SIMULTANEOUS INPUT AND STATE ESTIMATION THROUGH A UNIFYING MMSE FRAMEWORK WITH APPLICATIONS IN STRUCTURAL DYNAMICS

A Dissertation
Presented to
The Academic Faculty

by

Xi Liu

In Partial Fulfillment
of the Requirements for the Degree
Doctor of Philosophy in the
School of Civil and Environmental Engineering

Georgia Institute of Technology
December, 2019

SIMULTANEOUS INPUT AND STATE ESTIMATION THROUGH A UNIFYING MMSE FRAMEWORK WITH APPLICATIONS IN STRUCTURAL DYNAMICS

Approved by:

Dr. Yang Wang, Advisor
School of Civil and Environmental Engineering
Georgia Institute of Technology

Dr. Erik I. Verriest, Co-advisor
School of Electrical and Computer Engineering
Georgia Institute of Technology

Dr. Rafi L. Muhanna
School of Civil and Environmental Engineering
Georgia Institute of Technology

Dr. Lauren K. Stewart
School of Civil and Environmental Engineering
Georgia Institute of Technology

Dr. Donald W. White
School of Civil and Environmental Engineering
Georgia Institute of Technology

Date Approved: [August 16, 2019]

ACKNOWLEDGEMENTS

First and foremost, I would like to express my deepest gratitude to my advisor, Dr. Yang Wang, for his continuous support, advisement, and guidance throughout my time at Georgia Tech. Conducting research under his guidance has provided me with experiences in multidisciplinary topics such as estimation, control, and electronics, that have fascinated me ever since. The rigorous reasoning and critical thinking he has shown and taught me has not only helped me in academic research, but also in real life. These lessons will continue to influence my work and life in the future. I would also like to express my sincere thanks to my co-advisor Dr. Erik Verriest for his insightful advice and his generosity of time in our numerous discussions. The clarity of his explanation and his appreciation of mathematical beauty always inspired and motivated me as a researcher. My sincere thanks are also extended to my dissertation committee, Dr. Rafi Muhanna, Dr. Lauren Stewart, and Dr. Donald White, for offering their valuable time and constructive feedback on my research.

I would like to thank the Georgia Department of Transportation for funding the bridge weigh-in-motion test through grant PR 14-30. I would also like to thank Timothy R. Wright for his help with the full-scale dynamic testing on the concrete frame. This dissertation research is also partially supported by National Science Foundation (CMMI-1150700 and CMMI-1634483).

I have greatly enjoyed my time at the Laboratory for Smart Structural Systems at Georgia Tech. I would like to thank my research group members, Dapeng Zhu, Xiaohua Yi, Chunhee Cho, Xinjun Dong, Dan Li, Peter Lander, Yu Otsuki, and Nadine Fahed, for

their friendship and support in my research. I especially would like to thank Xinjun Dong and Dan Li for their assistance in finite element updating, developing the *Martlet* wireless sensing system, and carrying out various field testing. I would also like to thank Yu Hong, Jin Yan, Yidong Qin, and many other students used to work in our lab for their friendship and help with wireless system testing.

When I first started my studies at Georgia Tech, my friendships with Yu Feng, Farahnaz Soleimani, and Sujith Mangalathu helped me adapt to the new environment with excitement and joy. I will always cherish my fond memories with Chong Ye, Xiaojia Zhang and many other friends from Mason 4132 and Georgia Tech. I would also like to thank Hanyan Li and Yingping Zhao for going through the last mile of this Ph.D. journey together with me. My special gratitude goes to Edwin Lim for his company and support throughout my Ph.D. studies. He has shown me the virtues of accountability, endurance, and humbleness, which inspire me to be a better person.

Finally, I would like to express my profound gratitude to my parents and family for their unconditional love and support. I would not have come so far without their continued encouragement and belief in me. They have shown me how to live life with hope and gratitude, which will be treasured throughout my life.

TABLE OF CONTENTS

LIST OF TABLES

LIST OF FIGURES

SUMMARY

This research investigates simultaneous input-state estimation for stochastic linear systems in the presence of unknown input or disturbance. When prior knowledge of the unknown input is not available, an input-state estimator with a white Gaussian input model is proposed. Furthermore, delayed measurements are utilized to improve estimator performance. When some prior knowledge of the unknown input is available (such as maximum magnitude, statistical properties or frequency bandwidth), an input-state estimator with an exogenous input model is proposed to utilize such prior information. A unifying minimum-mean-square-error (MMSE) framework is presented for a comprehensive characterization and direct comparison among the proposed estimators and the conventional approaches. These include the augmented Kalman filter with a Gaussian random walk model and the weighted least squares approach.

The proposed recursive estimators can not only estimate inputs with fixed locations, but also estimate moving inputs with time-varying locations. The performance of the estimators is validated and compared in both structural dynamics simulation and field tests. Besides numerical examples, the first field validation is performed on a full-scale concrete frame under hydraulic shaker excitation, where the shaker force input for the full-scale frame is estimated using measured structural acceleration responses. The second field validation is performed on an in-service highway bridge under traffic excitation, where the moving vehicle loads are estimated using a set of heterogeneous sensor measurements obtained from a wireless sensing system instrumented on the bridge.

CHAPTER 1. INTRODUCTION

Simultaneous input and state estimation plays a vital role in many engineering applications, such as fault detection [1, 2], geophysical applications [3], target tracking and navigations [4] and disturbance-observer based control system design [5]. In civil engineering, it is oftentimes expensive or not feasible to measure the input excitation to a structure directly, such as earthquake, wind or traffic loads, while knowledge of the unknown inputs is essential for structural health monitoring, control and maintenance. In such scenarios, numerical techniques can be developed to explicitly estimate the unknown input from structural responses. A typical example can be bridge weigh-in-motion (B-WIM), which utilizes a bridge as a linear system to estimate moving vehicle loads based on structural responses. Estimation of the moving loads can be used to identify over-weighted vehicles, which helps to reduce structural maintenance cost, improve infrastructure durability and ensure public safety [6].

1.1 Background and Motivation

To illustrate the input-state estimation problem, structural dynamics is first modeled as a stochastic process using state space representation as shown in Figure 1-1. The continuous state space matrices are denoted as A_c, B_c, C_c and D_c; the system state is denoted as x, which includes displacement and velocity when modeling structural dynamics; the system input is denoted as u; and the system output is denoted as y, which usually represents sensor measurements. For example, in B-WIM, state x can be chosen as

displacement and velocity response of the bridge, input u represents vehicle axle loads, and measurement y can be acceleration, displacement and strain obtained from sensors instrumented on the bridge. The size of state x, i.e. dimension of the state space system, depends on the size of the meshed finite element model, which can easily go beyond over thousands of degrees-of-freedom (DOFs). The size of y is the number of measurements from sensors instrumented on the bridge. In practice, the measurements are contaminated by random measurement noise v, and the system may also be affected by random process noise (disturbance) w. As a result, an estimator is needed to estimate the input u and state x given noise contaminated measurements y along with knowledge of the state space system (A_c, B_c, C_c, D_c and statistical property of the noise processes).

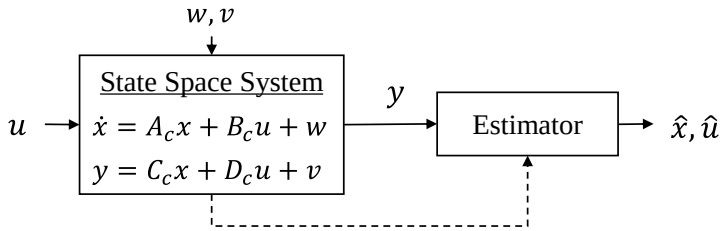

Figure 1-1 Linear dynamical system using state space representation

1.1.1 Introduction of Simultaneous Input-State Estimation

Simultaneous input-state estimation problems can be grouped into two major categories based on system models: (1) when the output y does not contain the unknown input u (i.e. $D_c = 0$, without direct feedthrough); (2) when the output contains the unknown input (i.e. $D_c \neq 0$, with direct feedthrough). Among early contributions addressing unknown input or bias during state estimation, Friedland [7] proposed to

estimate a constant bias by augmenting the state vector with the unknown bias vector. Verriest [8] generalized the constant bias assumption to time-varying bias/input signals with random initial conditions as well as for systems with delays. This generalization required a state space model of the unknown input. When a state space model of the input dynamics is not available, Kitanidis proposed a recursive state estimator by minimizing the trace of the state estimation error covariance for systems without direct feedthrough [3]. This approach provided an optimal state estimation in the sense of minimum mean square error (MMSE), but did not explicitly estimate the unknown input. Darouach, *et al.* [9] extended Kitanidis algorithm with stability and convergence conditions and further generalized to systems with direct feedthrough in [10]. To obtain an explicit estimation of the unknown input, Hsieh [11] generalized Kitanidis algorithm and proposed a two-stage Kalman filter for systems without direct feedthrough. Based on a weighted least squares (WLS) approach, Gillijns, *et al.* proposed a joint input-state estimation algorithm by combining MMSE estimation and a WLS objective along with optimality proof for both systems with and without feedthrough [12, 13]. Gillijns, *et al.* also showed that the proposed estimator in [12] yields the same input estimation as in [11] and the same state estimation as in [3] and [9]. Maes, *et al.* [14] generalized the algorithm to consider correlated process and measurement noise. Field measurements from a footbridge were used to validate the proposed WLS estimators for impact force identification [15, 16].

It should be noted that when WLS is used to estimate the unknown input, the input is treated as deterministic at each time step without utilizing any estimation results from prior time steps. Another approach to account for the unknown input is to treat the input as

a random variable at each time step. Lourens, *et al.* [17] proposed an augmented Kalman filter (AKF) by combining the unknown input with the state vector. This approach assumes a Gaussian random walk model for the unknown input, and the noise covariance corresponding to the input needs to be properly tuned through L-curve method [18]. It was also reported that when using acceleration measurements alone, a low-frequency drift occurs in both the estimated input and state, and the augmented system suffers from un-observability issue [17]. To examine the invertibility condition for linear systems, Maes, *et al.* [19] investigates the identifiability, stability and uniqueness conditions in simultaneous input-state estimation problems for modally reduced-order models. To improve the estimator performance and eliminate drift error, Azam, *et al.* [20] proposed a dual Kalman filter by switching the measurement update of the unknown input and time update of state, thus separating input and state estimation into two stages. This approach has the underlying assumption that the unknown input and state are uncorrelated. Although it is shown to be able to reduce drift error, similar as the augmented Kalman filter, it also required a properly tuned covariance and the estimator performance is quite sensitive to that parameter [21]. Other approaches to reduce the drift error include the use of post-processing high-pass filtering [16], fictitious displacement measurements [22], and an online high-pass filter [23]. In practice, when monitoring responses of civil structures, acceleration measurements are extensively used, and additional displacement measurement may not be available in each field test scenario. Therefore, the low-frequency drift error when displacement sensors are not available needs to be further studied to guarantee a good estimate of both the unknown input and state, especially for long-term applications.

In addition to the drift issue, the aforementioned approaches usually have full rank assumptions of matrix D_c (for systems with direct feedthrough) or matrix product $C_c B_c$ (for systems without direct feedthrough). These assumptions may be violated when only limited number of sensors are available in the field. To design estimators for rank deficient feedthrough matrix D_c, Yong, *et al.* [24] proposed a singular value decomposition based transformation approach as a generalization of the WLS estimator proposed by Gillijns, *et al.* in [12, 13]. This approach, however, still requires the matrix product $C_c B_c$ to be full rank. To further relax this assumption, delayed measurements can be introduced in the estimation [25]. The theoretical proof of minimum steps of delays required to obtain inversion of a linear deterministic discrete system is provided by Massey, *et al.* [26] in the late 1960s. For stochastic systems, Jin *et al.* [27] introduced time delays in the input estimation algorithm by augmenting measurement vector y, but ignoring the correlation between state estimation error and noise process after introducing delays [28]. To address the correlation issue, Sundaram, *et al.* [29] proposed to augment the noise process to the state vector, resulting in a state space model with a much higher dimension compared to the augmented measurement model. Maes, *et al.* [30] derived the correlation equations between state and noise processes by augmenting measurements from multiple time steps and provided experimental validation. This smoothing algorithm could improve the input estimation results when measurements and input are collocated, but still did not perform very well when the measurements and input were non-collocated.

As mentioned earlier, these estimation approaches generally assume no prior knowledge of the unknown input dynamics is available. However, in many engineering

applications, prior knowledge of the unknown input can be readily obtained, such as maximum magnitude, statistical properties or frequency bandwidth. When available, prior knowledge can be used to improve estimator performance. In control system design, the unknown input/disturbance can be assumed to be generated from a set of differential equations [31] or an exogenous system [32, 33]. Specifically, Chen [32] assumes the unknown disturbance is generated by a linear deterministic exogenous system and demonstrated that improved system performance can be achieved with a disturbance estimator/observer when the unknown disturbance can be modeled as a harmonic signal. Using these disturbance-model-based approaches, improved disturbance attenuation of the control system can be obtained.

In this dissertation, several simultaneous input-state estimators are proposed for systems with and without direct feedthrough. The estimators are especially designed with the ability to eliminate drift error when only acceleration measurements are available. In addition, multi-step delayed measurements are used to further improve estimator performance. To utilize any available prior knowledge of the unknown input, the input is assumed to be generated by a linear stochastic exogenous system.

Furthermore, most of the input-state estimators are commonly used in time invariant systems when the location of unknown inputs is fixed or time-invariant. A systematical way to modify the recursive estimators to account for moving inputs/loads needs to be developed for applications such as B-WIM.

1.1.2 Introduction of Bridge Weigh-in-Motion and Moving Load Estimation

The concept of using an instrumented bridge as a vehicle weighing platform was first proposed by Moses [34]. The algorithm was derived based on influence lines of a bridge to estimate equivalent static axle weights of a moving vehicle given measured bridge responses. Specifically, strain response of the bridge can be expressed as a function of axle weights based on the influence lines. The function is derived through the relationships among moving loads, bending moments and strain response of the bridge. To estimate equivalent static axle weights and gross vehicle weight, least-squares optimization was used to minimize the difference between theoretical bridge response and the experimentally measured strain response. Note that identification of the unknown vehicle weights using the response measurements is an inverse problem. Although Moses algorithm shows reasonable performance in determining gross vehicle weight, it can be ill-conditioned in determining axle weights [35, 36]. To improve the conditioning of conventional Moses algorithm, Tikhonov regularization [37] was introduced [35]. In addition to the ill-conditioning issue, the original Moses algorithm was based on theoretical influence lines, which can be inaccurate and different from the actual bridge response. O'Brien, *et al.* [38] proposed to obtain influence lines using experimental strain measurements from a pre-weighed calibration vehicle. Furthermore, probabilistic approach has also been introduced [39] to obtain influence lines.

The use of influence lines and strain measurements becomes the foundation of many B-WIM systems. In the 1980s, Peters [40] developed the AXWAY system in Australia, and later on developed a more efficient system named CULWAY [41]. The

CULWAY system uses existing concrete culverts as weighing scales. Because dynamic vibration of culverts can be quickly damped out by soil, dynamic interaction between the culvert and vehicle can be negligible [42]. In the late 1980s, Bridge Weighing Systems Inc. developed a B-WIM system [43] based on Moses algorithm. In the 1990s, several other B-WIM prototype systems were developed in Ireland [44] and Slovenia [45]. These systems, however, not only rely on static influence lines and strain measurements, but also require axle detectors installed on the road surface to estimate vehicle velocity and axle spacing. To improve the accuracy and durability of B-WIM systems, the European research project WAVE (Weigh-in-motion of Axles and Vehicles for Europe) [46] was launched in the mid-1990s. A highlight of the WAVE project was the introduction of the Free-of-Axle-Detector (FAD) concept [47]. Using strain gages instrumented under a bridge and eliminating axle detectors on the road surface, FAD systems can be installed without traffic interruption and reduce maintenance cost. In the early 2000s, A commercial FAD B-WIM system named SiWIM was developed by ZAG and Cestel, and has since become a popular B-WIM system used worldwide [48]. According to the accuracy classes specified by the European WIM specification (COST 323) [49], the SiWIM system can achieve accuracy classes ranging from the excellent class A(5) (i.e. $\pm 5\%$ error for 95% of the gross weight estimations) on ideal sites and classes B(10) or C(15) under average circumstances [50]. More recently, a portable B-WIM system is proposed to derive influence lines from bridge acceleration responses when only acceleration measurements are available, and a year-long field validation conducted by Sekiya reported the estimated gross vehicle weight was with $\pm 10.6\%$ error compared to static weights [51].

The aforementioned influence line method is a static approach to approximate dynamic behaviors, neglecting bridge-vehicle interactions and dynamical responses of the bridge. To account for the coupled dynamics between bridge and moving vehicles, moving force identification (MFI) algorithms have also been widely studied since the late 1980s, including the interpretive method [52, 53], time domain method [54], frequency-time domain method [55] and state space method [56-58]. Instead of estimating equivalent static axle weights, an MFI algorithm uses dynamic responses to estimate the entire time history of the dynamic axle forces applied by passing vehicles to the bridge. The system models used in the MFI algorithms can be categorized into analytical models [53-55, 57] and finite element models [52, 56, 59]. Because of the nature of inverse problems, i.e. estimating system input based on output, regularization and dynamic programming are also introduced to the MFI algorithms [58, 60, 61]. However, most of the existing approaches are based on deterministic system models without including uncertainties in systems and measurements [62]. Feng, *et al.* [63] proposed a Bayesian inference approach to estimate not only the moving force but also structural parameters with numerical validation.

The MFI algorithms in general, however, can be computationally expensive and real-time identification of axle weights can be challenging [64]. Furthermore, although besides strain measurements, the MFI algorithms allow the use of displacement and acceleration measurement, only a limited number of laboratory or field tests have been reported using accelerometers or heterogeneous measurements [65-68]. In this dissertation, a computationally efficient moving force estimator is proposed based on an MMSE framework. Heterogeneous sensor measurements, e.g. displacement, acceleration and

strain can be combined to estimate the moving force/load. The estimator is derived in state space form and the dynamical system is obtained from a finite element model. Statistical properties of system noise and measurement noise are incorporated in the estimator.

1.1.3 Motivating Structural Examples

One motivating structural example is a set of four full-scale two-story two-bay concrete frames (Figure 1-2(a)), located in the Structural Engineering and Materials Laboratory at Georgia Tech. The frames were built to investigate different seismic retrofitting methods [69]. This collaborative research project was funded by the Network for Earthquake Engineering Simulation (NEES) of National Science Foundation. The four concrete frames were built identical. While keeping the first frame as built, three different retrofitting methods were respectively applied to the other three frames. When testing a frame, a hydraulic linear inertia shaker provided by NEES@UCLA was installed on the roof of the frame [70]. Over tens of tests to each frame, the shaker generated excitation input to the structure with increasing magnitudes, gradually causing damage to the structure. Accelerometers, strain gages, and linear variable differential transformer (LVDTs) were instrumented on the frame to measure structural responses during a series of shaker tests [71]. Dynamic responses of the concrete frame can thus be used to estimate the shaker excitation time history.

Another motivating structural example is a pre-stressed concrete highway bridge (Figure 1-2(b)) in Bartow County of Georgia, United States. The bridge consists of three skewed spans, 70 feet long each. The continuous concrete slab is supported by five pre-

stressed concrete girders. The bridge is in good condition and can be used for B-WIM studies [72]. During a field test, a wireless sensing system named *Martlet* [73] is instrumented under the bridge to measure bridge dynamic responses under traffic loads [74]. Heterogeneous measurements acquired by the *Martlet* system can be used to estimate axle weights of two passing trucks.

(a) Full-scale concrete frame (NEES frame)

(b) Pre-stressed concrete highway bridge (Bartow bridge)

Figure 1-2 Motivating structural examples

1.2 Research Objectives

The main research objective of this dissertation is to develop simultaneous input-state estimators for various engineering applications, such as structural health monitoring and bridge weigh-in-motion (B-WIM).

1. An input-state estimator with an explicit estimation of the unknown input will be derived for systems with and without feedthrough, and especially designed to eliminate drift error when only acceleration measurements are available. Theoretical relationships between the proposed estimator and the conventional AKF and WLS estimators will be

provided. In addition, multi-step delayed measurements will be introduced during the estimation process to further improve estimator performance, especially when the input is not directly fed through to measurement or the feedthrough matrix is rank deficient.

2. To utilize any available prior knowledge of the unknown input, input-state estimators with an exogenous stochastic input model are derived for both systems with and without feedthrough. A special case of the estimator is then presented by assuming the input has a known frequency bandwidth.

3. For applications on large-scale structures, model reduction through modal decomposition will be included in the estimators with heterogeneous sensor measurement. To obtain a reliable finite element (FE) model for input estimation, model parameter updating is performed based on field measurement data. With the updated model, shaker excitation of the NEES concrete frame will be estimated using the measured structural responses.

4. This research will also extend the proposed input-state estimators to time varying systems, when the location of the input changes over time. The proposed estimators are especially designed for B-WIM applications with improved computational efficiency. An in-service highway bridge is used as the testbed. Given bridge vibration responses obtained by the low-cost *Martlet* wireless sensing system, the proposed moving load estimators will be used to identify moving vehicle loads.

1.3 Organization of Dissertation

The rest of this dissertation is organized as follows.

Chapter 2 presents the derivation of three input-state estimators based on a unifying minimum-mean-square-error (MMSE) framework for systems with and without direct feedthrough. The proposed estimators assume a white Gaussian input model with an explicit estimation of the unknown input. The estimators are short-named as FIC (finite input covariance) estimators, or FIC-d estimator when d time steps of delayed measurements are used during estimation. When the input covariance of the FIC estimator approaches infinity, theoretical proof of equivalence between the FIC and a conventional weighted least squares (WLS) estimator is provided. Numerical studies of a 4-story shear structure are presented using different sensor instrumentation scenarios. The proposed FIC and FIC-d estimators are validated, and their performance is compared with conventional augmented Kalman filter (AKF) and WLS estimators.

Chapter 3 extends the previously proposed estimators with an exogenous input model to utilize prior knowledge of input dynamics or frequency bandwidth. The combination of an exogenous input model provides more flexibility in estimator design, and the AKF and FIC estimators are shown to be special cases of the generalized input model. Furthermore, instead of assuming a white Gaussian input model (assumption from the FIC estimator), an estimator with a bandlimited frequency input model is proposed in this chapter for both systems with and without feedthrough, short-named as the LFB (limited frequency bandwidth) estimator. Numerical studies of a 4-story structure are used

to validate the proposed LFB estimator, in comparison with the FIC estimator for measurements both collocated and non-collocated with input.

Chapter 4 presents an experimental validation of the proposed FIC, FIC-d and LFB estimators using a full-scale concrete frame structure (NEES frame). System identification and finite element model updating are first performed to provide a reliable system model for input estimation. Modal decomposition is used to reduce the system order to increase computational efficiency. Based on the reduced-order model, effect of sensor instrumentation on shaker input estimation is investigated. Two different sensor instrumentation scenarios, i.e. when measurement locations include and exclude the shaker input location, are presented in this chapter to evaluate estimator performance. Based on measured acceleration responses of the frame, estimated shaker input is compared with the actual measured shaker input.

Chapter 5 extends the proposed input-state estimators to account for unknown inputs with time varying locations, especially for applications in bridge weigh-in-motion (B-WIM). The input matrix of the state space model is reformulated to describe the moving load. Numerical simulations based on a pair of simply supported girders are used to validate the FIC and LFB estimators for identifying moving load(s). Furthermore, an in-service highway bridge is used as the testbed bridge for B-WIM study. The moving load estimators are first validated in simulation using heterogeneous sensor measurements, including displacement, strain and acceleration. Three different sensor instrumentation scenarios are discussed here to investigate its effect on moving force estimation. In addition to simulated measurements, dynamical responses of a bridge span under moving vehicle loads were

recorded by the *Martlet* wireless sensing system during a B-WIM field test. Heterogeneous experimental measurements are used to estimate axle weights and gross vehicle weight of two different trucks passing through the bridge.

Chapter 6 presents a summary and main conclusions of this research along with recommendations for future research topics.

CHAPTER 2. SIMULTANEOUS ESTIMATION OF INPUT AND STATE BASED ON A UNIFYING MMSE FRAMEWORK

This chapter addresses the simultaneous input-state estimation problem for discrete-time linear stochastic systems with unknown input. A unifying minimum-mean-square-error (MMSE) estimation framework is presented for a comprehensive characterization and direct comparison with a few popular input estimation approaches. This chapter discusses systems both with and without direct feedthrough of the unknown input to the measurement output. For example, in structural dynamics, when acceleration measurements of a lumped-mass model are available for the excitation/input degrees-of-freedom (DOFs), the dynamical system is with direct feedthrough because of the corresponding non-zero feedthrough matrix in the measurement equation. In contrast, if no acceleration measurements are available for any input DOFs, the system is without direct feedthrough. The dynamical model of the input is assumed to be unknown in this chapter and the input is treated as a random variable at each time step. To account for the unknown input dynamics, an estimator that adopts a white Gaussian input model with a finite covariance is proposed, short-named as the FIC (finite input covariance) estimator.

Based on the unifying MMSE framework, it is shown that when the input covariance of the FIC estimator approaches infinity with some additional assumptions, the FIC estimator is equivalent to a well-known weighted-least-squares (WLS) estimator. Furthermore, when only acceleration measurements of a mechanical vibration system are available, the FIC estimator eliminates a low-frequency drift error in the estimated input

and states, providing a tight estimation confidence interval. To further generalize the input-state estimator, delayed measurements are used to improve the estimator performance and combine the estimators for both systems with and without direct feedthrough. Finally, the proposed estimators are validated using a simulated 4-story shear structure. The shear structure is excited by different types of inputs and the corresponding acceleration responses are used to compare estimator performance. Detailed discussions regarding the effect of estimator covariances on input estimation are also provided.

Three lemmas are first provided here to assist the derivation in this chapter. Since the lemmas are standard, they are provided without proof.

Lemma 2-1 (matrix push through identity) Let $A \in \mathbb{R}^{m\times n}$, $B \in \mathbb{R}^{n\times m}$, I_m is the identity matrix with dimension $m \times m$ and both $(I_n + BA)$ and $(I_m + AB)$ are invertible. As a result,

$$A(I_n + BA)^{-1} = (I_m + AB)^{-1}A \tag{2-1}$$

Lemma 2-2 (Sherman-Morrison-Woodbury formula) Let $A \in \mathbb{R}^{m\times m}$, $B \in \mathbb{R}^{m\times n}$, $C \in \mathbb{R}^{n\times n}$, $D \in \mathbb{R}^{n\times m}$. If A, C, $A + BCD$, and $C^{-1} + DA^{-1}B$ are nonsingular,

$$(A + BCD)^{-1} = A^{-1} - A^{-1}B(C^{-1} + DA^{-1}B)^{-1}DA^{-1} \tag{2-2a}$$

$$= A^{-1}(I_m - B(C^{-1} + DA^{-1}B)^{-1}DA^{-1}) \tag{2-2b}$$

Lemma 2-3 Suppose $x \in \mathbb{R}^n$ and $v \in \mathbb{R}^m$ are independent random vectors. We would like to estimate x based on a linear measurement $y = Ax + v$, where $A \in \mathbb{R}^{m \times n}$ is a constant matrix. As a result, we have $\mathbb{E}(y) = A\mathbb{E}(x) + \mathbb{E}(v)$, $\Sigma_{xy} = \Sigma_x A^T$ and $\Sigma_y = A\Sigma_x A^T + \Sigma_v$. If x, v are Gaussian, i.e. $x \sim \mathcal{N}(\mu_x, \Sigma_x)$, $v \sim \mathcal{N}(\mu_v, \Sigma_v)$, the MMSE estimate of x given y and the conditional estimation error covariance $\Sigma_{x|y}$ can be expressed as

$$\hat{x} = \mathbb{E}(x|y) = \mathbb{E}(x) + \Sigma_{xy}\Sigma_y^{-1}\big(y - \mathbb{E}(y)\big) \tag{2-3}$$

$$\Sigma_{x|y} \triangleq \mathrm{cov}(x|y) = \Sigma_x - \Sigma_{xy}\Sigma_y^{-1}\Sigma_{yx} \tag{2-4}$$

Note that x and y are also jointly Gaussian.

2.1 Estimation for Systems with Direct Feedthrough

This section introduces the problem of simultaneous input-state estimation for systems with direct feedthrough of the unknown input. Theoretical formulation of the FIC estimator is compared with two other estimators, one using a Gaussian random walk input model combined with augmented Kalman filter (AKF) and another one using a deterministic input model with WLS estimation. The basic unifying MMSE framework is first presented by augmenting the unknown input to the state vector in measurement update phase but keeping the estimation of input and state separate. Next, time update of input and state is derived based on the Gaussian random walk input model and the white noise input model. Finally, proof is provided to show that when input covariance of the FIC estimator

approaches infinity and the feedthrough matrix has full-column rank, the WLS estimator can be obtained.

2.1.1 Problem Formulation

Consider the following discrete-time stochastic linear system with direct feedthrough of input:

$$x_{k+1} = Ax_k + Bu_k + w_k \tag{2-5}$$

$$y_k = Cx_k + Du_k + v_k \tag{2-6}$$

Here $x_k \in \mathbb{R}^n$ is the state at time step k, $u_k \in \mathbb{R}^{n_u}$ is the unknown input, $w_k \in \mathbb{R}^n$ is the process noise or disturbance, $y_k \in \mathbb{R}^m$ is the measurement output, and $v_k \in \mathbb{R}^m$ is the measurement noise. The unknown input u_k is assumed to be a random vector at each time step with unknown dynamics. To account for the unknown dynamics, the AKF estimator, as proposed in [17], assumes a Gaussian random walk model of the unknown input with white Gaussian process noise $\xi_k \sim \mathcal{N}(0, \Sigma_{\xi_k})$, i.e. $u_{k+1} = u_k + \xi_k$, where ξ_k is independent from x_0, u_l, v_l and w_l for all k and l. The covariance of ξ_k is assumed to be time invariant, i.e. $\Sigma_{\xi_k} = \Sigma_{\xi}$. The FIC estimator assumes the input has white Gaussian distribution with a predefined finite input covariance Σ_u to utilize any prior knowledge related to the input. The WLS estimator extends the finite input covariance to be infinite, i.e. $\Sigma_u = \Sigma_\infty$, when assuming the input is highly uncertain.

The assumptions made in the section are: (1) the system is observable, i.e. (A, C) is observable; as a result, the rank of the observability matrix $\mathcal{O} = [C^T \quad (CA)^T \quad \cdots \quad (CA^{n-1})^T]^T$ equals the number of states n; (2) $v_k \sim \mathcal{N}(0, \Sigma_v)$ and $w_k \sim \mathcal{N}(0, \Sigma_w)$ are white Gaussian noise such that Σ_v and Σ_w are diagonal matrices and $\Sigma_v \succ 0$ and $\Sigma_w \succcurlyeq 0$; (3) v_k and w_l are independent for all k and l; (4) initial state is random $x_0 \sim \mathcal{N}(\mu_0, \Sigma_0)$ and independent from v_k and w_l for all k and l; (5) unknown input $u_{0:k}$ is Gaussian and independent from x_0, v_l and w_l for all k and l.

The following notations are used here: the minimum-mean-square-error (MMSE) estimate of x_k given cumulative sequential measurements $y_{0:l} \triangleq [y_0^T \quad y_1^T \quad \cdots \quad y_l^T]^T$ is denoted as $\hat{x}_{k|l} \triangleq \mathbb{E}(x_k|y_{0:l})$; the conditional covariance of x_k given $y_{0:l}$ is $\Sigma_{x_{k|l}} \triangleq \mathrm{cov}(x_k|y_{0:l})$; the MMSE of u_k is $\hat{u}_{k|l} \triangleq \mathbb{E}(u_k|y_{0:l})$ with conditional covariance $\Sigma_{u_{k|l}} \triangleq \mathrm{cov}(u_k|y_{0:l})$. The conditional cross-covariance between the state and input is denoted as $\Sigma_{x_k u_{k|l}} \triangleq \mathrm{cov}(x_k, u_k|y_{0:l})$, and the conditional cross-covariance between the state-input vector $\begin{Bmatrix} x_k \\ u_k \end{Bmatrix}$ and measurement y_k is denoted as $\Sigma_{\begin{Bmatrix} x_k \\ u_k \end{Bmatrix} y_{k|l}} \triangleq \mathrm{cov}\left(\begin{Bmatrix} x_k \\ u_k \end{Bmatrix}, y_k \middle| y_{0:l}\right)$. The following lemma is provided to derive the simultaneous input-state estimator for systems with direct feedthrough.

Lemma 2-4 For the system given by Eq. (2-5) and (2-6) with the assumptions made in this section, x_k, u_k and $y_{0:k}$ are jointly Gaussian. In addition, the three conditional random vectors, $x_k|y_{0:k-1}$, $u_k|y_{0:k-1}$ and $y_k|y_{0:k-1}$, are jointly (and individually) Gaussian.

Proof. Based on Eq. (2-5) and (2-6), we can derive that

$$x_k = A^k x_0 + H_{u_k} u_{0:k} + H_{w_k} w_{0:k-1} \tag{2-7}$$

$$y_{0:k} = \mathcal{O}_k x_0 + P_{u_k} u_{0:k} + P_{w_k} w_{0:k-1} + v_{0:k} \tag{2-8}$$

where $H_{u_k} \triangleq \begin{bmatrix} A^{k-1}B & \cdots & AB & B & 0_{n\times n_u} \end{bmatrix} \in \mathbb{R}^{n\times n_u(k+1)}$,

$H_{w_k} \triangleq [A^{k-1} \quad \cdots \quad A \quad I_n] \in \mathbb{R}^{n\times nk}$,

$\mathcal{O}_k \triangleq \begin{bmatrix} C \\ CA \\ \vdots \\ CA^k \end{bmatrix} \in \mathbb{R}^{m(k+1)\times n}$, $P_{u_k} \triangleq \begin{bmatrix} D & 0 & \cdots & 0 \\ CB & \ddots & \cdots & \vdots \\ \vdots & \ddots & D & 0 \\ CA^{k-1}B & \cdots & CB & D \end{bmatrix} \in \mathbb{R}^{m(k+1)\times n_u(k+1)}$ and

$P_{w_k} \triangleq \begin{bmatrix} 0 & 0 & 0 \\ C & \ddots & \vdots \\ \vdots & \ddots & 0 \\ CA^{k-1} & \cdots & C \end{bmatrix} \in \mathbb{R}^{m(k+1)\times nk}$.

Because x_0, $u_{0:k}$, $w_{0:k-1}$ and $v_{0:k}$ are Gaussian and independent from each other, they are jointly Gaussian. Since x_k, u_k, and $y_{0:k}$ can be expressed as a linear transformation of x_0, $u_{0:k}$, $w_{0:k-1}$ and $v_{0:k}$ with full row-rank as shown in Eq. (2-9), x_k, u_k, and $y_{0:k}$ are also jointly Gaussian.

$$\begin{Bmatrix} x_k \\ u_k \\ y_{0:k} \end{Bmatrix} = \begin{bmatrix} A^k & H_{u_k} & H_{w_k} & 0 \\ 0 & \check{I}_{n_u} & 0 & 0 \\ \mathcal{O}_k & P_{u_k} & P_{w_k} & I_{m(k+1)} \end{bmatrix} \begin{Bmatrix} x_0 \\ u_{0:k} \\ w_{0:k-1} \\ v_{0:k} \end{Bmatrix} \tag{2-9}$$

where $I_{n_u} \in \mathbb{R}^{n_u\times n_u}$, $I_m \in \mathbb{R}^{m(k+1)\times m(k+1)}$ are identity matrices, and $\check{I}_{n_u} = [0 \quad I_{n_u}]$. In addition, because conditional distributions of jointly Gaussian random vectors are Gaussian, each vector among $x_k|y_{0:k-1}$, $u_k|y_{0:k-1}$ and $y_k|y_{0:k-1}$ is Gaussian. ■

In the following, a recursive MMSE estimator for simultaneous input-state estimation is derived assuming a Gaussian random walk model (AKF estimator), a white noise model with finite input covariance (FIC estimator), and a white noise model with infinite input covariance (equivalent to the WLS estimator), respectively. Given prior estimates of input and state at time step k, i.e. $\hat{x}_{k|k-1}$, $\Sigma_{x_{k|k-1}}$, $\hat{u}_{k|k-1}$, $\Sigma_{u_{k|k-1}}$ and $\Sigma_{x_k u_{k|k-1}}$, the state x_k and input u_k at time step k given measurements $y_{0:k}$ are simultaneously estimated based on a unifying MMSE framework.

2.1.2 Measurement Update of Input and State

Equation (2-6) can be rewritten in the following form by combining the state x_k and input u_k as one vector

$$y_k = [C \quad D] \begin{Bmatrix} x_k \\ u_k \end{Bmatrix} + v_k \tag{2-10}$$

Considering the independence of measurement noise v_k from past measurement sequence $y_{0:k-1}$, Eq. (2-10) is conditioned on $y_{0:k-1}$ as

$$y_k | y_{0:k-1} = [C \quad D] \begin{Bmatrix} x_k \\ u_k \end{Bmatrix} \Big| y_{0:k-1} \Big\} + v_k \tag{2-11}$$

Recalling $v_k \sim \mathcal{N}(0, \Sigma_v)$, the corresponding conditional expectation can be written as

$$\mathbb{E}(y_k|y_{0:k-1}) = [C \quad D]\mathbb{E}\left(\begin{Bmatrix} x_k \\ u_k \end{Bmatrix}\middle| y_{0:k-1}\right) + \mathbb{E}(v_k) = C\hat{x}_{k|k-1} + D\hat{u}_{k|k-1} \tag{2-12}$$

Applying the affine transformation in Lemma 2-3 to Eq. (2-12), the conditional cross-covariance between $\begin{Bmatrix} x_k \\ u_k \end{Bmatrix}\middle| y_{0:k-1}$ and $y_k|y_{0:k-1}$ is

$$\Sigma_{\begin{Bmatrix} x_k \\ u_k \end{Bmatrix} y_{k|k-1}} = \begin{bmatrix} \Sigma_{x_{k|k-1}} & \Sigma_{x_k u_{k|k-1}} \\ \Sigma_{u_k x_{k|k-1}} & \Sigma_{u_{k|k-1}} \end{bmatrix} \begin{bmatrix} C^T \\ D^T \end{bmatrix} \tag{2-13}$$

The conditional covariance of $y_k|y_{0:k-1}$ is found as

$$\Sigma_{y_{k|k-1}} = [C \quad D] \begin{bmatrix} \Sigma_{x_{k|k-1}} & \Sigma_{x_k u_{k|k-1}} \\ \Sigma_{u_k x_{k|k-1}} & \Sigma_{u_{k|k-1}} \end{bmatrix} \begin{bmatrix} C^T \\ D^T \end{bmatrix} + \Sigma_v \tag{2-14}$$

Recall that measurement noise v_k is independent of x_k, u_k and $y_{0:k-1}$, thus $\Sigma_{x_k v_{k|k-1}}$ and $\Sigma_{u_k v_{k|k-1}}$ are zero matrices. Expanding Eq. (2-13) and Eq. (2-14) gives the following expressions

$$\Sigma_{x_k y_{k|k-1}} = \Sigma_{x_{k|k-1}} C^T + \Sigma_{x_k u_{k|k-1}} D^T \tag{2-15}$$

$$\Sigma_{u_k y_{k|k-1}} = \Sigma_{u_{k|k-1}} D^T + \Sigma_{u_k x_{k|k-1}} C^T \tag{2-16}$$

$$\Sigma_{y_{k|k-1}} = C\Sigma_{x_{k|k-1}} C^T + D\Sigma_{u_{k|k-1}} D^T + \Sigma_v + D\Sigma_{u_k x_{k|k-1}} C^T + C\Sigma_{x_k u_{k|k-1}} D^T \tag{2-17}$$

Recall that $x_k|y_{0:k-1}$, $u_k|y_{0:k-1}$ and $y_k|y_{0:k-1}$ are jointly Gaussian from Lemma 2-4. Based on Eq. (2-11) and Lemma 2-3, the MMSE estimate of x_k, u_k given y_k and $y_{0:k-1}$ are shown in the following

$$\begin{Bmatrix}\hat{x}_{k|k}\\ \hat{u}_{k|k}\end{Bmatrix} \triangleq \mathbb{E}\left(\begin{Bmatrix}x_k\\ u_k\end{Bmatrix}\middle| y_{0:k}\right)$$

$$= \mathbb{E}\left(\begin{Bmatrix}x_k\\ u_k\end{Bmatrix}\middle| y_{0:k-1}\right) + \Sigma_{\begin{Bmatrix}x_k\\ u_k\end{Bmatrix} y_{k|k-1}} \Sigma_{y_{k|k-1}}^{-1}\left(y_k - \mathbb{E}(y_k|y_{0:k-1})\right) \tag{2-18}$$

Substituting Eq. (2-12), Eq. (2-13) into Eq. (2-18), we obtain

$$\begin{Bmatrix}\hat{x}_{k|k}\\ \hat{u}_{k|k}\end{Bmatrix} = \begin{Bmatrix}\hat{x}_{k|k-1} + L_{x_k}\left(y_k - C\hat{x}_{k|k-1} - D\hat{u}_{k|k-1}\right)\\ \hat{u}_{k|k-1} + L_{u_k}\left(y_k - C\hat{x}_{k|k-1} - D\hat{u}_{k|k-1}\right)\end{Bmatrix} \tag{2-19}$$

where the estimation gains are defined as

$$L_{x_k} \triangleq \Sigma_{x_k y_{k|k-1}} \Sigma_{y_{k|k-1}}^{-1} = \Sigma_{x_{k|k-1}} C^T \Sigma_{y_{k|k-1}}^{-1} + \Sigma_{x_k u_{k|k-1}} D^T \Sigma_{y_{k|k-1}}^{-1} \tag{2-20}$$

$$L_{u_k} \triangleq \Sigma_{u_k y_{k|k-1}} \Sigma_{y_{k|k-1}}^{-1} = \Sigma_{u_{k|k-1}} D^T \Sigma_{y_{k|k-1}}^{-1} + \Sigma_{u_k x_{k|k-1}} C^T \Sigma_{y_{k|k-1}}^{-1} \tag{2-21}$$

Note that $\Sigma_{x_k y_{k|k-1}}$ and $\Sigma_{u_k y_{k|k-1}}$ are given by Eq. (2-15) and (2-16). Based on Eq. (2-4) in Lemma 2-3, the conditional covariance given $y_{0:k}$ can be obtained as

$$\operatorname{cov}\left(\begin{Bmatrix} x_k \\ u_k \end{Bmatrix} \middle| y_{0:k}\right) \triangleq \begin{bmatrix} \Sigma_{x_{k|k}} & \Sigma_{x_k u_{k|k}} \\ \Sigma_{u_k x_{k|k}} & \Sigma_{u_{k|k}} \end{bmatrix}$$

$$= \begin{bmatrix} \Sigma_{x_{k|k-1}} & \Sigma_{x_k u_{k|k-1}} \\ \Sigma_{u_k x_{k|k-1}} & \Sigma_{u_{k|k-1}} \end{bmatrix} - \begin{bmatrix} \Sigma_{x_k y_{k|k-1}} \\ \Sigma_{u_k y_{k|k-1}} \end{bmatrix} \Sigma_{y_{k|k-1}}^{-1} \begin{bmatrix} \Sigma_{y_k x_{k|k-1}} & \Sigma_{y_k u_{k|k-1}} \end{bmatrix} \tag{2-22}$$

Expand Eq. (2-22), simplify the equations with estimation gains, and substitute $\Sigma_{x_k y_{k|k-1}}$ and $\Sigma_{u_k y_{k|k-1}}$ with Eq. (2-15) and (2-16):

$$\begin{aligned} \Sigma_{x_{k|k}} &= \Sigma_{x_{k|k-1}} - \Sigma_{x_k y_{k|k-1}} \Sigma_{y_{k|k-1}}^{-1} \Sigma_{x_k y_{k|k-1}}^T \\ &= \Sigma_{x_{k|k-1}} - L_{x_k} \left(\Sigma_{x_{k|k-1}} C^T + \Sigma_{x_k u_{k|k-1}} D^T \right)^T \end{aligned} \tag{2-23}$$

$$\begin{aligned} \Sigma_{u_{k|k}} &= \Sigma_{u_{k|k-1}} - \Sigma_{u_k y_{k|k-1}} \Sigma_{y_{k|k-1}}^{-1} \Sigma_{u_k y_{k|k-1}}^T \\ &= \Sigma_{u_{k|k-1}} - L_{u_k} \left(\Sigma_{u_{k|k-1}} D^T + \Sigma_{u_k x_{k|k-1}} C^T \right)^T \end{aligned} \tag{2-24}$$

$$\begin{aligned} \Sigma_{x_k u_{k|k}} &= \Sigma_{x_k u_{k|k-1}} - \Sigma_{x_k y_{k|k-1}} \Sigma_{y_{k|k-1}}^{-1} \Sigma_{u_k y_{k|k-1}}^T \\ &= \Sigma_{x_k u_{k|k-1}} - \left(\Sigma_{x_{k|k-1}} C^T + \Sigma_{x_k u_{k|k-1}} D^T \right) L_{u_k}^T \end{aligned} \tag{2-25}$$

In summary, this subsection derives estimates of both state x_k and input u_k given measurement sequence $y_{0:k}$, as shown in Eq. (2-19). The corresponding estimation error covariances are given by Eq. (2-23) ~ (2-25).

2.1.3 Time Update of Input and State

Time update of state is straightforward using linear transformation. Based on Eq. (2-5), the state at time step $k+1$ can be re-written in the following form

$$x_{k+1} = [A \quad B \quad I]\begin{Bmatrix} x_k \\ u_k \\ w_k \end{Bmatrix} \tag{2-26}$$

Because the linear transformation in Eq. (2-26) has full row-rank, the estimate of x_{k+1} given $y_{0:k}$ can thus be written as

$$\hat{x}_{k+1|k} = \mathbb{E}(x_{k+1}|y_{0:k}) = [A \quad B \quad I]\mathbb{E}\left(\begin{Bmatrix} x_k \\ u_k \\ w_k \end{Bmatrix}\middle| y_{0:k}\right) = A\hat{x}_{k|k} + B\hat{u}_{k|k} \tag{2-27}$$

Note $\mathbb{E}(w_k|y_{0:k}) = 0$ because process noise $w_k \sim \mathcal{N}(0, \Sigma_w)$ is independent from $y_{0:k}$ (Eq. (2-8)). The conditional covariance is given by

$$\Sigma_{x_{k+1|k}} \triangleq \text{cov}(x_{k+1}|y_{0:k}) = [A \quad B]\begin{bmatrix} \Sigma_{x_{k|k}} & \Sigma_{x_k u_{k|k}} \\ \Sigma_{u_k x_{k|k}} & \Sigma_{u_{k|k}} \end{bmatrix}\begin{bmatrix} A^T \\ B^T \end{bmatrix} + \Sigma_w \tag{2-28}$$

Note here because the process noise w_k is independent from x_k, u_k and $y_{0:k}$, the cross-covariance of state-noise and input-noise are zero, i.e. $\Sigma_{x_k w_{k|k}} = 0$ and $\Sigma_{u_k w_{k|k}} = 0$. In addition, $\text{cov}(w_k|y_{0:k}) = \text{cov}(w_k) = \Sigma_w$.

In terms of time update of input, a state space model of the input can be used to propagate the input over time. When a Gaussian random walk model is assumed as $u_{k+1} = u_k + \xi_k$ with $\xi_k \sim \mathcal{N}(0, \Sigma_\xi)$, the conditional expectation and covariance are

$$\hat{u}_{k+1|k} \triangleq \mathbb{E}(u_{k+1}|y_{0:k}) = \mathbb{E}(u_k + \xi_k|y_{0:k}) = \hat{u}_{k|k} \tag{2-29}$$

$$\Sigma_{u_{k+1|k}} \triangleq \mathrm{cov}(u_{k+1}|y_{0:k}) = \mathrm{cov}(u_k + \xi_k|y_{0:k}) = \Sigma_{u_{k|k}} + \Sigma_\xi \tag{2-30}$$

$$\begin{aligned}\Sigma_{x_{k+1}u_{k+1|k}} &\triangleq \mathrm{cov}(x_{k+1}, u_{k+1}|y_{0:k}) = \mathrm{cov}(Ax_k + Bu_k + w_k, u_k + \xi_k|y_{0:k}) \\ &= A\Sigma_{x_k u_{k|k}} + B\Sigma_{u_{k|k}}\end{aligned} \tag{2-31}$$

This approach is the same as augmenting the state vector with the unknown input; the resulting augmented state can then be estimated using a regular Kalman filter [17]. Hereinafter, this estimator with a Gaussian random walk input model is referred to as the augmented Kalman filter (AKF). The resulting augmented system is found to suffer from un-observability issue when only acceleration measurements are available [17]. To resolve the issue, u_k can be assumed to be zero-mean white Gaussian with $u_k \sim \mathcal{N}(0, \Sigma_u)$. With this assumption, u_k is independent from x_0, $u_{0:k-1}$, $w_{0:k-1}$ and $v_{0:k-1}$. Therefore, based on Eq. (2-7) and Eq. (2-8), u_{k+1} is independent from x_{k+1} and $y_{0:k}$. As a result, we have

$$\hat{u}_{k+1|k} \triangleq \mathbb{E}(u_{k+1}|y_{0:k}) = \mathbb{E}(u_{k+1}) = 0 \tag{2-32}$$

$$\Sigma_{u_{k+1|k}} \triangleq \mathrm{cov}(u_{k+1}|y_{0:k}) = \Sigma_u \tag{2-33}$$

$$\Sigma_{x_{k+1}u_{k+1|k}} \triangleq \mathrm{cov}(x_{k+1}, u_{k+1}|y_{0:k}) = \Sigma^T_{u_{k+1}x_{k+1|k}} = 0 \tag{2-34}$$

Hereinafter, this estimator with a finite input covariance Σ_u is referred to as the finite input covariance (FIC) estimator. Thus far, simultaneous estimation of the state and input given $y_{0:k}$ have been derived based on the unifying MMSE framework, and the difference between AKF and FIC is shown to be only in the time update stage. Table 2-1 summarizes the proposed FIC estimator using the time updated priors given by Eq. (2-32) ~ (2-34) in comparison to the AKF.

Table 2-1 Input-state estimation using the augmented Kalman filter and finite input covariance estimator for systems with direct feedthrough

Augmented Kalman filter (AKF)		Finite input covariance (FIC) estimator	
Initialization:			
$\hat{x}_{0\|-1} = \mu_{x_0}, \Sigma_{x_{0\|-1}} = \Sigma_{x_0}$ $\hat{u}_{0\|-1} = \hat{u}_0, \Sigma_{u_{0\|-1}} = \Sigma_{u_0}, \Sigma_{x_0 u_{0\|-1}} = \Sigma_{x_0 u_0}$		$\hat{x}_{0\|-1} = \mu_{x_0},\ \Sigma_{x_{0\|-1}} = \Sigma_{x_0}$	
`for` $k = 0,\ 1, \dots, n$			
Measurement update of input:			
$\Sigma_{y_{k\|k-1}} = C\Sigma_{x_{k\|k-1}}C^T + D\Sigma_{u_{k\|k-1}}D^T + \Sigma_v + D\Sigma_{u_k x_{k\|k-1}}C^T + C\Sigma_{x_k u_{k\|k-1}}D^T$	Rept. (2-17)	$\Sigma_{y_{k\|k-1}} = C\Sigma_{x_{k\|k-1}}C^T + D\Sigma_u D^T + \Sigma_v$	(2-35)
$L_{u_k} = \left(\Sigma_{u_{k\|k-1}}D^T + \Sigma_{u_k x_{k\|k-1}}C^T\right)\Sigma^{-1}_{y_{k\|k-1}}$	Rept. (2-21)	$L_{u_k} = \Sigma_u D^T \Sigma^{-1}_{y_{k\|k-1}}$	(2-36)
$\hat{u}_{k\|k} = \hat{u}_{k\|k-1} + L_{u_k}\left(y_k - C\hat{x}_{k\|k-1} - D\hat{u}_{k\|k-1}\right)$	Rept. (2-19)	$\hat{u}_{k\|k} = L_{u_k}\left(y_k - C\hat{x}_{k\|k-1}\right)$	(2-37)
$\Sigma_{u_{k\|k}} = \Sigma_{u_{k\|k-1}} - L_{u_k}\left(\Sigma_{u_{k\|k-1}}D^T + \Sigma_{u_k x_{k\|k-1}}C^T\right)^T$	Rept. (2-24)	$\Sigma_{u_{k\|k}} = \Sigma_u - L_{u_k}D\Sigma_u$	(2-38)
$\Sigma_{x_k u_{k\|k}} = \Sigma_{x_k u_{k\|k-1}} - \left(\Sigma_{x_{k\|k-1}}C^T + \Sigma_{x_k u_{k\|k-1}}D^T\right)L_{u_k}^T$	Rept. (2-25)	$\Sigma_{x_k u_{k\|k}} = -\Sigma_{x_{k\|k-1}}C^T L_{u_k}^T$	(2-39)
Measurement update of state:			
$L_{x_k} = \left(\Sigma_{x_{k\|k-1}}C^T + \Sigma_{x_k u_{k\|k-1}}D^T\right)\Sigma^{-1}_{y_{k\|k-1}}$	Rept. (2-20)	$L_{x_k} = \Sigma_{x_{k\|k-1}}C^T\Sigma^{-1}_{y_{k\|k-1}}$	(2-40)
$\hat{x}_{k\|k} = \hat{x}_{k\|k-1} + L_{x_k}\left(y_k - C\hat{x}_{k\|k-1} - D\hat{u}_{k\|k-1}\right)$	Rept. (2-19)	$\hat{x}_{k\|k} = \hat{x}_{k\|k-1} + L_{x_k}\left(y_k - C\hat{x}_{k\|k-1}\right)$	(2-41)
$\Sigma_{x_{k\|k}} = \Sigma_{x_{k\|k-1}} - L_{x_k}\left(\Sigma_{x_{k\|k-1}}C^T + \Sigma_{x_k u_{k\|k-1}}D^T\right)^T$	Rept. (2-23)	$\Sigma_{x_{k\|k}} = \Sigma_{x_{k\|k-1}} - L_{x_k}C\Sigma_{x_{k\|k-1}}$	(2-42)
Time update of state:			
$\hat{x}_{k+1\|k} = A\hat{x}_{k\|k} + B\hat{u}_{k\|k}$	Rept. (2-27)		
$\Sigma_{x_{k+1\|k}} = \begin{bmatrix} A & B \end{bmatrix}\begin{bmatrix} \Sigma_{x_{k\|k}} & \Sigma_{x_k u_{k\|k}} \\ \Sigma_{u_k x_{k\|k}} & \Sigma_{u_{k\|k}} \end{bmatrix}\begin{bmatrix} A^T \\ B^T \end{bmatrix} + \Sigma_w$	Rept. (2-28)		
Time update of input:			
$\hat{u}_{k+1\|k} = \hat{u}_{k\|k}$	Rept. (2-29)	$\hat{u}_{k+1\|k} = 0$	Rept. (2-32)
$\Sigma_{u_{k+1\|k}} = \Sigma_{u_{k\|k}} + \Sigma_\xi$	Rept. (2-30)	$\Sigma_{u_{k+1\|k}} = \Sigma_u$	Rept. (2-33)
$\Sigma_{x_{k+1}u_{k+1\|k}} = A\Sigma_{x_k u_{k\|k}} + B\Sigma_{u_{k\|k}}$	Rept. (2-31)	$\Sigma_{x_{k+1}u_{k+1\|k}} = \Sigma^T_{u_{k+1}x_{k+1\|k}} = 0$	Rept. (2-34)
`end`			

Specifically, for input estimation of the FIC estimator, Eq. (2-35), (2-36) and (2-38) are obtained by substituting $\Sigma_{u_{k|k-1}}$ from Eq. (2-33) and $\Sigma_{x_k u_{k|k-1}}$ from Eq. (2-34) into Eq. (2-17), (2-21) and (2-24), respectively; Eq. (2-37) is obtained by substituting $\hat{u}_{k|k-1}$ from Eq. (2-32) into (2-19); and Eq. (2-39) is obtained by substituting $\Sigma_{x_k u_{k|k-1}}$ from Eq. (2-34) to (2-25). For state estimation of the FIC estimator, Eq. (2-40) and (2-42) are obtained by substituting $\Sigma_{x_k u_{k|k-1}}$ from Eq. (2-34) into Eq. (2-20) and (2-23), respectively; and Eq. (2-41) is obtained by substituting $\hat{u}_{k|k-1}$ from Eq. (2-32) into (2-19).

2.1.4 Measurement Update with Large and Infinite Input Covariance

Equation (2-35) may be ill-conditioned when the input covariance Σ_u is much larger than the state estimation covariance and $D\Sigma_u D^T$ does not have full rank. To improve the conditioning of Eq. (2-35), first define a symmetric positive definite matrix as:

$$\Sigma_{\tilde{y}_{k|k-1}} \triangleq C\Sigma_{x_{k|k-1}}C^T + \Sigma_v \tag{2-43}$$

Based on the matrix push through identity in Lemma 2-1, input estimation gain L_{u_k} from Eq. (2-36) can be rewritten as

$$L_{u_k} = \Sigma_u D^T \left(\Sigma_{\tilde{y}_{k|k-1}} + D\Sigma_u D^T\right)^{-1} = \Sigma_u D^T \left(I + \Sigma_{\tilde{y}_{k|k-1}}^{-1} D\Sigma_u D^T\right)^{-1} \Sigma_{\tilde{y}_{k|k-1}}^{-1}$$

$$= \left(\Sigma_u^{-1} + D^T\Sigma_{\tilde{y}_{k|k-1}}^{-1} D\right)^{-1} D^T\Sigma_{\tilde{y}_{k|k-1}}^{-1} \tag{2-44}$$

The corresponding input estimation error covariance in Eq. (2-38) can be rewritten using Eq. (2-2a) in Lemma 2-2 as

$$\Sigma_{u_{k|k}} = \Sigma_u - \Sigma_u D^T \Sigma_{y_{k|k-1}}^{-1} D\Sigma_u = \left(\Sigma_u^{-1} + D^T \Sigma_{\tilde{y}_{k|k-1}}^{-1} D\right)^{-1} \tag{2-45}$$

To improve the ill-conditioning of $\Sigma_{y_{k|k-1}}$ caused by the term $D\Sigma_u D^T$, the matrix inversion $\Sigma_{y_{k|k-1}}^{-1}$ in Eq. (2-40) can be rewritten as

$$\begin{aligned}\Sigma_{y_{k|k-1}}^{-1} &= \left(\Sigma_{\tilde{y}_{k|k-1}} + D\Sigma_u D^T\right)^{-1} \\ &= \Sigma_{\tilde{y}_{k|k-1}}^{-1}\left(I - D\left(\Sigma_u^{-1} + D^T\Sigma_{\tilde{y}_{k|k-1}}^{-1} D\right)^{-1} D^T \Sigma_{\tilde{y}_{k|k-1}}^{-1}\right)\end{aligned} \tag{2-46}$$

Therefore, an equivalent set of equations given by Eq. (2-44) ~ (2-46) can be used to rewrite Eq. (2-36), (2-38) and (2-40) to improve the condition of Eq. (2-35) in the FIC estimator.

Finally, if the unknown input is highly uncertain such that no prior knowledge can be used to estimate u_k, $\Sigma_{u_{k|k-1}} = \Sigma_u$ can be replaced with Σ_∞, which denotes a diagonal matrix with diagonal entries being infinity. When the number of unknown inputs is smaller than the number of measurements, i.e. D has full column rank ($n_u \leq m$ and $\text{rank}(D) = n_u$), $\Sigma_u^{-1} = \Sigma_\infty^{-1} = 0$ in Eq. (2-44) ~ (2-46) can be eliminated, resulting in Eq. (2-47) ~ (2-49) as follows.

$$L_{u_k} = \left(D^T \Sigma_{\tilde{y}_{k|k-1}}^{-1} D\right)^{-1} D^T \Sigma_{\tilde{y}_{k|k-1}}^{-1} = \Sigma_{u_{k|k}} D^T \Sigma_{\tilde{y}_{k|k-1}}^{-1} \tag{2-47}$$

$$\Sigma_{u_{k|k}} = \left(D^T \Sigma_{\tilde{y}_{k|k-1}}^{-1} D\right)^{-1} \tag{2-48}$$

$$\Sigma_{y_{k|k-1}}^{-1} = \Sigma_{\tilde{y}_{k|k-1}}^{-1} \left(I - D\left(D^T \Sigma_{\tilde{y}_{k|k-1}}^{-1} D\right)^{-1} D^T \Sigma_{\tilde{y}_{k|k-1}}^{-1}\right) = \Sigma_{\tilde{y}_{k|k-1}}^{-1} \left(I - D L_{u_k}\right) \tag{2-49}$$

As a result of Eq. (2-49), the state estimation gain in Eq. (2-40) can be rewritten as

$$L_{x_k} = \Sigma_{x_{k|k-1}} C^T \Sigma_{y_{k|k-1}}^{-1} = \Sigma_{x_{k|k-1}} C^T \Sigma_{\tilde{y}_{k|k-1}}^{-1} \left(I - D L_{u_k}\right) \tag{2-50}$$

To summarize, when assuming $\Sigma_u = \Sigma_\infty$ and D has full column rank, Eq. (2-35), (2-36), (2-38) and (2-40) for the finite input covariance (FIC) estimator in Table 2-1 can be replaced by Eq. (2-43), (2-47), (2-48) and (2-50). Time update of the state is the same as Eq. (2-27) and (2-28). The time update of input remains the same as in Eq. (2-32) and (2-33) for the FIC estimator.

Theorem 2-1 When the input covariance Σ_u of the FIC estimator approaches infinity (Σ_∞) and the feedthrough matrix D has full column rank, the FIC estimator with L_{u_k}, $\Sigma_{u_{k|k}}$ and L_{x_k} given by Eq. (2-47), (2-48) and (2-50) is equivalent to the WLS estimator proposed by Gillijns and De Moor in [13].

Proof. In comparison to the notations in [13], the symmetric positive definite matrix $\Sigma_{\tilde{y}_{k|k-1}}$ defined here is denoted as $\tilde{R}_k$ in [13]; the input estimation gain L_{u_k} is denoted as M_k; the state estimation gain L_{x_k} is denoted as L_k; and $\Sigma_{x_{k|k-1}} C^T \Sigma_{\tilde{y}_{k|k-1}}^{-1}$ is denoted as K_k.

Therefore, Eq. (2-43), (2-47), (2-37) and (2-48) here are equivalent to the unknown input estimation step in [13]. Substituting L_{x_k} from Eq. (2-50) into Eq. (2-41) and (2-42), the state measurement update step in [13] can be obtained. Finally, Eq. (2-27) and (2-28) are equivalent to the time update step in [13]. ■

Hereinafter, the FIC estimator with $\Sigma_u = \Sigma_\infty$ is referred to as the weighted-least-squares (WLS) estimator. Thus far, the relationship among all three estimators, i.e. AKF, FIC and WLS, has been demonstrated based on the unifying MMSE framework. In theory, neither the FIC nor the AKF estimator assumes the feedthrough matrix D has full column rank. However, to estimate the unknown inputs accurately, in practice full-column rank of D is needed and the magnitude of Du_k should be relatively large compared to the measurement noise v_k.

2.1.5 Numerical Study: Collocated Input and Measurements

A four-story lumped-mass shear structure, i.e. with four degrees-of-freedom (DOFs), is used to validate the proposed FIC estimator for systems with direct feedthrough of the input. The mass and stiffness values are provided in Figure 2-1 and the resonance frequencies of the structure are 0.92 Hz, 2.48 Hz, 3.84 Hz and 4.94 Hz. A 2% modal damping ratio is assumed for the first two modes based on a Rayleigh damping model. Acceleration responses of the structure under different types of excitations are used to simultaneously estimate the unknown input and system states.

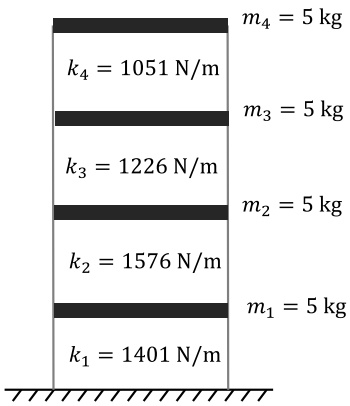

Figure 2-1 Four-story structural example

A state space dynamical model is formulated based on the following equations of motion of a multiple-DOF structure. The number of DOFs is denoted as n_{DOF}:

$$M\ddot{q}(t) + C_{\mathrm{damp}}\dot{q}(t) + Kq(t) = \Gamma_u u(t) \tag{2-51}$$

where M, K, $C_{\mathrm{damp}} \in \mathbb{R}^{n_{\mathrm{DOF}} \times n_{\mathrm{DOF}}}$ are the mass, stiffness and damping matrices; $q(t)$, $\dot{q}(t)$ and $\ddot{q}(t) \in \mathbb{R}^{n_{\mathrm{DOF}}}$ are displacement, velocity and acceleration vectors at time *t*; $\Gamma_u \in \mathbb{R}^{n_{\mathrm{DOF}} \times n_u}$ is the input location matrix, with ones at the input DOFs and zeros elsewhere; and $u(t) \in \mathbb{R}^{n_u}$ is the force input. To reformulate Eq. (2-51) in state space, define the state vector as $x \triangleq \begin{Bmatrix} q \\ \dot{q} \end{Bmatrix}$ with a length of $n = 2n_{\mathrm{DOF}}$. As a result, the equations of motion can be reformulated in state space as follows, together with corresponding measurement equation for m number of acceleration measurements.

$$\dot{x} = \begin{bmatrix} 0 & I \\ -M^{-1}K & -M^{-1}C_{\mathrm{damp}} \end{bmatrix} x + \begin{bmatrix} 0 \\ M^{-1}\Gamma_u \end{bmatrix} u \triangleq A_c x + B_c u \tag{2-52}$$

$$y = \Gamma_y\begin{bmatrix} -M^{-1}K & -M^{-1}C_{\text{damp}} \end{bmatrix}x + \Gamma_y M^{-1}\Gamma_u u + v \triangleq C_c x + D_c u + v \tag{2-53}$$

Here $y \in \mathbb{R}^m$ represents the acceleration measurement; $\Gamma_y \in \mathbb{R}^{m \times n_{\text{DOF}}}$ is the output location matrix; $v \in \mathbb{R}^m$ is the measurement noise; A_c, B_c, C_c and D_c represent the continuous-time system matrix, input matrix, output matrix and feedthrough matrix in state space. Because the estimators are implemented in discrete time, the continuous-time system given by Eq. (2-52) and (2-53) is discretized using zero-order-hold with a time step of 0.005s in this study.

In the scenario of systems with direct feedthrough, all the excitation inputs u and the acceleration measurements are collocated. Specifically, the input is fed directly to the measurements and the feedthrough matrix D is non-zero and has full column rank. In this example, a force excitation $u(t)$ is applied at the 4th DOF of the structure, i.e. at mass m_4, and measurement y contains simulated acceleration response of all four DOFs. Therefore, the input location matrix is $\Gamma_u = [0 \quad 0 \quad 0 \quad 1]^T$ and the output location matrix is an identity matrix $\Gamma_y = I$. As a result, the continuous-time feedthrough matrix $D_c = \Gamma_y M^{-1}\Gamma_u$ has full column rank, i.e. $D_c = [0 \quad 0 \quad 0 \quad 0.2]^T$, because the measured DOFs contain the input DOF.

Two types of input excitations are used here to compare the performance of the FIC estimator with the AKF and WLS estimator for systems with direct feedthrough. The first type is a white Gaussian input excitation with a standard deviation of 10 N, i.e. $u_k \sim \mathcal{N}(0, 10^2)$. The second type is a 3 Hz periodic sinusoidal input with a magnitude of

10 N (the sinusoidal input is chosen on purpose such that the white Gaussian noise assumption of the unknown input is violated). The simulated measurements are contaminated by measurement noise with a standard deviation of $\sigma_v = 10^{-3}\ \mathrm{m/s^2}$ and sampled at 200 Hz. For easier comparison of the input estimators, σ_v values available to the estimators are assumed to be the same as the one used in simulation. The initial state μ_{x_0} and the diagonal entries of state covariance Σ_{x_0} are set as zero for all estimators, assuming the initial condition of the structure is static. Moreover, for the AKF, $\hat{u}_0$, Σ_{u_0} and $\Sigma_{x_0 u_0}$ are set as zero (see Table 2-1 for the initialization requirements).

2.1.5.1 Effect of covariance knowledge on input estimation

In practice, the actual input covariance Σ_u and process noise covariance Σ_w are often unknown, while the measurement noise covariance Σ_v can be approximated based on sensor noise level. Knowledge of the covariances Σ_u and Σ_w by an estimator can have significant effect on the estimation performance. To study such effects, numerical simulations are performed first, where the actual/true values of these covariances are known. When generating time history data, the true input covariance and process noise covariance used in the dynamics simulation are denoted $\Sigma_{u,sim}$ and $\Sigma_{w,sim}$, respectively. These true values are intentionally kept blind to the estimators. On the other hand, for input estimation, all three estimators (FIC, AKF and WLS) require a value of process noise covariance Σ_w; the value available to the estimator is accordingly denoted as $\Sigma_{w,est}$. In addition, the FIC estimator requires a value of the input covariance (see Table 2-1), which is denoted as $\Sigma_{u,est}$. Similarly, operation of the AKF estimator requires the Gaussian

random walk covariance Σ_{ξ} (also see Table 2-1), which is denoted as $\Sigma_{\xi,est}$. Finally, operation of the WLS estimation does not require any input covariance Σ_u, as shown in Eq. (2-47) ~ (2-49). In summary, the covariances for the estimator operation includes $\Sigma_{u,est}$ of the FIC estimator, $\Sigma_{\xi,est}$ of the AKF and $\Sigma_{w,est}$ for all three estimators. Table 2-2 summarizes the data generation process and the estimator covariances during each trial run.

Table 2-2 Summary of data generation and estimator covariances

Covariances	Time history generation	Estimation		
		FIC	AKF	WLS
Input types	(1) White noise $\Sigma_{u,\,sim} = 100\ \mathrm{N}^2$ (2) Sinusoidal input	$\Sigma_{u,\,est}$ (1 to $10^7\ \mathrm{N}^2$)	$\Sigma_{\xi,est}$ (1 to $10^7\ \mathrm{N}^2$)	-
Initial state	Static	$\mu_{x_0} = 0,\ \Sigma_{x_0} = 0$		
Process noise	$\Sigma_{w,\,sim} = 0$ or $10^{-10}I$	$\Sigma_{w,\,est} = 0$		
Measurement noise	$\Sigma_{v,\,sim} = 10^{-6}\ (\mathrm{m/s^2})^2$	$\Sigma_{v,\,est} = 10^{-6}\ (\mathrm{m/s^2})^2$		

To study estimator covariance effects under white Gaussian excitation, 50 independent runs of dynamic simulation are performed, and each trial run is conducted using randomly generated 30 seconds of input u_k (with $\Sigma_{u,sim} = 100\mathrm{N}^2$ as shown in Table 2-2) and measurement noise v_k. Using data from each trial run, the root mean square (RMS) error e_u can be calculated based on the estimated input $\hat{u}_k$ and the actual input u_k, defined as $e_u \triangleq \sqrt{\frac{1}{\mathbb{K}}\sum_{k=1}^{\mathbb{K}}|u_k - \hat{u}_k|^2}$, where $\mathbb{K}$ is the total number of time steps. Because all three estimators require process noise covariance $\Sigma_{w,est}$, the same value is used when

performing estimation by all estimators and for 50 trials. When performing estimation for each trial run, the WLS estimator is operated only once, because the estimator does not require knowledge of input covariance $\Sigma_{u,est}$ or $\Sigma_{\xi,est}$; the averaged RMS error among 50 trials is then obtained as $\bar{e}_u = \frac{1}{n_{trial}} \sum_{i=1}^{n_{trial}} e_u^{(i)}$. On the other hand, the FIC estimator is performed for different values of $\Sigma_{u,est}$ ranging from 1 to 10^7 N^2 (see Table 2-2). At each value of $\Sigma_{u,est}$, one estimation time history $\hat{u}_k$ is generated and e_u is calculated accordingly for one trial; among 50 trials the averaged RMS $\bar{e}_u$ is obtained. Thus, the results provide the relationship between $\bar{e}_u$ and $\Sigma_{u,est}$. Likewise, the AKF estimator is performed for different values of $\Sigma_{\xi,est}$ in the same range of 1 to 10^7 N^2. After averaging among 50 trials, the relationship between $\bar{e}_u$ and $\Sigma_{\xi,est}$ can be obtained.

When no process noise is added to the system in all 50 trials, i.e. $\Sigma_{w,sim} = 0$, Figure 2-2(a) shows the change in $\bar{e}_u$ as $\Sigma_{u,est}$ of FIC and $\Sigma_{\xi,est}$ of AKF vary with $\Sigma_{w,est} = 0$. The smallest RMS error is achieved by the FIC estimator when $\Sigma_{u,est}$ is very close to the actual input covariance $\Sigma_{u,sim} = 100\ \mathrm{N}^2$. It is also observed that AKF is not sensitive to the change of $\Sigma_{\xi,est}$ and has a similar averaged RMS error as the WLS estimator, resulting in the coinciding curves in Figure 2-2(a). Specifically, the averaged RMS from both AKF and WLS estimator is around 0.35 N, and the smallest averaged RMS achieved by FIC is around 0.20 N. In addition, the RMS error of the FIC estimator is smaller than both the AKF and WLS when $\Sigma_{u,est}$ is in the range from 2.5 to 10^5 N^2. As $\Sigma_{u,est}$ becomes larger than 10^5 N^2, the FIC estimator converges to the WLS estimator, which is consistent with Theorem 2-1. To investigate the situation when process noise covariance is not exactly

known, a small amount of process noise is randomly generated in each of the 50 trial runs, while the estimators assume no process noise is present and the system model is accurate. Figure 2-2(b) illustrates the averaged RMS errors of estimated input given each $\Sigma_{u,est}$ and $\Sigma_{\xi,est}$ when $\Sigma_{w,sim} = 10^{-10}I$ and $\Sigma_{w,est} = 0$.

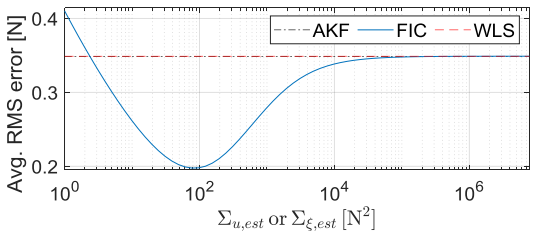

(a) $\Sigma_{w,sim} = \Sigma_{w,est} = 0$
(AKF and WLS coincide)

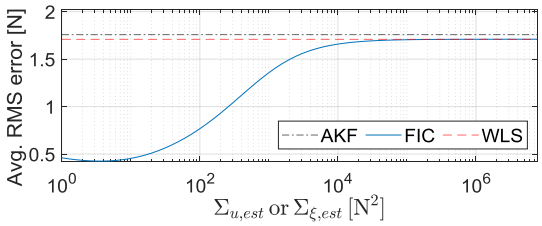

(b) $\Sigma_{w,sim} = 10^{-10}I, \Sigma_{w,est} = 0$

Figure 2-2 Averaged RMS error $\bar{e}_u$ of white input estimation ($\Sigma_{u,sim} = 100\text{N}^2$)

For the AKF and WLS estimator, the averaged input RMS error increase significantly to around 1.70 N, while the FIC estimator is able to achieve a much smaller RMS error of 0.43 N when $\Sigma_{u,est}$ is chosen around 4 N^2. The best choice of $\Sigma_{u,est}$ here is smaller than $\Sigma_{u,sim} = 100\ \text{N}^2$, when the $\Sigma_{w,est}$ used by the FIC estimator is smaller than the actual $\Sigma_{w,sim}$ used for simulation. In addition, the RMS error from FIC estimator is always smaller than AKF and WLS estimator when $\Sigma_{u,est}$ ranges from 1 to 10^5 N^2.

Next, a sinusoidal input excitation is adopted here on purpose to violate the white Gaussian assumption of the unknown input. Using the 3 Hz periodic sinusoidal input excitation with a magnitude of 10 N, 50 independent runs of 15 seconds dynamics simulation with randomly generated white Gaussian process noise and measurement noise are performed. The time history generation process and estimator covariances are set the

same as summarized in Table 2-2, except the input in time history generation is changed to sinusoidal excitation. Same as in the white Gaussian input simulation, the input RMS error e_u is calculated in each trial run for different values of $\Sigma_{u,est}$ and $\Sigma_{\xi,est}$ ranging from 1 to 10^7 N^2. After averaging among 50 trials, the relationship between $\bar{e}_u$ and $\Sigma_{u,est}$ of the FIC estimator can be obtained. Likewise, the relationship between $\bar{e}_u$ and $\Sigma_{\xi,est}$ of the AKF is obtained in the same manner.

Figure 2-3(a) shows the change in $\bar{e}_u$ as $\Sigma_{u,est}$ and $\Sigma_{\xi,est}$ vary, when there is no process noise added to the system in all 50 trials, i.e. $\Sigma_{w,sim} = 0$. Accordingly, all estimators use $\Sigma_{w,est} = 0$. The smallest RMS error $\bar{e}_u$ is 0.10 N, achieved by the FIC estimator when $\Sigma_{u,est}$ is around 20 N^2, when the actual input covariance $\Sigma_{u,sim}$ of the sinusoidal signal is 50 N^2. The best $\Sigma_{u,est}$ of FIC does not equal to the actual $\Sigma_{u,sim}$, which is as expected because the input signal is not white noise as assumed. However, compared to the AKF and WLS estimator, smaller RMS error can still be achieved by the FIC estimator when $\Sigma_{u,est}$ is within a large range around the actual $\Sigma_{u,sim}$. In addition, AKF is not sensitive to the changes of $\Sigma_{\xi,est}$ and has an averaged RMS error around 0.17 N, leading to the results coinciding with the WLS estimator in Figure 2-3(a). To investigate the situation when process noise covariance is not exactly known under sinusoidal excitation, a small amount of process noise with covariance $\Sigma_{w,sim} = 10^{-10}I$ is added to the system while the estimators assume $\Sigma_{w,est} = 0$. Figure 2-3(b) shows the change in $\bar{e}_u$ as $\Sigma_{u,est}$ and $\Sigma_{\xi,est}$ vary. For the AKF and WLS estimator, $\bar{e}_u$ increases significantly to 1.31 N, while the FIC estimator is again able to achieve a much smaller error of 0.32 N

when $\Sigma_{u,est}$ is 1 N^2 for the range given. In addition, the error $\bar{e}_u$ from the FIC estimator is always smaller than the AKF and WLS estimator when $\Sigma_{u,est}$ ranges from 1 to 10^5 N^2.

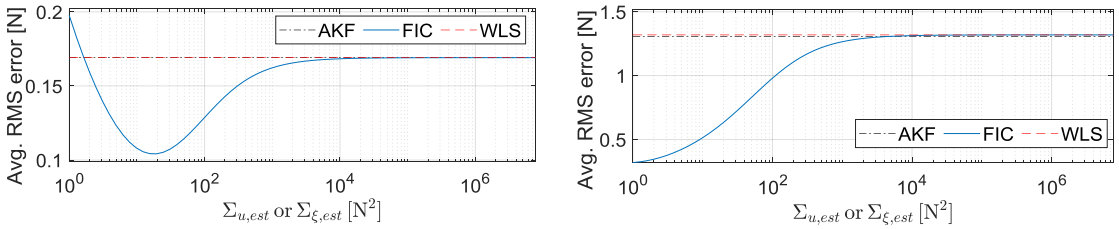

(a) $\Sigma_{w,sim} = \Sigma_{w,est} = 0$
(AKF and WLS coincide)

(b) $\Sigma_{w,sim} = 10^{-10}I, \Sigma_{w,est} = 0$
(AKF and WLS coincide)

Figure 2-3 Averaged input RMS error $\bar{e}_u$ of sinusoidal input estimation ($\Sigma_{u,sim} = 50N^2$)

It is also worth noting that for all cases presented thus far, the FIC estimator converges to the WLS estimator when $\Sigma_{u,est}$ is large, regardless of input types or covariances available to the estimator. In addition, if $\Sigma_{w,est}$ is smaller than the actual $\Sigma_{w,sim}$, the best choice of $\Sigma_{u,est}$ of the FIC estimator will be slightly smaller than $\Sigma_{u,sim}$, and vice versa. The difference in RMS error between AKF and WLS is relatively small compared to FIC estimation. This is partially due to the drift error when only acceleration measurements are available, which will be shown in the following subsection. Furthermore, by varying $\Sigma_{\xi,est}$ of the AKF, the performance could not be improved as much as the FIC estimator.

2.1.5.2 Simultaneous input-state estimation

This subsection first compares the time history of the estimated inputs for a single run of white Gaussian excitation for 60 seconds. Recall that the input has a standard deviation of 10 N, i.e. the input covariance $\Sigma_{u,sim} = 100$ N^2. The simulated process noise

is set as 0, i.e. $\Sigma_{w,sim} = 0$. Based on the discussion on white noise excitation, $\Sigma_{\xi,est}$ of AKF and $\Sigma_{u,est}$ of FIC are set as 100 N^2. The process noise covariance $\Sigma_{w,est}$ for all estimators is set as 0, the same as $\Sigma_{w,sim}$. Measurement noise covariance is kept the same as before, i.e. $\Sigma_{v,est} = \Sigma_{v,sim} = 10^{-6} I\ (m/s^2)^2$. The same initialization of state and the corresponding state estimation covariance is used, which assumes the initial condition of the structure is static and known.

Figure 2-4(a) shows the comparison of estimator performance when estimating the white Gaussian input during the first 1s. It is observed that all estimators perform almost equally well during the initial time period. However, the AKF and WLS estimator start to drift slightly over time. Because AKF and WLS have almost the same performance, close-up plot of only the WLS estimator is provided in comparison to the FIC estimator results. Figure 2-4(b) shows the close-up plot of FIC estimation results during the final 0.5s and Figure 2-4(c) shows the final 0.5s of the WLS estimation results. The confidence interval of three times square root of input estimation error covariance, $\pm 3\sigma_{u_{k|k}}$, is included in the close-up plots for the estimated input $\hat{u}_{k|k}$ obtained from each estimator. It can be seen that the FIC estimator performs consistently well over time with a tight confidence interval (Figure 2-4(b)), while the WLS estimator cannot provide a good estimate of the input as time increases (Figure 2-4(c)). In addition, Figure 2-4(d) shows the time history of input estimation error covariance $\Sigma_{u_{k|k}}$ of FIC and WLS estimation in logarithmic scale. Again, AKF has almost identical result as the WLS estimator and thus is not included in the plots. The input estimation error covariance of the WLS estimator is not able to converge to

steady state, while the error covariance of the FIC estimator converges to steady state after 10s. Similar phenomenon can be observed in state estimation that not all of the state estimates from the WLS estimator are able to converge, while all state estimates from the FIC estimator converge to steady state.

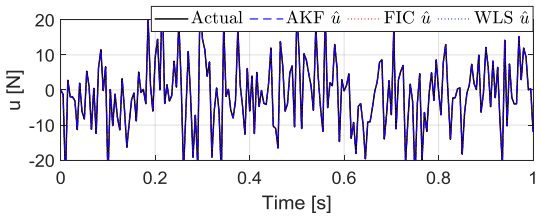

(a) 0~1s of AKF, FIC and WLS estimation

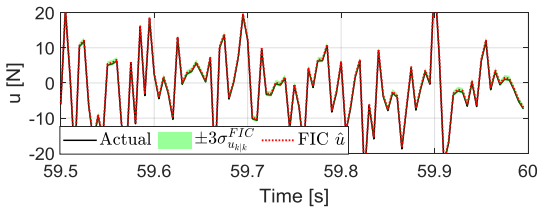

(b) 59.5~60s of FIC estimation

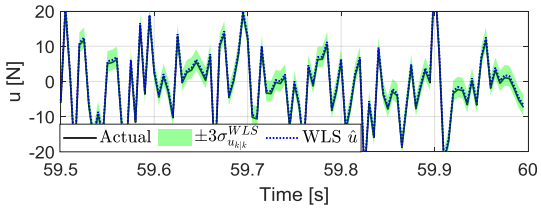

(c) 59.5~60s of WLS estimation

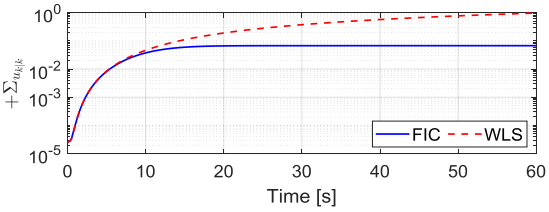

(d) input estimation error covariance $\Sigma_{u_{k|k}}$

Figure 2-4 Estimation of white Gaussian input: collocated input and measurements

Next for a single run of sinusoidal excitation, the same 3 Hz sinusoidal input with an amplitude of 10 N is again applied for 15 seconds. Because the dynamical state space system is accurate and no modeling error is assumed in this example, process noise covariance $\Sigma_{w,est}$ is set as 0. From the discussion on sinusoidal excitation, when no process is applied to the system, $\Sigma_{\xi,est}$ of AKF and $\Sigma_{u,est}$ of FIC are set as 25 N^2.

Figure 2-5(a) shows the comparison of estimated sinusoidal input from 0s to 15s. All estimators perform almost equally well during the initial time period. However, compared to the white input, the drift phenomenon of the AKF and WLS estimator

becomes more obvious under sinusoidal excitation. Because the AKF and WLS estimator have similar performance due to the drift error, close-up plots of only the WLS estimator are provided to compare with the FIC estimator. Figure 2-5(b) shows the close-up plot of the FIC estimator during the final 0.5s and Figure 2-5(c) shows the corresponding close-up plot of the WLS estimator. The confidence interval of three times square root of input estimation error covariance, $\pm 3\sigma_{u_{k|k}}$, is included in the close-up plots for the estimated input $\hat{u}_{k|k}$. Figure 2-5(b) shows that even though the white Gaussian assumption is violated because of the sinusoidal input, the FIC estimator can still estimate the input consistently well over time. Meanwhile, Figure 2-5(c) shows that drift error occurs in WLS estimation. Figure 2-5(d) plots the input estimation error covariance $\Sigma_{u_{k|k}}$ of the FIC and WLS estimator in logarithmic scale (again, AKF has almost the same result as WLS and thus is not included here).

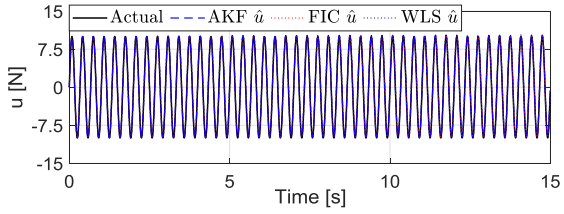

(a) 0~15s of FIC, AKF and WLS estimation

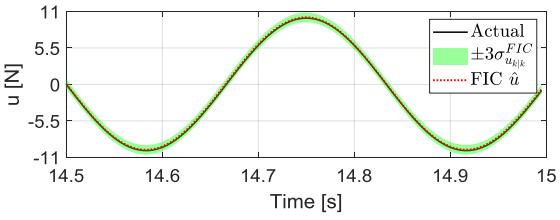

(b) 14.5~15s of FIC estimation

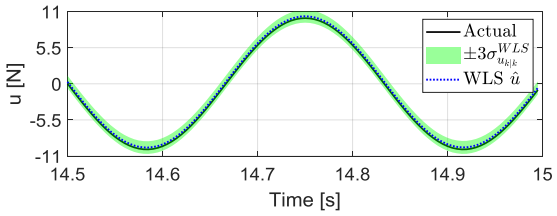

(c) 14.5~15s of WLS estimation

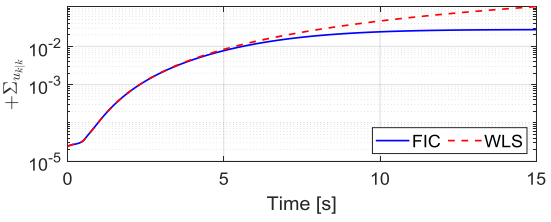

(d) input estimation error covariance $\Sigma_{u_{k|k}}$

Figure 2-5 Estimation of sinusoidal input: collocated input and measurements

The input estimation error covariance $\Sigma_{u_{k|k}}$ of the WLS estimator cannot converge to steady state, while $\Sigma_{u_{k|k}}$ of the FIC estimator converges after 9s. Indeed, not only the input error covariance $\Sigma_{u_{k|k}}$ but also part of the state estimation error covariance $\Sigma_{x_{k|k}}$ from the WLS estimator cannot converge to steady state. In contrast, the state estimation error covariances of all states from the FIC estimator converge to steady state.

In all cases presented so far, the FIC estimator achieves smallest RMS error (with a small estimation error covariance $\Sigma_{u_{k|k}}$) not only in input estimation but also in displacement and velocity estimation and eliminates the drift error. In addition, the AKF and WLS estimator perform similarly for both inputs because of the drift error present in the input-state estimation.

2.2 Estimation for Systems without Direct Feedthrough

This section introduces the problem of simultaneous input-state estimation for systems without direct feedthrough of the unknown input, i.e. systems with the input-to-output feedthrough matrix $D = 0$. A parallel version of the FIC estimator in Section 2.1 is derived for systems without feedthrough, based on the same MMSE framework. Proof is again provided to show that when Σ_u of the FIC estimator approaches infinity and matrix CB has full-column rank, a WLS estimator can be obtained.

2.2.1 Problem Formulation

Consider the following discrete-time stochastic linear system without direct feedthrough of input:

$$x_{k+1} = Ax_k + Bu_k + w_k \tag{2-54}$$

$$y_k = Cx_k + v_k \tag{2-55}$$

Here $x_k \in \mathbb{R}^n$ is the state at time step k, $u_k \in \mathbb{R}^{n_u}$ is the unknown input, $w_k \in \mathbb{R}^n$ is the process noise or disturbance, $y_k \in \mathbb{R}^m$ is the measurement output, and $v_k \in \mathbb{R}^m$ is the measurement noise. The unknown input u_k is assumed to be a random vector at each time step with unknown dynamics. To account for the unknown input dynamics, the input is first assumed to have white Gaussian distribution with a predefined finite input covariance Σ_u to utilize any prior knowledge related to the input. Next, for highly uncertain input, the input covariance is further assumed to be infinite, i.e. $\Sigma_u = \Sigma_\infty$. Similar to the previous Section 2.1.4, $\Sigma_u = \Sigma_\infty$ was found to be removable from the estimator.

The assumptions and notations used here are the same as in Section 2.1.1, except for assumption (5). Besides assuming the unknown input $u_{0:k}$ is Gaussian and independent from x_0, v_l and w_l for all k and l, the input is also to be white Gaussian with covariance Σ_u, i.e. $u_k \sim \mathcal{N}(0, \Sigma_u)$, which is the same as the assumption of the FIC estimation presented in Section 2.1.3. The following lemma is provided to help derive the simultaneous input-state estimator for systems without direct feedthrough.

Lemma 2-5 For the system given by Eq. (2-54) and (2-55) with the assumptions made in this section, x_{k-1}, u_{k-1}, w_{k-1} and $y_{0:k}$ are jointly Gaussian. In addition, the three

conditional random vectors, $x_{k-1}|y_{0:k-1}$, $u_{k-1}|y_{0:k-1}$, $w_{k-1}|y_{0:k-1}$ and $y_k|y_{0:k-1}$, are jointly (and individually) Gaussian.

Proof. Based on Eq. (2-54) and (2-55), we can derive that

$$x_{k-1} = A^{k-1}x_0 + H_{u_{k-1}}u_{0:k-1} + H_{w_{k-1}}w_{0:k-1} \tag{2-56}$$

$$y_{0:k} = \mathcal{O}_k x_0 + \check{P}_{u_{k-1}}u_{0:k-1} + P_{w_k}w_{0:k-1} + v_{0:k} \tag{2-57}$$

where $H_{u_{k-1}} \triangleq \begin{bmatrix} A^{k-2}B & \cdots & AB & B & 0_{n\times n_u} \end{bmatrix} \in \mathbb{R}^{n\times n_u k}$,

$H_{w_{k-1}} \triangleq [A^{k-2} \quad \cdots \quad A \quad I_n \quad 0_{n\times n}] \in \mathbb{R}^{n\times nk}$,

$\mathcal{O}_k \triangleq \begin{bmatrix} C \\ CA \\ \vdots \\ CA^k \end{bmatrix} \in \mathbb{R}^{m(k+1)\times n}$, $\check{P}_{u_{k-1}} \triangleq \begin{bmatrix} 0 & 0 & \cdots \\ CB & \ddots & \cdots \\ \vdots & \ddots & 0 \\ CA^{k-1}B & \cdots & CB \end{bmatrix} \in \mathbb{R}^{m(k+1)\times n_u k}$ and

$P_{w_k} \triangleq \begin{bmatrix} 0 & 0 & 0 \\ C & \ddots & \vdots \\ \vdots & \ddots & 0 \\ CA^{k-1} & \cdots & C \end{bmatrix} \in \mathbb{R}^{m(k+1)\times nk}$.

Because x_0, $u_{0:k-1}$, $w_{0:k-1}$ and $v_{0:k}$ are Gaussian and independent from each other, they are jointly Gaussian. Define notations $\check{I}_{n_u} \triangleq [0 \quad I_{n_u}]$ and $\check{I}_n \triangleq [0 \quad I_n]$. Vectors x_{k-1}, u_{k-1}, and $y_{0:k}$ can be expressed as a full row-rank linear transformation of x_0, $u_{0:k-1}$, $w_{0:k-1}$ and $v_{0:k}$:

$$\begin{Bmatrix} x_{k-1} \\ u_{k-1} \\ w_{k-1} \\ y_{0:k} \end{Bmatrix} = \begin{bmatrix} A^{k-1} & H_{u_{k-1}} & H_{w_{k-1}} & 0 \\ 0 & \check{I}_{n_u} & 0 & 0 \\ 0 & 0 & \check{I}_n & 0 \\ \mathcal{O}_k & \check{P}_{u_{k-1}} & P_{w_k} & I_{m(k+1)} \end{bmatrix} \begin{Bmatrix} x_0 \\ u_{0:k-1} \\ w_{0:k-1} \\ v_{0:k} \end{Bmatrix} \tag{2-58}$$

As a result, x_{k-1}, u_{k-1}, w_{k-1} and $y_{0:k}$ are also jointly Gaussian. In addition, because conditional distributions of jointly Gaussian random vectors are Gaussian, each vector among $x_{k-1}|y_{0:k-1}$, $u_{k-1}|y_{0:k-1}$, $w_{k-1}|y_{0:k-1}$ and $y_k|y_{0:k-1}$ is Gaussian. ■

With prior estimates and error covariance of input and state at time step k (i.e. $\hat{x}_{k-1|k-1}$, $\Sigma_{x_{k-1|k-1}}$, $\hat{u}_{k-1|k-1}$, $\Sigma_{u_{k-1|k-1}}$ and $\Sigma_{x_{k-1}u_{k-1|k-1}}$), the state x_{k-1} and input u_{k-1} at time step $k-1$ given measurements $y_{0:k}$ can be simultaneously estimated based on a unifying MMSE framework. The details are developed in the following subsections.

2.2.2 Measurement Update of Input and State

In order to include the unknown input in measurement equation, Eq. (2-55) is first propagated back one time step and rewritten as follows

$$y_k = \begin{bmatrix} CA & CB & C \end{bmatrix} \begin{Bmatrix} x_{k-1} \\ u_{k-1} \\ w_{k-1} \end{Bmatrix} + v_k \tag{2-59}$$

Compared to Eq. (2-10) for systems with direct feedthrough in Section 2.1.2, the back propagated measurement equation (2-59) here includes process noise w_{k-1}. Consequently,

$\mathbb{E}(w_{k-1}|y_{0:k})$ is not a zero vector and an estimate of w_{k-1} given $y_{0:k}$ with corresponding error covariances are needed by $\hat{x}_{k|k}$ and $\Sigma_{x_{k|k}}$ during time update step in Section 2.2.3.

Considering the independence of measurement noise v_k from past measurement sequence $y_{0:k-1}$, Eq. (2-59) is conditioned on $y_{0:k-1}$ as

$$y_k|y_{0:k-1} = [CA \quad CB \quad C]\begin{Bmatrix} x_{k-1} \\ u_{k-1} \\ w_{k-1} \end{Bmatrix}\Bigg| y_{0:k-1} + v_k \tag{2-60}$$

The corresponding conditional expectation can be found as

$$\mathbb{E}(y_k|y_{0:k-1}) = [CA \quad CB \quad C]\mathbb{E}\left(\begin{Bmatrix} x_{k-1} \\ u_{k-1} \\ w_{k-1} \end{Bmatrix}\Bigg| y_{0:k-1}\right) + \mathbb{E}(v_k)$$

$$= CA\hat{x}_{k-1|k-1} + CB\hat{u}_{k-1|k-1} \tag{2-61}$$

where $\hat{x}_{k-1|k-1}$ and $\hat{u}_{k-1|k-1}$ are the prior time-updated estimates from last time step. As a result of Eq. (2-61), define the measurement residual (innovation) as

$$r_k \triangleq y_k - \mathbb{E}(y_k|y_{0:k-1}) = y_k - CA\hat{x}_{k-1|k-1} - CB\hat{u}_{k-1|k-1} \tag{2-62}$$

Note that process noise $w_{k-1}\sim\mathcal{N}(0,\Sigma_w)$ is independent of $y_{0:k-1}$ based on Eq. (2-57). Therefore, $\mathbb{E}(w_{k-1}|y_{0:k-1}) = \mathbb{E}(w_{k-1}) = 0$ and $\Sigma_{w_{k-1|k-1}} = \mathrm{cov}(w_{k-1}|y_{0:k-1}) = \Sigma_w$.

Based on the affine transformation of Eq. (2-60), the conditional cross-covariance between $\begin{Bmatrix} x_{k-1} \\ u_{k-1} \\ w_{k-1} \end{Bmatrix} \Big| y_{0:k-1}$ and $y_k|y_{0:k-1}$ is found as

$$\begin{aligned} \Sigma_{\begin{Bmatrix} x_{k-1} \\ u_{k-1} \\ w_{k-1} \end{Bmatrix} y_{k|k-1}} &\triangleq \operatorname{cov}\left(\begin{Bmatrix} x_{k-1} \\ u_{k-1} \\ w_{k-1} \end{Bmatrix}, y_k \middle| y_{0:k-1} \right) \\ &= \begin{bmatrix} \Sigma_{x_{k-1|k-1}} & \Sigma_{x_{k-1}u_{k-1|k-1}} & 0 \\ \Sigma_{u_{k-1}x_{k-1|k-1}} & \Sigma_{u_{k-1|k-1}} & 0 \\ 0 & 0 & \Sigma_w \end{bmatrix} \begin{bmatrix} (CA)^T \\ (CB)^T \\ C^T \end{bmatrix} \end{aligned} \tag{2-63}$$

The covariance of $y_k|y_{0:k-1}$ is found as

$$\Sigma_{y_{k|k-1}} = \begin{bmatrix} CA & CB & C \end{bmatrix} \begin{bmatrix} \Sigma_{x_{k-1|k-1}} & \Sigma_{x_{k-1}u_{k-1|k-1}} & 0 \\ \Sigma_{u_{k-1}x_{k-1|k-1}} & \Sigma_{u_{k-1|k-1}} & 0 \\ 0 & 0 & \Sigma_w \end{bmatrix} \begin{bmatrix} (CA)^T \\ (CB)^T \\ C^T \end{bmatrix} + \Sigma_v \tag{2-64}$$

Equations (2-63) and (2-64) hold because process noise w_{k-1} and measurement noise v_k are independent of x_{k-1} and u_{k-1} given $y_{0:k-1}$. Thus, $\Sigma_{x_{k-1}w_{k-1|k-1}}$, $\Sigma_{u_{k-1}w_{k-1|k-1}}$, $\Sigma_{x_{k-1}v_{k|k-1}}$ and $\Sigma_{u_{k-1}v_{k|k-1}}$ are all zero matrices. Expanding Eq. (2-63) gives the following expressions

$$\Sigma_{x_{k-1}y_{k|k-1}} = \Sigma_{x_{k-1|k-1}}(CA)^T + \Sigma_{x_{k-1}u_{k-1|k-1}}(CB)^T \tag{2-65}$$

$$\Sigma_{u_{k-1}y_{k|k-1}} = \Sigma_{u_{k-1|k-1}}(CB)^T + \Sigma_{u_{k-1}x_{k-1|k-1}}(CA)^T \tag{2-66}$$

$$\Sigma_{w_{k-1}y_{k|k-1}} = \Sigma_w C^T \tag{2-67}$$

Expanding Eq. (2-64) gives

$$\Sigma_{y_{k|k-1}} = CA\Sigma_{x_{k-1|k-1}}(CA)^T + CB\Sigma_{u_{k-1|k-1}}(CB)^T$$
$$+CA\Sigma_{x_{k-1}u_{k-1|k-1}}(CB)^T + CB\Sigma_{u_{k-1}x_{k-1|k-1}}(CA)^T + C\Sigma_w C^T + \Sigma_v \quad (2\text{-}68)$$

Recall that $x_{k-1}|y_{0:k-1}$, $u_{k-1}|y_{0:k-1}$, $w_{k-1}|y_{0:k-1}$ and $y_k|y_{0:k-1}$ are jointly Gaussian from Lemma 2-5, and Eq. (2-60) is an affine transformation of the Gaussian random vector $\begin{Bmatrix} x_{k-1} \\ u_{k-1} \\ w_{k-1} \end{Bmatrix} \Big| y_{0:k-1}$. Applying Eq. (2-3) in Lemma 2-3 to Eq. (2-60), the MMSE estimate of $x_{k-1}, u_{k-1}, w_{k-1}$ given $y_{0:k}$ is found as

$$\begin{Bmatrix} \hat{x}_{k-1|k} \\ \hat{u}_{k-1|k} \\ \hat{w}_{k-1|k} \end{Bmatrix} \triangleq \mathbb{E}\left(\begin{Bmatrix} x_{k-1} \\ u_{k-1} \\ w_{k-1} \end{Bmatrix} \Big| y_{0:k} \right)$$
$$= \begin{Bmatrix} \hat{x}_{k-1|k-1} \\ \hat{u}_{k-1|k-1} \\ \hat{w}_{k-1|k-1} \end{Bmatrix} + \Sigma_{\begin{Bmatrix} x_{k-1} \\ u_{k-1} \\ w_{k-1} \end{Bmatrix} y_{k|k-1}} \Sigma_{y_{k|k-1}}^{-1} \left(y_k - \mathbb{E}(y_k|y_{0:k-1}) \right) \quad (2\text{-}69)$$

Using the measurement residual r_k defined in Eq. (2-62), Eq. (2-69) is simplified as:

$$\begin{Bmatrix} \hat{x}_{k-1|k} \\ \hat{u}_{k-1|k} \\ \hat{w}_{k-1|k} \end{Bmatrix} = \begin{Bmatrix} \hat{x}_{k-1|k-1} + L_{x_{k-1}} r_k \\ \hat{u}_{k-1|k-1} + L_{u_{k-1}} r_k \\ L_{w_{k-1}} r_k \end{Bmatrix} \quad (2\text{-}70)$$

where the estimation gains are defined as

$$L_{x_{k-1}} \triangleq \Sigma_{x_{k-1}y_{k|k-1}}\Sigma_{y_{k|k-1}}^{-1} = \Sigma_{x_{k-1|k-1}}(CA)^T\Sigma_{y_{k|k-1}}^{-1} + \Sigma_{x_{k-1}u_{k-1|k-1}}(CB)^T\Sigma_{y_{k|k-1}}^{-1} \quad (2\text{-}71)$$

$$L_{u_{k-1}} \triangleq \Sigma_{u_{k-1}y_{k|k-1}}\Sigma_{y_{k|k-1}}^{-1} = \Sigma_{u_{k-1|k-1}}(CB)^T\Sigma_{y_{k|k-1}}^{-1} + \Sigma_{u_{k-1}x_{k-1|k-1}}(CA)^T\Sigma_{y_{k|k-1}}^{-1} \quad (2\text{-}72)$$

$$L_{w_{k-1}} \triangleq \Sigma_{w_{k-1}y_{k|k-1}}\Sigma_{y_{k|k-1}}^{-1} = \Sigma_w C^T\Sigma_{y_{k|k-1}}^{-1} \quad (2\text{-}73)$$

Note that $\Sigma_{x_{k-1}y_{k|k-1}}$, $\Sigma_{u_{k-1}y_{k|k-1}}$ and $\Sigma_{w_{k-1}y_{k|k-1}}$ are given by Eq. (2-65) ~ (2-67). Based on Eq. (2-4) in Lemma 2-3, the conditional covariance given $y_{0:k}$ can be obtained as

$$\begin{aligned}\operatorname{cov}\left(\begin{Bmatrix}x_{k-1}\\u_{k-1}\\w_{k-1}\end{Bmatrix}\middle| y_{0:k}\right) &\triangleq \begin{bmatrix}\Sigma_{x_{k-1|k}} & \Sigma_{x_{k-1}u_{k-1|k}} & \Sigma_{x_{k-1}w_{k-1|k}}\\ \Sigma_{u_{k-1}x_{k-1|k}} & \Sigma_{u_{k-1|k}} & \Sigma_{u_{k-1}w_{k-1|k}}\\ \Sigma_{w_{k-1}x_{k-1|k}} & \Sigma_{w_{k-1}u_{k-1|k}} & \Sigma_{w_{k-1|k}}\end{bmatrix}\\ &= \begin{bmatrix}\Sigma_{x_{k-1|k-1}} & \Sigma_{x_{k-1}u_{k-1|k-1}} & 0\\ \Sigma_{u_{k-1}x_{k-1|k-1}} & \Sigma_{u_{k-1|k-1}} & 0\\ 0 & 0 & \Sigma_{w_{k-1|k-1}}\end{bmatrix}\\ &- \begin{bmatrix}\Sigma_{x_{k-1}y_{k|k-1}}\\ \Sigma_{u_{k-1}y_{k|k-1}}\\ \Sigma_{w_{k-1}y_{k|k-1}}\end{bmatrix}\Sigma_{y_{k|k-1}}^{-1}\begin{bmatrix}\Sigma_{y_k x_{k-1|k-1}} & \Sigma_{y_k u_{k-1|k-1}} & \Sigma_{y_k w_{k-1|k-1}}\end{bmatrix}\end{aligned} \quad (2\text{-}74)$$

The conditional covariance matrix is a symmetric 3×3 block matrix. Taking the (1,1)block for example, expansion of (2-74) provides

$$\Sigma_{x_{k-1|k}} = \Sigma_{x_{k-1|k-1}} - \Sigma_{x_{k-1}y_{k|k-1}}\Sigma_{y_{k|k-1}}^{-1}\Sigma_{x_{k-1}y_{k|k-1}}^T \quad (2\text{-}75)$$

Recall the estimation gain matrix $L_{x_{k-1}} = \Sigma_{x_{k-1}y_{k|k-1}}\Sigma_{y_{k|k-1}}^{-1}$ defined in (2-71), and substitute prior covariance $\Sigma_{x_{k-1}y_{k|k-1}}$ using Eq. (2-65):

$$\Sigma_{x_{k-1|k}} = \Sigma_{x_{k-1|k-1}} - L_{x_{k-1}}\left(\Sigma_{x_{k-1|k-1}}(CA)^T + \Sigma_{x_{k-1}u_{k-1|k-1}}(CB)^T\right)^T \quad (2\text{-}76)$$

Similarly, other blocks in the conditional covariance matrix can be found using estimation gains from Eq. (2-71) ~ (2-73) and prior covariances $\Sigma_{x_{k-1}y_{k|k-1}}$, $\Sigma_{u_{k-1}y_{k|k-1}}$ and $\Sigma_{w_{k-1}y_{k|k-1}}$ in Eq. (2-65) ~ (2-67):

$$\begin{aligned}\Sigma_{u_{k-1|k}} &= \Sigma_{u_{k-1|k-1}} - \Sigma_{u_{k-1}y_{k|k-1}}\Sigma_{y_{k|k-1}}^{-1}\Sigma_{u_{k-1}y_{k|k-1}}^{T} \\ &= \Sigma_{u_{k-1|k-1}} - L_{u_{k-1}}\left(\Sigma_{u_{k-1|k-1}}(CB)^T + \Sigma_{u_{k-1}x_{k-1|k-1}}(CA)^T\right)^T\end{aligned} \tag{2-77}$$

$$\Sigma_{w_{k-1|k}} = \Sigma_{w_{k-1|k-1}} - \Sigma_{w_{k-1}y_{k|k-1}}\Sigma_{y_{k|k-1}}^{-1}\Sigma_{w_{k-1}y_{k|k-1}}^{T} = \Sigma_w - L_{w_{k-1}}C\Sigma_w \tag{2-78}$$

$$\begin{aligned}\Sigma_{x_{k-1}u_{k-1|k}} &= \Sigma_{x_{k-1}u_{k-1|k-1}} - \Sigma_{x_{k-1}y_{k|k-1}}\Sigma_{y_{k|k-1}}^{-1}\Sigma_{u_{k-1}y_{k|k-1}}^{T} \\ &= \Sigma_{x_{k-1}u_{k-1|k-1}} - \left(\Sigma_{x_{k-1|k-1}}(CA)^T + \Sigma_{x_{k-1}u_{k-1|k-1}}(CB)^T\right)L_{u_{k-1}}^T\end{aligned} \tag{2-79}$$

$$\Sigma_{x_{k-1}w_{k-1|k}} = -\Sigma_{x_{k-1}y_{k|k-1}}\Sigma_{y_{k|k-1}}^{-1}\Sigma_{w_{k-1}y_{k|k-1}}^{T} = -L_{x_{k-1}}C\Sigma_w \tag{2-80}$$

$$\Sigma_{u_{k-1}w_{k-1|k}} = -\Sigma_{u_{k-1}y_{k|k-1}}\Sigma_{y_{k|k-1}}^{-1}\Sigma_{w_{k-1}y_{k|k-1}}^{T} = -L_{u_{k-1}}C\Sigma_w \tag{2-81}$$

Note that due to independence of w_{k-1} from $y_{0:k-1}$, the cross-covariances $\Sigma_{x_{k-1}w_{k-1|k-1}} = 0$ and $\Sigma_{u_{k-1}w_{k-1|k-1}} = 0$. The remaining three blocks in Eq. (2-74) are easily obtained through symmetry.

2.2.3 Time Update of Input and State

Time update of state is straightforward using linear transformation. Based on Eq. (2-54), the state at time step k can be re-written in the following form

$$x_k = [A \quad B \quad I]\begin{Bmatrix} x_{k-1} \\ u_{k-1} \\ w_{k-1} \end{Bmatrix} \tag{2-82}$$

Because linear transformation in Eq. (2-82), the estimate of x_k given $y_{0:k}$ can be found as

$$\begin{aligned} \hat{x}_{k|k} &= \mathbb{E}(x_k|y_{0:k}) = [A \quad B \quad I]\mathbb{E}\left(\begin{Bmatrix} x_{k-1} \\ u_{k-1} \\ w_{k-1} \end{Bmatrix}\middle| y_{0:k}\right) \\ &= A\hat{x}_{k-1|k} + B\hat{u}_{k-1|k} + \hat{w}_{k-1|k} \end{aligned} \tag{2-83}$$

Here the prior estimates $\hat{x}_{k-1|k}$, $\hat{u}_{k-1|k}$ and $\hat{w}_{k-1|k}$ are given in Eq. (2-70). An important fact is that $\mathbb{E}(w_{k-1}|y_{0:k})$ cannot be discarded as zero because $y_{0:k}$ contains process noise w_{k-1} based on Eq. (2-59). The conditional covariance of x_k given $y_{0:k}$ is

$$\Sigma_{x_{k|k}} \triangleq \mathrm{cov}(x_k|y_{0:k}) = [A \quad B \quad I]\begin{bmatrix} \Sigma_{x_{k-1|k}} & \Sigma_{x_{k-1}u_{k-1|k}} & \Sigma_{x_{k-1}w_{k-1|k}} \\ \Sigma_{u_{k-1}x_{k-1|k}} & \Sigma_{u_{k-1|k}} & \Sigma_{u_{k-1}w_{k-1|k}} \\ \Sigma_{w_{k-1}x_{k-1|k}} & \Sigma_{w_{k-1}u_{k-1|k}} & \Sigma_{w_{k-1|k}} \end{bmatrix}\begin{bmatrix} A^T \\ B^T \\ I \end{bmatrix} \tag{2-84}$$

In terms of time update of input, a state-space model of the input can be used to propagate the input over time. In this section, the input u_k at each time step is assumed to be white Gaussian. Based on Eq. (2-56), Eq. (2-57) and the white Gaussian assumption, u_k is independent from x_0, $u_{0:k-1}$, $w_{0:k-1}$ and $v_{0:k}$. Therefore, u_k is also independent from x_k and $y_{0:k}$. As a result,

$$\hat{u}_{k|k} \triangleq \mathbb{E}(u_k|y_{0:k}) = \mathbb{E}(u_k) = 0 \tag{2-85}$$

$$\Sigma_{u_{k|k}} \triangleq \mathrm{cov}(u_k|y_{0:k}) = \Sigma_u \tag{2-86}$$

$$\Sigma_{x_k u_{k|k}} \triangleq \mathrm{cov}(x_k, u_k | y_{0:k}) = \Sigma^T_{u_k x_{k|k}} = 0 \tag{2-87}$$

Thus far, the FIC estimator for systems without direct feedthrough of the input is derived. The state x_k and input u_k given $y_{0:k}$ are jointly estimated by propagating the measurement equation back one-time step. Table 2-3 summarizes the proposed FIC estimator using the time updated priors of input given by Eq. (2-85) ~ (2-87), assuming the unknown input is zero-mean white Gaussian with finite covariance Σ_u.

Table 2-3 Input-state estimation of FIC estimator for systems without feedthrough

Initialization: $\hat{x}_{0\|0} = \mu_{x_0}$, $\Sigma_{x_{0\|0}} = \Sigma_{x_0}$		
for $k = 1, 2, \ldots, n$		
Measurement update of input:		
$\Sigma_{y_{k\|k-1}} = CA\Sigma_{x_{k-1\|k-1}}(CA)^T + CB\Sigma_u(CB)^T + C\Sigma_w C^T + \Sigma_v$	(from (2-68), (2-86) and (2-87))	(2-88)
$L_{u_{k-1}} = \Sigma_u (CB)^T \Sigma^{-1}_{y_{k\|k-1}}$	(from (2-72), (2-86) and (2-87))	(2-89)
$\hat{u}_{k-1\|k} = L_{u_{k-1}}\left(y_k - CA\hat{x}_{k-1\|k-1}\right)$	(from (2-70) and (2-85))	(2-90)
$\Sigma_{u_{k-1\|k}} = \Sigma_u - L_{u_{k-1}} CB\Sigma_u$	(from (2-77), (2-86) and (2-87))	(2-91)
$\Sigma_{x_{k-1}u_{k-1\|k}} = -\Sigma_{x_{k-1\|k-1}}(CA)^T L^T_{u_{k-1}}$	(from (2-79) and (2-87))	(2-92)
Measurement update of state:		
$L_{x_{k-1}} = \Sigma_{x_{k-1\|k-1}}(CA)^T \Sigma^{-1}_{y_{k\|k-1}}$	(from (2-71) and (2-87))	(2-93)
$\hat{x}_{k-1\|k} = \hat{x}_{k-1\|k-1} + L_{x_{k-1}}\left(y_k - CA\hat{x}_{k-1\|k-1}\right)$		Rept. (2-70)
$\Sigma_{x_{k-1\|k}} = \Sigma_{x_{k-1\|k-1}} - L_{x_{k-1}} CA\Sigma_{x_{k-1\|k-1}}$	(from (2-75) and (2-87))	(2-94)
Measurement update of process noise:		
$L_{w_{k-1}} = \Sigma_w C^T \Sigma^{-1}_{y_{k\|k-1}}$		Rept. (2-73)
$\hat{w}_{k-1\|k} = L_{w_{k-1}}\left(y_k - CA\hat{x}_{k-1\|k-1}\right)$		Rept. (2-70)
$\Sigma_{w_{k-1\|k}} = \Sigma_w - L_{w_{k-1}} C\Sigma_w$		Rept. (2-78)

$$\Sigma_{x_{k-1}w_{k-1|k}} = -L_{x_{k-1}} C \Sigma_w \quad \text{Rept. (2-80)}$$

$$\Sigma_{u_{k-1}w_{k-1|k}} = -L_{u_{k-1}} C \Sigma_w \quad \text{Rept. (2-81)}$$

Time update:

$$\hat{x}_{k|k} = A\hat{x}_{k-1|k} + B\hat{u}_{k-1|k} + \hat{w}_{k-1|k} \quad \text{Rept. (2-83)}$$

$$\Sigma_{x_{k|k}} = \begin{bmatrix} A & B & I \end{bmatrix} \begin{bmatrix} \Sigma_{x_{k-1|k}} & \Sigma_{x_{k-1}u_{k-1|k}} & \Sigma_{x_{k-1}w_{k-1|k}} \\ \Sigma_{u_{k-1}x_{k-1|k}} & \Sigma_{u_{k-1|k}} & \Sigma_{u_{k-1}w_{k-1|k}} \\ \Sigma_{w_{k-1}x_{k-1|k}} & \Sigma_{w_{k-1}u_{k-1|k}} & \Sigma_{w_{k-1|k}} \end{bmatrix} \begin{bmatrix} A^T \\ B^T \\ I \end{bmatrix} \quad \text{Rept. (2-84)}$$

`end`

2.2.4 Measurement Update with Large and Infinite Input Covariance

Similar as in Section 2.1.4, when the input covariance is large, measurement update equations shown in Table 2-3 can be modified to improve the conditioning of Equation (2-88). Specifically, Equation (2-88) may be ill-conditioned when the input covariance Σ_u is much larger than the state estimation covariance and $CB\Sigma_u B^T C^T$ does not have full rank. To improve the conditioning of Eq. (2-88), define a symmetric positive definite matrix $\Sigma_{\tilde{y}_{k|k-1}}$ to represent part of $\Sigma_{y_{k|k-1}}$, such that $\Sigma_{y_{k|k-1}} = \Sigma_{\tilde{y}_{k|k-1}} + CB\Sigma_u(CB)^T$:

$$\Sigma_{\tilde{y}_{k|k-1}} \triangleq CA\Sigma_{x_{k-1|k-1}}(CA)^T + C\Sigma_w C^T + \Sigma_v \quad (2\text{-}95)$$

Based on the matrix push through identity in Lemma 2-1, input estimation gain $L_{u_{k-1}}$ from Eq. (2-89) can be modified as

$$L_{u_{k-1}} = \Sigma_u(CB)^T \left(\Sigma_{\tilde{y}_{k|k-1}} + CB\Sigma_u(CB)^T\right)^{-1}$$

$$= \Sigma_u (CB)^T \left(I + \Sigma_{\tilde{y}_{k|k-1}}^{-1} CB\Sigma_u (CB)^T \right)^{-1} \Sigma_{\tilde{y}_{k|k-1}}^{-1} \quad \text{invert } \Sigma_{\tilde{y}_{k|k-1}}$$

$$= \left(\Sigma_u^{-1} + (CB)^T \Sigma_{\tilde{y}_{k|k-1}}^{-1} CB \right)^{-1} (CB)^T \Sigma_{\tilde{y}_{k|k-1}}^{-1} \quad \text{apply Lemma 2-1, invert } \Sigma_u \qquad (2\text{-}96)$$

The corresponding input estimation error covariance $\Sigma_{u_{k-1|k}}$ (Eq. (2-91)) is rewritten as

$$\Sigma_{u_{k-1|k}} = \Sigma_u - \Sigma_u (CB)^T \Sigma_{y_{k|k-1}}^{-1} CB\Sigma_u \quad \text{substitute } L_{u_{k-1}} \text{ with (2-89)}$$

$$= \Sigma_u - \Sigma_u (CB)^T \left(\Sigma_{\tilde{y}_{k|k-1}} + CB\Sigma_u (CB)^T \right)^{-1} CB\Sigma_u \quad \text{substitute } \Sigma_{y_{k|k-1}}$$

$$= \left(\Sigma_u^{-1} + (CB)^T \Sigma_{\tilde{y}_{k|k-1}}^{-1} CB \right)^{-1} \quad \text{apply Lemma (2-2a) in reverse} \qquad (2\text{-}97)$$

For $\Sigma_{y_{k|k-1}}^{-1}$, the matrix inversion can be rewritten by applying Lemma (2-2b) as

$$\Sigma_{y_{k|k-1}}^{-1} = \left(\Sigma_{\tilde{y}_{k|k-1}} + CB\Sigma_u (CB)^T \right)^{-1}$$

$$= \Sigma_{\tilde{y}_{k|k-1}}^{-1} \left(I - CB \left(\Sigma_u^{-1} + (CB)^T \Sigma_{\tilde{y}_{k|k-1}}^{-1} CB \right)^{-1} (CB)^T \Sigma_{\tilde{y}_{k|k-1}}^{-1} \right) \qquad (2\text{-}98)$$

Therefore, Eq. (2-98) can be used to evaluate $\Sigma_{y_{k|k-1}}^{-1}$ in Eq. (2-93) and (2-73) to improve the conditioning of Eq. (2-88) of the FIC estimator. In addition, an equivalent set of equations given by Eq. (2-96) and (2-97) can be used to replace Eq. (2-89), (2-91),. Furthermore, if the unknown input is highly uncertain such that no prior knowledge can be used to estimate u_{k-1}, $\Sigma_{u_{k-1|k-1}} = \Sigma_u$ can be replaced with Σ_∞, which denotes a diagonal matrix with diagonal entries being infinity. When the number of unknown inputs is smaller than the number of measurements, $n_u \leq m$, and $\text{rank}(CB) = n_u$ (i.e. CB has full column

rank), $\Sigma_u^{-1} = \Sigma_\infty^{-1}$ in Eq. (2-96)~(2-98) can be eliminated, and Eq. (2-99) ~ (2-101) are obtained.

$$L_{u_{k-1}} = \left((CB)^T \Sigma_{\tilde{y}_{k|k-1}}^{-1} CB\right)^{-1} (CB)^T \Sigma_{\tilde{y}_{k|k-1}}^{-1} = \Sigma_{u_{k-1|k}} (CB)^T \Sigma_{\tilde{y}_{k|k-1}}^{-1} \tag{2-99}$$

$$\Sigma_{u_{k-1|k}} = \left((CB)^T \Sigma_{\tilde{y}_{k|k-1}}^{-1} CB\right)^{-1} \tag{2-100}$$

$$\begin{aligned} \Sigma_{y_{k|k-1}}^{-1} &= \Sigma_{\tilde{y}_{k|k-1}}^{-1} \left(I - CB\left((CB)^T \Sigma_{\tilde{y}_{k|k-1}}^{-1} CB\right)^{-1} (CB)^T \Sigma_{\tilde{y}_{k|k-1}}^{-1}\right) \\ &= \Sigma_{\tilde{y}_{k|k-1}}^{-1} \left(I - CBL_{u_{k-1}}\right) \end{aligned} \tag{2-101}$$

As a result of Eq. (2-101), the state estimation gain $L_{x_{k-1}}$ in Eq. (2-93) and the process noise estimation gain $L_{w_{k-1}}$ in Eq. (2-73) can be rewritten as

$$L_{x_{k-1}} = \Sigma_{x_{k-1|k-1}} (CA)^T \Sigma_{\tilde{y}_{k|k-1}}^{-1} \left(I - CBL_{u_k}\right) \tag{2-102}$$

$$L_{w_{k-1}} = \Sigma_w C^T \Sigma_{\tilde{y}_{k|k-1}}^{-1} \left(I - CBL_{u_k}\right) \tag{2-103}$$

To summarize, when assuming $\Sigma_{u_{k-1|k-1}} = \Sigma_u = \Sigma_\infty$ and CB has full column rank, Eq. (2-88), (2-89), (2-91), (2-93) and (2-73) in Table 2-3 can be replaced by Eq. (2-95), (2-99), (2-100), (2-102) and (2-103), respectively. Time update of the state is the same as given by Eq. (2-83) and (2-84) while there is no time update of input.

Theorem 2-2 For systems without direct feedthrough, when the input covariance Σ_u of the FIC estimator approaches infinity (Σ_∞) and CB has full column rank, the FIC estimator with $L_{u_{k-1}}$, $\Sigma_{u_{k-1|k}}$, $L_{x_{k-1}}$ and $L_{w_{k-1}}$ given by Eq. (2-99), (2-100), (2-102) and (2-103) is equivalent to the WLS estimator proposed by Gillijns and De Moor in [12].

Proof. In comparison to the notations in [12], the symmetric positive definite matrix $\Sigma_{\tilde{y}_{k|k-1}}$ defined here in Eq. (2-95) is denoted as $\tilde{R}_k$ in (12) of [12]; the input estimation gain L_{u_k} here is denoted as M_k. For state estimation, by substituting $\hat{x}_{k-1|k}$, $\hat{u}_{k-1|k}$ and $\hat{w}_{k-1|k}$ in Eq. (2-70) into Eq. (2-83), a one-step state update equation from $\hat{x}_{k-1|k}$ to $\hat{x}_{k|k}$ can be obtained. Accordingly, the same one-step state estimate $\hat{x}_{k|k}$ from [12] can be found by substituting $\hat{x}_{k|k-1}$ in (3) into (19). In addition, the same one-step state covariance update equation from $\Sigma_{x_{k-1|k}}$ to $\Sigma_{x_{k|k}}$ can be found in a similar way. The same one-step covariance equation from [12] can be found by substituting $P_{k|k-1}$ into $P_{k|k}$ of (25). Note that because the MMSE derivation here simultaneously estimate x_{k-1} and u_{k-1}, the notations $\hat{x}_{k|k-1}$ and $P_{k|k-1}$ in [12] are not used in this derivation. Therefore, substitution of $\hat{x}_{k|k-1}$ and $P_{k|k-1}$ in [12] is needed to show the equivalence. ■

In theory, the FIC estimator in Table 2-3 does not assume CB has full column rank. However, to provide a good estimation of all the unknown inputs, in practice full column-rank of CB is needed and the magnitude of CBu_k should be relatively large compared to the measurement noise v_k.

2.2.5 Numerical Study: Non-collocated Input and Measurements

This section presents the simulation results for systems without direct feedthrough. The same four-story structure from Section 2.1.5 is used here. In this scenario, however, the inputs and acceleration measurements are not collocated and thus the feedthrough matrix D is zero. A force excitation $u(t)$ is applied at the 4th DOF of the structure, i.e. at

mass m_4, and measurement y contains simulated acceleration response of only the first three DOFs, excluding the input DOF. The input location matrix is $\Gamma_u = [0 \quad 0 \quad 0 \quad 1]^T$ and the output location matrix is $\Gamma_y = \begin{bmatrix} 1 & 0 & 0 & 0 \\ 0 & 1 & 0 & 0 \\ 0 & 0 & 1 & 0 \end{bmatrix}$. Therefore, the feedthrough matrix of Eq. (2-53) $D_c = \Gamma_y M^{-1} \Gamma_u = 0$, leading to a system without direct feedthrough of the unknown input. The same Rayleigh damping model is used here with a 2% modal damping ratio assumed for the first two modes.

Two types of input excitations are used here to compare the performance of the FIC estimator and the WLS estimator. The first type is a white Gaussian input excitation with a standard deviation of 10 N, i.e. $u_k \sim \mathcal{N}(0, 10^2)$, same as the one described in Section 2.1.5. The second type is a mixed sinusoidal input from 1 Hz to 10 Hz with uniformly randomly generated magnitudes ranging from 0 to 10 N. Measurement noise with a standard deviation $\sigma_v = 10^{-3}$ m/s^2 is added to structural acceleration responses, sampled at 200 Hz. The standard deviation σ_v available to the estimators is assumed to be the same as the one used in the simulated measurements. Moreover, no process noise is used during simulation or estimation process, i.e. $\Sigma_{w,sim} = \Sigma_{w,est} = 0$. Because the initial condition of the structure is assumed to be static and known, μ_{x_0} and Σ_{x_0} are set zero.

2.2.5.1 Effect of covariance knowledge on input estimation

To study estimator covariance effects, multiple trial runs of numerical simulations are performed when the unknown input is not directly fed through measurements. Similar

as in Section 2.1.5.1, Table 2-4 summarizes the time history generation process and the estimator covariances during each trial run.

Table 2-4 Summary of data generation and estimator covariances

Covariances	Time history generation	Estimation	
		FIC	WLS
Input types	(1) White noise: $\Sigma_{u,\,sim} = 100\ \mathrm{N}^2$ (2) Mixed sinusoidal input	$\Sigma_{u,\,est}$ (10 to $10^7\ \mathrm{N}^2$)	-
Initial state	Static	$\mu_{x_0} = 0,\ \Sigma_{x_0} = 0$	
Process noise	$\Sigma_{w,\,sim} = 0$	$\Sigma_{w,\,est} = 0$	
Measurement noise	$\Sigma_{v,\,sim} = 10^{-6}\ (\mathrm{m/s^2})^2$	$\Sigma_{v,\,est} = 10^{-6}\ (\mathrm{m/s^2})^2$	

For white Gaussian excitation, 50 independent runs of dynamic simulation are performed; each trial is conducted using randomly generated 30 seconds of input u_k with $\Sigma_{u,sim} = 100\mathrm{N}^2$ and measurement noise v_k. The input RMS error e_u is calculated in each trial run for different values of $\Sigma_{u,est}$ ranging from 10 to $10^7\ \mathrm{N}^2$. Figure 2-6(a) shows the relationship between the averaged RMS $\bar{e}_u$ and $\Sigma_{u,est}$ of FIC for white Gaussian input. The smallest error $\bar{e}_u$ is 2.78 N, achieved by the FIC estimator when $\Sigma_{u,est}$ is very close to the actual input covariance $\Sigma_{u,sim} = 100\ \mathrm{N}^2$. As $\Sigma_{u,est}$ becomes larger than $10^5\ \mathrm{N}^2$, the FIC estimator converges to the WLS estimator, which is consistent with Theorem 2-2.

For the mixed sinusoidal input excitation, 50 independent runs of 15 seconds dynamics simulation with randomly generated measurement noise are performed. Same as in the white Gaussian input simulation, the input RMS error e_u is calculated in each trial

run for different values of $\Sigma_{u,est}$ ranging from 10 to 10^7 N^2. Figure 2-6(b) shows the relationship between $\bar{e}_u$ and $\Sigma_{u,est}$ of FIC for mixed sinusoidal input. The smallest RMS error $\bar{e}_u$ is 2.54 N, achieved by the FIC estimator when $\Sigma_{u,est}$ is around 40 N^2. Although different from the calculated input covariance $\Sigma_{u,sim} = 155\ \mathrm{N}^2$ based on the mixed sinusoidal signal, the best choice of $\Sigma_{u,est}$ is close to the maximum magnitude of the input. Similar as in the sinusoidal input in Section 2.1.5.1, the best $\Sigma_{u,est}$ of FIC does not equal to the actual $\Sigma_{u,sim}$, when the white noise assumption is violated. However, compared to the WLS estimator, smaller RMS error can still be achieved by the FIC estimator when $\Sigma_{u,est}$ is within a large range around the actual $\Sigma_{u,sim}$.

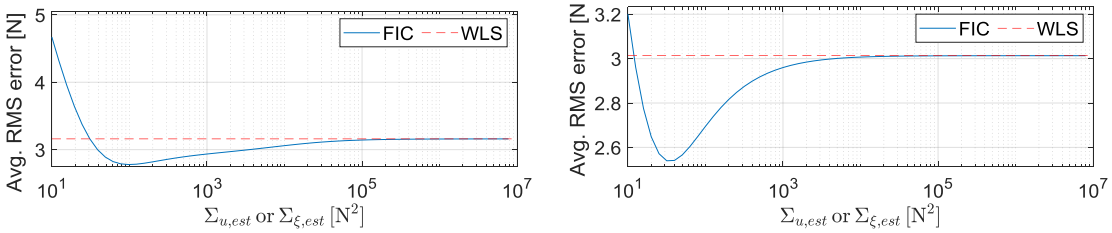

(a) White Gaussian input (b) Mixed sinusoidal input

Figure 2-6 Averaged input RMS error $\bar{e}_u$ for white Gaussian and mixed sinusoidal inputs: noncollocated input and measurements without process nosie

2.2.5.2 Simultaneous input-state estimation

This subsection first compares the time history of the estimated inputs for a single run of white Gaussian excitation for 60 seconds. Process noise covariance is set as zero in both simulation and estimation, i.e. $\Sigma_{w,sim} = \Sigma_{w,est} = 0$. Measurement noise covariance in estimation is set the same as in simulation, i.e. $\Sigma_{v,sim} = \Sigma_{v,est} = 10^{-6} I\ (\mathrm{m/s^2})^2$. The initial state and corresponding state estimation covariance are set as zero. Input covariance $\Sigma_{u,est}$ of the FIC estimator is set as $100\ \mathrm{N}^2$, same as the covariance of the Gaussian

excitation. Figure 2-7(a) shows the input estimation comparison between the FIC estimator and WLS estimator during the first 1s of simulation. Both estimators perform similarly at the beginning. However, compared to results of systems with direct feedthrough (Section 2.1.5.2), drift error of the WLS estimator becomes more significant when input is not directly fed to measurements as time increases. Figure 2-7(b) shows the close-up plot of the estimated input by FIC estimation from 59.5s to 60s, and Figure 2-7(c) shows the corresponding close-up plot of WLS estimation. Again, the FIC estimator performs consistently well over time with a tight confidence interval, while the WLS estimator cannot provide a good estimate of the input as time increases. Figure 2-7(d) shows the time history of input estimation error covariance $\Sigma_{u_{k|k}}$ of FIC and WLS estimation in logarithmic scale. The FIC estimator converges slowly after around 11s, while the WLS estimator is not able to converge to steady state. Compared to the scenario in Section 2.1.5 when input and measurements are collocated, the steady state value of the input error covariance is much larger in this non-collocated scenario.

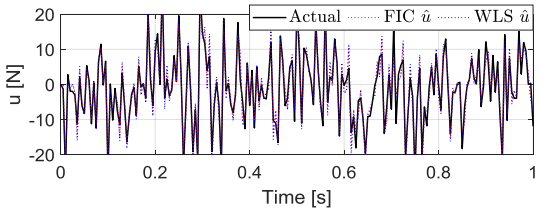

(a) 0~1s of FIC and WLS estimation

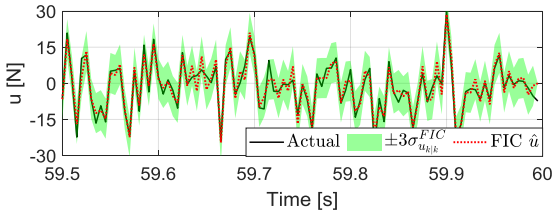

(b) 59.5~60s of FIC estimation

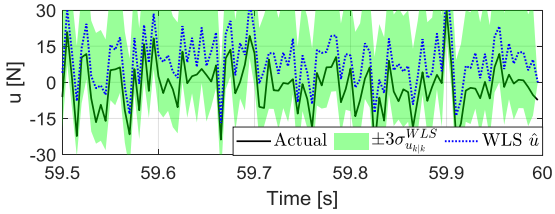

(c) 59.5~60 of WLS estimation

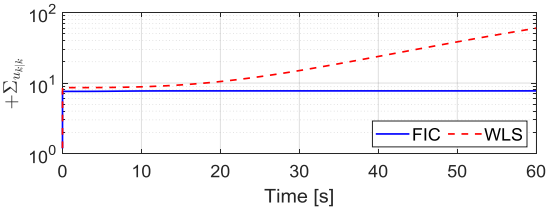

(d) input estimation error covariance $\Sigma_{u_{k|k}}$

Figure 2-7 Estimation of white Gaussian input: non-collocated input and measurements

Next for a single run of a mixed sinusoidal input from 1 Hz to 10 Hz with uniformly randomly generated magnitude from 0 to 10 N is applied to the structure for 15 seconds. With a mixed sinusoidal input, the white Gaussian noise assumption of the unknown input is violated on purpose in order to check the estimator performance. The process and measurement noise covariances are set as those in white noise simulation, i.e. $\Sigma_{w,sim} = \Sigma_{w,est} = 0$ and $\Sigma_{v,sim} = \Sigma_{v,est} = 10^{-6} I\ (\mathrm{m/s^2})^2$. The initial state and corresponding state estimation covariance are set as zero. Input covariance $\Sigma_{u,est}$ of the FIC estimator is set as $40\ \mathrm{N}^2$.

Figure 2-8(a) shows the input estimation comparison between the FIC and WLS estimators from 0s to 15s. Compared to the white input, the drift error of the WLS estimator becomes less obvious under mixed sinusoidal excitation. Figure 2-8(b) shows the close-up plot of the estimated input by FIC estimation from 13s to 14s, and Figure 2-8(c) shows the corresponding close-up plot of WLS estimation. Because the unknown input is not fed directly to measurements, the estimated input from both FIC and WLS estimators is affected by measurement noise more significantly than the direct feedthrough results in Section 2.1.5.2. Figure 2-8(d) shows the time history of input estimation error covariance $\Sigma_{u_{k|k}}$ of FIC and WLS estimation in logarithmic scale. The WLS estimator cannot converge to steady state with a slow divergence over time. The FIC estimator shows a relatively large increase in the error covariance at the beginning, and converges slowly to steady state after around 8s. Compared to the collocated scenario shown in Figure 2-5(d), the steady state value of the input error covariance from the FIC estimator is relatively large.

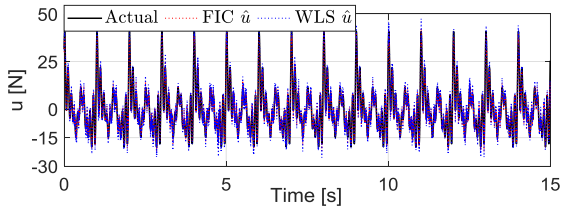

(a) 0~15s of FIC and WLS estimation results

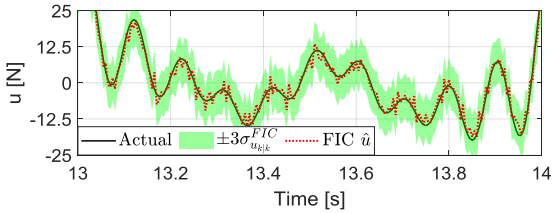

(b) 13~14s of FIC estimation results

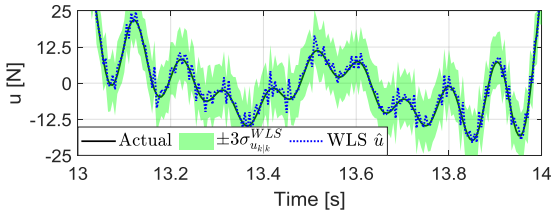

(c) 13~14s of WLS estimation results

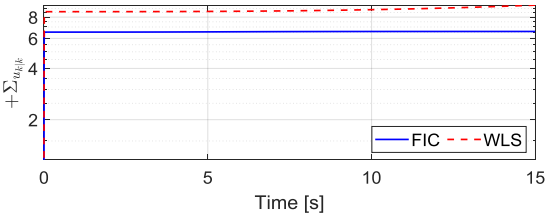

(d) input estimation error covariance $\Sigma_{u_{k|k}}$

Figure 2-8 Estimation of mixed sinusoidal input: non-collocated input and measurements

For systems without direct feedthrough, compared to the WLS estimator, the FIC estimator achieves smaller RMS error and a smaller estimation error covariance $\Sigma_{u_{k|k}}$ not only in input estimation but also in state (displacement and velocity) estimation.

2.3 Estimation with Delayed Measurements

This section derives an input-state estimator with delayed measurements to improve estimator performance and relax the full column rank assumption needed by the FIC estimator for accurate input estimation.

2.3.1 Problem Formulation

Consider the same discrete-time stochastic linear system:

$$x_{k+1} = Ax_k + Bu_k + w_k \tag{2-104}$$

$$y_k = Cx_k + Du_k + v_k \tag{2-105}$$

where $x_k \in \mathbb{R}^n$ is the state at time step k, $u_k \in \mathbb{R}^{n_u}$ is the unknown input, $w_k \in \mathbb{R}^n$ is the process noise or disturbance, $y_k \in \mathbb{R}^m$ is the measurement output, and $v_k \in \mathbb{R}^m$ is the measurement noise. Note that when the feedthrough matrix D is non-zero, the system is the same as the one in Section 2.1; when D is zero, the system is the same as the one in Section 2.2. In addition to the assumptions made in Section 2.1.1, the system is assumed to be invertible with a non-negative integer delay d, defined by Theorem 4 in [26]. Note that based on Corollary 2 in [26], the minimum required number of delays to make the system invertible needs to be smaller than the number of state n. Following lemma is provided to derive the simultaneous input-state estimator for systems with d-step delayed measurements.

Lemma 2-6 For the system given by Eq. (2-104) and (2-105) with the same assumptions made in Section 2.1.1 along with the invertibility requirement, x_{k-d}, $u_{k-d:k}$ and $y_{0:k}$ are jointly Gaussian, where d is the number of delayed time steps used for estimation and $d \geq 1$. In addition, each vector among $x_{k-d}|y_{0:k-1}$, $u_{k-d:k}|y_{0:k-1}$ and $y_k|y_{0:k-1}$, is Gaussian.

Proof. Based on Eq. (2-104) and (2-105), we can derive

$$x_{k-d} = A^{k-d}x_0 + H_{u_{k-d}}u_{0:k} + H_{w_{k-d}}w_{0:k-1} \tag{2-106}$$

$$y_{0:k} = \mathcal{O}_k x_0 + P_{u_k}u_{0:k} + P_{w_k}w_{0:k-1} + v_{0:k} \tag{2-107}$$

where

(1) $H_{u_{k-d}} \triangleq \begin{bmatrix} A^{k-d-1}B & \cdots & AB & B & 0_{n\times n_u(d+1)} \end{bmatrix} \in \mathbb{R}^{n\times n_u(k+1)}$;

(2) $H_{w_{k-d}} \triangleq \begin{bmatrix} A^{k-d-1} & \cdots & A & I_n & 0_{n\times nd} \end{bmatrix} \in \mathbb{R}^{n\times nk}$;

(3) $\mathcal{O}_k \triangleq \begin{bmatrix} C \\ CA \\ \vdots \\ CA^k \end{bmatrix} \in \mathbb{R}^{m(k+1)\times n}$;

(4) $P_{u_k} \triangleq \begin{bmatrix} D & 0 & \cdots & 0 \\ CB & \ddots & \cdots & \vdots \\ \vdots & \ddots & D & 0 \\ CA^{k-1}B & \cdots & CB & D \end{bmatrix} \in \mathbb{R}^{m(k+1)\times n_u(k+1)}$;

(5) $P_{w_k} \triangleq \begin{bmatrix} 0 & 0 & 0 \\ C & \ddots & \vdots \\ \vdots & \ddots & 0 \\ CA^{k-1} & \cdots & C \end{bmatrix} \in \mathbb{R}^{m(k+1)\times nk}$.

Here $P_{u_0} = D$, $P_{w_0} = 0$ and define $\text{rank}(P_{u_{-1}}) \triangleq 0$. The system invertibility assumption mentioned earlier can thus be specified as $\text{rank}\left(P_{u_d}\right) - \text{rank}\left(P_{u_{d-1}}\right) = n_u$ [26]. Because x_0, $u_{0:k}$, $w_{0:k-1}$ and $v_{0:k}$ are Gaussian and independent from each other, they are jointly Gaussian. Equation (2-108) shows that x_{k-d}, $u_{k-d:k}$, $w_{k-d:k-1}$ and $y_{0:k}$ can be expressed as a linear transformation of x_0, $u_{0:k}$, $w_{0:k-1}$ and $v_{0:k}$.

$$\begin{Bmatrix} x_{k-d} \\ u_{k-d:k} \\ w_{k-d:k-1} \\ y_{0:k} \end{Bmatrix} = \begin{bmatrix} A^{k-d} & H_{u_{k-d}} & H_{w_{k-d}} & 0 \\ 0 & \check{I}_{u_{k-d:k}} & 0 & 0 \\ 0 & 0 & \check{I}_{w_{k-d:k-1}} & 0 \\ \mathcal{O}_k & P_{u_k} & P_{w_k} & I_{m(k+1)} \end{bmatrix} \begin{Bmatrix} x_0 \\ u_{0:k} \\ w_{0:k-1} \\ v_{0:k} \end{Bmatrix} \tag{2-108}$$

Here $\check{I}_{u_{k-d:k}} \triangleq [0_{n_u(d+1)\times n_u(k-d)} \quad I_{n_u(d+1)}] \in \mathbb{R}^{n_u(d+1)\times n_u(k+1)}$ and $\check{I}_{w_{k-d:k-1}} \triangleq [0_{nd\times n(k-d)} \quad I_{nd}] \in \mathbb{R}^{nd\times nk}$. Because of the identity matrices $I_{n_u(d+1)}$, I_{nd} and $I_{m(k+1)}$, the second to the fourth rows of the transformation matrix in Eq. (2-108) have full row-rank. To examine the first row of the transformation matrix, recall $H_{w_{k-d}}$ as

$$H_{w_{k-d}} = [A^{k-d-1} \quad \cdots \quad A \quad I_n \quad 0_{n\times nd}]$$

Due to the identity matrix I_n, $H_{w_{k-d}}$ has full row rank, and so does the first row. Because I_n in $H_{w_{k-d}}$, $I_{n_u(d+1)}$ in $\check{I}_{u_{k-d:k}}$, I_{nd} in $\check{I}_{w_{k-d:k-1}}$ and $I_{m(k+1)}$ in the last row are in different block columns, the entire transformation matrix in Eq. (2-108) has full row rank. It is also straightforward to verify that the matrix is fat. Therefore, x_{k-d}, $u_{k-d:k}$, $w_{k-d:k-1}$ and $y_{0:k}$ are also jointly Gaussian. Finally, as conditional distributions of jointly Gaussian random vector are Gaussian, given $y_{0:k-1}$, vectors x_{k-d}, $u_{k-d:k}$, $y_{0:k-1}$ and y_k are jointly Gaussian (and thus individually Gaussian). ■

In the following section, a recursive MMSE estimator for joint input-state estimation using d-step delayed measurements is derived.

2.3.2 Measurement Update of Input and State

To simplify later presentation, we define a compact notation xuw_{k-d} as follows:

$$xuw_{k-d} \triangleq \begin{Bmatrix} x_{k-d} \\ u_{k-d:k} \\ w_{k-d:k-1} \end{Bmatrix}$$

Prior estimates at time step $k-d$ are denoted as $\hat{x}_{k-d|k-1}$, $\hat{u}_{k-d:k|k-1}$, $\hat{w}_{k-d:k-1|k-1}$, and prior covariance is defined as

$$\Sigma_{xuw_{k-d|k-1}} \triangleq \begin{bmatrix} \Sigma_{x_{k-d|k-1}} & \Sigma_{x_{k-d}u_{k-d:k|k-1}} & \Sigma_{x_{k-d}w_{k-d:k-1|k-1}} \\ \Sigma_{u_{k-d:k}x_{k-d|k-1}} & \Sigma_{u_{k-d:k|k-1}} & \Sigma_{u_{k-d:k}w_{k-d:k-1|k-1}} \\ \Sigma_{w_{k-d:k-1}x_{k-d|k-1}} & \Sigma_{w_{k-d:k-1}u_{k-d:k|k-1}} & \Sigma_{w_{k-d:k-1|k-1}} \end{bmatrix} \tag{2-109}$$

With the prior estimates and prior covariances, state x_{k-d} and input $u_{k-d:k}$ given measurements $y_{0:k}$ are simultaneously estimated. The measurement equation (2-105) is first propagated back d steps to include the terms x_{k-d} and $u_{k-d:k}$:

$$\begin{aligned} y_k &= CA^d x_{k-d} + \tilde{P}_{u_d} u_{k-d:k} + \tilde{P}_{w_d} w_{k-d:k-1} + v_k \\ &= \begin{bmatrix} CA^d & \tilde{P}_{u_d} & \tilde{P}_{w_d} \end{bmatrix} xuw_{k-d} + v_k \end{aligned} \tag{2-110}$$

where $\tilde{P}_{u_d} \triangleq [CA^{d-1}B \quad \cdots \quad CB \quad D]$ as the last row of P_{u_d} (defined through P_{u_k} in Eq. (2-107)) and $\tilde{P}_{w_d} \triangleq [\,CA^{d-1} \quad \cdots \quad CA \quad C]$ as the last row of P_{w_d} (defined through P_{w_k} in Eq. (2-107)). Considering the independence of measurement noise v_k from past measurement sequence $y_{0:k-1}$, the conditional expectation of Eq. (2-110) given $y_{0:k-1}$ can be found as

$$\begin{aligned} \mathbb{E}(y_k|y_{0:k-1}) &= \begin{bmatrix} CA^d & \tilde{P}_{u_d} & \tilde{P}_{w_d} \end{bmatrix} \mathbb{E}(xuw_{k-d}|y_{0:k-1}) + \mathbb{E}(v_k) \\ &= CA^d \hat{x}_{k-d|k-1} + \tilde{P}_{u_d} \hat{u}_{k-d:k|k-1} + \tilde{P}_{w_d} \hat{w}_{k-d:k-1|k-1} \end{aligned} \tag{2-111}$$

As a result of Eq. (2-111), define the measurement residual (innovation) as

$$r_k \triangleq y_k - \mathbb{E}(y_k|y_{0:k-1})$$

$$= y_k - CA^d\hat{x}_{k-d|k-1} - \tilde{P}_{u_d}\hat{u}_{k-d:k|k-1} - \tilde{P}_{w_d}\hat{w}_{k-d:k-1|k-1} \tag{2-112}$$

Note that because process noise w_{k-1} is independent of $y_{0:k-1}$ based on Eq. (2-107), $\hat{w}_{k-1|k-1} = \mathbb{E}(w_{k-1}|y_{0:k-1}) = \mathbb{E}(w_{k-1}) = 0$. However, $w_{k-d:k-2}$ is not independent of $y_{0:k-1}$ and $\hat{w}_{k-d:k-2|k-1} = \mathbb{E}(w_{k-d:k-2}|y_{0:k-1}) \neq 0$. Based on the affine transformation in Eq. (2-110), the conditional cross-covariances is found as

$$\Sigma_{xuw_{k-d}y_{k|k-1}} = \Sigma_{xuw_{k-d|k-1}}\begin{bmatrix}(CA^d)^T\\ \tilde{P}_{u_d}^T\\ \tilde{P}_{w_d}^T\end{bmatrix} \tag{2-113}$$

The conditional variance of y_k given $y_{0:k-1}$ is

$$\Sigma_{y_{k|k-1}} = \begin{bmatrix}CA^d & \tilde{P}_{u_d} & \tilde{P}_{w_d}\end{bmatrix}\Sigma_{xuw_{k-d|k-1}}\begin{bmatrix}(CA^d)^T\\ \tilde{P}_{u_d}^T\\ \tilde{P}_{w_d}^T\end{bmatrix} + \Sigma_v \tag{2-114}$$

Note here according to Eq. (2-106) and (2-107) given $y_{0:k-1}$, the process noise vector $w_{k-d:k-2}$ is also not independent of x_{k-d} and $u_{k-d:k}$. On the other hand, because given $y_{0:k-1}$, measurement noise v_k is independent of x_{k-d}, $u_{k-d:k}$ and $w_{k-d:k-1}$, cross-covariances $\Sigma_{x_{k-d}v_{k|k-1}}$, $\Sigma_{u_{k-d:k}v_{k|k-1}}$ and $\Sigma_{w_{k-d:k-1}v_{k|k-1}}$ are all zero matrices. Expanding

the covariance matrix at right hand side of Eq. (2-113) with the nine block entries in (2-109) gives the following conditional covariances

$$\Sigma_{x_{k-d}y_{k|k-1}} = \Sigma_{x_{k-d|k-1}}(CA^d)^T + \Sigma_{x_{k-d}u_{k-d:k|k-1}}\tilde{P}_{u_d}^T + \Sigma_{x_{k-d}w_{k-d:k-1|k-1}}\tilde{P}_{w_d}^T \tag{2-115}$$

$$\Sigma_{u_{k-d:k}y_{k|k-1}} = \Sigma_{u_{k-d:k}x_{k-d|k-1}}(CA^d)^T + \Sigma_{u_{k-d:k|k-1}}\tilde{P}_{u_d}^T + \Sigma_{u_{k-d:k}w_{k-d:k-1|k-1}}\tilde{P}_{w_d}^T \tag{2-116}$$

$$\begin{aligned}\Sigma_{w_{k-d:k-1}y_{k|k-1}} = {} & \Sigma_{w_{k-d:k-1}x_{k-d|k-1}}(CA^d)^T + \Sigma_{w_{k-d:k-1}u_{k-d:k|k-1}}\tilde{P}_{u_d}^T \\ & + \Sigma_{w_{k-d:k-1|k-1}}\tilde{P}_{w_d}^T\end{aligned} \tag{2-117}$$

Recall given $y_{0:k-1}$, vectors x_{k-d}, $u_{k-d:k}$, $w_{k-d:k-1}$ and y_k are jointly Gaussian from Lemma 2-6, and Eq. (2-110) is an affine transformation of the Gaussian random vector xuw_{k-d}. Applying Eq. (2-3) in Lemma 2-3 to Eq. (2-110), the MMSE estimate of $x_{k-d}, u_{k-d:k}, w_{k-d:k-1}$ given y_k and $y_{0:k-1}$ (i.e. given $y_{0:k}$) is found as

$$\begin{aligned}\begin{Bmatrix}\hat{x}_{k-d|k}\\ \hat{u}_{k-d:k|k}\\ \hat{w}_{k-d:k-1|k}\end{Bmatrix} &\triangleq \mathbb{E}(xuw_{k-d}|y_{0:k}) \\ &= \begin{Bmatrix}\hat{x}_{k-d|k-1}\\ \hat{u}_{k-d:k|k-1}\\ \hat{w}_{k-d:k-1|k-1}\end{Bmatrix} + \Sigma_{xuw_{k-d|k-1}}\Sigma_{y_{k|k-1}}^{-1}\left(y_k - \mathbb{E}(y_k|y_{0:k-1})\right)\end{aligned} \tag{2-118}$$

Substitute Eq. (2-112) and (2-113) into (2-118),

$$\begin{Bmatrix}\hat{x}_{k-d|k}\\ \hat{u}_{k-d:k|k}\\ \hat{w}_{k-d:k-1|k}\end{Bmatrix} = \begin{Bmatrix}\hat{x}_{k-d|k-1} + L_{x_{k-d}}r_k\\ \hat{u}_{k-d:k|k-1} + L_{u_{k-d:k}}r_k\\ \hat{w}_{k-d:k-1|k-1} + L_{w_{k-d:k-1}}r_k\end{Bmatrix} \tag{2-119}$$

where the estimation gains are defined as

$$L_{x_{k-d}} \triangleq \Sigma_{x_{k-d}y_{k|k-1}}\Sigma_{y_{k|k-1}}^{-1} \tag{2-120}$$

$$L_{u_{k-d:k}} \triangleq \Sigma_{u_{k-d:k}y_{k|k-1}}\Sigma_{y_{k|k-1}}^{-1} \tag{2-121}$$

$$L_{w_{k-d:k-1}} \triangleq \Sigma_{w_{k-d:k-1}y_{k|k-1}}\Sigma_{y_{k|k-1}}^{-1} \tag{2-122}$$

Note that $\Sigma_{y_{k|k-1}}$, $\Sigma_{x_{k-d}y_{k|k-1}}$, $\Sigma_{u_{k-d:k}y_{k|k-1}}$ and $\Sigma_{w_{k-d:k-1}y_{k|k-1}}$ are given by Eq. (2-114) ~ (2-117). Based on Eq. (2-4) in Lemma 2-3, the conditional covariance after measurement update is given by

$$\Sigma_{xuw_{k-d|k}} \triangleq \begin{bmatrix} \Sigma_{x_{k-d|k}} & \Sigma_{x_{k-d}u_{k-d:k|k}} & \Sigma_{x_{k-d}w_{k-d:k-1|k}} \\ \Sigma_{u_{k-d:k}x_{k-d|k}} & \Sigma_{u_{k-d:k|k}} & \Sigma_{u_{k-d:k}w_{k-d:k-1|k}} \\ \Sigma_{w_{k-d:k-1}x_{k-d|k}} & \Sigma_{w_{k-d:k-1}u_{k-d:k|k}} & \Sigma_{w_{k-d:k-1|k}} \end{bmatrix}$$

$$= \Sigma_{xuw_{k-d|k-1}} - \begin{bmatrix} \Sigma_{x_{k-d}y_{k|k-1}} \\ \Sigma_{u_{k-d:k}y_{k|k-1}} \\ \Sigma_{w_{k-d:k-1}y_{k|k-1}} \end{bmatrix} \Sigma_{y_{k|k-1}}^{-1} \begin{bmatrix} \Sigma_{y_k x_{k-d|k-1}} & \Sigma_{y_k u_{k-d:k|k-1}} & \Sigma_{y_k w_{k-d:k-1|k-1}} \end{bmatrix} \tag{2-123}$$

In the following, Eq. (2-123) is expanded. The equations are simplified with the estimation gains defined in Eq. (2-120) ~ (2-122) as

$$\Sigma_{x_{k-d|k}} = \Sigma_{x_{k-d|k-1}} - L_{x_{k-d}}\Sigma_{x_{k-d}y_{k|k-1}}^{T} \tag{2-124}$$

$$\Sigma_{u_{k-d:k|k}} = \Sigma_{u_{k-d:k|k-1}} - L_{u_{k-d:k}}\Sigma_{u_{k-d:k}y_{k|k-1}}^{T} \tag{2-125}$$

$$\Sigma_{w_{k-d:k-1|k}} = \Sigma_{w_{k-d:k-1|k-1}} - L_{w_{k-d:k-1}}\Sigma_{w_{k-d:k-1}y_{k|k-1}}^{T} \tag{2-126}$$

$$\Sigma_{x_{k-d}u_{k-d:k|k}} = \Sigma_{x_{k-d}u_{k-d:k|k-1}} - \Sigma_{x_{k-d}y_{k|k-1}}L_{u_{k-d:k}}^{T} \tag{2-127}$$

$$\Sigma_{x_{k-d}w_{k-d:k-1|k}} = \Sigma_{x_{k-d}w_{k-d:k-1|k-1}} - \Sigma_{x_{k-d}y_{k|k-1}} L_{w_{k-d:k-1}}^T \tag{2-128}$$

$$\Sigma_{u_{k-d:k}w_{k-d:k-1|k}} = \Sigma_{u_{k-d:k}w_{k-d:k-1|k-1}} - L_{u_{k-d:k}} \Sigma_{w_{k-d:k-1}y_{k|k-1}}^T \tag{2-129}$$

Here $\Sigma_{x_{k-d|k-1}}$, $\Sigma_{u_{k-d:k|k-1}}$, $\Sigma_{w_{k-d:k-1|k-1}}$, $\Sigma_{x_{k-d}u_{k-d:k|k-1}}$, $\Sigma_{x_{k-d}w_{k-d:k-1|k-1}}$ and $\Sigma_{u_{k-d:k}w_{k-d:k-1|k-1}}$ are priors defined in Eq. (2-109). In practice, the measurement update equations of covariance in Eq. (2-124) ~ (2-129) do not guarantee the updated posterior covariance $\Sigma_{xuw_{k-d|k}}$ is symmetric positive definite. For example, for state covariance update equation (2-124), numerical errors may render the updated covariance $\Sigma_{x_{k-d|k}}$ to be non-symmetric positive definite. One simple technique (used in this implementation) is to first force the updated covariance $\Sigma_{x_{k-d|k}}$ to be symmetric by $\Sigma_{x_{k-d|k}} := \frac{1}{2}\left(\Sigma_{x_{k-d|k}} + \Sigma_{x_{k-d|k}}^T\right)$, and check the positive definiteness at each time step. Other techniques include modification of eigenvalues and square root filtering [75].

Thus far, measurement updates of state $\hat{x}_{k-d|k}$, input vector $\hat{u}_{k-d:k|k}$ and correlated process noise $\hat{w}_{k-d:k-1|k}$ have been derived. Based on Eq. (2-110), one advantage to include d-step delays is that not only the unknown input u_k at current time step is fed to measurement y_k, but also the input sequence from previous time steps $u_{k-d:k-1}$ is also fed to y_k. As a result, the unknown input at each time step is updated not just once but d times through the Markov parameters in the extended feedthrough matrix $\tilde{P}_{u_d} = [CA^{d-1}B \quad \cdots \quad CAB \quad CB \quad D]$.

2.3.3 Time Update of Input and State

Time update of state is straightforward using linear transformation. Based on (2-104), the state at time step $k-d+1$ can be re-written in the following form

$$x_{k-d+1} = [A \quad B \quad I]\begin{Bmatrix} x_{k-d} \\ u_{k-d} \\ w_{k-d} \end{Bmatrix} \tag{2-130}$$

Based on the linear transformation of Eq. (2-130), the estimate of x_{k-d+1} given $y_{0:k}$ is

$$\begin{aligned} \hat{x}_{k-d+1|k} &= \mathbb{E}(x_{k-d+1}|y_{0:k}) = [A \quad B \quad I]\mathbb{E}\left(\begin{Bmatrix} x_{k-d} \\ u_{k-d} \\ w_{k-d} \end{Bmatrix}\middle| y_{0:k}\right) \\ &= A\hat{x}_{k-d|k} + B\hat{u}_{k-d|k} + \hat{w}_{k-d|k} \end{aligned} \tag{2-131}$$

Note that $\mathbb{E}(w_{k-d}|y_{0:k})$ is no longer a zero vector because of the delayed measurements. The conditional covariance of state is given by

$$\begin{aligned} \Sigma_{x_{k-d+1|k}} &\triangleq \mathrm{cov}(x_{k-d+1}|y_{0:k}) \\ &= [A \quad B \quad I]\begin{bmatrix} \Sigma_{x_{k-d|k}} & \Sigma_{x_{k-d}u_{k-d|k}} & \Sigma_{x_{k-d}w_{k-\mathrm{d}|k}} \\ \Sigma_{u_{k-d}x_{k-d|k}} & \Sigma_{u_{k-d|k}} & \Sigma_{u_{k-d}w_{k-\mathrm{d}|k}} \\ \Sigma_{w_{k-d}x_{k-\mathrm{d}|k}} & \Sigma_{w_{k-d}u_{k-\mathrm{d}|k}} & \Sigma_{w_{k-d|k}} \end{bmatrix}\begin{bmatrix} A^T \\ B^T \\ I \end{bmatrix} \end{aligned} \tag{2-132}$$

In terms of time update of input, $u_{0:k}$ is assumed to be zero-mean white Gaussian. Based on Eq. (2-106), (2-107) and the white Gaussian assumption, u_{k+1} is independent from x_0, $u_{0:k}$, $w_{0:k}$ and $v_{0:k+1}$. Therefore, u_{k+1} is independent from x_{k-d+1} and $y_{0:k}$. As a result,

$$\hat{u}_{k-d+1:k+1|k} = \mathbb{E}\left(\begin{Bmatrix} u_{k-d+1:k} \\ u_{k+1} \end{Bmatrix} \middle| y_{0:k}\right) = \begin{Bmatrix} \hat{u}_{k-d+1:k|k} \\ 0 \end{Bmatrix} \tag{2-133}$$

$$\Sigma_{u_{k-d+1:k+1|k}} = \mathrm{cov}\left(\begin{Bmatrix} u_{k-d+1:k} \\ u_{k+1} \end{Bmatrix} \middle| y_{0:k}\right) = \begin{bmatrix} \Sigma_{u_{k-d+1:k|k}} & 0 \\ 0 & \Sigma_u \end{bmatrix} \tag{2-134}$$

For time update of the input-state cross-covariance $\Sigma_{x_{k-d+1}u_{k-d+1:k+1|k}} \triangleq \mathrm{cov}(x_{k-d+1}, u_{k-d+1:k+1}|y_{0:k})$, substitute x_{k-d+1} with Eq. (2-130):

$$\begin{aligned} \Sigma_{x_{k-d+1}u_{k-d+1:k+1|k}} &= \mathrm{cov}\left(Ax_{k-d} + Bu_{k-d} + w_{k-d}, \begin{Bmatrix} u_{k-d+1:k} \\ u_{k+1} \end{Bmatrix} \middle| y_{0:k}\right) \\ &= \begin{bmatrix} A\Sigma_{x_{k-d}u_{k-d+1:k|k}} + B\Sigma_{u_{k-d}u_{k-d+1:k|k}} + \Sigma_{w_{k-d}u_{k-d+1:k|k}} & 0 \end{bmatrix} \end{aligned} \tag{2-135}$$

Here $\Sigma_{x_{k-d}u_{k-d+1:k|k}}$, $\Sigma_{u_{k-d}u_{k-d+1:k|k}}$, and $\Sigma_{w_{k-d}u_{k-d+1:k|k}}$ can be obtained from the measurement update Eqs. (2-127), (2-125) and (2-129). For time update of the cross-covariance between state and process noise, recall that w_k is independent of x_{k-d+1} and $y_{0:k}$. As a result,

$$\begin{aligned} \Sigma_{x_{k-d+1}w_{k-d+1:k|k}} &\triangleq \mathrm{cov}(x_{k-d+1}, w_{k-d+1:k}|y_{0:k}) \\ &= \mathrm{cov}\left(Ax_{k-d} + Bu_{k-d} + w_{k-d}, \begin{Bmatrix} w_{k-d+1:k-1} \\ w_k \end{Bmatrix} \middle| y_{0:k}\right) \\ &= \begin{bmatrix} A\Sigma_{x_{k-d}w_{k-d+1:k-1|k}} + B\Sigma_{u_{k-d}w_{k-d+1:k-1|k}} + \Sigma_{w_{k-d}w_{k-d+1:k-1|k}} & 0 \end{bmatrix} \end{aligned} \tag{2-136}$$

For time update of the cross-covariance between input and process noise, recall that w_k is independent of $u_{k-d+1:k+1}$ and $y_{0:k}$. As a result,

$$\Sigma_{u_{k-d+1:k+1}w_{k-d+1:k|k}} \triangleq \mathrm{cov}(u_{k-d+1:k+1}, w_{k-d+1:k}|y_{0:k}) \tag{2-137}$$

$$= \operatorname{cov}\left(\begin{Bmatrix} u_{k-d+1:k} \\ u_{k+1} \end{Bmatrix}, \begin{Bmatrix} w_{k-d+1:k-1} \\ w_k \end{Bmatrix} \middle| y_{0:k}\right)$$

$$= \begin{bmatrix} \Sigma_{u_{k-d+1:k} w_{k-d+1:k-1|k}} & 0 \\ 0 & 0 \end{bmatrix}$$

Thus far, we have simultaneously estimated the state x_{k-d+1} and input u_{k-d+1} given $y_{0:k}$ when assuming $u_{0:k}$ is zero-mean white Gaussian with covariance Σ_u. Table 2-5 summarizes the FIC estimator with d-step delayed measurements.

Table 2-5 Input-state estimation of FIC estimator with d-step delayed measurements

Initialization:	
$\hat{x}_{0\|d-1} = \mu_{x_0},\ \Sigma_{x_{0\|d-1}} = \Sigma_{x_0}, \hat{u}_{0:d\|d-1} = \mu_{x_0}, \Sigma_{u_{0:d\|d-1}} = \operatorname{diag}(\Sigma_u),$ $\hat{w}_{0:d-1\|d-1} = 0, \Sigma_{w_{0:d-1\|d-1}} = \operatorname{diag}(\Sigma_w), \Sigma_{x_0 u_{0:d\|d-1}} = \Sigma_{x_0 w_{0:d-1\|d-1}} = \Sigma_{u_{0:d} w_{0:d-1\|d-1}} = 0$	
`for` $k = d, d+1, \ldots, n$	
Measurement update of input:	
$\Sigma_{y_{k\|k-1}} = \begin{bmatrix} CA^d & \tilde{P}_{u_d} & \tilde{P}_{w_d} \end{bmatrix} \Sigma_{xuw_{k-d\|k-1}} \begin{bmatrix} (CA^d)^T \\ \tilde{P}_{u_d}^T \\ \tilde{P}_{w_d}^T \end{bmatrix} + \Sigma_v$	Rept. (2-114)
$r_k = y_k - CA^d \hat{x}_{k-d\|k-1} - \tilde{P}_{u_d} \hat{u}_{k-d:k\|k-1} - \tilde{P}_{w_d} \hat{w}_{k-d:k-1\|k-1}$	Rept. (2-112)
$L_{u_{k-d:k}} = \Sigma_{u_{k-d:k} y_{k\|k-1}} \Sigma_{y_{k\|k-1}}^{-1}$	Rept. (2-121)
$\hat{u}_{k-d:k\|k} = \hat{u}_{k-d:k\|k-1} + L_{u_{k-d:k}} r_k$	Rept. (2-119)
$\Sigma_{u_{k-d:k\|k}} = \Sigma_{u_{k-d:k\|k-1}} - L_{u_{k-d:k}} \Sigma_{u_{k-d:k} y_{k\|k-1}}^T$	Rept. (2-125)
Measurement update of process noise:	
$L_{w_{k-d:k-1}} = \Sigma_{w_{k-d:k-1} y_{k\|k-1}} \Sigma_{y_{k\|k-1}}^{-1}$	Rept. (2-122)
$\hat{w}_{k-d:k-1\|k} = \hat{w}_{k-d:k-1\|k-1} + L_{w_{k-d:k-1}} r_k$	Rept. (2-119)
$\Sigma_{w_{k-d:k-1\|k}} = \Sigma_{w_{k-d:k-1\|k-1}} - L_{w_{k-d:k-1}} \Sigma_{w_{k-d:k-1} y_{k\|k-1}}^T$	Rept. (2-126)
Measurement update of state:	
$L_{x_{k-d}} = \Sigma_{x_{k-d} y_{k\|k-1}} \Sigma_{y_{k\|k-1}}^{-1}$	Rept. (2-120)

$$\hat{x}_{k-d|k} = \hat{x}_{k-d|k-1} + L_{x_{k-d}} r_k \quad \text{Rept. (2-119)}$$

$$\Sigma_{x_{k-d|k}} = \Sigma_{x_{k-d|k-1}} - L_{x_{k-d}} \Sigma^T_{x_{k-d} y_{k|k-1}} \quad \text{Rept. (2-124)}$$

Measurement update of cross-covariances

$$\Sigma_{x_{k-d} u_{k-d:k|k}} = \Sigma_{x_{k-d} u_{k-d:k|k-1}} - \Sigma_{x_{k-d} y_{k|k-1}} L^T_{u_{k-d:k}} \quad \text{Rept. (2-127)}$$

$$\Sigma_{x_{k-d} w_{k-d:k-1|k}} = \Sigma_{x_{k-d} w_{k-d:k-1|k-1}} - \Sigma_{x_{k-d} y_{k|k-1}} L^T_{w_{k-d:k-1}} \quad \text{Rept. (2-128)}$$

$$\Sigma_{u_{k-d:k} w_{k-d:k-1|k}} = \Sigma_{u_{k-d:k} w_{k-d:k-1|k-1}} - L_{u_{k-d:k}} \Sigma^T_{w_{k-d:k-1} y_{k|k-1}} \quad \text{Rept. (2-129)}$$

Time update of state:

$$\hat{x}_{k-d+1|k} = A\hat{x}_{k-d|k} + B\hat{u}_{k-d|k} + \hat{w}_{k-d|k} \quad \text{Rept. (2-131)}$$

$$\Sigma_{x_{k-d+1|k}} = \begin{bmatrix} A & B & I \end{bmatrix} \begin{bmatrix} \Sigma_{x_{k-d|k}} & \Sigma_{x_{k-d} u_{k-d|k}} & \Sigma_{x_{k-d} w_{k-d|k}} \\ \Sigma_{u_{k-d} x_{k-d|k}} & \Sigma_{u_{k-d|k}} & \Sigma_{u_{k-d} w_{k-d|k}} \\ \Sigma_{w_{k-d} x_{k-d|k}} & \Sigma_{w_{k-d} u_{k-d|k}} & \Sigma_{w_{k-d|k}} \end{bmatrix} \begin{bmatrix} A^T \\ B^T \\ I \end{bmatrix} \quad \text{Rept. (2-132)}$$

Time update of input:

$$\hat{u}_{k-d+1:k+1|k} = \begin{Bmatrix} \hat{u}_{k-d+1:k|k} \\ 0 \end{Bmatrix} \quad \text{Rept. (2-133)}$$

$$\Sigma_{u_{k-d+1:k+1|k}} = \begin{bmatrix} \Sigma_{u_{k-d+1:k|k}} & 0 \\ 0 & \Sigma_u \end{bmatrix} \quad \text{Rept. (2-134)}$$

Time update of cross-covariances:

$$\Sigma_{x_{k-d+1} w_{k-d+1:k|k}} = \begin{bmatrix} A\Sigma_{x_{k-d} w_{k-d+1:k-1|k}} + B\Sigma_{u_{k-d} w_{k-d+1:k-1|k}} + \Sigma_{w_{k-d} w_{k-d+1:k-1|k}} & 0 \end{bmatrix} \quad \text{Rept. (2-136)}$$

$$\Sigma_{u_{k-d+1:k+1} w_{k-d+1:k|k}} = \begin{bmatrix} \Sigma_{u_{k-d+1:k} w_{k-d+1:k-1|k}} & 0 \\ 0 & 0 \end{bmatrix} \quad \text{Rept. (2-137)}$$

$$\Sigma_{x_{k-d+1} u_{k-d+1:k+1|k}} = \begin{bmatrix} A\Sigma_{x_{k-d} u_{k-d+1:k|k}} + B\Sigma_{u_{k-d} u_{k-d+1:k|k}} + \Sigma_{w_{k-d} u_{k-d+1:k|k}} & 0 \end{bmatrix} \quad \text{Rept. (2-135)}$$

`end`

With delayed measurements, the estimator proposed in this section is able to relax the full column rank requirement without compromising estimator performance. Note that the invertibility condition in Section 2.3.1 is needed to guarantee all unknown inputs can be estimated. In addition, the two FIC estimators proposed in Section 2.1 and Section 2.2 can be combined by the delayed estimator.

2.3.4 Numerical Study: Partially Collocated Inputs and Measurements

This section discusses the scenario when there are multiple inputs and only a subset of inputs is collocated with the measurements, the feedthrough matrix D is non-zero but rank deficient. In this example, two input excitations are applied to the structure at the same time (Figure 2-9). The first input u_1 is again applied at the 4th DOF of the structure and an additional input u_2 is applied at the 2nd DOF, i.e. at mass m_2.

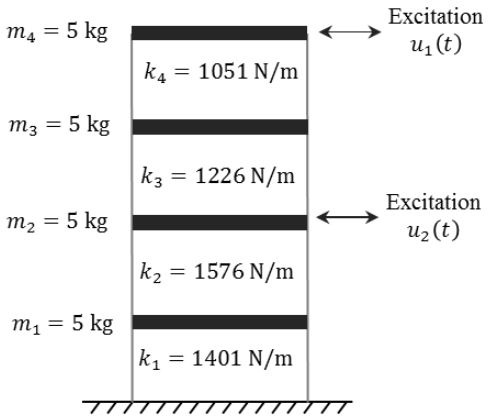

Figure 2-9 Four-story structural example: partially collocated inputs and measurements

Two types of input excitations are studied here. The first type of excitation is white Gaussian with a standard deviation of 10 N, i.e. $u_k \sim \mathcal{N}(0, 10^2)$. The second type of excitation is a mixed sinusoidal signal ranging from 1 Hz to 10 Hz. To study partially collocated inputs and measurements, acceleration measurement y is assumed available only at the first three DOFs, excluding the 4th DOF where input u_1 is applied. Therefore, the input location matrix is $\Gamma_u = \begin{bmatrix} 0 & 0 & 0 & 1 \\ 0 & 1 & 0 & 0 \end{bmatrix}^T$ and the output location matrix is $\Gamma_y = \begin{bmatrix} 1 & 0 & 0 & 0 \\ 0 & 1 & 0 & 0 \\ 0 & 0 & 1 & 0 \end{bmatrix}$. As a result, the continuous-time feedthrough matrix $D_c = \Gamma_y M^{-1} \Gamma_u =$

$\begin{bmatrix} 0 & 0 \\ 0 & 1/m_2 \\ 0 & 0 \end{bmatrix}$ is non-zero but does not have full column rank. The reason is one of the inputs, i.e. u_1, is not fed directly to the measurements, while the other input u_2 is fed to the measurements. A 2% modal damping ratio is assumed for the first two modes for the Rayleigh damping model. In addition, the continuous-time system is discretized through zero-order-hold with a time step of 0.005s. The simulated measurements are contaminated by noise with a standard deviation of $\sigma_v = 10^{-3}$ m/s^2 and sampled at 200 Hz.

Using simulated acceleration measurements, the performance of the FIC estimator (proposed in Section 2.1) and FIC estimator with delayed measurements (proposed in Section 2.2.5) are compared. For the delayed FIC estimator, the number of delayed time steps is denoted as d and the d-step delayed FIC estimator is denoted as FIC-d. Before applying the FIC-d delayed estimator, the minimum delayed time steps d required by the system invertibility condition, i.e. $\text{rank}(P_{u_d}) - \text{rank}(P_{u_{d-1}}) = n_u$, needs to be determined first. In this example, the resulting discrete feedthrough matrix D and the product of measurement and input matrices CB are

$$D = \begin{bmatrix} 0 & 0 \\ 0 & 0.2 \\ 0 & 0 \end{bmatrix}, CB = \begin{bmatrix} 1.87 \times 10^{-9} & 1.37 \times 10^{-3} \\ 1.52 \times 10^{-6} & -2.60 \times 10^{-3} \\ 9.15 \times 10^{-4} & 1.06 \times 10^{-3} \end{bmatrix}, CAB = \begin{bmatrix} 3.52 \times 10^{-8} & 2.87 \times 10^{-3} \\ 1.09 \times 10^{-5} & -5.31 \times 10^{-3} \\ 1.94 \times 10^{-3} & 2.24 \times 10^{-3} \end{bmatrix}$$

The rank of following matrices can thus be obtained.

$$P_{u_0} = D, P_{u_1} = \begin{bmatrix} D & 0 \\ CB & D \end{bmatrix}, P_{u_2} = \begin{bmatrix} D & 0 & 0 \\ CB & D & 0 \\ CAB & CB & D \end{bmatrix}, \cdots$$

Note that because CB has full column rank, i.e. $\text{rank}(CB) = n_u = 2$, we have $\text{rank}(P_{u_1}) - \text{rank}(P_{u_0}) = n_u$. Therefore, the minimum delayed time step d required by the invertibility condition is one. Furthermore, when d is larger than the minimum required steps, the invertibility condition still holds, e.g. when $d = 2$, $\text{rank}(P_{u_2}) - \text{rank}(P_{u_1}) = n_u$. As a result, the delayed time step is chosen as 1 in this example, denoted as FIC-1.

First, two independently generated white Gaussian inputs are applied to the structure for 15 seconds. For both FIC and FIC-1 estimators, the covariances and initial values are set the same as the white Gaussian scenario in Section 2.2.5.2, where the process and measurement noise covariances are set as $\Sigma_{w,sim} = \Sigma_{w,est} = 0$ and $\Sigma_{v,sim} = \Sigma_{v,est} = 10^{-6} I\ (\text{m/s}^2)^2$. The initial state and corresponding state estimation covariance are set as zero. The input covariances $\Sigma_{u,est}$ of the FIC estimator and the delayed FIC-1 estimator are both set as $100\ \text{N}^2$. Figure 2-10(a) shows the estimated inputs from both FIC and FIC-1 estimators during the initial 1s. Figure 2-10(b) shows the estimated inputs from FIC estimator during 13s ~ 14s, with the corresponding confidence interval $\pm 3\sigma_{u_{k|k}}$. While good estimate of the collocated input u_2 can be obtained, the FIC estimator cannot estimate the non-collocated input u_1. In contrast, the delayed FIC-1 estimator can estimate both inputs with a slightly larger error of the non-collocated input u_1 compared to the collocated input u_2 (Figure 2-10(a) and (c)). Figure 2-10(d) shows the time history of input estimation error covariance $\Sigma_{u_{k|k}}$ of FIC and FIC-1 estimators. The covariance of the collocated input from both estimators coincide. While the non-collocated input covariance from the FIC-1

estimator converges to a smaller steady state value, the one from the FIC estimator stays constant at the initial value.

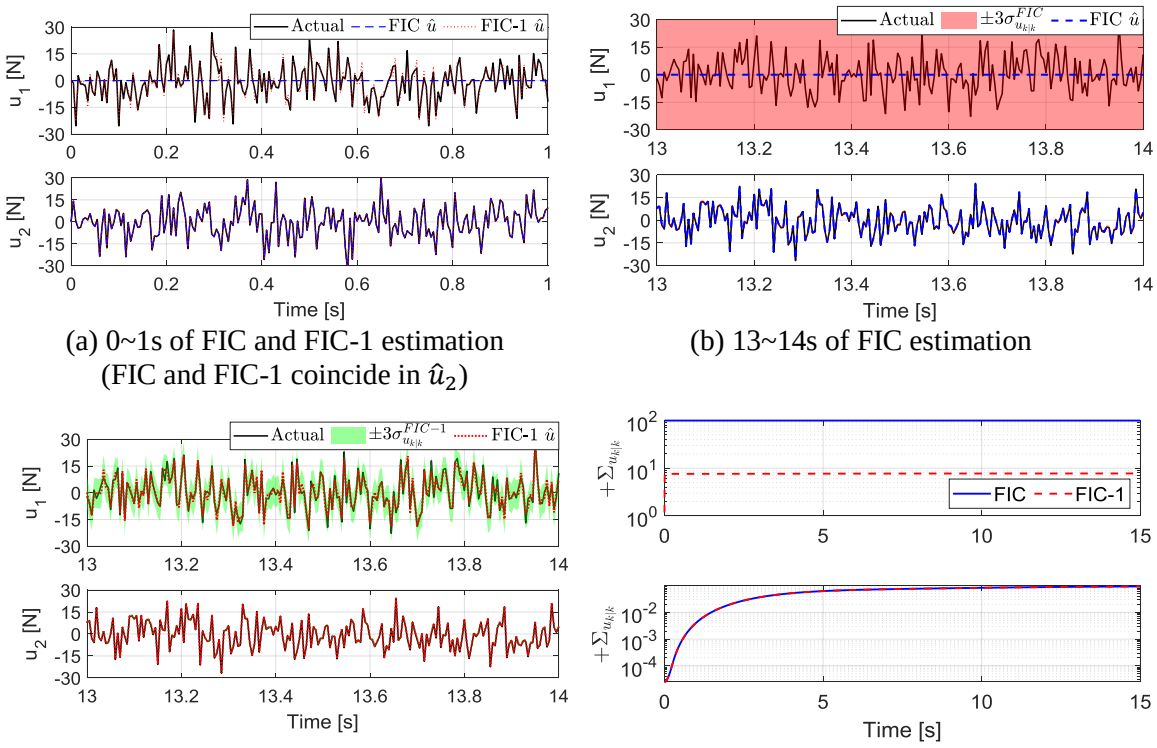

(a) 0~1s of FIC and FIC-1 estimation (FIC and FIC-1 coincide in $\hat{u}_2$)

(b) 13~14s of FIC estimation

(c) 13~14s of FIC-1 estimation

(d) Input estimation error covariance $\Sigma_{u_{k|k}}$ (FIC and FIC-1 coincide in $\Sigma_{u_{k|k}}$ of u_2)

Figure 2-10 Estimation of whtie Gaussian inputs: partially collocated scenario

Next, two mixed sinusoidal inputs from 1 Hz to 10 Hz with an increment of 1 Hz are used in this example. Magnitudes of each sinusoidal signal are uniformly randomly generated ranging from 1 N to 10 N. The sinusoidal signals are then added together as the mixed input, applied to excite the structure for 15 seconds. For both FIC and FIC-1 estimators, the process and measurement noise covariances are set as $\Sigma_{w,sim} = \Sigma_{w,est} = 0$ and $\Sigma_{v,sim} = \Sigma_{v,est} = 10^{-6} I\ (\mathrm{m/s^2})^2$. The initial state and corresponding state estimation covariance are set as zero. The input covariances $\Sigma_{u,est}$ of the FIC estimator and the

delayed FIC estimator are both set as 40 N^2. Figure 2-11(a) shows the input estimation of the FIC and FIC-1 estimators during the entire 15s. The FIC estimator can provide a relatively good estimate of the fed through input u_2, but unable to estimate the non-fed through input u_1 (Figure 2-11(b)). Figure 2-11(c) shows the corresponding input estimation of the FIC-1. After combining one-step delayed measurements, the FIC-1 estimator is able to estimate both inputs u_1 and u_2, with a better estimate of u_2. Figure 2-11(d) shows the time history of input estimation error covariance $\Sigma_{u_{k|k}}$ of FIC and FIC-1 estimation in logarithmic scale.

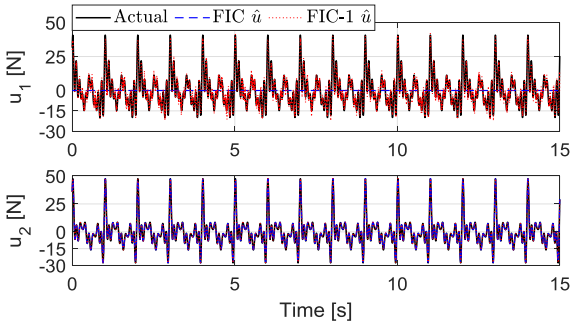

(a) 0~15s of FIC and FIC-1 estimation
(FIC and FIC-1 coincide in $\hat{u}_2$)

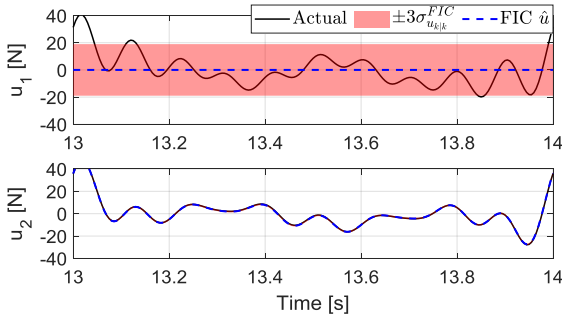

(b) 13~14s of FIC estimation

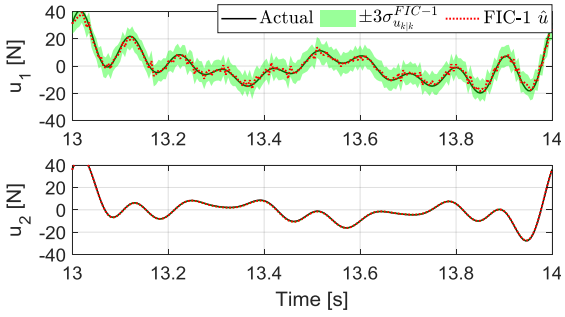

(c) 13~14s of FIC-1 estimation

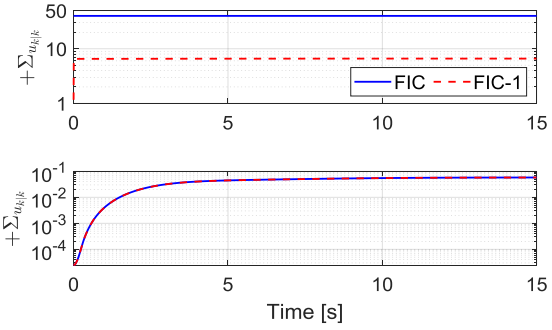

(d) Input estimation error covariance $\Sigma_{u_{k|k}}$
(FIC and FIC-1 coincide in $\Sigma_{u_{k|k}}$ of u_2)

Figure 2-11 Estimation of mixed sinusoidal inputs: partially collocated scenario

For the FIC estimator, the error covariance of the first input is constant over time and equal to $\Sigma_{u,est} = 40\ \mathrm{N}^2$, which means the estimator could not reduce the uncertainty in the unknown input from its initially assigned value $\Sigma_{u,est}$. In contrast, the input error covariance of the FIC-1 estimator converges to a relatively smaller value during steady state especially for the non-collocated input.

2.4 Summary

This chapter presents an MMSE framework to unify several different input-state estimators. For systems with direct feedthrough of the unknown input, a finite input covariance (FIC) estimator is proposed and compared with an augmented Kalman filter (AKF) and a weighted-least-squares (WLS) estimator. Detailed discussion on the choice of input covariance of the FIC estimator is also provided. Prior knowledge of the statistical property of the unknown input can be utilized to achieve good estimator performance. When only acceleration measurements are available, the FIC estimator is shown to reduce drift error with a tight estimation confidence interval. Compared to the AKF and WLS estimator, the FIC estimator is able to provide better estimation results for both input and state. In addition, based on the convergence plot of the input estimation covariances, both AKF and WLS estimator could not converge to steady state, while the FIC estimator converges within a few seconds.

For systems without direct feedthrough, the FIC estimator is again derived by propagating measurement equation one time step backward. Compared to the corresponding WLS estimator for systems without direct feedthrough, the FIC estimator is

again able to perform consistently better than the WLS estimator when acceleration measurements are not collocated with the unknown input. However, because the unknown input is not directly fed through to the measurements, both the FIC and WLS estimators perform worse than the results from systems with direct feedthrough.

To improve the estimator performance, delayed measurements are introduced and combined with the FIC estimator. The proposed delayed estimator is able to combine both systems with and without direct feedthrough of the input by relaxing the full-column rank requirement of the feedthrough matrix. Numerical study of partially collocated inputs and measurements, i.e. one measured input and one unmeasured input, is provided to show the improved performance after combining delayed measurements with the FIC estimator.

CHAPTER 3. SIMULTANEOUS ESTIMATION OF INPUT AND STATE WITH AN EXOGENOUS INPUT MODEL

This chapter generalizes the previous input-state estimator with an exogenous input model for systems with and without direct feedthrough. The generalization serves as a unified approach to obtain an input-state estimator in situations when the characteristics of the input is entirely unknown, partially known or fully known. Specifically, instead of assuming the input to be white Gaussian as in the previous chapter, knowledge of input frequency bandwidth can be incorporated into the exogenous input model to improve estimator performance. The same MMSE framework is used for both systems with and without direct feedthrough. Numerical studies using the same 4-story shear structure are provided, demonstrating improved input-state estimation results after combining an exogenous input model.

In this chapter, the unknown input u_k is assumed to be generated by an exogenous dynamical system with an internal state η_k as follows

$$\eta_{k+1} = A_\eta \eta_k + B_\eta \xi_k \tag{3-1}$$

$$u_k = C_\eta \eta_k + D_\eta \xi_k \tag{3-2}$$

Here A_η, B_η, C_η and D_η are the state space matrices of the input model; $\eta_k \in \mathbb{R}^{n_\eta}$ is the internal state of the input model at time step k; $\xi_k \in \mathbb{R}^{n_u}$ is a zero-mean white Gaussian

noise, i.e. $\xi_k \sim \mathcal{N}(0, \Sigma_\xi)$, which drives the exogenous input system and is set to have the same dimension as the input u_k. The number of internal state n_η is recommended to be equal or larger than the number of unknown inputs n_u. In addition, the exogenous input system is assumed to be both controllable and observable, i.e. the state space realization is minimal.

3.1 Exogenous Input Model for Systems with Direct Feedthrough

This section introduces simultaneous input-state estimation for systems with direct feedthrough and with an exogenous input model. The derivation process is similar as the previous chapter, while the state and input are augmented here to simply notations. The estimation is separated into three main stages, i.e. measurement update of the augmented states, input-state estimation and time update of the augmented states.

3.1.1 Problem Formulation

Consider the following discrete-time stochastic linear system with direct feedthrough of input:

$$x_{k+1} = Ax_k + Bu_k + w_k \tag{3-3}$$

$$y_k = Cx_k + Du_k + v_k \tag{3-4}$$

Here $x_k \in \mathbb{R}^n$ is the state at time step k, $u_k \in \mathbb{R}^{n_u}$ is the unknown input, $w_k \in \mathbb{R}^n$ is the process noise or disturbance, $y_k \in \mathbb{R}^m$ is the measurement output, and $v_k \in \mathbb{R}^m$ is the

measurement noise. The exogenous input model is combined with the dynamical system by substituting u_k from Eq. (3-1) into system equation (3-3) and measurement equation (3-4). The augmented state space system can be found as

$$x_{k+1} = Ax_k + BC_\eta \eta_k + BD_\eta \xi_k + w_k \tag{3-5}$$

$$y_k = Cx_k + DC_\eta \eta_k + DD_\eta \xi_k + v_k \tag{3-6}$$

In the augmented system, the state vector x_k in Eq. (3-5) and (3-6) and the state vector η_k of the exogenous input model form the augmented state $z_k \triangleq \begin{Bmatrix} x_k \\ \eta_k \end{Bmatrix} \in \mathbb{R}^{n_z}$, where $n_z = n + n_\eta$. The augmented system equations are:

$$z_{k+1} \triangleq \begin{Bmatrix} x_{k+1} \\ \eta_{k+1} \end{Bmatrix} = \begin{bmatrix} A & BC_\eta \\ 0 & A_\eta \end{bmatrix} \begin{Bmatrix} x_k \\ \eta_k \end{Bmatrix} + \begin{bmatrix} BD_\eta \\ B_\eta \end{bmatrix} \xi_k + \begin{bmatrix} I \\ 0 \end{bmatrix} w_k \triangleq A^a z_k + B^a \xi_k + \begin{bmatrix} I \\ 0 \end{bmatrix} w_k \tag{3-7}$$

$$y_k = \begin{bmatrix} C & DC_\eta \end{bmatrix} \begin{Bmatrix} x_k \\ \eta_k \end{Bmatrix} + DD_\eta \xi_k + v_k \triangleq C^a z_k + D^a \xi_k + v_k \tag{3-8}$$

Here A^a, B^a, C^a and D^a denote the state space matrices of the augmented system. The assumptions in this section are: (1) the original system is observable, i.e. (A, C) is observable; as a result, the rank of the observability matrix $\mathcal{O} = [C^T \quad (CA)^T \quad \cdots \quad (CA^{n-1})^T]^T$ equals the number of states n; (2) the exogenous input system is controllable and observable, i.e. (A_η, B_η) is controllable and (A_η, C_η) is observable; as a result, the controllability matrix $\mathcal{C}_\eta = \begin{bmatrix} B_\eta & A_\eta B_\eta & \cdots & A_\eta^{n_\eta - 1} B_\eta \end{bmatrix}$ and

the observability matrix $\mathcal{O}_\eta = \left[C_\eta^T \quad \left(C_\eta A_\eta\right)^T \quad \cdots \quad \left(C_\eta A_\eta^{n_\eta - 1}\right)^T\right]^T$ have full rank; (3) $v_k \sim \mathcal{N}(0, \Sigma_v)$, $w_k \sim \mathcal{N}(0, \Sigma_w)$ and $\xi_k \sim \mathcal{N}(0, \Sigma_\xi)$ are white Gaussian noise and Σ_v, Σ_w and Σ_ξ are diagonal matrices with $\Sigma_v \succ 0$, $\Sigma_w \succcurlyeq 0$ and $\Sigma_\xi \succ 0$; (4) v_k, w_l and ξ_m are independent for all k, l and m; (5) the initial augmented state is random $z_0 \sim \mathcal{N}\left(\mu_{z_0}, \Sigma_{z_0}\right)$ and independent from v_l, w_l and ξ_l for all l; in addition, $x_0 \sim \mathcal{N}(\mu_0, \Sigma_0)$ and $\eta_0 \sim \mathcal{N}\left(\mu_{\eta_0}, \Sigma_{\eta_0}\right)$ are independent, therefore, $\Sigma_{z_0} = \begin{bmatrix} \Sigma_0 & 0 \\ 0 & \Sigma_{\eta_0} \end{bmatrix}$. The following lemmas are provided to derive the joint input-state estimation algorithm.

Lemma 3-1 For the system given by Eq. (3-7) and (3-8) with the assumptions made in this section, z_k, ξ_k and $y_{0:k}$ are jointly Gaussian when $k \geq n_\eta$. If the augmented system matrix A^a has full row rank, z_k, ξ_k and $y_{0:k}$ are jointly Gaussian for all k. In addition, given $y_{0:k-1}$, the three random vectors z_k, ξ_k and y_k are jointly Gaussian under the same condition.

Proof. Based on Eq. (3-7) and (3-8), we can derive

$$z_k = (A^a)^k z_0 + H_{\xi_k} \xi_{0:k} + \breve{H}_{w_k} w_{0:k-1} \tag{3-9}$$

$$y_{0:k} = \mathcal{O}_{z_k} z_0 + P_{\xi_k} \xi_{0:k} + P_{w_k} w_{0:k-1} + v_{0:k} \tag{3-10}$$

where $H_{\xi_k} = \left[(A^a)^{k-1} B^a \quad \cdots \quad A^a B^a \quad B^a \quad 0_{n_z \times n_u}\right]$, $\breve{H}_{w_k} = \begin{bmatrix} A^{k-1} & \cdots & A & I_n \\ 0 & \cdots & 0 & 0 \end{bmatrix}$,

$$\mathcal{O}_{z_k} = \begin{bmatrix} C^a \\ C^a A^a \\ \vdots \\ C^a (A^a)^k \end{bmatrix}, P_{\xi_k} = \begin{bmatrix} D^a & 0 & \cdots & 0 \\ C^a B^a & \ddots & \cdots & \vdots \\ \vdots & \ddots & D^a & 0 \\ C^a (A^a)^{k-1} B^a & \cdots & C^a B^a & D^a \end{bmatrix}, P_{w_k} = \begin{bmatrix} 0 & 0 & 0 \\ C & \ddots & \vdots \\ \vdots & \ddots & 0 \\ CA^{k-1} & \cdots & C \end{bmatrix}.$$

Note that $z_0 \triangleq \begin{Bmatrix} x_0 \\ \eta_0 \end{Bmatrix}$, $\xi_{0:k}$, $w_{0:k-1}$ and $v_{0:k}$ are Gaussian and independent from each other, they are jointly Gaussian. Equation (3-11) shows that z_k, ξ_k and $y_{0:k}$ can be expressed as a linear transformation of z_0, $\xi_{0:k}$, $w_{0:k-1}$ and $v_{0:k}$

$$\begin{Bmatrix} z_k \\ \xi_k \\ y_{0:k} \end{Bmatrix} = \begin{bmatrix} (A^a)^k & H_{\xi_k} & \check{H}_{w_k} & 0 \\ 0 & \check{I}_{n_u} & 0 & 0 \\ \mathcal{O}_{z_k} & P_{\xi_k} & P_{w_k} & I_{m(k+1)} \end{bmatrix} \begin{Bmatrix} z_0 \\ \xi_{0:k} \\ w_{0:k-1} \\ v_{0:k} \end{Bmatrix} \tag{3-11}$$

where $\check{I}_{n_u} \triangleq [0 \quad I_{n_u}]$. Because of the identity matrices I_{n_u} and $I_{m(k+1)}$, the second and third rows of the transformation matrix in Eq. (3-11) have full row-rank. If the augmented matrix A^a has full row rank, the first row of the transformation matrix also has full row rank. To examine the rank of the first row when A^a does not have full row rank, H_{ξ_k} can be expanded as

$$H_{\xi_k} = \begin{bmatrix} * & \cdots & * & BD_\eta & 0_{n \times n_u} \\ A_\eta^{k-1} B_\eta & \cdots & A_\eta B_\eta & B_\eta & 0_{n_\eta \times n_u} \end{bmatrix}$$

Here $*$ denotes a non-zero block. Note that the number of the last zero columns in H_{ξ_k} equals to the dimension of $\xi_k \in \mathbb{R}^{n_u}$, i.e. there are n_u number of zero columns in H_{ξ_k}. Furthermore, these zero columns in H_{ξ_k} align with I_{n_u} in the second row of the

transformation matrix in Eq. (3-11) as $\check{I}_{n_u} \triangleq [0 \quad I_{n_u}]$. Therefore, with the expanded H_{ξ_k}, the 2×2 block $\begin{bmatrix} H_{\xi_k} & \check{H}_{w_k} \\ \check{I}_{n_u} & 0 \end{bmatrix}$ from the first two rows can be written as

$$\begin{bmatrix} H_{\xi_k} & \check{H}_{w_k} \\ \check{I}_{n_u} & 0 \end{bmatrix} = \begin{bmatrix} * & \cdots & * & BD_\eta & 0_{n\times n_u} & A^{k-1} & \cdots & A & I_n \\ A_\eta^{k-1}B_\eta & \cdots & A_\eta B_\eta & B_\eta & 0_{n_\eta \times n_u} & 0 & \cdots & 0 & 0 \\ 0 & \cdots & 0 & 0 & I_{n_u} & 0 & \cdots & 0 & 0 \end{bmatrix}$$

Because the input system is assumed to be controllable and $\mathcal{C}_\eta = \begin{bmatrix} B_\eta & A_\eta B_\eta & \cdots & A_\eta^{n_\eta - 1} B_\eta \end{bmatrix} \in \mathbb{R}^{n_\eta \times (n_u n_\eta)}$ has full row rank, $\begin{bmatrix} H_{\xi_k} & \check{H}_{w_k} \end{bmatrix}$ has full row rank for $k \geq n_\eta$.

As a result, the entire transformation matrix in Eq. (3-11) has full row rank. Therefore, z_k , ξ_k and $y_{0:k}$ are also jointly Gaussian. In addition, as conditional distributions of jointly Gaussian random vector are Gaussian, given $y_{0:k-1}$, vectors z_k, ξ_k and y_k are jointly and individually Gaussian. ■

In the following subsection, a recursive MMSE estimator for simultaneous input-state estimation of the augmented system is derived.

3.1.2 Measurement Update of Augmented State

Given prior estimates of the augmented state at time step k, i.e. $\hat{z}_{k|k-1}$ and $\Sigma_{z_{k|k-1}}$, the estimate of z_k given measurements $y_{0:k}$ is derived as follows. Considering the independence of measurement noise v_k from past measurement sequence $y_{0:k-1}$, given $y_{0:k-1}$ the conditional expectation of Eq. (3-8) is found as

$$\mathbb{E}(y_k|y_{0:k-1}) = \mathbb{E}(C^a z_k + D^a \xi_k + v_k|y_{0:k-1}) = [C^a \quad D^a]\mathbb{E}\left(\begin{Bmatrix} z_k \\ \xi_k \end{Bmatrix}\middle| y_{0:k-1}\right) \tag{3-12}$$

The input noise ξ_k is independent of $y_{0:k-1}$ based on Eq. (3-8), therefore

$$\hat{\xi}_{k|k-1} \triangleq \mathbb{E}(\xi_k|y_{0:k-1}) = \mathbb{E}(\xi_k) = 0 \tag{3-13}$$

$$\Sigma_{\xi_{k|k-1}} \triangleq \text{cov}(\xi_k|y_{0:k-1}) = \Sigma_\xi \tag{3-14}$$

Equation (3-12) can thus be simplified as

$$\mathbb{E}(y_k|y_{0:k-1}) = C^a \hat{z}_{k|k-1} \tag{3-15}$$

Similarly, because given $y_{0:k-1}$, ξ_k is also independent of z_k (from Eq. (3-7)) and v_k, $\Sigma_{z_k \xi_{k|k-1}} = 0$ and $\Sigma_{v_k \xi_{k|k-1}} = 0$. Recall Lemma 3-1 shows that given $y_{0:k-1}$, $\begin{Bmatrix} z_k \\ \xi_k \end{Bmatrix}$ and y_k are jointly Gaussian, and Eq. (3-8) is an affine transformation of the conditional Gaussian random vector $\begin{Bmatrix} z_k \\ \xi_k \end{Bmatrix}$. Based on the affine transformation, the conditional covariance of y_k given $y_{0:k-1}$ can be obtained as

$$\begin{aligned} \Sigma_{y_{k|k-1}} &= [C^a \quad D^a] \begin{bmatrix} \Sigma_{z_{k|k-1}} & 0 \\ 0 & \Sigma_\xi \end{bmatrix} \begin{bmatrix} (C^a)^T \\ (D^a)^T \end{bmatrix} + \Sigma_v \\ &= C^a \Sigma_{z_{k|k-1}} (C^a)^T + D^a \Sigma_\xi (D^a)^T + \Sigma_v \end{aligned} \tag{3-16}$$

In addition, given $y_{0:k-1}$ the conditional cross-covariance between $\begin{Bmatrix} z_k \\ \xi_k \end{Bmatrix}$ and y_k is found as

$$\Sigma_{\begin{Bmatrix} z_k \\ \xi_k \end{Bmatrix} y_{k|k-1}} \triangleq \begin{bmatrix} \Sigma_{z_k y_{k|k-1}} \\ \Sigma_{\xi_k y_{k|k-1}} \end{bmatrix} = \begin{bmatrix} \Sigma_{z_{k|k-1}} & 0 \\ 0 & \Sigma_{\xi} \end{bmatrix} \begin{bmatrix} (C^a)^T \\ (D^a)^T \end{bmatrix} = \begin{bmatrix} \Sigma_{z_{k|k-1}} (C^a)^T \\ \Sigma_{\xi} (D^a)^T \end{bmatrix} \tag{3-17}$$

Because the input noise ξ_k appears in measurement y_k, an estimate of ξ_k is needed for the input estimation later. Applying Eq. (2-3) in Lemma 2-3 to Eq. (3-12), the MMSE estimate of $\begin{Bmatrix} z_k \\ \xi_k \end{Bmatrix}$ given y_k and $y_{0:k-1}$ are shown in the following

$$\begin{aligned} \begin{Bmatrix} \hat{z}_{k|k} \\ \hat{\xi}_{k|k} \end{Bmatrix} &\triangleq \mathbb{E}\left(\begin{Bmatrix} z_k \\ \xi_k \end{Bmatrix} \middle| y_{0:k} \right) \\ &= \mathbb{E}\left(\begin{Bmatrix} z_k \\ \xi_k \end{Bmatrix} \middle| y_{0:k-1} \right) + \Sigma_{\begin{Bmatrix} z_k \\ \xi_k \end{Bmatrix} y_{k|k-1}} \Sigma_{y_{k|k-1}}^{-1} \left(y_k - \mathbb{E}(y_k | y_{0:k-1}) \right) \end{aligned} \tag{3-18}$$

Substituting Eq. (3-15) and (3-17) into Eq. (3-18), we obtain

$$\begin{Bmatrix} \hat{z}_{k|k} \\ \hat{\xi}_{k|k} \end{Bmatrix} = \begin{Bmatrix} \hat{z}_{k|k-1} + L_{z_k} \left(y_k - C^a \hat{z}_{k|k-1} \right) \\ L_{\xi_k} \left(y_k - C^a \hat{z}_{k|k-1} \right) \end{Bmatrix} \tag{3-19}$$

Here the estimation gains are defined and found as follows, using cross-covariances $\Sigma_{z_{k-1} y_{k|k-1}}$ and $\Sigma_{\xi_k y_{k|k-1}}$ from Eq. (3-17)

$$L_{z_k} \triangleq \Sigma_{z_k y_{k|k-1}} \Sigma_{y_{k|k-1}}^{-1} = \Sigma_{z_{k|k-1}} (C^a)^T \Sigma_{y_{k|k-1}}^{-1} \tag{3-20}$$

$$L_{\xi_k} \triangleq \Sigma_{\xi_k y_{k|k-1}} \Sigma_{y_{k|k-1}}^{-1} = \Sigma_{\xi} (D^a)^T \Sigma_{y_{k|k-1}}^{-1} \tag{3-21}$$

Based on Eq. (2-4) in Lemma 2-3, the measurement update of the conditional covariance of the augmented state is

$$\operatorname{cov}\left(\begin{Bmatrix} z_k \\ \xi_k \end{Bmatrix} \middle| y_{0:k}\right) \triangleq \begin{bmatrix} \Sigma_{z_{k|k}} & \Sigma_{z_k \xi_{k|k}} \\ \Sigma_{\xi_k z_{k|k}} & \Sigma_{\xi_{k|k}} \end{bmatrix}$$

$$= \begin{bmatrix} \Sigma_{z_{k|k-1}} & \Sigma_{z_k \xi_{k|k-1}} \\ \Sigma_{\xi_k z_{k|k-1}} & \Sigma_{\xi_{k|k-1}} \end{bmatrix} - \begin{bmatrix} \Sigma_{z_k y_{k|k-1}} \\ \Sigma_{\xi_k y_{k|k-1}} \end{bmatrix} \Sigma_{y_{k|k-1}}^{-1} \begin{bmatrix} \Sigma_{z_k y_{k|k-1}}^T & \Sigma_{\xi_k y_{k|k-1}}^T \end{bmatrix}$$

$$= \begin{bmatrix} \Sigma_{z_{k|k-1}} & 0 \\ 0 & \Sigma_{\xi} \end{bmatrix} - \begin{bmatrix} \Sigma_{z_k y_{k|k-1}} \\ \Sigma_{\xi_k y_{k|k-1}} \end{bmatrix} \Sigma_{y_{k|k-1}}^{-1} \begin{bmatrix} \Sigma_{z_k y_{k|k-1}}^T & \Sigma_{\xi_k y_{k|k-1}}^T \end{bmatrix} \tag{3-22}$$

This is further expanded and simplified with estimation gains L_{z_k} and L_{ξ_k}

$$\Sigma_{z_{k|k}} = \Sigma_{z_{k|k-1}} - \Sigma_{z_k y_{k|k-1}} \Sigma_{y_{k|k-1}}^{-1} \Sigma_{z_k y_{k|k-1}}^T = \Sigma_{z_{k|k-1}} - L_{z_k} C^a \Sigma_{z_{k|k-1}} \tag{3-23}$$

$$\Sigma_{\xi_{k|k}} = \Sigma_{\xi} - \Sigma_{\xi_k y_{k|k-1}} \Sigma_{y_{k|k-1}}^{-1} \Sigma_{\xi_k y_{k|k-1}}^T = \Sigma_{\xi} - L_{\xi_k} D^a \Sigma_{\xi} \tag{3-24}$$

The last step of Eq. (3-23) holds as a result of substituting Eq. (3-17) and (3-20). Similarly, the last step of Eq. (3-24) holds as a result of substituting Eq. (3-17) and (3-21). The cross-covariance measurement update equations from Eq. (3-22) is given by

$$\Sigma_{z_k \xi_{k|k}} = \Sigma_{\xi_k z_{k|k}}^T = -\Sigma_{z_k y_{k|k-1}} \Sigma_{y_{k|k-1}}^{-1} \Sigma_{\xi_k y_{k|k-1}}^T = -L_{z_k} D^a \Sigma_{\xi} \tag{3-25}$$

3.1.3 State and Input Estimation

Recall that the augmented state is defined as $z_k \triangleq \begin{Bmatrix} x_k \\ \eta_k \end{Bmatrix}$, the estimate of state x_k given measurement sequence $y_{0:k}$ can be found from the augmented state estimate $\hat{z}_{k|k}$:

$$\hat{x}_{k|k} = [I_n \quad 0]\hat{z}_{k|k} \tag{3-26}$$

$$\Sigma_{x_{k|k}} = [I_n \quad 0]\Sigma_{z_{k|k}}\begin{bmatrix} I_n \\ 0 \end{bmatrix} \tag{3-27}$$

From Eq. (3-2), the estimate of the input can be derived as follows

$$\begin{aligned}\hat{u}_{k|k} &\triangleq \mathbb{E}(u_k|y_{0:k}) = \mathbb{E}\big(C_\eta\eta_k + D_\eta\xi_k\big|y_{0:k}\big) = C_\eta\hat{\eta}_{k|k} + D_\eta\hat{\xi}_{k|k} \\ &= C_\eta[0 \quad I_\eta]\hat{z}_{k|k} + D_\eta\hat{\xi}_{k|k}\end{aligned} \tag{3-28}$$

where $I_\eta \in \mathbb{R}^{n_\eta \times n_\eta}$ is an identity matrix. Therefore, the noise estimate $\hat{\xi}_{k|k}$ is needed and can be found in Eq. (3-19). The input estimation error covariance is given as

$$\begin{aligned}\Sigma_{u_{k|k}} &\triangleq \mathrm{cov}(u_k|y_{0:k}) = \mathrm{cov}\big(C_\eta\eta_k + D_\eta\xi_k\big|y_{0:k}\big) \\ &= C_\eta\Sigma_{\eta_{k|k}}C_\eta^T + D_\eta\Sigma_{\xi_{k|k}}D_\eta^T + C_\eta\Sigma_{\eta_k\xi_{k|k}}D_\eta^T + D_\eta\Sigma_{\xi_k\eta_{k|k}}C_\eta^T \\ &= C_\eta[0 \quad I_{n_u}]\Sigma_{z_{k-1|k}}\begin{bmatrix} 0 \\ I_{n_u} \end{bmatrix}C_\eta^T + D_\eta\Sigma_{\xi_{k|k}}D_\eta^T \\ &\quad + C_\eta[0 \quad I_\eta]\Sigma_{z_k\xi_{k|k}}D_\eta^T + D_\eta\Sigma_{\xi_k z_{k|k}}\begin{bmatrix} 0 \\ I_\eta \end{bmatrix}C_\eta^T\end{aligned} \tag{3-29}$$

The relevant (cross-) covariance matrices can be found in Eq. (3-23) ~ (3-25).

3.1.4 Time Update of Augmented State

Time update of the augmented state is straightforward using linear transformation and system equations. Based on Eq. (3-7), the state at time step $k+1$ can be re-written in the following form

$$z_{k+1} = A^a z_k + B^a \xi_k + \begin{bmatrix} I \\ 0 \end{bmatrix} w_k = \begin{bmatrix} A^a & B^a \end{bmatrix} \begin{Bmatrix} z_k \\ \xi_k \end{Bmatrix} + \begin{bmatrix} I \\ 0 \end{bmatrix} w_k \tag{3-30}$$

Based on the affine transformation in Eq. (3-30), the estimate of z_{k+1} given $y_{0:k}$ can be written as

$$\hat{z}_{k+1|k} = \mathbb{E}\left(A^a z_k + B^a \xi_k + \begin{bmatrix} I \\ 0 \end{bmatrix} w_k \middle| y_{0:k} \right) = A^a \hat{z}_{k|k} + B^a \hat{\xi}_{k|k} \tag{3-31}$$

Because w_k is independent of $y_{0:k}$, $\mathbb{E}(w_k|y_{0:k}) = \mathbb{E}(w_k) = 0$ and $\operatorname{cov}\left(\begin{bmatrix} I \\ 0 \end{bmatrix} w_k \middle| y_{0:k} \right) = \operatorname{cov}\left(\begin{bmatrix} I \\ 0 \end{bmatrix} w_k \right) = \begin{bmatrix} \Sigma_w & 0 \\ 0 & 0 \end{bmatrix}$. In addition, because w_k is independent of z_k and ξ_k (Eq. (3-9)), cross-covariances $\Sigma_{z_k w_{k|k}} = 0$ and $\Sigma_{\xi_k w_{k|k}} = 0$. Based on the linear transformation in Eq. (3-30), the conditional covariance is thus given by

$$\Sigma_{z_{k+1|k}} = \operatorname{cov}(z_{k+1}|y_{0:k}) = \begin{bmatrix} A^a & B^a \end{bmatrix} \begin{bmatrix} \Sigma_{z_{k|k}} & \Sigma_{z_k \xi_{k|k}} \\ \Sigma_{\xi_k z_{k|k}} & \Sigma_{\xi_{k|k}} \end{bmatrix} \begin{bmatrix} (A^a)^T \\ (B^a)^T \end{bmatrix} + \begin{bmatrix} \Sigma_w & 0 \\ 0 & 0 \end{bmatrix} \tag{3-32}$$

Thus far, we have estimated the time updated augmented state $\hat{z}_{k+1|k}$ along with the measurement updated state estimate $\hat{x}_{k|k}$ and input estimate $\hat{u}_{k|k}$. Table 3-1 summarizes the proposed estimator for systems with direct feedthrough of the unknown input, assuming the input is generated by an exogenous system given by Eq. (3-1) and (3-2).

Table 3-1 Input-state estimation with exogenous input model for systems with feedthrough

Initialization: $\hat{z}_{0\|-1} = \mu_{z_0}, \Sigma_{z_{0\|-1}} = \Sigma_{z_0}$	
`for` $k = 0,\ 1,\ 2, \ldots, n$	
Measurement update of augmented state:	
$\Sigma_{y_{k\|k-1}} = C^a \Sigma_{z_{k\|k-1}} (C^a)^T + D^a \Sigma_\xi (D^a)^T + \Sigma_v$	Rept. (3-16)
$L_{z_k} = \Sigma_{z_{k\|k-1}} (C^a)^T \Sigma_{y_{k\|k-1}}^{-1}$	Rept. (3-20)
$\hat{z}_{k\|k} = \hat{z}_{k\|k-1} + L_{z_k}\left(y_k - C^a \hat{z}_{k\|k-1}\right)$	Rept. (3-19)
$\Sigma_{z_{k\|k}} = \Sigma_{z_{k\|k-1}} - L_{z_k} C^a \Sigma_{z_{k\|k-1}}$	Rept. (3-23)
Measurement update of correlated noise:	
$L_{\xi_k} = \Sigma_\xi (D^a)^T \Sigma_{y_{k\|k-1}}^{-1}$	Rept. (3-21)
$\hat{\xi}_{k\|k} = L_{\xi_k}\left(y_k - C^a \hat{z}_{k\|k-1}\right)$	Rept. (3-19)
$\Sigma_{\xi_{k\|k}} = \Sigma_\xi - L_{\xi_k} D^a \Sigma_\xi$	Rept. (3-24)
$\Sigma_{z_k \xi_{k\|k}} = \Sigma_{\xi_k z_{k\|k}}^T = -L_{z_k} D^a \Sigma_\xi$	Rept. (3-25)
Estimate of state and input:	
$\hat{x}_{k\|k} = [I_n \quad 0]\hat{z}_{k\|k}$	Rept. (3-26)
$\Sigma_{x_{k\|k}} = [I_n \quad 0]\Sigma_{z_{k\|k}} \begin{bmatrix} I_n \\ 0 \end{bmatrix}$	Rept. (3-27)
$\hat{u}_k = C_\eta [0 \quad I_\eta]\hat{z}_{k\|k} + D_\eta \hat{\xi}_{k\|k}$	Rept. (3-28)
$\Sigma_{u_{k\|k}} = C_\eta [0 \quad I_{n_u}]\Sigma_{z_{k-1\|k}} \begin{bmatrix} 0 \\ I_{n_u} \end{bmatrix} C_\eta^T + D_\eta \Sigma_{\xi_{k\|k}} D_\eta^T + C_\eta [0 \quad I_\eta]\Sigma_{z_k \xi_{k\|k}} D_\eta^T + D_\eta \Sigma_{\xi_k z_{k\|k}} \begin{bmatrix} 0 \\ I_\eta \end{bmatrix} C_\eta^T$	Rept. (3-29)
Time update of augmented state:	
$\hat{z}_{k+1\|k} = A^a \hat{z}_{k\|k} + B^a \hat{\xi}_{k\|k}$	Rept. (3-31)
$\Sigma_{z_{k+1\|k}} = [A^a \quad B^a] \begin{bmatrix} \Sigma_{z_{k\|k}} & \Sigma_{z_k \xi_{k\|k}} \\ \Sigma_{\xi_k z_{k\|k}} & \Sigma_{\xi_{k\|k}} \end{bmatrix} \begin{bmatrix} (A^a)^T \\ (B^a)^T \end{bmatrix} + \begin{bmatrix} \Sigma_w & 0 \\ 0 & 0 \end{bmatrix}$	Rept. (3-32)
`end`	

3.2 Exogenous Input Model for Systems without Direct Feedthrough

3.2.1 Problem Formulation

Consider the following discrete-time stochastic linear system without direct feedthrough of input:

$$x_{k+1} = Ax_k + Bu_k + w_k \tag{3-33}$$

$$y_k = Cx_k + v_k \tag{3-34}$$

Here $x_k \in \mathbb{R}^n$ is the state at time step k, $u_k \in \mathbb{R}^{n_u}$ is the unknown input, $w_k \in \mathbb{R}^n$ is the process noise or disturbance, $y_k \in \mathbb{R}^m$ is the measurement output, and $v_k \in \mathbb{R}^m$ is the measurement noise.

The exogenous input model given by Eq. (3-1) and (3-2) is combined with the dynamical system by substituting u_k and u_{k-1} with Eq. (3-2) into system equation Eq. (3-33) and back-propagated measurement equation (3-34), the state space system can then be expressed as

$$x_{k+1} = Ax_k + BC_\eta \eta_k + BD_\eta \xi_k + w_k \tag{3-35}$$

$$\begin{aligned} y_k &= CAx_{k-1} + CBu_{k-1} + Cw_{k-1} + v_k \\ &= CAx_{k-1} + CBC_\eta \eta_{k-1} + CBD_\eta \xi_{k-1} + Cw_{k-1} + v_k \end{aligned} \tag{3-36}$$

Similar as in Section 3.1, the state x_k in Eq. (3-35) and (3-36) is augmented with state η_k of the exogenous input model. The augmented state is denoted as $z_k \triangleq \begin{Bmatrix} x_k \\ \eta_k \end{Bmatrix} \in \mathbb{R}^{n_z}$. Augmented system equations can thus be rewritten as

$$z_k \triangleq \begin{Bmatrix} x_k \\ \eta_k \end{Bmatrix} = \begin{bmatrix} A & BC_\eta \\ 0 & A_\eta \end{bmatrix} \begin{Bmatrix} x_{k-1} \\ \eta_{k-1} \end{Bmatrix} + \begin{bmatrix} BD_\eta & I_n \\ B_\eta & 0 \end{bmatrix} \begin{Bmatrix} \xi_{k-1} \\ w_{k-1} \end{Bmatrix} \triangleq A^a z_{k-1} + B^a w_{k-1}^a \tag{3-37}$$

$$y_k = [CA \quad CBC_\eta] \begin{Bmatrix} x_{k-1} \\ \eta_{k-1} \end{Bmatrix} + [CBD_\eta \quad C] \begin{Bmatrix} \xi_{k-1} \\ w_{k-1} \end{Bmatrix} + v_k \triangleq C^a z_{k-1} + D^a w_{k-1}^a + v_k \tag{3-38}$$

Here A^a, B^a, C^a and D^a denote the state space matrices of the augmented system. Note that notations B^a, C^a and D^a in this subsection are different from those defined in Section 3.1 and will only be applicable in this subsection. The process noise w_k from the original system and the noise ξ_k from the exogenous input system are combined as the process noise of the augmented system, defined as $w_k^a \triangleq \begin{Bmatrix} \xi_k \\ w_k \end{Bmatrix} \in \mathbb{R}^{(n_u+n)}$. Similar as the systems without direct feedthrough from Chapter 2, the augmented process noise term w_{k-1}^a appears in measurement equation, making the process noise w_{k-1}^a in Eq. (3-37) correlated with the measurement y_k in Eq. (3-38). The augmented process noise covariance is given as follows

$$\Sigma_{w^a} \triangleq \mathbb{E}\left(\begin{Bmatrix} \xi_{k-1} \\ w_{k-1} \end{Bmatrix} \begin{Bmatrix} \xi_{k-1} \\ w_{k-1} \end{Bmatrix}^T \right) = \begin{bmatrix} \Sigma_\xi & 0 \\ 0 & \Sigma_w \end{bmatrix} \tag{3-39}$$

The assumptions in this section are the same as those stated in Section 3.1.1. The following lemma is provided to derive the joint input-state estimation algorithm for systems without feedthrough.

Lemma 3-2 For the system given by Eq. (3-37) and (3-38) with the assumptions made in Section 3.1.1, z_{k-1}, ξ_{k-1}, w_{k-1} and $y_{0:k}$ are jointly Gaussian when $k \geq n_\eta$. If the augmented system matrix A^a has full row rank, z_{k-1}, ξ_{k-1}, w_{k-1} and $y_{0:k}$ are jointly Gaussian for all k. In addition, given $y_{0:k-1}$, the four random vectors z_{k-1}, ξ_{k-1}, w_{k-1} and y_k are all jointly Gaussian under the same condition.

Proof. Based on Eq. (3-37) and (3-38), we can derive

$$z_{k-1} = (A^a)^{k-1} z_0 + H_{w_{k-1}^a} w_{0:k-1}^a \tag{3-40}$$

$$y_{0:k} = \mathcal{O}_{z_{k-1}} z_0 + P_{w_{k-1}^a} w_{0:k-1}^a + v_{0:k} \tag{3-41}$$

where $H_{w_{k-1}^a} = [(A^a)^{k-2}B^a \quad \cdots \quad A^aB^a \quad B^a \quad 0]$,

$$\mathcal{O}_{z_{k-1}} = \begin{bmatrix} \check{C} \\ C^a \\ C^aA^a \\ \vdots \\ C^a(A^a)^{k-1} \end{bmatrix} \text{ with } \check{C} = [C \quad 0],\ P_{w_{k-1}^a} = \begin{bmatrix} 0 & 0 & \cdots & 0 \\ D^a & 0 & \cdots & 0 \\ C^aB^a & D^a & \ddots & \vdots \\ \vdots & \ddots & \ddots & 0 \\ C^a(A^a)^{k-2}B^a & \cdots & C^aB^a & D^a \end{bmatrix}.$$

Note that because z_0, $w_{0:k-1}^a$ and $v_{0:k}$ are Gaussian and independent from each other, they are jointly Gaussian. In addition, z_{k-1}, w_{k-1}^a and $y_{0:k}$ can be expressed as a linear transformation of z_0, $w_{0:k-1}^a$ and $v_{0:k}$

$$\begin{Bmatrix} z_{k-1} \\ w_{k-1}^{a} \\ y_{0:k} \end{Bmatrix} = \begin{bmatrix} (A^{a})^{k-1} & H_{w_{k-1}^{a}} & 0 \\ 0 & \check{I}_{w^{a}} & 0 \\ \mathcal{O}_{z_{k-1}} & P_{w_{k-1}^{a}} & I_{m(k+1)} \end{bmatrix} \begin{Bmatrix} z_0 \\ w_{0:k-1}^{a} \\ v_{0:k} \end{Bmatrix} \tag{3-42}$$

where $\check{I}_{w^{a}} = [0 \quad I_{w^{a}}]$ contains the identity matrix $I_{w^{a}} \in \mathbb{R}^{(n_u+n)\times(n_u+n)}$. Because of the identity matrices $I_{w^{a}}$ and $I_{m(k+1)}$, the second and third rows of the transformation matrix in Eq. (3-42) have full row rank. If the augmented matrix A^{a} has full row rank, the first row of the transformation matrix also has full row rank. To examine the first two rows of the transformation matrix when A^{a} does not have full row rank, the two center blacks $\begin{bmatrix} H_{w_{k-1}^{a}} \\ \check{I}_{w^{a}} \end{bmatrix}$ can be expanded as

$$\begin{bmatrix} H_{w_{k-1}^{a}} \\ \check{I}_{w^{a}} \end{bmatrix} = \begin{bmatrix} (A^{a})^{k-2}B^{a} & \cdots & A^{a}B^{a} & B^{a} & 0 \\ 0 & \cdots & 0 & 0 & I_{w^{a}} \end{bmatrix}$$

$$= \begin{bmatrix} * & * & \cdots & * & A & BD_{\eta} & I_n & 0 \\ A_{\eta}^{k-1}B_{\eta} & 0 & \cdots & A_{\eta}B_{\eta} & 0 & B_{\eta} & 0 & 0 \\ 0 & 0 & \cdots & 0 & 0 & 0 & 0 & I_{w^{a}} \end{bmatrix}$$

Here $*$ denotes a non-zero block. Note that the number of the last zero columns in $H_{w_{k-1}^{a}}$ equals to the dimension of $w_k^{a} \in \mathbb{R}^{(n_u+n)}$, i.e. there are $n_u + n$ number of zero columns in $H_{w_{k-1}^{a}}$. Furthermore, these zero columns in $H_{w_{k-1}^{a}}$ align with $I_{w^{a}}$ in the second row of the transformation matrix in Eq. (3-42) as $\check{I}_{w^{a}} = [0 \quad I_{w^{a}}]$. Because the input system is assumed to be controllable and $\mathcal{C}_{\eta} = \begin{bmatrix} B_{\eta} & A_{\eta}B_{\eta} & \cdots & A_{\eta}^{n_{\eta}-1}B_{\eta} \end{bmatrix} \in \mathbb{R}^{n_{\eta}\times(n_u n_{\eta})}$ has full row rank, $H_{w_{k-1}^{a}}$ has full row rank for $k \geq n_{\eta}$. In addition, the entire transformation matrix

in Eq. (3-42) has full row rank. Therefore, z_{k-1}, w_{k-1}^a and $y_{0:k}$ are also jointly Gaussian. In addition, as conditional distributions of jointly Gaussian random vector are Gaussian, given $y_{0:k-1}$, each vector among z_{k-1}, w_{k-1}^a and y_k is Gaussian. ■

In the following section, a recursive MMSE estimator for joint input-state estimation of the augmented system is derived.

3.2.2 Measurement Update of Augmented State

Given prior estimates of the augmented state at time step $k-1$ (i.e. $\hat{z}_{k-1|k-1}$, $\Sigma_{z_{k-1|k-1}}$ and $\Sigma_{x_{k-1}u_{k-1|k-1}}$), the estimate of z_{k-1} given measurements $y_{0:k}$ is derived as follows. Considering the independence of measurement noise v_k from $y_{0:k-1}$, Eq. (3-38) is conditioned on $y_{0:k-1}$ as

$$\begin{aligned}\mathbb{E}(y_k|y_{0:k-1}) &= \mathbb{E}(C^a z_{k-1} + D^a w_{k-1}^a + v_k|y_{0:k-1}) \\ &= [C^a \quad D^a]\mathbb{E}\left(\begin{Bmatrix} z_{k-1} \\ w_{k-1}^a \end{Bmatrix}\middle| y_{0:k-1}\right)\end{aligned} \tag{3-43}$$

Recalling the independence assumptions, based on Eq. (3-41), the augmented process noise $w_{k-1}^a \triangleq [\xi_{k-1}^T \quad w_{k-1}^T]^T$ is independent of $y_{0:k-1}$,

$$\widehat{w}_{k-1|k-1}^a = \mathbb{E}(w_{k-1}^a|y_{0:k-1}) = \mathbb{E}(w_{k-1}^a) = 0 \tag{3-44}$$

$$\Sigma_{w_{k-1|k-1}^a} = \mathrm{cov}(w_{k-1}^a|y_{0:k-1}) = \Sigma_{w^a} \tag{3-45}$$

Equation (3-43) can thus be simplified as

$$\mathbb{E}(y_k|y_{0:k-1}) = C^a \hat{z}_{k-1|k-1} \tag{3-46}$$

Similarly, because given $y_{0:k-1}$, w_{k-1}^a is also independent of z_{k-1} (from Eq. (3-40) and (3-41)) and v_k, $\Sigma_{z_{k-1}w_{k-1|k-1}^a} = 0$ and $\Sigma_{v_k w_{k-1|k-1}^a} = 0$. Recall Eq. (3-42) shows that given $y_{0:k-1}$, $\begin{Bmatrix} z_{k-1} \\ w_{k-1}^a \end{Bmatrix}$ and y_k are jointly Gaussian, and Eq. (3-38) is an affine transformation of the Gaussian random vector $\begin{Bmatrix} z_{k-1} \\ w_{k-1}^a \end{Bmatrix}$. Based on the affine transformation given $y_{0:k-1}$, the conditional covariance of y_k can be obtained as

$$\begin{aligned} \Sigma_{y_{k|k-1}} &= \begin{bmatrix} C^a & D^a \end{bmatrix} \begin{bmatrix} \Sigma_{z_{k-1|k-1}} & 0 \\ 0 & \Sigma_{w^a} \end{bmatrix} \begin{bmatrix} (C^a)^T \\ (D^a)^T \end{bmatrix} + \Sigma_v \\ &= C^a \Sigma_{z_{k-1|k-1}} (C^a)^T + D^a \Sigma_{w^a} (D^a)^T + \Sigma_v \end{aligned} \tag{3-47}$$

In addition, given $y_{0:k-1}$, the conditional cross-covariance between z_{k-1}, w_{k-1}^a and y_k is found as

$$\Sigma_{\begin{Bmatrix} z_{k-1} \\ w_{k-1}^a \end{Bmatrix} y_{k|k-1}} \triangleq \begin{bmatrix} \Sigma_{z_{k-1}y_{k|k-1}} \\ \Sigma_{w_{k-1}^a y_{k|k-1}} \end{bmatrix} = \begin{bmatrix} \Sigma_{z_{k-1|k-1}} & 0 \\ 0 & \Sigma_{w^a} \end{bmatrix} \begin{bmatrix} (C^a)^T \\ (D^a)^T \end{bmatrix} = \begin{bmatrix} \Sigma_{z_{k-1|k-1}} (C^a)^T \\ \Sigma_{w^a} (D^a)^T \end{bmatrix} \tag{3-48}$$

Because the augmented process noise w_{k-1}^a appears in measurement y_k, an estimate of w_{k-1}^a is needed for the input estimation later. Applying Eq. (2-3) in Lemma 2-3 to Eq. (3-43), the MMSE estimate of $\begin{Bmatrix} z_{k-1} \\ w_{k-1}^a \end{Bmatrix}$ given y_k and $y_{0:k-1}$ are shown in the following

$$\begin{Bmatrix} \hat{z}_{k-1|k} \\ \hat{w}^a_{k-1|k} \end{Bmatrix} \triangleq \mathbb{E}\left(\begin{Bmatrix} z_{k-1} \\ w^a_{k-1} \end{Bmatrix} \middle| y_{0:k} \right)$$

$$= \mathbb{E}\left(\begin{Bmatrix} z_{k-1} \\ w^a_{k-1} \end{Bmatrix} \middle| y_{0:k-1} \right) + \Sigma_{\begin{Bmatrix} z_{k-1} \\ w^a_{k-1} \end{Bmatrix} y_{k|k-1}} \Sigma^{-1}_{y_{k|k-1}} \left(y_k - \mathbb{E}(y_k | y_{0:k-1}) \right) \tag{3-49}$$

Substitute Eq. (3-46) and (3-48) into Eq. (3-49),

$$\begin{Bmatrix} \hat{z}_{k-1|k} \\ \hat{w}^a_{k-1|k} \end{Bmatrix} = \begin{Bmatrix} \hat{z}_{k-1|k-1} + L_{z_{k-1}} \left(y_k - C^a \hat{z}_{k-1|k-1} \right) \\ L_{w^a_{k-1}} \left(y_k - C^a \hat{z}_{k-1|k-1} \right) \end{Bmatrix} \tag{3-50}$$

where the estimation gains are defined as follows

$$L_{z_{k-1}} \triangleq \Sigma_{z_{k-1} y_{k|k-1}} \Sigma^{-1}_{y_{k|k-1}} = \Sigma_{z_{k-1|k-1}} (C^a)^T \Sigma^{-1}_{y_{k|k-1}} \tag{3-51}$$

$$L_{w^a_{k-1}} \triangleq \Sigma_{w^a_{k-1} y_{k|k-1}} \Sigma^{-1}_{y_{k|k-1}} = \Sigma_{w^a} (D^a)^T \Sigma^{-1}_{y_{k|k-1}} \tag{3-52}$$

Note that $\Sigma_{z_{k-1} y_{k|k-1}}$ and $\Sigma_{w^a_{k-1} y_{k|k-1}}$ are given by Eq. (3-48). Based on Eq. (2-4) in Lemma 2-3, the measurement update of the augmented state covariance is

$$\begin{aligned} \operatorname{cov}\left(\begin{Bmatrix} z_{k-1} \\ w^a_{k-1} \end{Bmatrix} \middle| y_{0:k} \right) &\triangleq \begin{bmatrix} \Sigma_{z_{k-1|k}} & \Sigma_{z_{k-1} w^a_{k-1|k}} \\ \Sigma_{w^a_{k-1} z_{k-1|k}} & \Sigma_{w^a_{k-1|k}} \end{bmatrix} \\ &= \begin{bmatrix} \Sigma_{z_{k-1|k-1}} & 0 \\ 0 & \Sigma_{w^a} \end{bmatrix} - \begin{bmatrix} \Sigma_{z_{k-1} y_{k|k-1}} \\ \Sigma_{w^a_{k-1} y_{k|k-1}} \end{bmatrix} \Sigma^{-1}_{y_{k|k-1}} \begin{bmatrix} \Sigma^T_{z_{k-1} y_{k|k-1}} & \Sigma^T_{w^a_{k-1} y_{k|k-1}} \end{bmatrix} \end{aligned} \tag{3-53}$$

Equation (3-53) is further expanded and simplified with estimation gains $L_{z_{k-1}}$ and $L_{w^a_{k-1}}$

$$\Sigma_{z_{k-1|k}} = \Sigma_{z_{k-1|k-1}} - \Sigma_{z_{k-1}y_{k|k-1}}\Sigma_{y_{k|k-1}}^{-1}\Sigma_{z_{k-1}y_{k|k-1}}^{T} = \Sigma_{z_{k-1|k-1}} - L_{z_{k-1}}C^{a}\Sigma_{z_{k-1|k-1}} \quad (3\text{-}54)$$

$$\Sigma_{w_{k-1|k}^{a}} = \Sigma_{w^{a}} - \Sigma_{w_{k-1}^{a}y_{k|k-1}}\Sigma_{y_{k|k-1}}^{-1}\Sigma_{w_{k-1}^{a}y_{k|k-1}}^{T} = \Sigma_{w^{a}} - L_{w_{k-1}^{a}}D^{a}\Sigma_{w^{a}} \quad (3\text{-}55)$$

The last step of Eq. (3-54) holds as a result of substituting Eq. (3-48) and (3-51). Similarly, the last step of Eq. (3-55) holds as a result of substituting Eq. (3-48) and (3-52). The cross-covariance measurement update equations from Eq. (3-53) is given by

$$\Sigma_{z_{k-1}w_{k-1|k}^{a}} = \Sigma_{w_{k-1}^{a}z_{k-1|k}}^{T} = -\Sigma_{z_{k-1}y_{k|k-1}}\Sigma_{y_{k|k-1}}^{-1}\Sigma_{w_{k-1}^{a}y_{k|k-1}}^{T} = -L_{z_{k-1}}D^{a}\Sigma_{w^{a}} \quad (3\text{-}56)$$

3.2.3 State and Input Estimation

Recall that the augmented state is defined as $z_{k-1} \triangleq \begin{Bmatrix} x_{k-1} \\ \eta_{k-1} \end{Bmatrix}$. The estimate of state x_{k-1} given measurement sequence $y_{0:k}$ can be found from the augmented state estimate:

$$\hat{x}_{k-1|k} = [I_n \quad 0]\hat{z}_{k-1|k} \quad (3\text{-}57)$$

$$\Sigma_{x_{k-1|k}} = [I_n \quad 0]\Sigma_{z_{k-1|k}}\begin{bmatrix} I_n \\ 0 \end{bmatrix} \quad (3\text{-}58)$$

Recall that the augmented process noise is defined as $w_{k-1}^{a} \triangleq \begin{Bmatrix} \xi_{k-1} \\ w_{k-1} \end{Bmatrix}$. The estimate of the input noise ξ_{k-1} can thus be obtained from $\hat{w}_{k-1|k}^{a}$ by $\hat{\xi}_{k-1|k} = [I_\xi \quad 0]\hat{w}_{k-1|k}^{a}$, where

$\hat{w}^a_{k-1|k}$ is given by Eq. (3-50). From Eq. (3-2), the estimate of the input u_{k-1} can thus be found as follows

$$\begin{aligned}\hat{u}_{k-1|k} &\triangleq \mathbb{E}(u_{k-1}|y_{0:k}) = \mathbb{E}\left(C_\eta \eta_{k-1} + D_\eta \xi_{k-1}\middle| y_{0:k}\right) = C_\eta \hat{\eta}_{k-1|k} + D_\eta \hat{\xi}_{k-1|k} \\ &= C_\eta [0 \quad I_\eta] \hat{z}_{k-1|k} + D_\eta [I_\xi \quad 0] \hat{w}^a_{k-1|k}\end{aligned} \tag{3-59}$$

Therefore, the noise estimate $\hat{\xi}_{k-1|k}$ is needed to obtain $\hat{u}_{k-1|k}$. The corresponding conditional covariance $\Sigma_{\xi_{k-1|k}}$ can be obtained from $\Sigma_{w^a_{k-1|k}}$ as $\Sigma_{\xi_{k-1|k}} = [I_\xi \quad 0]\Sigma_{w^a_{k-1|k}} \begin{bmatrix} I_\xi \\ 0 \end{bmatrix}^T$, and the cross-covariance between the augmented state and input noise can be obtained as $\Sigma_{z_{k-1}\xi_{k-1|k}} = \Sigma_{z_{k-1}w^a_{k-1|k}} \begin{bmatrix} I_\xi \\ 0 \end{bmatrix}^T$. The corresponding input estimation error covariance is thus given as

$$\begin{aligned}\Sigma_{u_{k-1|k}} &\triangleq \mathrm{cov}(u_{k-1}|y_{0:k}) = \mathrm{cov}\left(C_\eta \eta_{k-1} + D_\eta \xi_{k-1}\middle| y_{0:k}\right) \\ &= C_\eta \Sigma_{\eta_{k-1|k}} C_\eta^T + D_\eta \Sigma_{\xi_{k-1|k}} D_\eta^T + C_\eta \Sigma_{\eta_{k-1}\xi_{k-1|k}} D_\eta^T + D_\eta \Sigma_{\xi_{k-1}\eta_{k-1|k}} C_\eta^T \\ &= C_\eta [0 \quad I_{n_u}] \Sigma_{z_{k-1|k}} \begin{bmatrix} 0 \\ I_{n_u} \end{bmatrix} C_\eta^T + D_\eta [I_\xi \quad 0] \Sigma_{w^a_{k-1|k}} \begin{bmatrix} I_\xi \\ 0 \end{bmatrix}^T D_\eta^T \\ &\quad + C_\eta [0 \quad I_\eta] \Sigma_{z_{k-1}w^a_{k-1|k}} \begin{bmatrix} I_\xi \\ 0 \end{bmatrix}^T D_\eta^T + D_\eta [I_\xi \quad 0] \Sigma_{w^a_{k-1}z_{k-1|k}} \begin{bmatrix} 0 \\ I_\eta \end{bmatrix} C_\eta^T\end{aligned} \tag{3-60}$$

The relevant (cross-) covariance matrices can be found in Eq. (3-54) ~ (3-56).

3.2.4 Time Update of Augmented State

Time update of the augmented state is straightforward using linear transformation and system equations. Based on Eq. (3-37), the augmented state at time step k can be re-written as follows

$$z_k = A^a z_{k-1} + B^a w_{k-1}^a = [A^a \quad B^a] \begin{Bmatrix} z_{k-1} \\ w_{k-1}^a \end{Bmatrix} \tag{3-61}$$

Based on the linear transformation in Eq. (3-61), the estimate of z_k given $y_{0:k}$ can be written as

$$\hat{z}_{k|k} = \mathbb{E}(A^a z_{k-1} + B^a w_{k-1}^a | y_{0:k}) = A^a \hat{z}_{k-1|k} + B^a \hat{w}_{k-1|k}^a \tag{3-62}$$

where $\hat{z}_{k-1|k}$ and $\hat{w}_{k-1|k}^a$ are given in Eq. (3-50). Note that $\mathbb{E}(w_{k-1}^a | y_{0:k})$ is not a zero vector according to Eq. (3-41). The conditional covariance is

$$\Sigma_{z_{k|k}} = \text{cov}(z_k | y_{0:k}) = [A^a \quad B^a] \begin{bmatrix} \Sigma_{z_{k-1|k}} & \Sigma_{z_{k-1} w_{k-1|k}^a} \\ \Sigma_{w_{k-1}^a z_{k-1|k}} & \Sigma_{w_{k-1|k}^a} \end{bmatrix} \begin{bmatrix} (A^a)^T \\ (B^a)^T \end{bmatrix} \tag{3-63}$$

Thus far, we have estimated the time updated augmented state $\hat{z}_{k|k}$ and found the measurement updated state estimate $\hat{x}_{k-1|k}$ and input estimate $\hat{u}_{k-1|k}$. Table 3-2 summarizes the proposed estimator for systems without direct feedthrough of the unknown input, assuming the input is generated by an exogenous system given by Eq. (3-1) and (3-2).

Table 3-2 Input-state estimation with exogenous input model for systems without feedthrough

Initialization: $\hat{z}_{0|0} = \mu_{z_0}, \Sigma_{z_{0|0}} = \Sigma_{z_0}$

`for` $k = 1,\ 2, \ldots, n$

Measurement update of augmented state:

$$\Sigma_{y_{k|k-1}} = C^a \Sigma_{z_{k-1|k-1}} (C^a)^T + D^a \Sigma_{w^a} (D^a)^T + \Sigma_v \quad \text{Rept. (3-47)}$$

$$L_{z_{k-1}} = \Sigma_{z_{k-1|k-1}} (C^a)^T \Sigma_{y_{k|k-1}}^{-1} \quad \text{Rept. (3-51)}$$

$$\hat{z}_{k-1|k} = \hat{z}_{k-1|k-1} + L_{z_{k-1}} \left(y_k - C^a \hat{z}_{k-1|k-1} \right) \quad \text{Rept. (3-50)}$$

$$\Sigma_{z_{k-1|k}} = \Sigma_{z_{k-1|k-1}} - L_{z_{k-1}} C^a \Sigma_{z_{k-1|k-1}} \quad \text{Rept. (3-54)}$$

Measurement update of correlated noise:

$$L_{w_{k-1}^a} = \Sigma_{w^a} (D^a)^T \Sigma_{y_{k|k-1}}^{-1} \quad \text{Rept. (3-52)}$$

$$\hat{w}_{k-1|k}^a = L_{w_{k-1}^a} \left(y_k - C^a \hat{z}_{k-1|k-1} \right) \quad \text{Rept. (3-50)}$$

$$\Sigma_{w_{k-1|k}^a} = \Sigma_{w^a} - L_{w_{k-1}^a} D^a \Sigma_{w^a} \quad \text{Rept. (3-55)}$$

$$\Sigma_{z_{k-1} w_{k-1|k}^a} = -L_{z_{k-1}} D^a \Sigma_{w^a} \quad \text{Rept. (3-56)}$$

Estimate of state and input:

$$\hat{x}_{k-1|k} = [I_n \quad 0] \hat{z}_{k-1|k} \quad \text{Rept. (3-57)}$$

$$\Sigma_{x_{k-1|k}} = [I_n \quad 0] \Sigma_{z_{k-1|k}} \begin{bmatrix} I_n \\ 0 \end{bmatrix} \quad \text{Rept. (3-58)}$$

$$\hat{u}_{k-1|k} = C_\eta [0 \quad I_\eta] \hat{z}_{k-1|k} + D_\eta [I_\xi \quad 0] \hat{w}_{k-1|k}^a \quad \text{Rept. (3-59)}$$

$$\begin{aligned} \Sigma_{u_{k-1|k}} = {} & C_\eta [0 \quad I_{n_u}] \Sigma_{z_{k-1|k}} \begin{bmatrix} 0 \\ I_{n_u} \end{bmatrix} C_\eta^T + D_\eta [I_\xi \quad 0] \Sigma_{w_{k-1|k}^a} \begin{bmatrix} I_\xi \\ 0 \end{bmatrix}^T D_\eta^T \\ & + C_\eta [0 \quad I_\eta] \Sigma_{z_{k-1} w_{k-1|k}^a} \begin{bmatrix} I_\xi \\ 0 \end{bmatrix}^T D_\eta^T + D_\eta [I_\xi \quad 0] \Sigma_{w_{k-1}^a z_{k-1|k}} \begin{bmatrix} 0 \\ I_\eta \end{bmatrix} C_\eta^T \end{aligned} \quad \text{Rept. (3-60)}$$

Time update of augmented state:

$$\hat{z}_{k|k} = A^a \hat{z}_{k-1|k} + B^a \hat{w}_{k-1|k}^a \quad \text{Rept. (3-62)}$$

$$\Sigma_{z_{k|k}} = [A^a \quad B^a] \begin{bmatrix} \Sigma_{z_{k-1|k}} & \Sigma_{z_{k-1} w_{k-1|k}^a} \\ \Sigma_{w_{k-1}^a z_{k-1|k}} & \Sigma_{w_{k-1|k}^a} \end{bmatrix} \begin{bmatrix} (A^a)^T \\ (B^a)^T \end{bmatrix} \quad \text{Rept. (3-63)}$$

`end`

3.3 Input Model with Limited Frequency Bandwidth

In this section, the proposed estimator with exogenous input model is first shown to be a generalized model of the previous estimators presented in Chapter 2. To improve estimator performance, an input model with limited frequency bandwidth is introduced next. In contrast to the white Gaussian assumption of the FIC estimator from Chapter 2, the input is assumed to have limited bandwidth in frequency domain.

First recall that the augmented Kalman filter (AKF), as described in Chapter 2, assumes a Gaussian random walk model for the unknown input. Table 3-3 shows that the input estimator for system with feedthrough (derived in Section 3.1) can be converted to AKF by setting the input u_k equal to the state η_k of the input model while keeping ξ_{k-1} as the noise term. Similarly, the FIC estimator for systems with and without feedthrough can be also obtained by setting the unknown input u_k directly equal to the noise term ξ_{k-1}. For AKF and FIC, the controllability condition of the input model is satisfied. In addition, because D_η is zero for both AKF and FIC estimators, noise term ξ_{k-1} does not appear in measurement y_k according to Eq. (3-6) and (3-38). Therefore, an estimate of ξ_{k-1} is not needed by the AKF and FIC estimators.

Table 3-3 Relationship between exogenous input models and other estimators

Estimator	Input model	State space matrices
AKF (Gaussian random walk)	$u_k = \eta_k = \eta_{k-1} + \xi_{k-1}$	$A_\eta = I, B_\eta = I, C_\eta = I, D_\eta = 0$
FIC (white Gaussian)	$u_k = \eta_k = \xi_{k-1}$	$A_\eta = 0, B_\eta = I, C_\eta = I, D_\eta = 0$

When prior knowledge of frequency property of the unknown input is available, an estimator combined with an input model with limited frequency bandwidth (LFB) is proposed here, short named as the LFB estimator. The filter input model of the LFB estimator can be low-pass, high-pass or bandpass filters based on the prior knowledge of the input frequency spectrum. Generally, when choosing a filter with limited frequency bandwidth, important design factors to consider include passband flatness and passband to stopband transition [76]. For example, if a steep transition is desired, Chebyshev type I filter can be used by allowing small passband ripples. If a maximally flat passband is desired, Butterworth filter may be used at an expense of the steepness in the transition. In terms of phase response of filter, because the input estimator is recursive and adaptive, phase shift from the filter does not have a significant effect on the estimated input, but a relatively linear phase response or constant time delay is recommended.

In this work, a digital Chebyshev type I filter with a specified frequency bandwidth is used in the LFB estimator with a small passband ripple. The filter is converted to discrete state space form and used as the input model. The dimension n_η of the resulting input state space model (Eq. (3-1)) equals the specified filter order multiplies number of unknown inputs, i.e. $n_\eta = n_u n_{\text{filter}}$. Note that D_η of the input model is no longer zero and an estimate of ξ_{k-1} is needed. One advantage of the LFB estimator over the FIC estimator is to utilize prior knowledge of frequency property of the unknown input, reducing the adverse effect of high-frequency noise on the estimator performance.

3.4 Numerical Studies

This section provides numerical validations of the LFB estimator in comparison to the FIC estimator for collocated and non-collocated input and measurements. The four-story lumped-mass shear structure from Chapter 2 is used to validate the LFB estimator when an input excitation force applied at the 4th DOF, i.e. at mass m_4 (Figure 3-1).

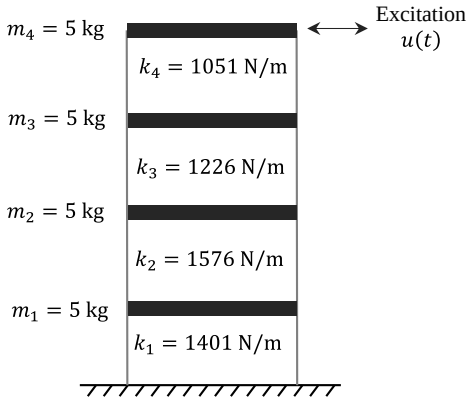

Figure 3-1 Four-story structural example

A 2% modal damping ratio is assumed for the first two modes based on the same Rayleigh damping model. Zero-order-hold discretization with a time step of 0.005s is used. For collocated input and measurements, the same 3Hz sinusoidal excitation described in Section 2.1.5.2 with an increased measurement noise level is used. For non-collocated input and measurements, the same mixed sinusoidal excitation described in Section 2.2.5.2 is used with a larger measurement noise level.

3.4.1 Collocated Input and Measurements

In this example, acceleration responses of all four DOFs of the structure are assumed to be measured, including the input DOF, which resulting in a non-zero

feedthrough matrix. A 3 Hz periodic sinusoidal input excitation with a magnitude of 10 N is used to excite the structure for 15 seconds. The simulated measurements are sampled at 200 Hz and contaminated by a relatively large measurement noise with a standard deviation of $\sigma_v = 10^{-1}\ \mathrm{m/s^2}$ (one hundred times larger than the one used in Section 2.1.5.2).

For direct comparison of the estimators, the standard deviation of measurement noise σ_v available to the estimators is assumed to be the same as the one used in the simulated measurements. Because the original state space system is accurate, and no modeling error is assumed in this example, process noise covariance Σ_w used in simulation and available to the estimators are both set as zero. The initial value μ_{x_0} and the diagonal entries of Σ_{x_0} are zero for both estimators, assuming the initial condition of the structure is static and known. For the input covariance required by the FIC estimator, Σ_u is set as 25 $\mathrm{N^2}$. For the LFB estimator, assuming prior knowledge of the input has a main frequency component between 2Hz to 4Hz, an 10^{th} order bandpass Chebyshev filter with a passband of 2 Hz to 4 Hz and a passband ripple of 0.1dB is used. The filter magnitude and phase response are shown in Figure 3-2.

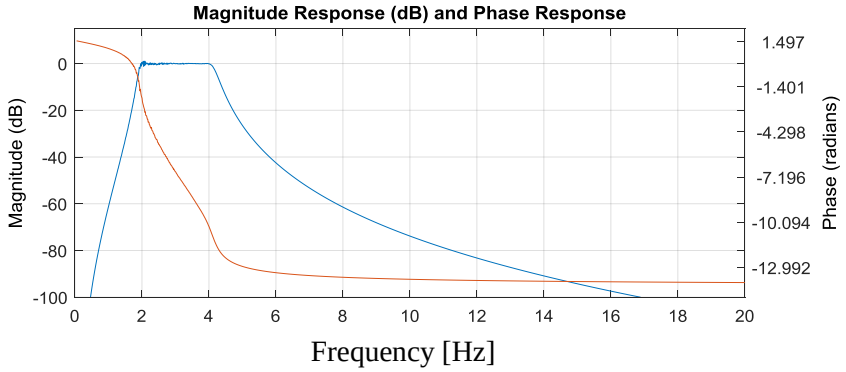

Figure 3-2 Filter response of the input model

The noise covariance Σ_ξ of the LFB estimator is set as 250, ten times larger than Σ_u of the FIC estimator. Compared to Σ_u of the FIC estimator, a larger covariance Σ_ξ of the LFB estimator is used because of the bandpass filter input model, which attenuates the input magnitude. Given the advantage of its limited bandwidth model, a large covariance Σ_ξ makes the LFB estimator more responsive to measurements without being affected by the increased measurement noise. In addition, the initial state $\hat{\eta}_0$ of the LFB estimator is set as zero and the initial state covariance Σ_{η_0} is set the same as Σ_ξ.

Figure 3-3 shows the comparison of input estimation results from the FIC estimator and the LFB estimator during the initial 0~1s and 13.5~14.5s. The confidence interval of three times square root of input estimation error covariance, $\pm 3\sigma_{u_{k|k}}$, is included in each of the close-up plot for the estimated input $\hat{u}_{k|k}$. With a large measurement noise level, the estimated input from the FIC estimator becomes noisier and less accurate (Figure 3-3(a)) than the one presented in Section 2.1.5.2. In contrast, the LFB estimator performs consistently better during the entire simulation, as shown in Figure 3-3(b).

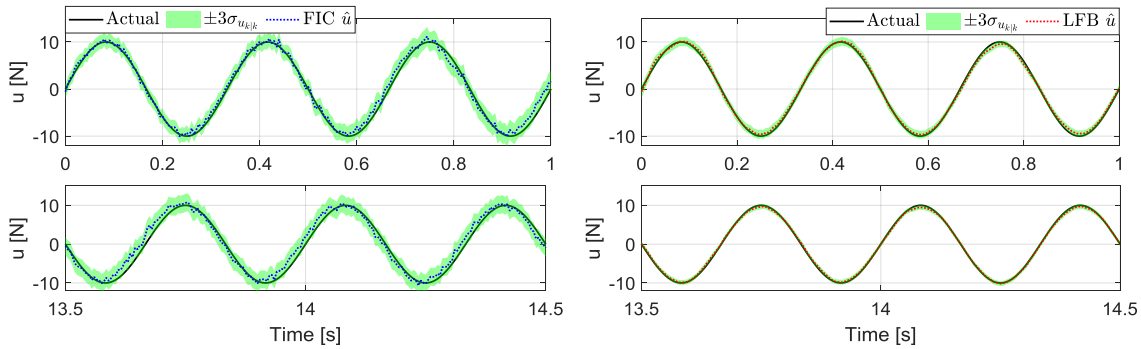

(a) 0~1s and 13.5~14.5s of FIC estimation (b) 0~1s and 13.5~14.5s of LFB estimation

Figure 3-3 Estimation of sinusoidal input: collocated input and measurements

Figure 3-4 shows the time history of input estimation error covariance $\Sigma_{u_{k|k}}$ from the FIC and LFB estimators in logarithmic scale. Both estimators converge to steady state, while the FIC estimator converges after around 3s and the LFB converges after around 5s. Similar phenomenon can be observed in states estimation results: estimation error covariances $\Sigma_{x_{k|k}}$ of all states from both estimators are able to converge within 5s, while the LFB estimator taking a slightly longer time to converge than the FIC estimator.

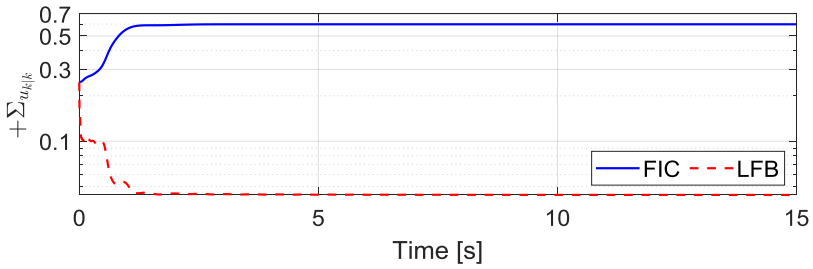

Figure 3-4 Time history of input estimation error covariance $\Sigma_{u_{k|k}}$: collocated input and measurements

3.4.2 Non-collocated Input and Measurements

In this example, acceleration responses of the first three DOFs of the structure, excluding the input DOF, are assumed to be measured. Because of the non-collocated input and measurements, the unknown input is not fed directly to the measurements. A mixed sinusoidal input excitation from 1 Hz to 10 Hz with an increment of 1 Hz is used in this example. Magnitudes of each sinusoidal signal are uniformly randomly generated ranging from 1 N to 10 N. The sinusoidal signals are then added together as the mixed input, applied to excite the structure for 15 seconds. The simulated measurements are contaminated by a

relatively large measurement noise with a standard deviation of $\sigma_v = 10^{-2}\ \mathrm{m/s^2}$ (ten times larger than the one used in Section 2.2.5.2) and sampled at 200 Hz.

Same as in Section 3.4.1, σ_v available to the estimators is assumed to be the same as the one used in the simulated measurements. No process noise w is used during simulation or estimation process, and the initial condition of the structure is assumed to be known. For the input covariance required by the FIC estimator, Σ_u is set as 150. For the LFB estimator, an 8th order low-pass Chebyshev filter with a cutoff frequency of 10 Hz and a passband ripple of 0.1dB is used. The noise covariance Σ_ξ of the LFB estimator is set as 1500 in this example, ten times larger than Σ_u of the FIC estimator. In addition, the initial state $\hat{\eta}_0$ of the LFB estimator is again set as zero and the initial state covariance Σ_{η_0} is set the same as Σ_ξ.

Figure 3-5 shows the input estimation comparison between the FIC and LFB estimators during the initial 0~1s and 13.5~14.5s. Because the input and measurements are not collocated in this example, measurement noise affects the performance of the FIC estimator more significantly (Figure 3-5(a)). Generally, a larger input covariance Σ_u makes the FIC estimator more responsive to measurements, but at the same time amplifies the noise effect in the input estimation results. In contrast, the LFB estimator mitigates the effect of large measurement noise on input estimation (Figure 3-5(b)) because of the limited bandwidth model, without losing responsiveness at the same time. Moreover, the input estimation interval from the LFB estimator is consistently smaller than the one from the FIC estimator.

Figure 3-6 shows the convergence time history of input estimation error covariance $\Sigma_{u_{k|k}}$ from the FIC and LFB estimators in logarithmic scale. The FIC estimator converges to steady state after around 0.05s, while the LFB estimator converges after 8s. However, the steady state value of $\Sigma_{u_{k|k}}$ from the FIC estimator is significantly larger than the LFB estimator, representing a larger uncertainty in the input estimation result.

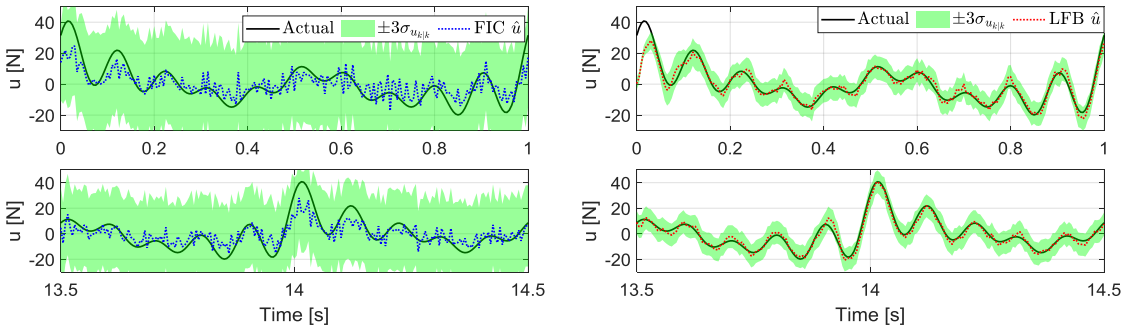

(a) 0~1s and 13.5~14.5s of FIC estimation

(b) 0~1s and 13.5~14.5s of LFB estimation

Figure 3-5 Estimation of mixed sinusoidal input: non-collocated input and measurements

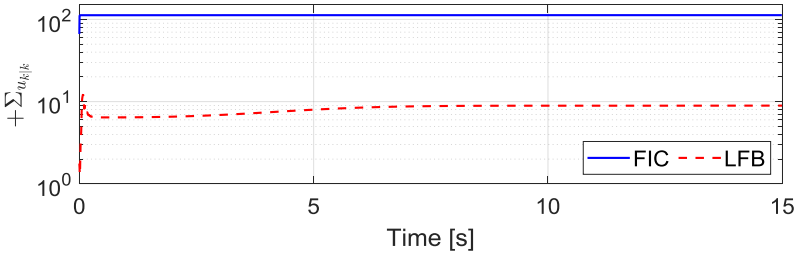

Figure 3-6 Time history of input estimation error covariance $\Sigma_{u_{k|k}}$: non-collocated input and measurements

3.5 Summary

This chapter presents derivations of an input-state estimator combined with an exogenous input model for systems with and without direct feedthrough of the unknown input. The input-state estimator is a generalization of the estimators described in Chapter

2. A limited frequency bandwidth (LFB) estimator is proposed as a special case of the exogenous input model to improve estimator performance, especially when measurement noise level is relatively high. Numerical examples of a 4-story shear structure are used to validate the proposed LFB estimator in comparison to the FIC estimator for collocated and non-collocated input and measurements. The LFB estimator is shown to be able to utilize prior frequency properties of the unknown input with improved estimation accuracy. The improvement by the LFB estimator is especially significant when sensor noise level is high, and the unknown input is not directly fed to the measurements.

CHAPTER 4. EXPERIMENTAL VALIDATION ON A FULL-SCALE CONCRETE FRAME

In this chapter, experimental acceleration measurements from a full-scale concrete frame structure are used to validate the proposed input-state estimators, including the finite input covariance (FIC) estimator from Section 2.1, the FIC estimator with delayed measurements (FIC-d) from Section 2.3 and the limited frequency bandwidth (LFB) estimator from Section 3.1. In addition, the traditional weighted least squares (WLS) estimator combined with an online drift filter is included for comparison. The test structure, sensor instrumentation and corresponding input excitation are first introduced. Based on experimental measurements from the concrete frame, structural modal properties are extracted using the Numerical Algorithms for Subspace State Space System Identification (N4SID) algorithm. To obtain a reliable system model for input-state estimation, material parameter values of a finite element (FE) model are updated by minimizing the differences between the experimentally identified modal properties and those generated from the FE model through non-convex optimization with multiple starting points.

Based on the updated FE model, structural mass and stiffness matrices are used to construct a state space dynamical model for simultaneous input-state estimation. To increase computational efficiency, modal decomposition is performed to reduce the system order. Based on the magnitude of the feedthrough matrix of the reduced-order system, effect of sensor instrumentation is also discussed. Two different sensor instrumentation scenarios are presented to compare the performance of different estimators. In the first

scenario, acceleration measurements including the input excitation location are used to estimate the input and state of the structure. In the second scenario, only measurements away from the input location are used during estimation.

4.1 Test Structure and Sensor Instrumentation

As shown in Figure 4-1(a), a set of four identical two-story two-bay concrete frames were constructed to compare different seismic retrofitting approaches. Each frame was constructed with a gap from its neighboring frames, allowing free in-plane longitudinal movement and can thus be tested independently from the other frames. Experimental data from frame #1 is used in this study. Figure 4-1(b) shows the frame consisting of two stories with a story height of 3.66 meters (12 ft) and two bays with a column spacing of 5.49 meters (18 ft). The width of the two elevated slabs are 2.74 meters (9 ft). When constructing the frame, concrete pouring was conducted in five stages, indicated by five different colors shown in Figure 4-1(b).

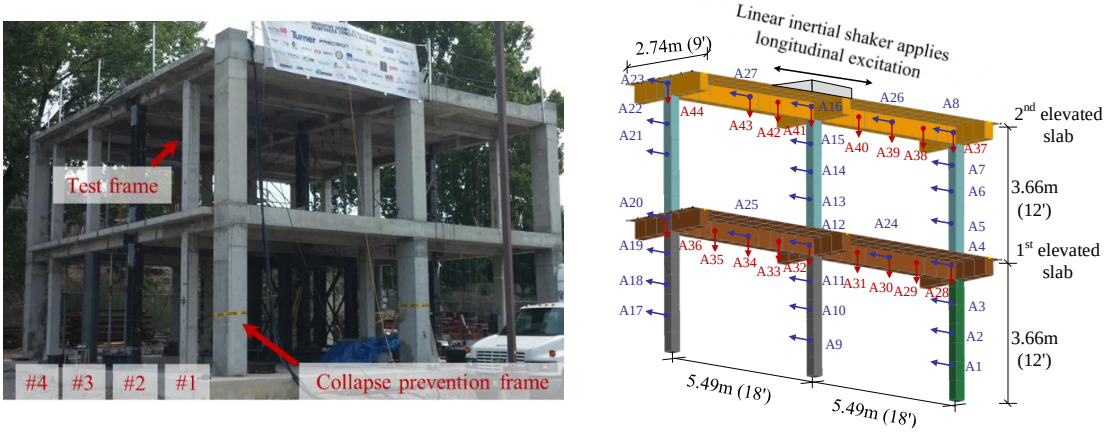

(a) Reinforced concrete frame (b) Accelerometer instrumentation

Figure 4-1 Full-scale test frame and sensor instrumentation

To provide excitation, a hydraulic linear inertia shaker was installed at the middle beam-column joint on the roof, i.e. the second elevated slab (Figure 4-1(b)). The moving mass on the shaker was used to generate in-plane excitation to the structure with a prescribed displacement record [70, 71]. In this study, the input is a scaled El Centro earthquake record with the maximum displacement of the shaker mass scaled to 25.4 mm (1 inch). The low-amplitude El Centro excitation caused little to no damage to the structure, thus the structure can be approximated as a linear system in this study. In order to calculate the exact shaker excitation force during the test, an accelerometer was installed on the moving mass of the shaker.

To measure the dynamic response of the frame, a total of 44 acceleration channels (Kinemetrics EpiSensor ES-T and ES-U) were instrumented on the structure, including 27 in-plane longitudinal directions and 17 vertical directions. Figure 4-1(b) illustrates the detailed sensor instrumentation of the frame. Specifically, the accelerometers were instrumented at mid-length and quarter length locations of columns and longitudinal beams. Structural acceleration response was sampled at 200 Hz during the shaker test. In post processing, the measured shaker input and structural responses were filtered by an 8^{th} order bandpass (1~40 Hz) Butterworth filter in both the forward and reverse directions to remove phase distortion.

Figure 4-2(a) shows the time history of 27 in-plane longitudinal acceleration measurements under shaker (El Centro 1 inch) excitation. Figure 4-2(b) shows the corresponding frequency spectrum of the longitudinal measurements. It can be seen that the shaker excited the structure more significantly in low frequency domain, i.e. below 10

Hz, while peaks with higher frequencies can still be observed. Figure 4-2(c) shows 17 in-plane vertical acceleration measurements. The magnitude of vertical structural response is smaller than those of in-plane longitudinal response as expected. Figure 4-2(d) shows the corresponding frequency spectrum of the vertical measurements. The main frequency components of the measured vertical response are in the range of 10 ~ 23 Hz. In the following section, structural modal properties, i.e. resonance frequencies and mode shapes, are extracted using both in-plane longitudinal and vertical measurements.

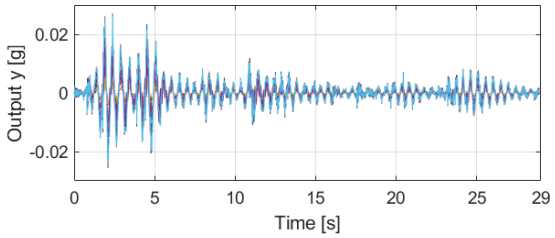

(a) Acceleration measurements of 27 in-plane longitudinal channels

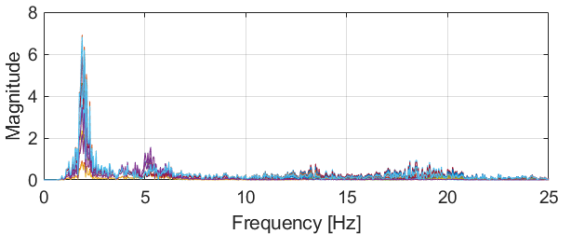

(b) Frequency spectrum of 27 in-plane longitudinal channels

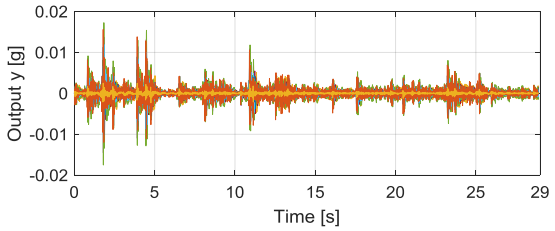

(c) Acceleration measurements of 17 in-plane vertical channels

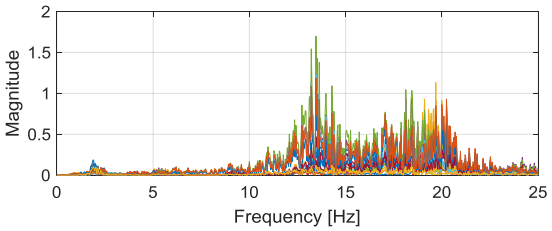

(d) Frequency spectrum of 17 in-plane vertical channels

Figure 4-2 Time history and frequency sepctrum of acceleration measurements

4.2 System Identification and Finite Element Model Updating

To a certain degree, an as-built civil structure always behaves differently from its corresponding FE model. The reason can be attributed to both model idealizations and inaccuracy in material property values. In order to provide a more reliable system model for later input-state estimation, parameter values of the FE model need to be updated based

on experimental measurements. This section utilizes a frequency domain approach to update the material parameter values of an FE model by minimizing the difference between experimentally identified modal properties and those of the FE model.

4.2.1 Modal Property Identification

Using in-plane longitudinal and vertical acceleration measurements during the shaker test, modal properties of the concrete frame are identified using the N4SID algorithm [77]. The N4SID algorithm is a numerical algorithm for subspace identification, which requires determination of system order. To obtain a reasonable system order and reliable identification results, a stabilization diagram (Figure 4-3) is used to visualize the identified resonance frequencies based on different system orders ranging from 20 to 80. A damping ratio threshold of 6% and a modal phase collinearity (MPC) [78] threshold of 0.85 are introduced in the stabilization diagram to remove fictitious identified modes. Specifically, MPC quantifies the collinearity between the real and imaginary parts of each identified complex-valued mode shape vector. The closer MPC value gets to one, the more likely the identified mode shape is an actual mode of a lightly damped civil structure.

Based on the stabilization diagram, four modes are reliably identified and a system order of 50 is chosen for the system, which gives the best overall identification results. The corresponding MPC values of the four modes are relatively high (above 0.9), and the MPC values of the first two modes are very close to one, which means the entries of the complex vector almost reside on a straight line across the origin on the complex plane.

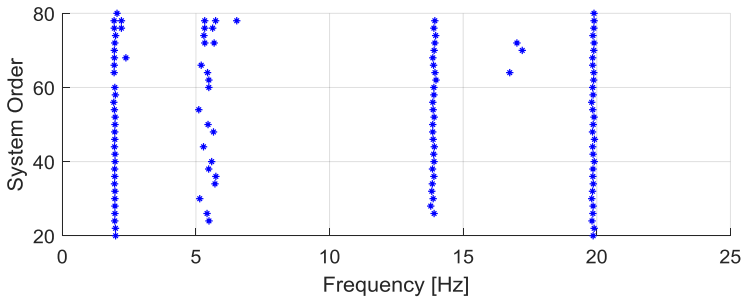

Figure 4-3 Stabilization diagram of N4SID system identification results

To plot the identified mode shapes, the complex-valued mode shape vectors are converted to real-valued vectors using the mean phase angle obtained from MPC calculation. Specifically, the complex-valued vectors are rotated first based on the mean phase angle to align with the real axis. By taking the real part of the rotated vectors, the real-valued mode shape vectors can be obtained. Figure 4-4 shows the resulting real-valued mode shapes of the four identified modes along with the corresponding identified resonance frequencies and damping ratios. Sensor locations are marked as solid blue dots. The first two modes mainly consist of in-plane longitudinal movement of columns, which is in the same direction as the shaker excitation. In contrast, higher modes are mainly characterized by vertical movement of beams.

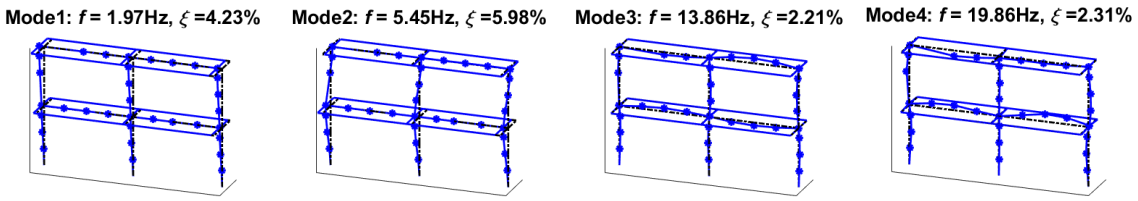

Figure 4-4 Experimentally identified modes under shaker excitation

4.2.2 Finite Element Model Updating with Experimental Measurements

An FE model of the concrete frame is built in SAP2000 (Figure 4-5). The beams and columns are modeled using beam elements and the two elevated slabs are modeled using thin-shell elements. The mesh size of the FE model is around 50.8 cm (20 in), and there is a total of 2,482 degrees-of-freedom (DOFs). The total weight of the structure includes both structural self-weight and the weight of the shaker. The initial FE model utilizes nominal material properties of the concrete, obtained from cylinder tests from five concrete pours. Fixed-end boundary condition is applied at the end of the three columns. In addition, out-of-plane translational DOF of each transverse beam is restrained to match with the experimental setup.

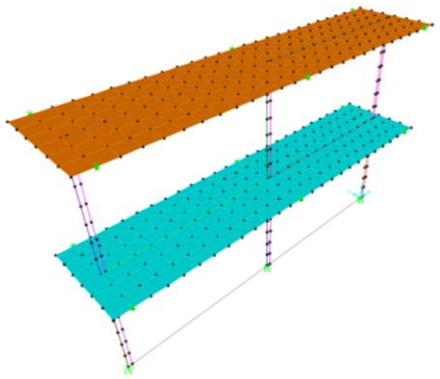

Figure 4-5 FE model of the concrete frame

To update the model, five concrete moduli of the FE model (corresponding to the five pours indicated by different colors in Figure 4-1(b)) are selected for updating. Note that in this study, the mass density of the structure is assumed to be relatively close to the assigned nominal value and hence structural stiffness is chosen for updating. The structural

stiffness matrix can thus be parameterized on the five concrete moduli as $K(\alpha) = K_0 + \sum_{i=1}^{n_\alpha} \alpha_i K_i$. Here $\alpha \in \mathbb{R}^{n_\alpha}$ is a vector representing the relative changes of elastic moduli from nominal values and treated as the updating variables ($n_\alpha = 5$); K_0 is the initial stiffness matrix before model updating and using nominal concrete moduli; and K_i is a constant stiffness matrix contributed by structural members from one pour and corresponding to one α_i. In the following, two updating approaches are used to update the concrete elastic moduli based on experimental modal analysis results from Section 4.2.1. The main difference between the two updating approaches is in handling the differences between mode shape vectors: the first approach uses modal assurance criterion (MAC) to quantify the similarity between the experimentally identified mode shape vectors and those of the FE model, while the second approach minimizes the difference of the normalized mode shape vectors from experiment and FE model directly.

4.2.2.1 MAC Value Approach

First, the MAC value approach is used to update the concrete moduli of the FE model. Similarities in mode shape vectors between the FE model and experimental results are quantified using MAC in this approach. For the *i*-th mode, the criterion is defined as $\mathrm{MAC}_i = \left(\left(\psi_i^{\mathrm{EXP,m}}\right)^{\mathrm{T}} \psi_i^{\mathrm{m}}\right)^2 \Big/ \left(\left\|\psi_i^{\mathrm{EXP,m}}\right\|_2^2 \|\psi_i^{\mathrm{m}}\|_2^2\right)$. Here, $\psi_i^{\mathrm{EXP,m}}$ denotes the experimentally identified mode shape vector, and ψ_i^{m} denotes the simulated mode shape vector at measured DOFs, obtained by solving the generalized eigenvalue problem between the stiffness matrix and mass matrix of the FE model. An optimization problem is

formulated as follows to minimize the modal property differences between the FE model and experiments.

$$\underset{\alpha}{\text{minimize}} \quad \sum_{i=1}^{n_{\text{modes}}} \left\{ \left(\frac{\lambda_i^{\text{EXP}} - \lambda_i(\alpha)}{\lambda_i^{\text{EXP}}} \cdot w_{\lambda_i} \right)^2 + \left(\frac{1 - \sqrt{\text{MAC}_i}}{\sqrt{\text{MAC}_i}} \cdot w_{\psi_i} \right)^2 \right\} \tag{4-1a}$$

$$\text{subject to} \quad L_\alpha \leq \alpha \leq U_\alpha \tag{4-1b}$$

Here L_α and U_α denote the lower and upper bounds of the updating variable α; n_{modes} denotes the number of modes used for updating; λ_i denotes the *i*-th eigenvalue of FE model obtained by solving the generalized eigenvalue problem between the stiffness matrix $K(\alpha)$ and mass matrix M; λ_i^{EXP} denotes the experimentally identified *i*-th eigenvalue; w_{λ_i} and w_{ψ_i} denote the weightings of the eigenvalues and MAC values of the *i*-th mode, respectively. Note here the objective function is an oracle formulation of the updating variable α, i.e. a non-explicit expression of the updating variable α, which results in a nonconvex optimization problem.

An open-source MATLAB package for structural model updating (SMU) is used to solve the optimization problem with the trust-region-reflective algorithm [79]. The upper and lower bounds of α are set as 0.3 and -0.3. In this example, the weightings are set the same to all four modes as $w_{\lambda_i} = 1, 1, 1, 1$, for $i = 1, \dots, 4$. The weightings for MAC values are set as $w_{\psi_i} = w_{\lambda_i}$. Starting from 100 randomized points of $\alpha \in [L_\alpha, U_\alpha]$, optimization searches are performed. Figure 4-6(a) plots the objective function values of the 100 runs,

among which the 96th run (marked as a star) finishes as the smallest. Correspondingly, Figure 4-6(b) shows the optimal/updated values of α from the 96th run.

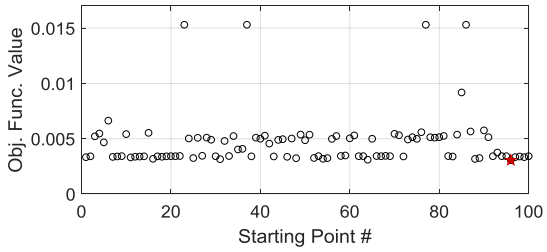

(a) Objective function values of 100 starting points

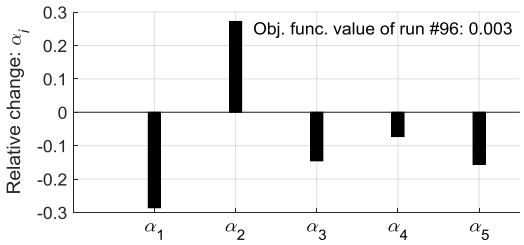

(b) Updated parameters α_i from the 96th run

Figure 4-6 FE model updating results from 100 starting points: MAC value formulation

4.2.2.2 Eigenvector Difference Approach

The second approach to update the FE model is to directly minimize the differences between the eigenvectors of the FE model and experimental results. Specifically, the entry of experimentally identified mode shape vector $\psi_i^{\mathrm{EXP,m}}$ with the largest magnitude is denoted as the q_i-th entry. Before updating, the experimentally identified vector $\psi_i^{\mathrm{EXP,m}}$ and the one from the FE model ψ_i^{m} are first normalized so that both q_i-th entries equal to one. An optimization problem (Eq. (4-2)) is formulated as follows.

$$\underset{\alpha}{\text{minimize}} \quad \sum_{i=1}^{n_{\text{modes}}} \left\{ \left(\frac{\lambda_i^{\mathrm{EXP}} - \lambda_i(\alpha)}{\lambda_i^{\mathrm{EXP}}} \cdot w_{\lambda_i} \right)^2 + \left\| Q_i \{ \psi_i^{\mathrm{EXP,m}} - \psi_i^{\mathrm{m}}(\alpha) \} \cdot w_{\psi_i} \right\|_2^2 \right\} \tag{4-2a}$$

$$\text{subject to} \quad L_\alpha \le \alpha \le U_\alpha \tag{4-2b}$$

The selection matrix $Q_i \in \mathbb{R}^{(n_\mathrm{m}-1)\times n_\mathrm{m}}$ is used to exclude the q_i-th entry of the normalized eigenvector from updating and defined as

$$Q_i = \begin{bmatrix} I_{q_i-1} & 0_{(q_i-1)\times 1} & 0_{(q_i-1)\times(n_\mathrm{m}-q_i)} \\ 0_{(n_\mathrm{m}-q_i)\times(q_i-1)} & 0_{(n_\mathrm{m}-q_i)\times 1} & I_{n_\mathrm{m}-q_i} \end{bmatrix} \tag{4-3}$$

Here $\|\cdot\|_2$ denotes the $\mathcal{L}2$-norm of a vector and n_m denotes the number of measured DOFs. Other notations are the same as those of Eq. (4-1). Note that the first eigenvalue term of Eq. (4-2) is the same as the one from the MAC value formulation of Eq. (4-1). For eigenvectors, however, Eq. (4-2) minimizes the $\mathcal{L}2$-norm of the differences between the experimentally identified vector and the one from the FE model instead of MAC values.

The same open-source MATLAB package for SMU is used to solve the optimization problem with the trust-region-reflective algorithm [79]. The upper and lower bounds of updating variable α are set the same as in Section 4.2.2.1, i.e. 0.3 and -0.3. In addition, the weightings are also set the same for all four modes, i.e. $w_{\lambda_i} = 1, 1, 1, 1$, for $i = 1, \dots, 4$, and the weightings for each eigenvector entries are all set as $w_{\psi_i} = w_{\lambda_i}$. Starting from 100 randomized points of $\alpha \in [L_\alpha, U_\alpha]$, optimization searches are performed. Figure 4-7(a) plots the objective function values of the 100 runs, among which the 13$^{\text{th}}$ run (marked as a star) finishes as the smallest. Correspondingly, Figure 4-7(b) shows the optimal/updated values of α from the 13$^{\text{th}}$ run.

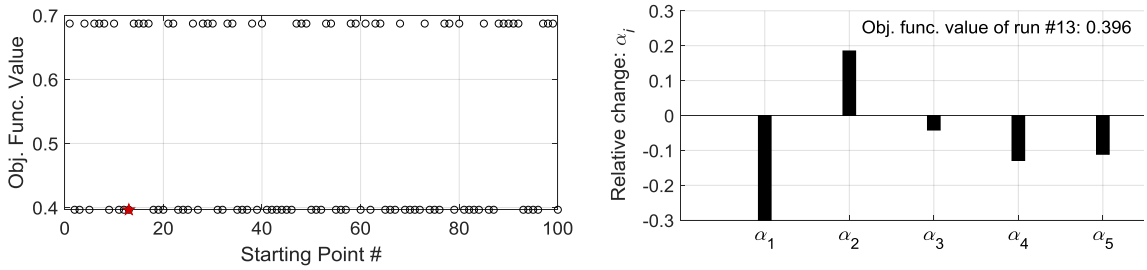

(a) Objective function values of 100 starting points

(b) Updated parameters α_i from the 13th run

Figure 4-7 FE model updating results from 100 starting points: eigenvector differernce formulation

4.2.2.3 Summary of FE model Updating Results

Given the updated material parameters, the resonance frequencies of the updated FE model can be obtained as $f_i = \sqrt{\lambda_i}/(2\pi)$. For both the initial FE model and the updated model, Table 4-1 summarizes the relative differences in resonance frequencies and the MAC values. The relative difference is defined as $\Delta f \triangleq \left(f_i - f_i^{\mathrm{EXP}}\right)/f_i^{\mathrm{EXP}}$. In terms of the updating results from MAC value approach, a much better match in resonance frequencies of the 2nd to 4th modes is obtained, with a relatively small sacrifice in MAC values and a slight increase in the relative errors of the first mode. Similar phenomenon can be observed in the updating results from the eigenvector difference approach. A better match in resonance frequencies of the 2nd to 4th modes and all four mode shapes is obtained, with a relatively small sacrifice in the first mode. Compared to the results from MAC value approach, the difference in the updated resonance frequencies from the eigenvector difference approach are slightly larger, but the updated mode shapes match better with experimental results when using the eigenvector difference approach.

Table 4-1 Comparison of modal properties before and after FE model updating

Mode	Exp.	Initial FE model			Updated FE model (MAC value)			Updated FE model (Eigvec. diff)		
	f_i^{EXP} (Hz)	f_i (Hz)	Δf (%)	MAC	f_i (Hz)	Δf (%)	MAC	f_i (Hz)	Δf (%)	MAC
1st	1.97	1.96	-0.40	0.999	1.95	-1.02	0.997	1.95	-1.24	0.998
2nd	5.45	5.63	3.27	0.990	5.50	0.84	0.990	5.58	2.28	0.990
3rd	13.86	14.96	7.91	0.959	14.03	1.18	0.936	14.25	2.83	0.974
4th	19.86	20.61	3.76	0.974	19.67	-0.98	0.969	19.48	-1.95	0.975
Object. function value	MAC value	0.0380			0.0031			0.0079		
	Eigvec. diff.	0.5023			0.6778			0.3964		

In addition, Table 4-1 also shows the objective function values of the two formulations, evaluated using the initial FE model and the updated FE model obtained from MAC value formulation and eigenvector difference formulation, respectively. As expected, the optimization results from the MAC value approach decreases the corresponding objective function from Eq. (4-1) from 0.038 to 0.0031, and achieves smaller value compared to the eigenvector difference approach with a result of 0.0079. Similarly, the optimization results from the eigenvector difference approach decreases the corresponding objective function from Eq. (4-2) from 0.5023 to 0.3964, and achieves smaller value compared to the result 0.6778 from MAC value approach. In the following input-state estimation, results from the MAC value approach are used to construct the updated model.

4.3 Input-State Estimation with Experimental Measurements

This section presents the input-state estimation results using experimental measurements. Performance of three previously proposed estimators for systems with direct feedthrough are compared here, including the FIC estimator (Section 2.1), FIC estimator with delayed measurements (Section 2.3) and the LFB estimator (Section 3.1). In addition to the three estimators, the well-known WLS estimator is also included and combined with an online drift filter to resolve the drift problem [23]. The resulting WLS estimator with drift filter denoted here as the WLSF estimator.

Because of the large size of the FE model resulting in a large state space system model, model order reduction is needed to improve computational efficiency of the estimators. Modal decomposition is first introduced to reduce the system model order. Next, effect of sensor instrumentation on input estimation is discussed by examining the magnitude of the feedthrough matrix of the reduced-order system. Based on the results, the number of modes used in model reduction is determined. Finally, two scenarios of sensor instrumentations are presented to compare the performance of the input-state estimators.

4.3.1 Model Order Reduction through Modal Decomposition

To reduce the system model order, modal decomposition is performed by converting physical coordinates to modal coordinates. When n_{mode} of modes are used for model order reduction, let Ω denote a diagonal matrix with diagonal entries as the first n_{mode} number of angular natural frequencies; let $\Psi = [\psi_1 \quad \psi_2 \quad \cdots \quad \psi_{n_{\text{mode}}}] \in \mathbb{R}^{n_{\text{DOF}} \times n_{\text{mode}}}$ denote the corresponding mass-normalized eigenvectors (vibrating mode

shapes). Note that ψ_i is a column vector denoting the eigenvector of the i-th mode, i.e. $\psi_i = [\psi_{1,i} \quad \psi_{2,i} \quad \cdots \quad \psi_{n_{\mathrm{DOF}},i}]^T$. The displacement vector q in physical coordinates is transformed to z in modal coordinates as $q = \Psi z$, where $z \in \mathbb{R}^{n_{\mathrm{mode}}}$. Therefore, the reduced order model is given by Eq. (4-4) and (4-5).

$$\dot{x}_{\mathrm{mod}} = \begin{Bmatrix} \dot{z} \\ \ddot{z} \end{Bmatrix} = \begin{bmatrix} 0 & \mathrm{I} \\ -\Omega^2 & -\Psi^T C_{\mathrm{damp}} \Psi \end{bmatrix} \begin{Bmatrix} z \\ \dot{z} \end{Bmatrix} + \begin{bmatrix} 0 \\ \Psi^T \Gamma_u \end{bmatrix} u$$

$$\triangleq A_{\mathrm{c,mod}} x_{\mathrm{mod}} + B_{\mathrm{c,mod}} u \tag{4-4}$$

$$y = \Gamma_y \ddot{q} + v = \Gamma_y \Psi \begin{bmatrix} -\Omega^2 & -\Psi^T C_{\mathrm{damp}} \Psi \end{bmatrix} \begin{Bmatrix} z \\ \dot{z} \end{Bmatrix} + \Gamma_y \Psi \Psi^T \Gamma_u u + v$$

$$\triangleq C_{\mathrm{c,mod}} x_{\mathrm{mod}} + D_{\mathrm{c,mod}} u + v \tag{4-5}$$

To obtain the continuous-time reduced-order state space model characterized by $A_{\mathrm{c,mod}}$, $B_{\mathrm{c,mod}}$, $C_{\mathrm{c,mod}}$ and $D_{\mathrm{c,mod}}$, a Rayleigh damping model is used to construct the damping matrix C_{damp} based on the identified damping ratios of the first two modes (Figure 4-4). The natural frequency matrix Ω and the mode shape matrix Ψ are obtained from the updated FE model in Section 4.2.2. Determination of the number of modes n_{mode} used in model reduction can be based on sensor instrumentation and unknown input location. Because the estimators are derived in discrete time, the continuous-time system from Eq. (4-4) and (4-5) is discretized using zero-order-hold.

4.3.2 Effect of Sensor Instrumentation on Input Estimation

For the reduced order model, the effect of sensor instrumentation on input estimation is investigated by examining the magnitude of the feedthrough matrix $D_{\mathrm{c,mod}}$ of Eq. (4-5), which degenerates to a column vector in this single input example. Because zero-order-hold discretization is used, the discrete feedthrough vector D of the estimators is the same as the continuous-time feedthrough matrix $D_{\mathrm{c,mod}}$. From Eq. (4-5), a relatively large $D_{\mathrm{c,mod}}$ is needed such that the unknown input u can be distinguished from measurement noise v.

To derive an expression of the feedthrough vector of the reduced order model, denote the input DOF as the r-th DOF of the full-order FE model. As a result, the input location matrix $\Gamma_u \in \mathbb{R}^{n_{\mathrm{DOF}} \times n_u}$ (which again degenerates to a column vector in this example) has value one at the r-th DOF and zero elsewhere. Recall that a total of m measurements are used during estimation. The measured DOFs of the FE model are thus denoted as the s_1, …, s_m-th DOFs. As a result, the output location matrix $\Gamma_y \in \mathbb{R}^{m \times n_{\mathrm{DOF}}}$ has value one at the j-th row and the s_j-th column with $j = 1, \ldots, m$; all other entries of Γ_y are zero. The $m \times 1$ feedthrough vector of the reduced order model can thus be expanded as follows.

$$D = D_{\mathrm{c,mod}} = \Gamma_y \Psi \Psi^T \{\Gamma_u\}$$

$$= \Gamma_y \sum_{i=1}^{n_{\mathrm{mode}}} \begin{bmatrix} \psi_{1,i}^2 & \psi_{1,i}\psi_{2,i} & \cdots & \psi_{1,i}\psi_{n_{\mathrm{DOF}},i} \\ \psi_{2,i}\psi_{1,i} & \psi_{2,i}^2 & \cdots & \psi_{2,i}\psi_{n_{\mathrm{DOF}},i} \\ \vdots & \vdots & \ddots & \vdots \\ \psi_{n_{\mathrm{DOF}},i}\psi_{1,i} & \psi_{n_{\mathrm{DOF}},i}\psi_{2,i} & \cdots & \psi_{n_{\mathrm{DOF}},i}^2 \end{bmatrix} \{\Gamma_u\}$$

$$= \sum_{i=1}^{n_{\text{mode}}} \begin{Bmatrix} \psi_{s_1,i}\psi_{r,i} \\ \psi_{s_2,i}\psi_{r,i} \\ \vdots \\ \psi_{s_m,i}\psi_{r,i} \end{Bmatrix} \tag{4-6}$$

Equation (4-6) shows that the magnitude of feedthrough vector $D_{c,mod}$ is determined by the product of eigenvector entries between the input DOF and the measured DOFs summed over each mode. For the j-th measurement, the product of $\psi_{s_j,i}$ and $\psi_{r,i}$ summed over n_{mode} modes needs to be large enough to ensure a relatively large value on the j-th row of $D_{\text{c,mod}}$.

In this structural example, a total of 44 acceleration measurements are available, i.e. $m = 44$, including 27 longitudinal measurements and 17 vertical measurements. Figure 4-8 shows the values of $\{D_{\text{c,mod}}\}_j$ with $j = 1, \dots, 44$, when the number of modes n_{mode} used in model reduction equals to 2 and 10, respectively. Each entry of $\{D_{\text{c,mod}}\}_j$ corresponds to an acceleration measurement A_j as numbered in Figure 4-1(b). Regardless of the choice of n_{mode} value, larger entries of $D_{\text{c,mod}}$ are from the longitudinal measurements located above the first elevated slab, i.e. A5~A8, A13~A16, A21~A23, A26 and A27. On the other hand, the entries of $D_{\text{c,mod}}$ corresponding to longitudinal measurements on and below the first elevated slab and all the vertical measurements are relatively small. Correspondingly, these measurements contribute less to the estimation of the longitudinal shaker input on the 2nd elevated slab. In addition, as shown in Figure 4-8(b), when a larger number of n_{mode} is used, the entries corresponding to vertical measurements located on the transverse beams of the second elevated slab increase slightly,

i.e. A38~A40, A42 and A43. Comparing Figure 4-8(a) and (b), it can be seen that a larger number of modes used in model reduction does not increase the magnitude of $D_{\mathrm{c,mod}}$ significantly, because only the first two modes contribute the most to structural in-plane longitudinal response under the longitudinal shaker excitation (see Figure 4-4). In addition, as n_{mode} increases, the dimension of the reduced-order system also increases. Based on this observation, n_{mode} is chosen as ten in the following input-state estimation.

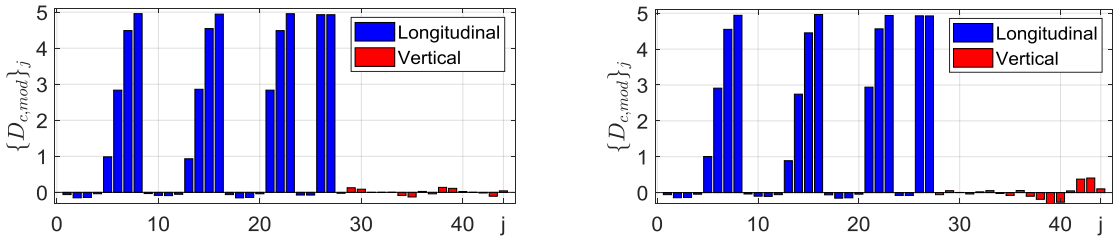

(a) $n_{\mathrm{mode}} = 2$ (b) $n_{\mathrm{mode}} = 10$

Figure 4-8 Entries of feedthrough vector $\{D_{\mathrm{c,mod}}\}_j$, $j = 1, \ldots, 44$. Each entry corresponds to acceleration measurement A_j

4.3.3 Measurements Including Input Location

All 44 acceleration measurements, including the one at the shaker input location, are used during the estimation process. Recall that the weight of the shaker is modeled as part of the structural weight. Therefore, the benchmark shaker force input to the structure is obtained by multiplying the moving mass of the shaker with the relative acceleration between the shaker mass and the beam-column joint of the 2nd elevated slab right below the shaker. In this subsection, the effect of estimator covariances on input estimation accuracy is discussed first. Input estimation results using experimental acceleration measurements are then presented.

4.3.3.1 Effect of Covariance Knowledge on Input Estimation

Before performing estimation using field measurements, the effect of covariance parameters available to the input-state estimators is investigated in simulation first, where the actual/true values of these covariances are known. Because the FIC-d estimator is derived based on the FIC estimator using delayed measurements, the effect of covariance knowledge of the FIC-d estimator is similar as the FIC estimator and thus is not included.

Measured shaker excitation force is used as the input to simulate 44 structural acceleration response (as shown in Figure 4-1(b)), contaminated by white Gaussian measurement noise. The standard deviation of measurement noise is set as $\sigma_{v,sim} = 50$ μg, obtained from sensor specification. Similar as in Section 2.1.5.1 and 2.2.5.1, a total of 20 trials are performed, and each trial lasts 30 seconds with randomly generated measurements noise. In practice, measurement noise covariance $\Sigma_{v,est}$ available to the estimators can be approximated based on sensor specification. In this simulation, all estimators assume the same standard deviation of measurement noise of 50 μg. Because no modeling error is assumed in simulation, i.e. $\Sigma_{w,sim} = 0$, the same zero-valued process noise covariance $\Sigma_{w,est}$ is used by all estimators in this subsection.

During estimation, the FIC estimator requires a value of the input covariance denoted $\Sigma_{u,est}$ (see Table 2-1). Similarly, operation of the LFB estimator requires the noise covariance Σ_{ξ} (see Table 3-1); accordingly, the value available is denoted $\Sigma_{\xi,est}$. Furthermore, based on the frequency spectrum of the measured response (Figure 4-2) and prior knowledge of the input El Centro record, the input model of the LFB estimator is

chosen as a 6th order Chebyshev filter with a bandwidth of 0.2 ~ 25 Hz. For the WLSF estimator, the online drift filter is tuned to be a 4th order high-pass Chebyshev Type I filter with cut-off frequency of 10^{-4} Hz and peak-to-peak passband ripple of 0.05 dB. Note that same as the WLS estimator, operation of the WLSF estimator does not require any input covariance $\Sigma_{u,est}$ or noise covariances other than $\Sigma_{w,est}$ and $\Sigma_{v,est}$.

In summary, the covariances for the estimator operation include $\Sigma_{u,est}$ of the FIC estimator, $\Sigma_{\xi,est}$ of the LFB, $\Sigma_{w,est}$ and $\Sigma_{v,est}$ for all estimators. The initial value of state estimation μ_{x_0} is set as 0 and the diagonal entries of Σ_{x_0} are set as 10^{-10} for all estimators to account for uncertainty in the initial condition of the structure. In addition, for the LFB estimator, the initial state $\hat{\eta}_0$ is set as zero and the initial state covariance Σ_{η_0} is set the same as $\Sigma_{\xi,est}$. Table 4-2 summarizes the data generation process and the estimator covariances during each trial run.

Table 4-2 Summary of data generation and estimator covariances

Covariances	Time history generation	Estimation		
		FIC	LFB	WLS/WLSF
Input	Shaker force input	$\Sigma_{u,\,est}$ (0.1 to 10^6 kN^2)	$\Sigma_{\xi,est}$ (0.1 to 10^6 kN^2)	-
Initial state	Static	$\mu_{x_0} = 0,\ \Sigma_{x_0} = 10^{-10}I$		
Process noise	$\Sigma_{w,\,sim} = 0$	$\Sigma_{w,\,est} = 0$		
Measurement noise	$\Sigma_{v,\,sim} = 50^2$ (μg)^2	$\Sigma_{v,\,est} = 50^2$ (μg)^2		

To study the effect of estimator covariances on input estimation, the averaged input RMS error $\bar{e}_u$ is obtained from 20 trials in the same way described in Section 2.1.5.1. To quantify the estimator performance, recall that the root mean square (RMS) error e_u from the i-th trial can be calculated as $e_u^{(i)} \triangleq \sqrt{\frac{1}{\mathbb{K}}\sum_{k=1}^{\mathbb{K}}|u_k - \hat{u}_k|^2}$, and the averaged RMS error among 20 trials is calculated as $\bar{e}_u = \frac{1}{n_{trial}}\sum_{i=1}^{n_{trial}} e_u^{(i)}$. Specifically, in each trial, the WLS and the WLSF estimators are operated only once, and the corresponding RMS error e_u is calculated for both estimators respectively. After averaging among 20 trials, the averaged RMS error $\bar{e}_u$ of WLS and WLSF estimators can be obtained. On the other hand, the FIC estimator is performed for different values of $\Sigma_{u,est}$ ranging from 0.1 to 10^6 kN^2 in each trial. Similarly, the LFB estimator is performed for different values of $\Sigma_{\xi,est}$ in the same range as $\Sigma_{u,est}$. In each trial, input RMS error e_u is calculated for the FIC estimator at each value of $\Sigma_{u,est}$ and the LFB estimator at each value of $\Sigma_{\xi,est}$ accordingly. Among 20 trials, the averaged $\bar{e}_u$ corresponding to each value of $\Sigma_{u,est}$ of the FIC estimator and $\Sigma_{\xi,est}$ of the LFB estimator can be obtained.

Figure 4-9 shows the relationship between $\bar{e}_u$ and the covariance of FIC and LFB estimators in comparison to the results from the WLS and WLSF estimators when no process noise is applied. Both the FIC and LFB estimators can achieve small RMS error of 0.14 kN when $\Sigma_{u,est}$ is around 6 kN^2 and $\Sigma_{\xi,est}$ is around 8 kN^2. This is on the same magnitude as the calculated variance 1.2 kN^2 of the actual input signal during 1s ~ 6s, when the large excitation happens. For the WLS estimator, the averaged RMS error $\bar{e}_u$ is close to 0.49 kN. After combining the online drift filter in WLS estimation, the RMS error

is significantly reduced to 0.16 kN. In summary, the FIC and the LFB estimators performs better than the WLSF estimator when $\Sigma_{u,est}$ is in the range of 1 to 30 $\text{kN}^2$and $\Sigma_{\xi,est}$ is in the range of 1 to 120 kN^2. In addition, when $\Sigma_{u,est}$ becomes larger than 10^5, the results from the FIC estimator converge to those of the WLS estimator.

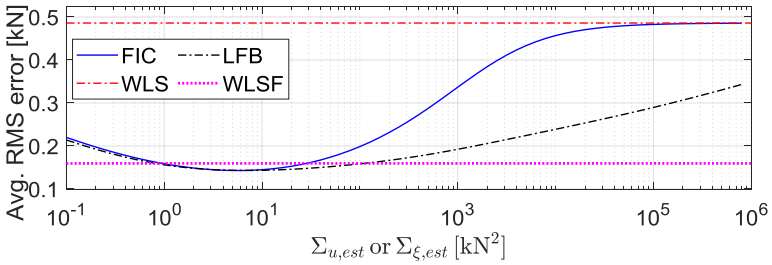

Figure 4-9 Averaged RMS error $\bar{e}_u$ of shaker input estimation: $\Sigma_{w,sim} = \Sigma_{w,est} = 0$

4.3.3.2 Input estimation with experimental acceleration measurements

A total of 44 acceleration measurements (Figure 4-1(b)) are used to compare the estimated inputs from all estimators. An 8th order bandpass (0.5 ~ 40 Hz) Chebyshev type I filter with a 0.5 dB bandpass ripple is applied to the measured shaker input and structural responses in both forward and reverse directions to remove phase distortion. To account for potential modeling error when using experimental acceleration measurements, a non-zero process noise covariance $\Sigma_{w,est}$ is used by the estimators. The process noise covariance $\Sigma_{w,est}$ is set to a relatively small value of $10^{-12}I$. Furthermore, $\Sigma_{u,est}$ of the FIC estimator is set as 6 kN^2. For the LFB estimator, the same value of 6 kN^2 is set for the covariance $\Sigma_{\xi,est}$. The measurement noise covariance $\Sigma_{v,est}$ and initial state covariance are set the same as those in Section 4.3.3.1. For the LFB estimator, the same input model is used, i.e. a 6th order Chebyshev filter with a bandwidth of 0.2 ~ 25 Hz.

For the delayed estimator FIC- d, Figure 4-9 shows the input RMS error e_u as a function of delay d. Smaller error can be achieved when $d = 7$, which is chosen as the number of delays used in the estimator considering the tradeoff between accuracy and computational efficiency. The estimator with $d = 7$ is therefore denoted as FIC-7.

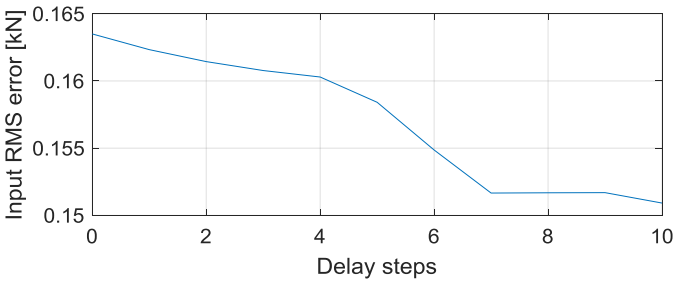

Figure 4-10 Input RMS error e_u of FIC- d estimator as a function of delay d

The estimated inputs from all four estimators are shown in Figure 4-11. Specifically, Figure 4-11(a) shows the comparison of estimated inputs from 0s to 30s; Figure 4-11(b) shows the close-up plots of the initial 2s to 4s of all four estimators; Figure 4-11(c) ~ (f) shows the estimated input from the FIC, WLSF, FIC-7 and LFB estimators during the final 24s to 29s, respectively. All four estimators perform similarly at the beginning (Figure 4-11(b)). During the final 24s to 29s, the FIC, FIC-7 and LFB estimators can estimate the input well with a small error covariance (Figure 4-11(c), (e) and (f)). As for WLSF, Figure 4-11(d) shows the online drift filter can reduce drift error of the WLS estimator but could not decrease the estimation error covariance.

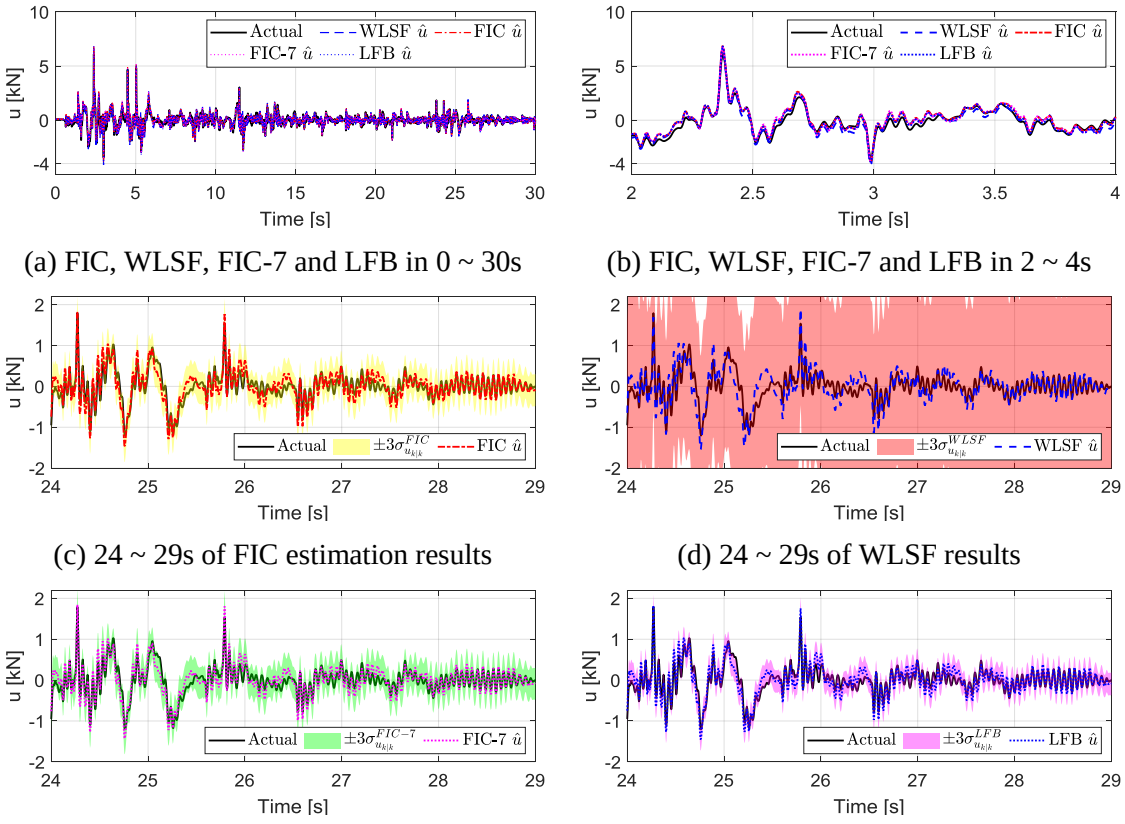

(a) FIC, WLSF, FIC-7 and LFB in 0 ~ 30s

(b) FIC, WLSF, FIC-7 and LFB in 2 ~ 4s

(c) 24 ~ 29s of FIC estimation results

(d) 24 ~ 29s of WLSF results

(e) 24 ~ 29s of FIC-7 results

(f) 24 ~ 29s of LFB results

Figure 4-11 Estimation of shaker input with 44 experimental measurements including input location

To quantify the performance of the input estimators, Table 4-3 shows the input RMS error e_u of all four estimators calculated for the entire 30s along with corresponding computational time using an Intel i7-4790 CPU and 16 GB RAM. The input error from the WLSF estimator is relatively larger than the other estimators with a larger error covariance (Figure 4-11(d)). The FIC estimator achieves smaller input RMS error compared to the WLSF estimator with a smaller error covariance. The delayed FIC estimator, i.e. FIC-7, is able to reduce the input estimation error of the FIC estimator with a longer computational time. As for the LFB estimator, the error e_u is slightly smaller than those of the other

estimators. In addition, the computational time of the LFB estimator is relatively short compared to the delayed FIC estimator. Therefore, prior knowledge of the frequency bandwidth of the unknown input can help improve estimator performance.

Table 4-3 Input RMS error comparison among different estimators using 44 measurements including input location

Estimator	WLSF	FIC	FIC-7	LFB
Input RMS error e_u (unit: kN)	0.265	0.195	0.193	0.185
Computational time (unit: s)	1.86	1.29	9.40	1.32

To check the convergence of the estimators, time history of the input estimation error covariances $\Sigma_{u_{k|k}}$ from four estimators is presented here. Figure 4-12 shows that for both the FIC and FIC-7 estimators, the input estimation error covariances $\Sigma_{u_{k|k}}$ converge to an almost same steady state value after 5s with the two lines almost coinciding. For the LFB estimator, the error covariance is able to converge to a smaller steady state value compared to the FIC estimator. In contrast, the input error covariance of WLSF cannot converge to steady state. It should be noted that a longer simulation time could not help the error covariance of WLSF to converge. Instead, the error covariance keeps increasing over time. Although an online drift filter can reduce drift error, the estimator cannot converge to steady state.

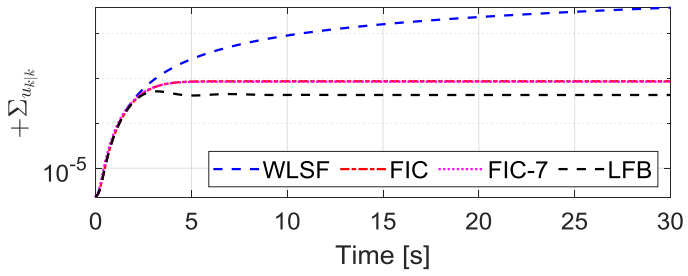

Figure 4-12 Convergence of input estimation error covariance $\Sigma_{u_{k|k}}$ of the FIC, WLSF, FIC-7, LFB estimators (FIC and FIC-7 coincide)

4.3.4 Measurements Away from Input Location

Results from Section 4.3.3 show that all estimators generally perform well in estimating the shaker input when all measurements are used. In practice, however, it may not be feasible to place sensors close to the unknown input location. To make the estimation problem more challenging, this subsection compares the estimator performance using measurements far from the input location only. A total of 25 acceleration measurements are used in this subsection, including 2 in-plane longitudinal channels on the columns above the first elevated slab, 14 longitudinal and 9 vertical channels on and below the first elevated slab, as shown in Figure 4-13. The same model reduction approach using two modes is applied and the system is discretized using zero-order-hold. Because the benchmark shaker input signal is the same as in Section 4.3.3, discussion about the effect of covariance knowledge on input estimation is not included here.

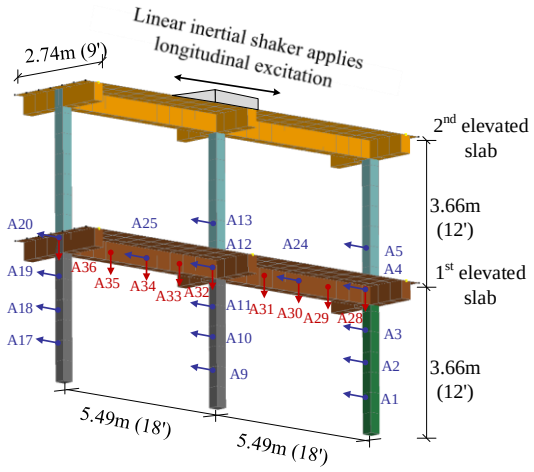

Figure 4-13 Accelerometer instrumentation: measurements away from shaker location

For consistency, the estimator parameter values and initial conditions are set the same as in Section 4.3.3. The estimated inputs from all four estimators are shown in Figure 4-14. Specifically, Figure 4-14(a) shows the comparison of estimated inputs from 0s to 30s; Figure 4-14(b) shows the close-up plots of the initial 2s to 4s of all four estimators; Figure 4-14(c) ~ (f) shows the estimated input from the FIC, WLSF, FIC-7 and LFB estimators during the final 24s to 29s, respectively.

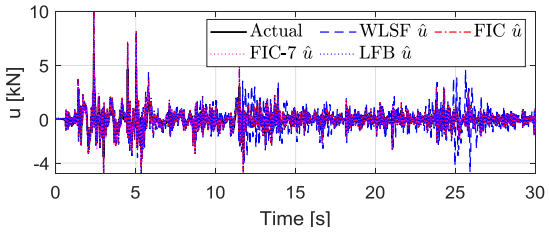

(a) FIC, WLSF, FIC-7 and LFB in 0 ~ 30s

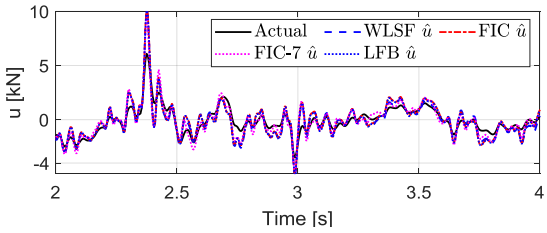

(b) FIC, WLSF, FIC-7 and LFB in 2 ~ 4s

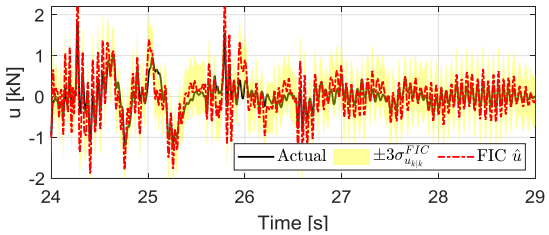

(c) 24 ~ 29s of FIC estimation results

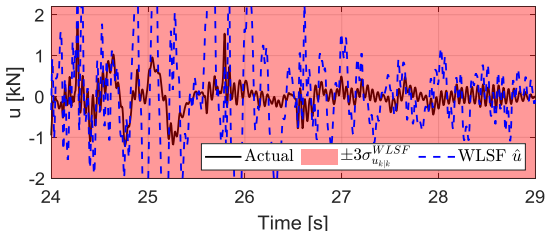

(d) 24 ~ 29s of WLSF results

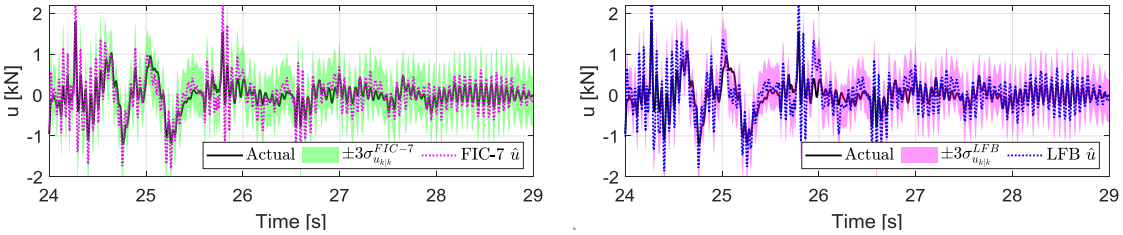

(e) 24 ~ 29s of FIC-7 results (f) 24 ~ 29s of LFB results

Figure 4-14 Estimation of shaker input with 25 experimental measurements excluding shaker input location

Compared to the results in Section 4.3.3.2, the estimated input using only measurements away from the input location is more prone to measurement noise and tends to overestimate the actual input. During the first few seconds, all four estimators perform similarly with acceptable results, as shown in Figure 4-14(b). During the final 24s to 29s, the FIC, FIC-7 and LFB estimators can still estimate the input with similar acceptable performance (Figure 4-14(c), (e) and (f)). However, the WLSF estimator is not able to provide a good estimate of the input as shown in Figure 4-14(d).

To quantify the performance of the input estimators, Table 4-4 shows the input RMS error e_u of all four estimators calculated for the entire 30s along with corresponding computational time using an Intel i7-4790 CPU and 16 GB RAM. Overall, the FIC, FIC-7 and LFB estimators perform similarly in terms of input RMS error. Specifically, both the LFB and the delayed estimator FIC-7 improves the performance of the FIC estimator, while the computational time of the FIC-7 estimator is longer that of the LFB estimator. On the other hand, the WLSF estimator is not able to provide a good estimate of the input, resulting in a large input RMS error.

Table 4-4 Input RMS error comparison among different estimators using 25 measurements excluding input location

Estimator	WLSF	FIC	FIC-7	LFB
Input RMS error e_u (unit: kN)	0.847	0.458	0.376	0.453
Computational time (unit: second)	0.88	0.58	8.54	0.75

To check the convergence of the estimators, time history of the input estimation error covariances $\Sigma_{u_{k|k}}$ from four estimators is shown in Figure 4-15. Similar as the results in Section 4.3.3.2, the input estimation error covariances $\Sigma_{u_{k|k}}$ of both the FIC and FIC-7 estimators converge to an almost same steady state value after 4s. The error covariance of the LFB estimator is able to converge to a smaller steady state value compared to the FIC estimator. However, the steady state values of input error covariances of the FIC, FIC-7 and LFB estimators are larger than those in Section 4.3.3.2 where all measurements are used. As expected, the larger steady state values indicate a higher uncertainty of the estimated input when the measurements are away from the input location. On the other hand, the input error covariance of WLSF cannot converge to steady state (Figure 4-15).

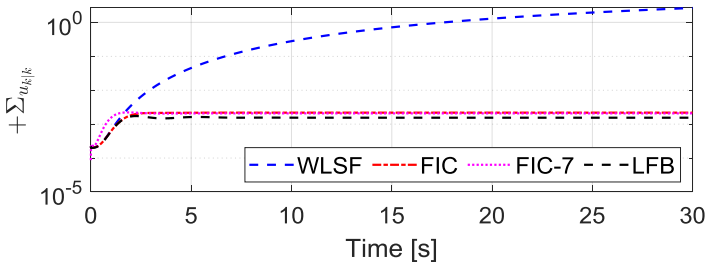

Figure 4-15 Convergence of input estimation error covariance of FIC, WLSF, FIC-7, LFB (FIC and FIC-7 coincide): measurements excluding input location

4.4 Summary

This chapter validates and compares the performance of the proposed estimators based on a full-scale concrete frame using experimental measurements. To obtain a reliable model for input-state estimation, modal properties of the frame are first identified. Based on the identified modal properties, the material parameters of an FE model are updated through non-convex optimization with randomized starting points. The updated FE model is then used to formulate a reduced-order state space model through modal decomposition to improve computational efficiency without significantly compromising accuracy.

For input-state estimation, two sensor instrumentation scenarios are included for comparison, using measurements including the input location and measurements excluding the input location. Performance of the FIC, WLSF, FIC-d and the LFB estimators are compared for both scenarios. For the WLSF estimator, the previous drift error from the WLS estimator can be reduced by the properly tuned online drift filter. However, the estimation error covariance of the WLSF is not able to converge when only acceleration measurements are used here. On the other hand, the FIC, FIC- d and the LFB estimators perform well overall in both cases. Specifically, after combining delayed measurements, the FIC- d improves the performance of the FIC estimator at the expense of a slightly longer computational time. The LFB also outperforms the FIC estimator when prior knowledge of the frequency bandwidth of the unknown input is incorporated into the estimator.

CHAPTER 5. ESTIMATION OF MOVING LOADS WITH APPLICATIONS IN BRIDGE WEIGH-IN-MOTION

Previous chapters focus on linear time invariant systems with unknown inputs applied at a fixed location. This chapter generalizes the previously proposed estimators when the inputs have time-varying locations. The estimators in this chapter are especially designed for applications in bridge weigh-in-motion (B-WIM). The previously proposed estimators are generalized with time varying input and feedthrough matrices $B(t)$ and $D(t)$ to account for moving loads. In Section 5.1, the state space model is reformulated and presented with heterogeneous measurements. To improve the computational efficiency of the estimators, modal decomposition is used to reduce the system order. For estimator validation, Section 5.2 presents the results of moving load estimation based on a pair of simply supported bridge girders. The modified FIC and LFB estimators can identify the moving loads using displacement and acceleration responses. In Section 5.3, the input estimators are applied to an in-service highway bridge to estimate truck axle weights and gross vehicle weight as it passes through the bridge. The FIC, LFB and FIC-d estimators are used to estimate the moving vehicle loads using both simulated and experimentally measured displacement, strain and acceleration responses of the bridge.

5.1 State Space Formulation with Moving Input

To account for moving loads, a time-varying input location matrix $\Gamma_u(t) \in \mathbb{R}^{n_{\mathrm{DOF}} \times n_u}$ is introduced to both system equations and measurement equations. The load

input u corresponds to vehicle axle loads in B-WIM as the vehicle passes through the bridge. The system equation is given by Eq. (5-1)

$$\dot{x}(t) = \begin{Bmatrix} \dot{q}(t) \\ \ddot{q}(t) \end{Bmatrix} = \begin{bmatrix} 0 & I \\ -M^{-1}K & -M^{-1}C_{\text{damp}} \end{bmatrix} \begin{Bmatrix} q(\text{t}) \\ \dot{q}(\text{t}) \end{Bmatrix} + \begin{bmatrix} 0 \\ M^{-1} \end{bmatrix} \Gamma_u(t)u(t)$$

$$\triangleq A_c x(t) + B_c(t)u(t) \tag{5-1}$$

Here A_c is the time-invariant system matrix and $B_c(t)$ is the time varying input matrix of the continuous system. The time-varying part of B_c comes from the input location matrix $\Gamma_u(t)$ that maps moving load locations to specific degrees-of-freedom (DOFs) of a bridge model. For simplification, the input location matrix $\Gamma_u(t)$ is obtained assuming the velocity of the moving load can be obtained with good accuracy. Detailed derivation of $\Gamma_u(t)$ is presented in Section 5.2 and 5.3 for the simply supported girders and the full-scale highway bridge, respectively.

Heterogeneous sensor measurements can be fused together to estimate the moving loads. Displacement, strain and acceleration measurement equations are given by Eq. (5-2).

$$\begin{Bmatrix} y_d(t) \\ y_s(t) \\ y_a(t) \end{Bmatrix} = \begin{Bmatrix} \Gamma_{y,d} q(t) \\ \Gamma_{y,s} q(t) \\ \Gamma_{y,a} \ddot{q}(t) \end{Bmatrix} + v(t)$$

$$= \begin{bmatrix} \Gamma_{y,d} & 0 \\ \Gamma_{y,s} & 0 \\ -\Gamma_{y,a}M^{-1}K & -\Gamma_{y,a}M^{-1}C_{\text{damp}} \end{bmatrix} \begin{Bmatrix} q(t) \\ \dot{q}(t) \end{Bmatrix} + \begin{bmatrix} 0 \\ 0 \\ \Gamma_{y,a}M^{-1} \end{bmatrix} \Gamma_u(t)u + v(t)$$

$$\triangleq C_c x(t) + D_c(t)u(t) + v(t) \tag{5-2}$$

Here C_c is the time-invariant measurement matrix and $D_c(t)$ is the time varying feedthrough matrix of the continuous system. For the measurement matrix C_c, $\Gamma_{y,d}$ is the displacement measurement output matrix, $\Gamma_{y,s}$ is the strain measurement matrix and $\Gamma_{y,a}$ is the acceleration measurement matrix, all of which are time-invariant. The time varying part of the feedthrough matrix $D_c(t)$ comes from the input location matrix $\Gamma_u(t)$, same as $B_c(t)$ in the system equation (5-1).

When the system order is large, modal decomposition is commonly used to reduce the system order. Similar as presented in Section 4.3.1, displacement vector q in physical coordinates is transformed to z in modal coordinates using the mass-normalized eigenvectors Ψ as $q(t) = \Psi z(t)$, where $z(t) \in \mathbb{R}^{n_{\text{mode}}}$. The reduced-order system of Eq. (5-1) and (5-2) are then given as follows

$$\dot{x}_{\text{mod}}(t) = \begin{Bmatrix} \dot{z}(t) \\ \ddot{z}(t) \end{Bmatrix} = \begin{bmatrix} 0 & I \\ -\Omega^2 & -\Psi^T C_{\text{damp}} \Psi \end{bmatrix} \begin{Bmatrix} z(t) \\ \dot{z}(t) \end{Bmatrix} + \begin{bmatrix} 0 \\ \Psi^T \end{bmatrix} \Gamma_u(t) u(t)$$

$$\triangleq A_{\text{c,mod}} x_{\text{mod}}(t) + B_{\text{c,mod}}(t) u(t) \tag{5-3}$$

$$\begin{Bmatrix} y_d(t) \\ y_s(t) \\ y_a(t) \end{Bmatrix} = \begin{Bmatrix} \Gamma_{y,d} q(t) \\ \Gamma_{y,s} q(t) \\ \Gamma_{y,a} \ddot{q}(t) \end{Bmatrix} + v(t)$$

$$= \begin{bmatrix} \Gamma_{y,d}\Psi & 0 \\ \Gamma_{y,s}\Psi & 0 \\ -\Gamma_{y,a}\Psi\Omega^2 & -\Gamma_{y,a}\Psi\Psi^T C_{\text{damp}}\Psi \end{bmatrix} \begin{Bmatrix} z(t) \\ \dot{z}(t) \end{Bmatrix} + \begin{bmatrix} 0 \\ 0 \\ \Gamma_{y,a}\Psi\Psi^T \end{bmatrix} \Gamma_u(t) u(t) + v(t)$$

$$\triangleq C_{\text{c,mod}} x_{\text{mod}}(t) + D_{\text{c,mod}}(t) u(t) + v(t) \tag{5-4}$$

Here $A_{\mathrm{c,mod}}$ and $B_{\mathrm{c,mod}}$ are the system and input matrices of the continuous reduced-order system; $C_{\mathrm{c,mod}}$ and $D_{\mathrm{c,mod}}$ are the measurement and feedthrough matrices of the continuous reduced-order system; $\Gamma_u(t)$ is the same input location matrix as presented in the full-order system.

Compared to Eq. (4-4) and (4-5) in Section 4.3.1 where the input location is time invariant, the only difference of the moving load system is in the input location matrix $\Gamma_u(t)$, resulting in the time varying matrices $B_{\mathrm{c,mod}}(t)$ and $D_{\mathrm{c,mod}}(t)$. To modify the previously proposed FIC and LFB estimators, the original discrete time-invariant input matrix B and feedthrough matrix D of the recursive estimators are replaced with the time varying matrices B_k and D_k, obtained by discretizing $B_{\mathrm{c,mod}}(t)$ and $D_{\mathrm{c,mod}}(t)$, to account for the moving inputs.

5.2 Numerical Studies with Simply Supported Girders

The proposed estimators are first validated in simulation using a pair of simply supported concrete I-girders, which are modeled based on the actual girders of an in-service highway bridge. The girders are built in LS-DYNA using Hughes-Liu beam element with cross section integration [80, 81]. The girders are 70 ft long and 8.75 ft apart from each other (Figure 5-1(a)). Each girder consists of 28 beam elements with an element length of 30 inches. There are 165 DOFs per girder. The concrete modulus of the girder is 4.415×10^6 psi. The first five resonance frequencies of the girder are 2.92 Hz, 4.68 Hz, 8.04 Hz, 15.72 Hz and 17.96 Hz. A Rayleigh damping model is assumed using 2% modal damping ratio for the first two modes to simulate structural response under moving loads. To model

the moving vehicle load, Figure 5-1(b) illustrates a spring-damper model used in this simulation. The spring stiffness is denoted as k and the damping coefficient is denoted as c. The spring stiffness and damping coefficient are set as $k = 7000\ \text{lbf/inch}$ and $c = 100\ \text{lbf} \cdot \text{s/inch}$. The vehicle mass of each spring and damper part is 234 slugs or 3415 kg, denoted as m_1 in Figure 5-1(b). As a result, the vehicle has a bouncing frequency around 3Hz. The contact relationship between the moving load and the girder is modeled as a train/rail contact from LS-DYNA [80]. A contact mass is added at each contact node between the vehicle model and the girders, denoted as m_2 in Figure 5-1(b).

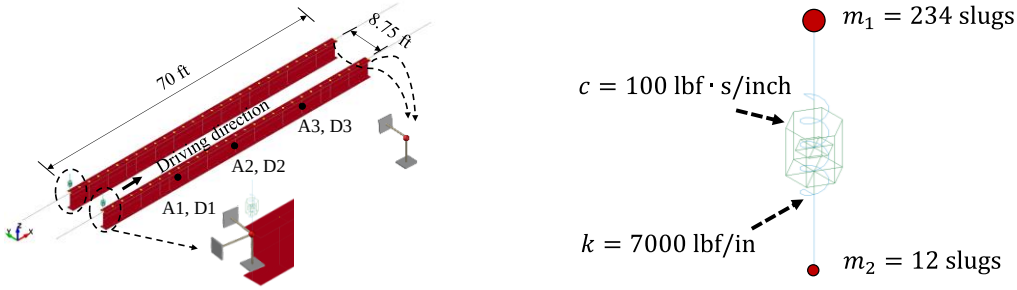

(a) Bridge girder (b) Spring-damper vehicle model

Figure 5-1 LS-DYNA model: simply supported girders with moving vehicle loads

Two numerical examples are presented in the following. Section 5.2.1 presents the input estimation results when only one moving load moves along each girder. Section 5.2.2 presents the results when two moving loads with a fixed distance move along each girder, corresponding to a vehicle with two axles. In both examples, three vertical displacement responses (denoted as D1 ~ D3 in Figure 5-1(a)) and three vertical acceleration responses (denoted as A1 ~ A3) at the mid-length and quarter lengths of the right girder are used to estimate the moving load(s).

5.2.1 A Single Pair of Moving Loads

First, a single pair of moving loads are used to validate the proposed moving input estimators. The total weights applied to the vehicle model are set as 15,054 lbs, evenly distributed between the two girders, i.e. 7,527 lbs each. The velocity of the moving loads is set as 440 inch/s, i.e. 25 miles per hour (mph). Therefore, the time of the loads passing through the girder is 1.91s. Because the element length is around 30 inches, the time of the loads passing each element is around 0.068 s. Since the two girders are identical in this example, results from only the right girder are included in this section.

When constructing the state space matrices (A_c, B_c, C_c and D_c in Eq. (5-1) and (5-2)) in MATLAB, the mass matrix M and stiffness matrix K are obtained from the LS-DYNA model and the damping matrix C_{damp} is obtained using a Rayleigh damping model with 2% damping ratios assumed for the first two modes of the girder. The time-varying input location matrix $\Gamma_u(t)$ is obtained by distributing the moving load to nearby nodes based on their relative distance, as illustrated in Figure 5-2.

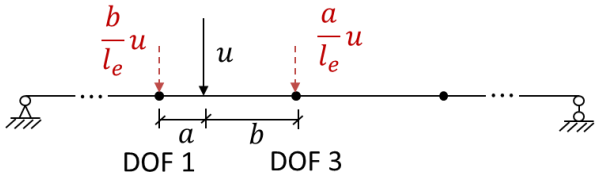

Figure 5-2 Illustration of a single moving load location at time t

Specifically, given prior knowledge of the moving load velocity, location of the load u at time t and the corresponding element can be determined. The load u is then distributed to the two nodes of the current element proportional to their relative distance,

i.e. b/l_e and a/l_e, where l_e is the length of current element. The distributed loads can thus be mapped to the corresponding vertical DOFs of the FE model through the input location matrix Γ_u. For example, assuming the vertical DOFs of the two nodes are the 1st DOF and the 3rd DOF of the FE model (denoted in Figure 5-2), the input location matrix $\Gamma_u \in \mathbb{R}^{n_{\text{DOF}} \times n_u}$ of the moving input u at time t is given as

$$\Gamma_u(t) = \begin{bmatrix} 1 & 0 \\ 0 & 0 \\ 0 & 1 \\ \vdots & \vdots \\ 0 & 0 \end{bmatrix} \begin{bmatrix} b/l_e \\ a/l_e \end{bmatrix} \tag{5-5}$$

Note that given the FE model of the girder and prior knowledge of the moving load(s) velocity, input location matrix $\Gamma_u(t)$ can be pre-calculated for the entire time interval when the vehicle is on the girder. Therefore, both the full-order state space model (Eq. (5-1), (5-2)) and the reduced-order model (Eq. (5-3), (5-4)) can be obtained before applying the moving input estimators.

Because the estimators are derived in discrete time, first-order-hold discretization is applied to the reduced-order continuous system given by Eq. (5-3) and (5-4) with a time step of 0.001s. Recall that the magnitude of discrete input-output feedthrough matrix D has a significant role in the input estimator as shown in previous chapters, the magnitude of feedthrough matrix corresponding to each measurement is first examined. Figure 5-3(a) shows the magnitude of feedthrough matrix D_k of the full-order model corresponding to the three displacement measurements and three acceleration measurements as the load moves through one girder. The magnitude of the feedthrough matrix is only sufficiently

large when the moving load is close to the measurement locations. This indicates that when the moving load is located in between measurements, the estimator cannot estimate the load well because of the small magnitude of the feedthrough matrix.

For the reduced-order model, Figure 5-3(b) shows the feedthrough matrix after modal decomposition using the first five modes. After transforming physical coordinates to modal coordinates using mass-normalized eigenvectors, the magnitude of the feedthrough matrix becomes relatively large even when the moving load is located between measurement locations. Therefore, the reduced-order model is used as the system model for the following input estimation, considering both the magnitude of feedthrough matrix and computational efficiency.

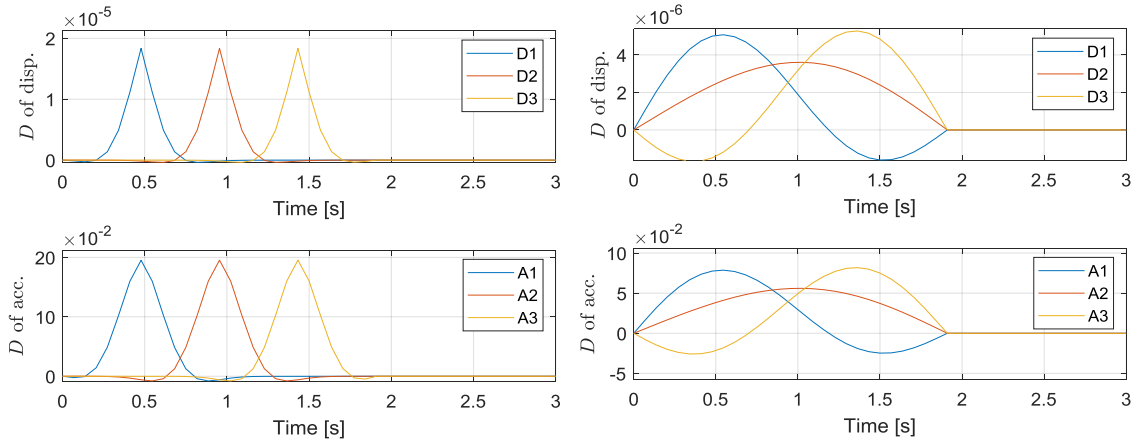

(a) Full-order model (b) Reduced-order model with 5 modes

Figure 5-3 Time history of feedthrough matrix

The simulated displacement and acceleration responses of the bridge are recorded at 1000 Hz in LS-DYNA. The responses are then contaminated with artificial measurement noise with a standard deviation of $\sigma_{v,sim}^{\text{disp}} = 10^{-3}$ inch for displacement measurements and

$\sigma_{v,sim}^{\text{acc}} = 0.5$ mg for acceleration measurements. For easier comparison of the estimators, σ_v values available to the estimators are assumed to be the same as the one used in simulation, thus the corresponding covariances $\Sigma_{v,est} = \Sigma_{v,sim}$. Because the girder model is assumed to be accurate and no external disturbance is present, the simulated process noise is set as zero, i.e. $\Sigma_{w,sim} = 0$. The corresponding process noise covariance available to the estimators are set as $\Sigma_{w,est} = \Sigma_{w,sim} = 0$. The initial state μ_{x_0} is set as zero for both estimators and the corresponding initial state covariance Σ_{x_0} are set to a small value as $10^{-12}I$, assuming the initial condition of the structure is not exactly known.

Recall that for FIC estimator, input covariance $\Sigma_{u,est}$ is needed to perform the estimation. Similarly, for the LFB estimator, noise covariance $\Sigma_{\xi,est}$ is required. The value of $\Sigma_{u,est}$ can be determined by prior knowledge of the input, e.g. the standard weight of a vehicle. Because half of vehicle axle weight used in the road test is over 5000 lbs, the covariances $\Sigma_{u,est}$ and $\Sigma_{\xi,est}$ are set as 10^7 lbs^2. In addition, because the vehicle model simulated in LS-DYNA has a bouncing frequency of 3Hz, the input model of the LFB estimator is chosen as a low-pass 4$^{\text{th}}$ order Chebyshev filter with a cutoff frequency of 5 Hz and a peak-to-peak passband ripple of 0.1 dB. The estimated moving input from the FIC and LFB estimators are shown in Figure 5-4. The actual input/load is indicated as the dashed red line with a corresponding $\pm 5\%$ error interval in the plot. For both estimators, the estimated input is mostly within the $\pm 5\%$ error interval when the moving input is on the girder from 0s to 1.91s. Slightly larger error can be observed when the input just enters the girder and shortly before exiting the girder.

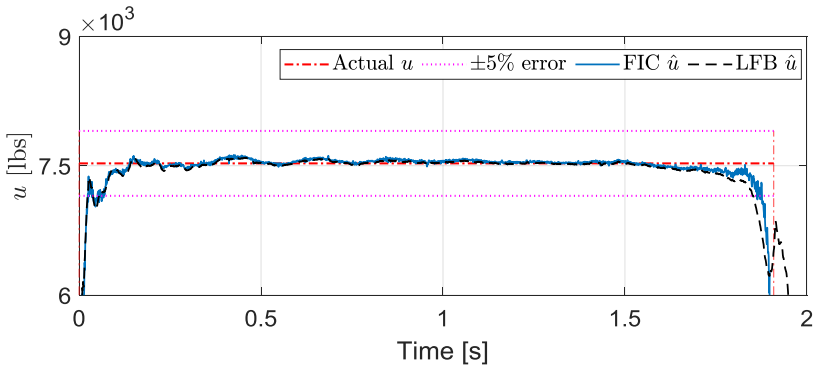

Figure 5-4 Estimated moving load with reduced-order model

The initial 0.2s after load entering the girder and the last 0.4s before load exiting the girder are excluded in the averaging process. The mean value of the input estimation time history during 0.20s to 1.51s is used as the final estimated input value. Using both estimators, the final estimated weight is very close to the actual applied weight, with a relative error of 0.25% for the FIC estimator and 0.069% for the LFB estimator.

5.2.2 Two Pairs of Moving Loads

Section 5.2.1 validates the moving input estimator with only one pair of loads, moving along the girders. To apply the estimators in B-WIM applications, however, the number of vehicle axles is always larger than one. In this subsection, two pairs of loads moving in tandem are applied with a velocity of 25 mph (Figure 5-5). The distance between the front and rear axles are 210 inches (17.5 ft), similar as the axle distance of a small truck. The total front load is set as 15,054 lbs, evenly distributed between the two spring-damper parts, i.e. 7,527 lbs on each girder. The rear load is set as 21,230 lbs and evenly distributed to the girders, i.e. 10,615 lbs on each girder. To simulate the moving loads in MATLAB, a state space model given by Eq. (5-1) and (5-2) is constructed in a similar manner as Section

5.2.1. The main difference is in the input location matrix Γ_u, which is modified to account for two moving loads.

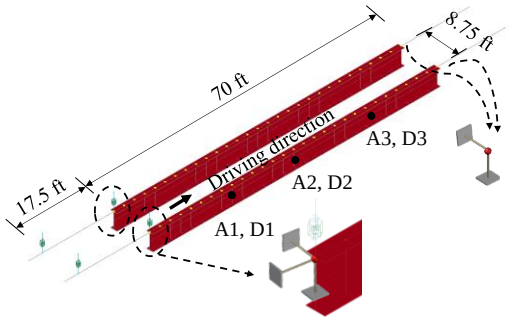

Figure 5-5 LS-DYNA model: simply supported girders with two pairs of moving loads

As illustrated in Figure 5-6, the two moving loads can be distributed to the vertical DOFs of neighboring nodes. Specifically, given prior knowledge of the moving loads velocity, location of u_1 and u_2 at time t can be determined. The loads u_1 and u_2 are then distributed to nearby nodes based on their relative distance, i.e. b/l_e, a/l_e for u_1 and d/l_e, c/l_e for u_2. The distributed loads can thus be mapped to the corresponding vertical DOFs of the FE model through an input location matrix Γ_u.

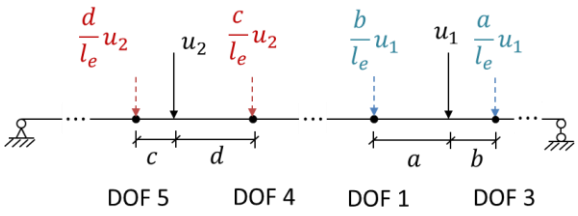

Figure 5-6 Illustration of two moving loads locations on one girder at time t

For example, if the vertical DOFs of the corresponding nodes are the same as shown in Figure 5-6, the input location matrix $\Gamma_u \in \mathbb{R}^{n_{\mathrm{DOF}} \times n_u}$ at time t is given by

$$\Gamma_u(t) = \begin{bmatrix} 1 & 0 & 0 & 0 \\ 0 & 0 & 0 & 0 \\ 0 & 1 & 0 & 0 \\ 0 & 0 & 0 & 1 \\ 0 & 0 & 1 & 0 \\ \vdots & \vdots & \vdots & \vdots \\ 0 & 0 & 0 & 0 \end{bmatrix} \begin{bmatrix} b/l_e & 0 \\ a/l_e & 0 \\ 0 & d/l_e \\ 0 & c/l_e \end{bmatrix} \tag{5-6}$$

Before applying the estimator, the magnitude of the feedthrough matrix D is again checked first. As explained in Section 5.2.1, compared to the full-order model, the reduced-order model through modal decomposition provides a larger time interval of non-zero feedthrough matrix, which is needed by the estimators to achieve desired input estimation. Therefore, the following results are based on the reduced-order model using the first five modes. Figure 5-7(a) shows the time history plot of the first column of feedthrough matrix (corresponding to the front load u_1) for three displacement and three acceleration measurements, respectively. Figure 5-7(b) shows the plots of the feedthrough matrix corresponding to the rear load u_2.

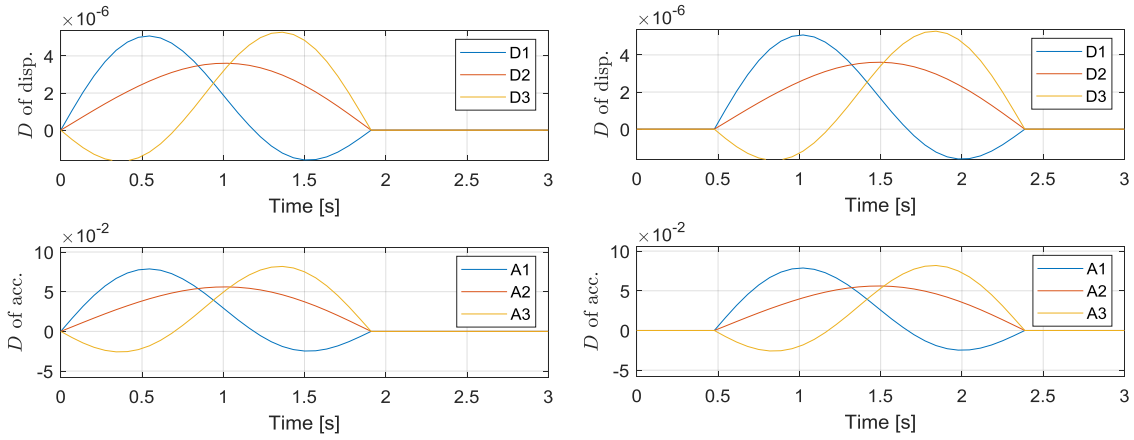

(a) Feedthrough matrix of front load u_1 (b) Feedthrough matrix of rear load u_2

Figure 5-7 Time history of feedthrough matrix using five modes for model reduction

Note that the front load plots in Figure 5-7(a) are the same as Figure 5-3(b) because the starting position and velocity between these two cases are the same. Furthermore, Figure 5-7(b) of load u_2 is a time-shifted version of Figure 5-7(a), because both loads have the same velocity and move along the same path on the girder.

Because the two girders are identical in this example, results from only the responses of the right girder are included here. To estimate the corresponding moving load, three vertical displacement responses (denoted as D1 ~ D3 in Figure 5-5(a)) and three vertical acceleration responses (denoted as A1 ~ A3) at the mid-length and near quarter lengths of the right girder are used. Same as Section 5.2.1, the simulated displacement and acceleration measurements are sampled at 1000 Hz and contaminated with measurement noise with a standard deviation of $\sigma_{v,sim}^{\text{disp}} = 10^{-3}$ inch and $\sigma_{v,sim}^{\text{acc}} = 0.5$ mg, respectively. The measurement covariance of the estimators is set as $\Sigma_{v,est} = \Sigma_{v,sim}$ and the process noise covariance is set as $\Sigma_{w,est} = \Sigma_{w,sim} = 0$. For initial condition of the state, μ_{x_0} is set as zero and the corresponding covariance is set as $\Sigma_{x_0} = 10^{-12}I$.

Recall that the actual front weight is 7,527 lbs and the rear weight is 10,615 lbs on each girder. Accordingly, the input covariance $\Sigma_{u,est}$ is set as $10^7 I$ lbs^2 for estimating both loads. Time history of the estimated loads u_1 and u_2 from the FIC and LFB estimators is shown in Figure 5-8. The estimated total load u_t is obtained as the sum of estimated axle loads u_1 and u_2 at each time step. For both estimators, the estimated loads are generally within the $\pm 5\%$ error interval of the actual load except after the second load just enters the girder at 0.48s and shortly before the first load exits the girder at 1.91s.

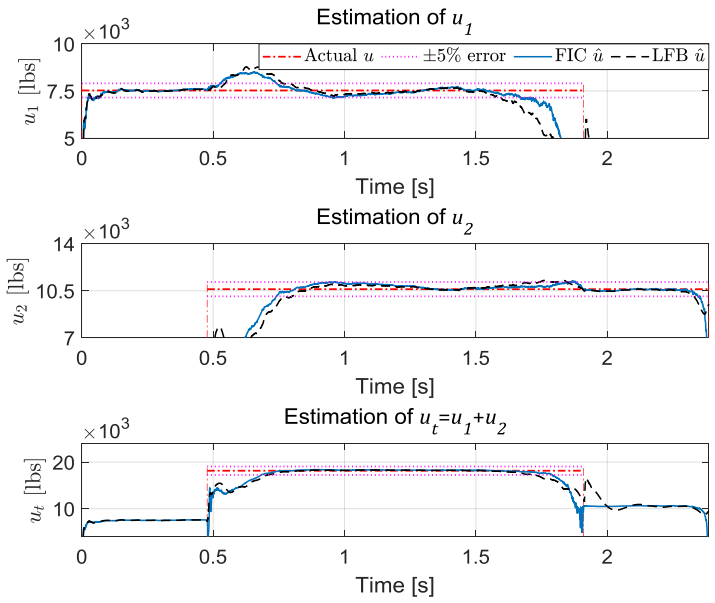

Figure 5-8 Estimated moving load with reduced-order model

The mean value of the input estimation time history during 0.20s to 1.51s is again used to calculate the front weight. For the rear weight, the mean value of the estimated input during 0.68s to 2.09s is taken as the estimated value. The mean value of the total load between 0.68s and 1.51s (when both loads are on the girder) is taken as the estimated total weight. For the FIC estimator, the final estimated input has a relative error of 1.19% for the front weight, 0.98% for the rear weight and 0.38% for the total weight. For the LFB estimator, a similar small error can be achieved, i.e. 1.92% for the front weight, 0.29% for the rear weight and -0.18% for the total weight. Overall, both estimators can achieve relatively good estimate of both weights.

5.3 Validation on an In-Service Highway Bridge

An in-service highway bridge located in Bartow County of Georgia in United States is used as the validation bridge for B-WIM study. The bridge will be referred to as the

Bartow bridge hereinafter. In Section 5.3.4, the proposed FIC and LFB estimators are first applied to estimate vehicle axle weights using simulated bridge response from LS-DYNA. In Section 5.3.5, experimentally measured bridge responses obtained from a wireless sensing system are used to estimate axle weights and gross vehicle weights of two different passing trucks.

5.3.1 Test Bridge and Sensor Instrumentation

The Bartow bridge consists of three skewed 70-feet long concrete spans supported by five I-shaped pre-stressed concrete girders. Figure 5-9 shows the plan and elevation view of the entire bridge. The five pre-stressed concrete girders, denoted as G1 to G5 in Figure 5-9(a), are spaced at 8 feet 9 inches and simply supported at both ends. The direction of the two-lane traffic passing through the bridge is from west to east as marked in Figure 5-9(a). The west span here is the first span of the bridge excited by vehicles with easy accessibility. Therefore, the west span is chosen for B-WIM instrumentation in this study.

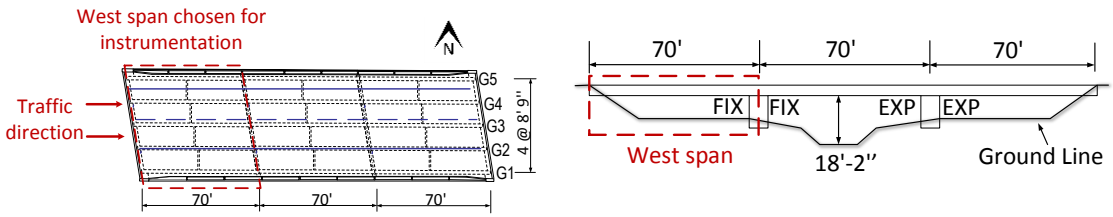

(a) Bridge plan view (b) Bridge elevation view

Figure 5-9 Plan and elevation view of Bartow bridge

Figure 5-10(a) illustrates sensor instrumentation of the west span in a field test, including 3 magnetostrictive displacement sensors, 7 strain gages and 9 accelerometers. The displacement sensors were installed at mid-span to measure vertical displacement of

the girders. On the bottom of girders, strain gages were installed at quarter and mid-span locations to measure longitudinal strain. Accelerometers were installed at the same locations as strain gages to measure vertical acceleration. Figure 5-10(b) illustrates the elevation view of sensor instrumentation of girder G2. In this study, these heterogeneous sensor measurements are fused together to estimate truck loads as it passes through the bridge.

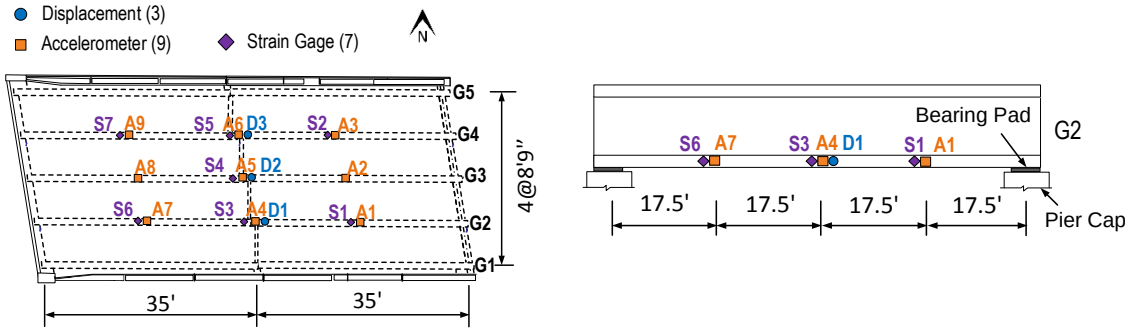

(a) Plan view of west span instrumentation (b) Elevation view of girder G2

Figure 5-10 Instrumentation plan of Bartow bridge

5.3.2 Bridge and Vehicle Models

A finite element (FE) model of the Bartow bridge is built in LS-DYNA. The FE model is used to simulate bridge response under moving vehicle loads and provide stiffness and mass matrices to construct the state-space system matrices required by the estimators. Figure 5-11 shows the top and bottom view of the FE model. The structural components include five concrete girders with pre-stressed steel strands, bridge deck, barriers, diaphragm, end wall and end beam at both sides of the span. The girders, barriers, diaphragm, end wall and end beam are modeled using Hughes-Liu beam element with cross section integration; the pre-stressed strands are modeled using discrete beam/cable

elements; and the deck is modeled using Belytschko-Tsay shell element. The resulting FE model has a mesh size of 76 cm (30 inches) with a total of 1,708 degrees-of-freedom (DOFs).

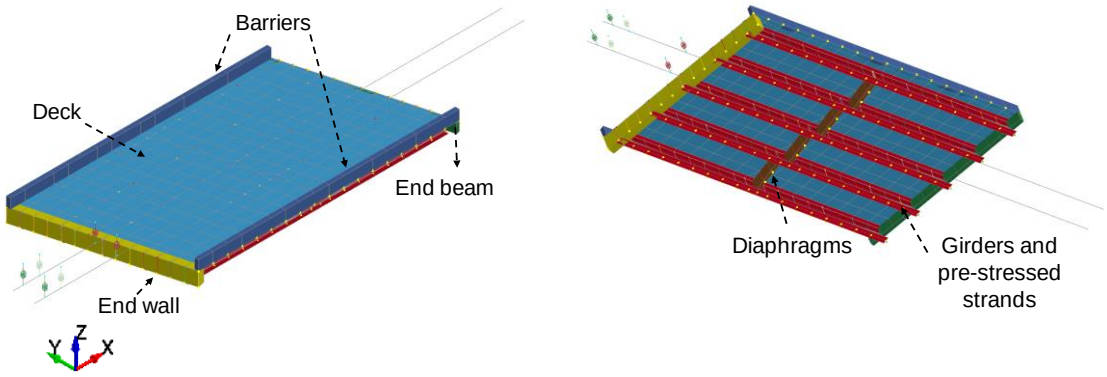

(a) Top view of FE model (b) Bottom view of FE model

Figure 5-11 LS-DYNA Bartow bridge model with moving vehicle loads

To model the connection between girders, pre-stressed strands and bridge deck, the meshed nodes from these components are connected using rigid body links. For boundary conditions, the longitudinal (i.e. x-axis) translational DOFs and rotational DOFs about global y-axis are released at the end wall side. At the end beam side, rotational DOFs about global y-axis of the bridge deck are restrained with rotational boundary springs, and the vertical DOFs of the girders are restrained with translational boundary springs. Specifically, to account for the bending stiffness contribution from the neighboring span, rotational springs about y-axis are added to each node of the bridge deck at the end beam side. Based on the bending stiffness of the deck, the stiffness value of the rotational spring at each node is set as 2.73×10^{10} lbf $\cdot$ inch/rad. In addition, the vertical translational spring are used to model bearing support at the bottom of the girders. The stiffness value of the translational spring is set as 4.60×10^{6} lbf/inch, based on the vertical stiffness of

the bearing pad. The concrete modulus of the concrete girder is set as 4.415×10^6 psi, based on the nominal design parameter. The moduli for all other concrete components are set as 3.372×10^6 psi. The steel modulus of the pre-stressed strands is set as 2.9×10^7 psi. The first four resonance frequencies of the bridge model are 7.79 Hz, 8.63 Hz, 12.91 Hz and 20.35 Hz and the mode shapes are shown in Figure 5-12. A Rayleigh damping model is assumed using 2% modal damping ratio for the first two modes to simulate structural response under moving loads.

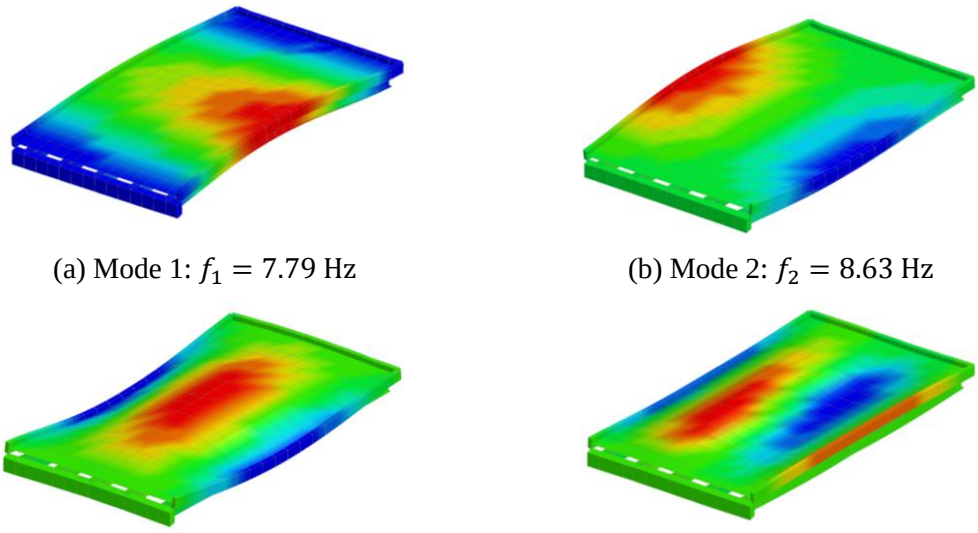

(a) Mode 1: $f_1 = 7.79$ Hz

(b) Mode 2: $f_2 = 8.63$ Hz

(c) Mode 3: $f_3 = 12.91$ Hz

(d) Mode 4: $f_4 = 20.35$ Hz

Figure 5-12 First four modes of the Bartow bridge FE model

To model the moving vehicle load, the same spring-damper model from Section 5.2 is used here. Three pairs of loads, each corresponding to a pair of truck axle loads, passes through the bridge at a velocity of 25 mph. The distance between the front axle and 2nd axle is 182 inches (4.62 meters) and 53 inches (1.35 meters) between the 2nd axle and 3rd axle. In this simulation, the front axle enters the span after 0.05s and exits the span after

2.03s, the 2nd axle enters after 0.47s and exits after 2.45s, and the 3rd axle enters the span after 0.59s and exits after 2.57s. The total weight of the front axle is set as 15,150 lbs, evenly distributed between the two spring-damper parts, i.e. 7,575 lbs each. The total weights of the two rear axles are set as 10,800 lbs and 10,500 lbs, respectively. The spring stiffness and damping coefficient of all three axles are set as $k = 7000$ lbf/inch and $c = 100$ lbf $\cdot$ s/inch, resulting in a bouncing frequency around 3Hz. The contact relationship between the moving vehicle and the girder is modeled using a train/rail model from LS-DYNA. A unit contact mass is added at each contact node between the vehicle model and the bridge. The bridge displacement, strain and acceleration response are simulated in LS-DYNA and sampled at 1000 Hz. The responses are contaminated with measurement noise with a standard deviation of $\sigma_{v,sim}^{\text{disp}} = 10^{-4}$ inch, $\sigma_{v,sim}^{\text{strain}} = 0.1$ με and $\sigma_{v,sim}^{\text{acc}} = 0.3$ mg.

5.3.3 State Space Model

To formulate the state space system used by the estimators in MATLAB, the mass matrix M and stiffness matrix K obtained from the LS-DYNA model are used to construct A_c, B_c, C_c and D_c in Eq. (5-1) and (5-2). In addition, the damping matrix C_{damp} is obtained using a Rayleigh damping model with 2% damping ratios assumed for the first two modes. To simulate the moving loads, the time-varying input location matrix $\Gamma_u(t)$ is obtained in a similar manner as in Section 5.2. Prior knowledge of the moving load velocity is used to determine the locations of all three axle loads (u_1, u_2 and u_3) at a time instant. Figure 5-13 illustrates the moving load locations.

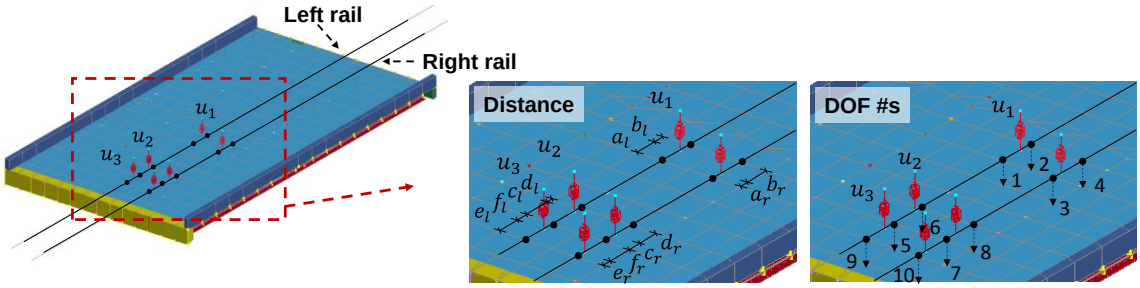

Figure 5-13 Illustration of moving load locations

First, based on the load locations, the corresponding elements are determined. Next, the load from each axle is distributed to four nodes (marked as black dots in Figure 5-13) of the corresponding elements, based on their distance to the nodes. Equation (5-7) shows the load distribution vectors for each of the three axle loads.

$$v_{u1} = \begin{bmatrix} b_l/l_{e,u1,l} \\ a_l/l_{e,u1,l} \\ b_r/l_{e,u1,r} \\ a_r/l_{e,u1,r} \end{bmatrix}_{4\times1}, \quad v_{u2} = \begin{bmatrix} d_l/l_{e,u2,l} \\ c_l/l_{e,u2,l} \\ d_r/l_{e,u2,r} \\ c_r/l_{e,u2,r} \end{bmatrix}_{4\times1}, \quad v_{u3} = \begin{bmatrix} f_l/l_{e,u3,l} \\ e_l/l_{e,u3,l} \\ f_r/l_{e,u3,r} \\ e_r/l_{e,u3,r} \end{bmatrix}_{4\times1} \tag{5-7}$$

In the distribution vector v_{u1} of the first axle load u_1, notations a_l, b_l represent the distance between u_1 on the left rail and the corresponding two neighboring nodes, and a_r, b_r represent the corresponding distance for the right rail. Notations $l_{e,u1,l} = a_l + b_l$ and $l_{e,u1,r} = a_r + b_r$ represent the current element lengths from both left and right rails. The distribution vectors v_{u2} and v_{u3} of the 2nd and 3rd axles are defined in the same way for the left and right rails.

Using the distribution vectors, the distributed nodal loads can thus be mapped to the corresponding vertical DOFs of the FE model through an input location matrix $\Gamma_u \in \mathbb{R}^{n_{\mathrm{DOF}} \times n_u}$. In this section, the number of inputs is $n_u = 3$, corresponding to the three truck axles, i.e. three pairs of moving loads. For simplicity, assume the vertical DOFs are numbered as in Figure 5-13, i.e. the two vertical DOFs corresponding to the first axle load at the left rail are the first two DOFs of the FE model, *etc*. Note that in this specific example, because the distance of rear axles is slightly smaller than twice of the shell element size, the two rear axles share a pair of distribution nodes (Figure 5-13). As a result, the input location matrix $\Gamma_u \in \mathbb{R}^{n_{\mathrm{DOF}} \times n_u}$ at time t is given by

$$\Gamma_u(t) = \begin{bmatrix} I_4 & 0 & 0 \\ 0 & I_4 & I_{u3}^{(2)} \\ 0 & 0 & I_{u3}^{(1)} \\ 0 & 0 & 0 \\ \vdots & \vdots & \vdots \\ 0 & 0 & 0 \end{bmatrix}_{n_{\mathrm{DOF}} \times 12} \begin{bmatrix} v_{u1} & 0 & 0 \\ 0 & v_{u2} & 0 \\ 0 & 0 & v_{u3} \end{bmatrix}_{12 \times 3} \tag{5-8}$$

where $I_4 = \begin{bmatrix} 1 & 0 & 0 & 0 \\ 0 & 1 & 0 & 0 \\ 0 & 0 & 1 & 0 \\ 0 & 0 & 0 & 1 \end{bmatrix}$, $I_{u3}^{(1)} = \begin{bmatrix} 1 & 0 & 0 & 0 \\ 0 & 0 & 0 & 0 \\ 0 & 0 & 1 & 0 \\ 0 & 0 & 0 & 0 \end{bmatrix}$ and $I_{u3}^{(2)} = \begin{bmatrix} 0 & 1 & 0 & 0 \\ 0 & 0 & 0 & 0 \\ 0 & 0 & 0 & 1 \\ 0 & 0 & 0 & 0 \end{bmatrix}$.

Because the FE model of the Bartow bridge has over thousands of DOFs, model reduction is applied to the full-order state space model using modal decomposition (Eq. (5-3) and (5-4)). Model reduction is applied to the full-order state space model. Recall that the distance between the axle u_2 and axle u_3 is only 53 inches in this example. Because of the closely spaced two rear axles, during input estimation, the two rear loads u_2 and u_3 are

combined as one rear load $u_{2,3}$ and equally distributed to all the rear nodes. Therefore, the input location matrix of the reduced-order estimator model is modified as follows. Accordingly, the estimated $\hat{u}_1$ is the front axle load; and the estimated $\hat{u}_{2,3}$ is the combined rear axle load.

$$\Gamma_{u,est}(t) = \begin{bmatrix} I_4 & 0 & 0 \\ 0 & I_4 & I_{u3}^{(2)} \\ 0 & 0 & I_{u3}^{(1)} \\ 0 & 0 & 0 \\ \vdots & \vdots & \vdots \\ 0 & 0 & 0 \end{bmatrix}_{n_{\mathrm{DOF}}\times 12} \begin{bmatrix} v_{u1} & 0 \\ 0 & \frac{v_{u2}}{2} \\ 0 & \frac{v_{u3}}{2} \end{bmatrix}_{12\times 2} \tag{5-9}$$

To obtain strain measurement equation in state space form, longitudinal nodal displacement from two nodes of a beam element divided by corresponding element length are used to approximate the axial strain. Specifically, the nodal displacements are shifted to the bottom of the girder based on the rotation of the cross-section. Because the estimators are derived in discrete time, first-order-hold discretization is applied to the reduced-order continuous system given by Eq. (5-3) and (5-4) with a time step of 0.001s. The resulting discrete feedthrough matrix D is shown in Figure 5-14. Specifically, three different types of measurements from Figure 5-10, i.e. displacement, strain and acceleration, are shown in separate plots.

Figure 5-14(a) shows the time history plot of the first column of feedthrough matrix corresponding to the front load u_1 using 15 modes for model reduction with the highest resonance frequency $f_{15} = 38.8$ Hz. Because the trajectory of the moving loads is close to girder G2 and G3, only the measurements from girders G2 and G3 are labeled in the plots.

Figure 5-14(b) shows the results using 70 modes for model reduction with the highest resonance frequency $f_{70} = 104$ Hz. When a larger number of modes are used to reduce the system order, the entries of the feedthrough matrix corresponding to the measurements close to the vehicle trajectory (girder G2 and G3) have larger magnitudes than other measurements. Note that for the combined rear load $u_{2,3}$, the corresponding column in the feedthrough matrix is similar as the result of u_1 but shifted in time. Therefore, those plots are not further included.

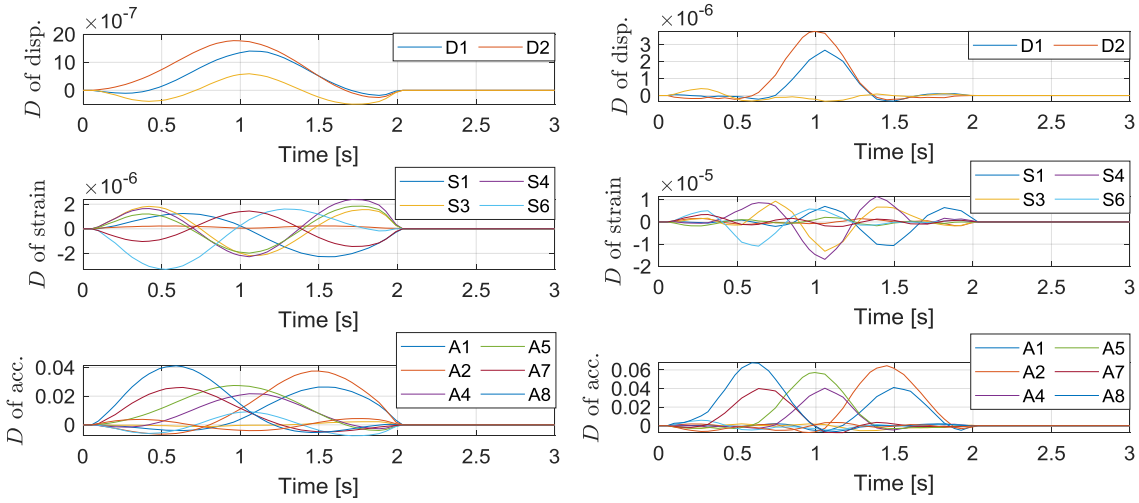

(a) Feedthrough matrix of front load u_1 with 15 modes

(b) Feedthrough matrix of front load u_1 with 70 modes

Figure 5-14 Time history of feedthrough matrix after model reduction

5.3.4 Moving Load Estimation with Simulated Measurements

The FIC and LFB estimators are applied to estimate the moving vehicle loads using simulated bridge responses. Three different sensor instrumentation scenarios are compared here. In the first scenario, simulated response from all three types of sensors are used, including 3 displacement, 7 strain and 9 acceleration (Figure 5-10(a)). In the second

scenario, only displacement and acceleration responses are used. In the third scenario, only displacement and strain responses are used. Note that in the last scenario, because of the small magnitude of the feedthrough matrix corresponding to the displacement and strain responses, the FIC estimator is not able to perform well. Therefore, the FIC-d estimator is used instead when no acceleration measurements are available. In all scenarios, the measurement covariance of the estimators is set as $\Sigma_{v,est} = \Sigma_{v,sim}$ and the process noise covariance is set as $\Sigma_{w,est} = 10^{-12}I$. For initial condition of the state, μ_{x_0} is set as zero and the corresponding covariance is set as $\Sigma_{x_0} = 10^{-10}I$.

For the FIC estimator used in the first two scenarios, input covariance $\Sigma_{u,est}$ is required to perform the estimation. Recall that the front axle has a pair of 7,575 lbs weights, and the two combined rear axles has a pair of 10,650 lbs weights. Accordingly, the input covariance $\Sigma_{u,est}$ is assumed as $10^8 I$ lbs^2 for estimating both loads. For the LFB estimator, because vehicles generally have a bouncing frequency from 1 Hz to 3 Hz [42], the input model of the LFB estimator is chosen as a low-pass 4th order Chebyshev filter with a cutoff frequency of 5 Hz and a peak-to-peak passband ripple of 0.1 dB for both loads. The noise covariance $\Sigma_{\xi,est}$ of the LFB estimator is set as $10^8 I$ lbs^2, same as the covariance $\Sigma_{u,est}$ of the FIC estimator.

5.3.4.1 Scenario #1: displacement, strain and acceleration measurements

The FIC and LFB estimators are applied to estimate the moving loads using all three types of measurements. Figure 5-15(a) shows the estimation of front axle load u_1, combined rear axle loads $u_{2,3}$ and total load u_t using 15 modes for model reduction. The

estimated total load is obtained as the sum of all estimated axle loads at each time step. Figure 5-15(b) shows the estimation results using 70 modes for model reduction. The actual axle weights are indicated as the dashed red line with the corresponding $\pm 5\%$ and $\pm 10\%$ error intervals in each plot.

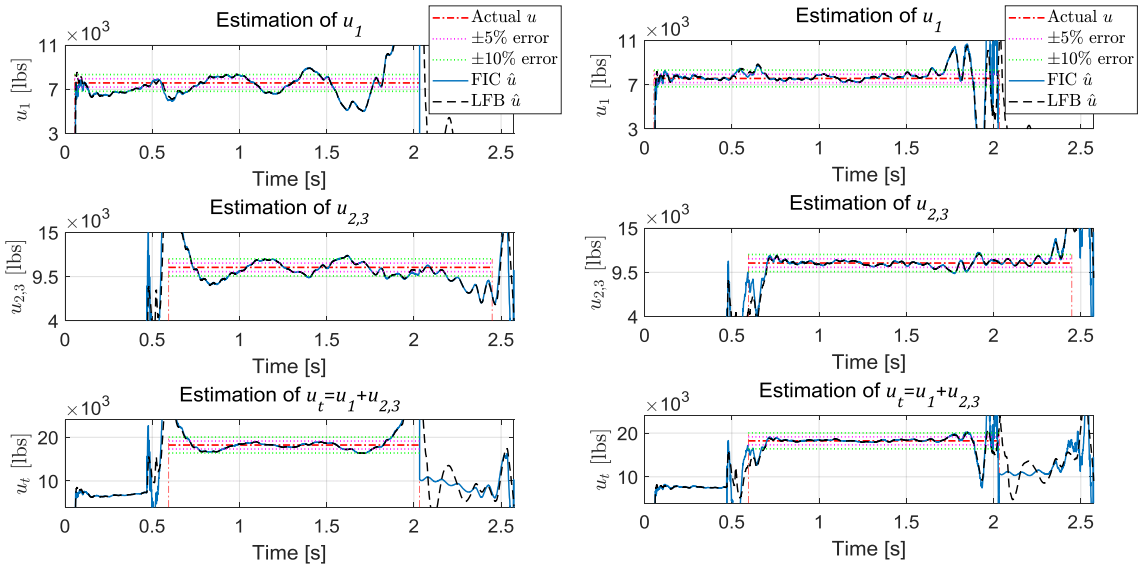

(a) 15 modes (b) 70 modes

Figure 5-15 Estimated loads using displacement, strain and acceleration responses

The FIC and LFB estimators generally perform similarly and the estimation of gross vehicle weights is more better than axle weights. Large fluctuations in the estimated loads can be observed when the 2nd axle enters the span at 0.47s and the first axle exits the span at 2.03s. When both axles are on the span, the estimated total load has less fluctuation and close to the actual applied weights. Furthermore, when a larger number of modes are used in model reduction, better estimation results of both axle weights and gross vehicle weight can be obtained with less fluctuation (Figure 5-15(b)).

5.3.4.2 Scenario #2: displacement and acceleration measurements

The FIC and LFB estimators are again applied to estimate the moving loads using 3 displacement and 9 acceleration measurements, excluding strain. Figure 5-16 shows the estimated front load u_1, combined rear loads $u_{2,3}$ and total load u_t using 15 modes and 70 modes for model reduction, respectively. Compared to scenario #1, larger oscillation in the axle load estimation can be observed, because more acceleration measurements are included than displacements, resulting in a larger contribution in the estimation results. On the other hand, because less low-frequency measurements are used, the estimated front load and total load are relatively constant and close to the actual applied weights even when only 15 modes are used in model reduction (Figure 5-16(a)).

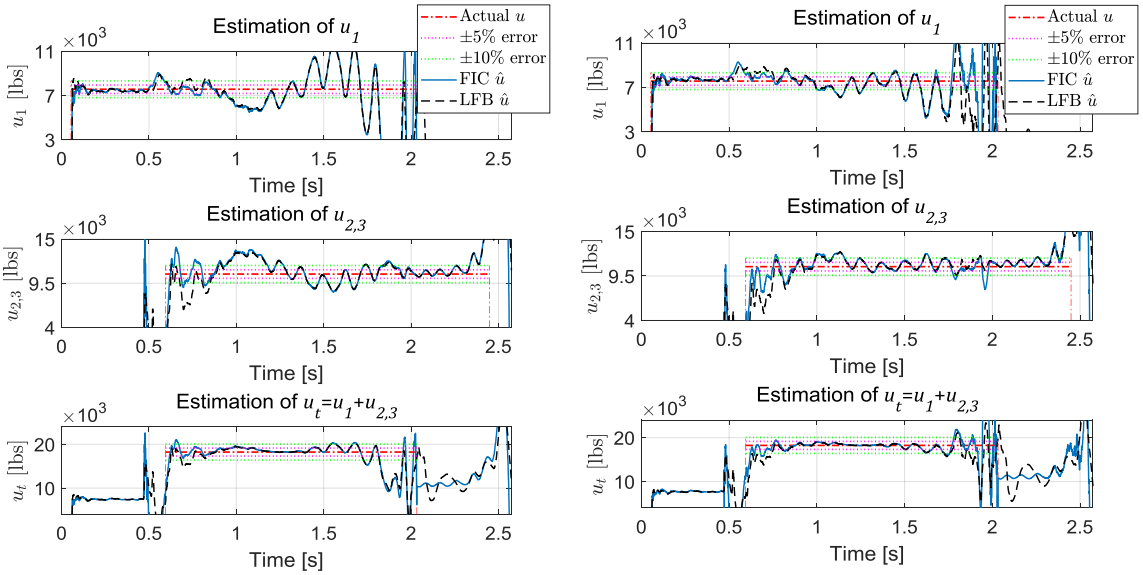

(a) 15 modes (b) 70 modes

Figure 5-16 Estimated loads using displacement and acceleration responses

5.3.4.3 Scenario #3: displacement and strain measurements

In this scenario, only 3 displacement and 7 strain measurements are used to estimate the moving loads without any acceleration measurements. Because of the small magnitude of the displacement and strain entries in the discrete feedthrough matrix, the FIC estimator is not able to provide good results. Therefore, the FIC-d estimator with delayed measurements from Section 2.3 are used instead. Figure 5-17 shows the estimation error e_{u_t} of the gross vehicle weight as a function of delay d when the input covariance $\Sigma_{u,est}$ is $10^6 I$ lbs^2. The delayed time step d is thus set as 10 to balance between accuracy and computational efficiency. The estimation results from the FIC-10 and LFB estimators are compared in Figure 5-18 using 15 modes and 70 modes for model reduction, respectively. Compared to the previous two scenarios, the estimated loads from the FIC-10 estimator appear to be more sensitive to measurement noise when only displacement and strain measurements are used. On the other hand, because the LFB estimator has a built-in low-pass filter, the estimated loads are less sensitive to noise than the FIC-10 estimator. Furthermore, when a larger number of modes are used in model reduction, better estimation results can be obtained with less fluctuation in the estimated loads (Figure 5-18(b)).

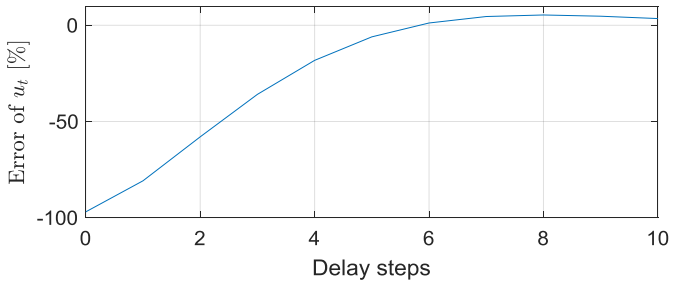

Figure 5-17 Estimation error e_{u_t} from the FIC-d estimator as a function of delay d

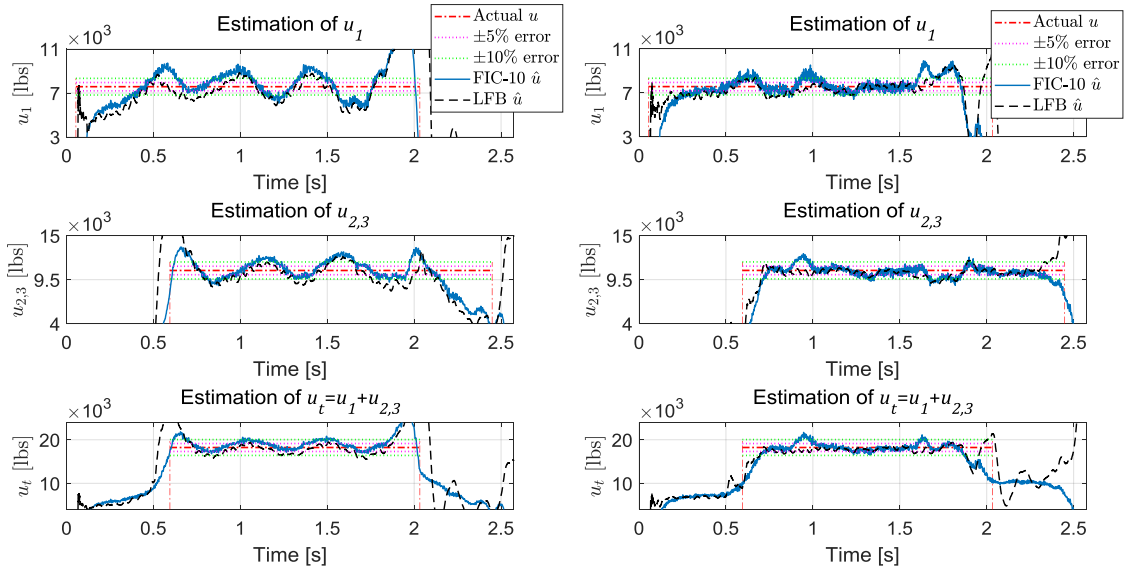

(a) 15 modes (b) 70 modes

Figure 5-18 Estimated loads using displacement and strain responses

5.3.4.4 Discussion of estimation results

Due to load fluctuations, mean values of the input estimation time history are calculated as estimation of axle weights and gross vehicle weight (GVW). Recall that the front axle is on the bridge span from 0.05s to 2.03s, and both the rear axles are on the span from 0.59s to 2.45s. In the first two scenarios, front axle weight estimation is obtained from the mean value of estimated front axle load $\hat{u}_1$ calculated between 0.10s to 0.54s. For rear axle weight estimation, the mean value of combined rear loads $\hat{u}_{2,3}$ is calculated between 1.09s to 2.15s. For GVW estimation, the mean value of total load $\hat{u}_t$ is calculated between 1.09s to 1.73s. In the third scenario, because of the delayed measurements, a longer time interval is used in the front axle estimation, which is obtained from the mean value of $\hat{u}_1$ calculated between 0.10s to 1.98s. Mean value intervals for rear weight and GVW are kept

the same as the first two scenarios. Table 5-1 summarizes the estimation error for the three scenarios and the smallest error in each scenario is in bold font.

Table 5-1 Weight estimation comparison among different estimators

Scenario	Estimator		Front axle e_{u_1} (%)	Rear axles $e_{u_{2,3}}$ (%)	GVW e_{u_t} (%)	Computation time (unit: second)
#1	FIC	15 modes	-8.34	-0.88	-1.40	0.59
		70 modes	1.45	-0.81	0.26	3.04
	LFB	15 modes	-8.66	**-0.61**	1.45	0.85
		70 modes	**0.77**	-0.79	**0.21**	4.04
#2	FIC	15 modes	**-0.72**	1.30	2.80	0.48
		70 modes	2.77	1.79	**-0.98**	3.10
	LFB	15 modes	-1.40	**1.10**	2.63	0.63
		70 modes	1.78	3.12	-1.05	4.86
#3	FIC-10	15 modes	-3.82	-4.34	2.98	7.59
		70 modes	**-3.43**	**-2.57**	**0.72**	203
	LFB	15 modes	-3.01	-3.78	-3.73	0.55
		70 modes	-4.93	-3.43	-2.51	4.36

Compared to the front axle, the estimation of rear axle weights and the GVW are closer to the actual applied weight in general. Specifically, smallest error e_{u_t} of the estimated GVW is achieved by the FIC estimator with 70 modes using all three types of measurements. The FIC and LFB estimators consume similar amount of computation time. Furthermore, the computation time is provided based on an Intel i7-4790 CPU and 16 GB RAM. The FIC-10 estimator in scenario #3 requires a longer time as a result of using

measurements at multiple time steps. When 70 modes are used in model reduction, longer estimation time is needed but resulting in improved estimation results, especially for scenario #1. In addition, when only displacement and strain measurements are available (scenario #3), although the delayed estimator performs better than the LFB estimator, a much longer computation time is required.

5.3.5 Moving Load Estimation with Experimental Measurements

In this section, the proposed moving load estimators are applied to estimate truck weights using experimental measurements from a B-WIM field test on the Bartow bridge. The same estimators from Section 5.3.4 are used here, including the FIC and LFB estimators. Two testing trucks used in this B-WIM test are introduced first. To measure bridge vibration responses, the *Martlet* wireless sensing system is used for data acquisition. In addition to the displacement, strain and acceleration measurements used in Section 5.3.4, three pairs of laser sensors interfaced with *Martlet* system are used to detect the actual truck speed during the field test. The speed is then used as prior knowledge provided to the moving load estimators.

5.3.5.1 Testing Trucks

The two trucks used in the B-WIM field test are manufactured by Navistar International Transportation Corporation and provided by Georgia Department of Transportation. Truck A is model 7600 6×4 (Figure 5-19(a)) and truck B is model 2674 6×4 (Figure 5-19(b)). As shown in Figure 5-19(c), each truck has three axles with similar axle distances. Truck A is half-loaded and truck B is fully loaded.

(a) Truck A (model 2674 6×4)

(b) Truck B (model 7600 6×4)

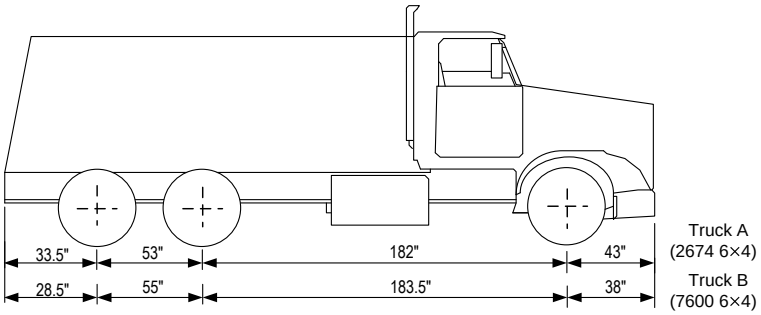

(c) Dimensions of two testing trucks

Figure 5-19 Trucks used in Bartow bridge B-WIM test

Static axle weights of each vehicle are measured by portable wheel scales and used to compare with the weight estimation results obtained from the moving load estimators. Table 5-2 summarizes the measured static axle weights and the corresponding GVW of both trucks.

Table 5-2 Axle weight and gross vehicle weight of the testing trucks

Vehicle	Axle weight (lbf)			GVW
	1st axle	2nd axle	3rd axle	
Truck A	15,150	10,800	10,500	36,450
Truck B	16,200	14,900	14,190	45,290

5.3.5.2 *Martlet* Wireless Sensing System

A wireless sensing system named *Martlet* is used to measure the bridge dynamical responses during traffic [73, 74]. In this field test, different types of sensors are interfaced with *Martlet* sensing node through corresponding sensor boards. As shown in Figure 5-20, the sensors include linear-position magnetostrictive displacement sensors (MTS CS194AV), 90mm strain gages, integrated MEMS accelerometers [82] and Silicon Designs accelerometers (2012-002). The amplification gains and the low-pass cutoff frequencies are set as ×50 and 25Hz for the displacement sensors, ×477 and 50Hz for the strain gages and ×20 and 25Hz for accelerometers. The sampling frequency is set to be 200Hz for all sensing channels.

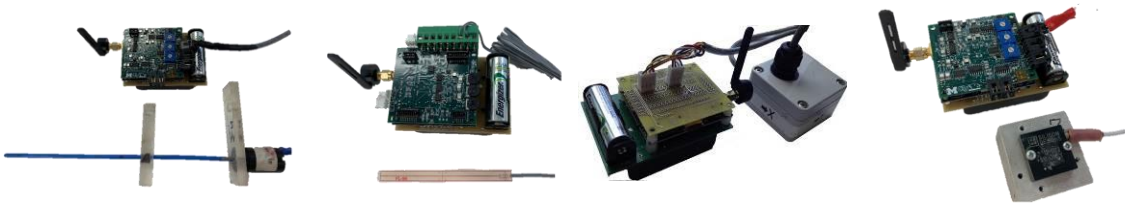

(a) Displacement sensor (b) Strain gage (c) Integrated accelerometer (d) Silicon Designs accelerometer

Figure 5-20 Sensors interfaced with *Martlet* wireless sensing system to measure bridge dynamical response

Figure 5-21(a) shows the sensor instrumentation of the bridge span, including 3 displacement sensors, 7 strain gages and 9 accelerometers, installed at mid-length and quarter lengths of bridge girders G2 ~ G4. Same as in Section 5.3.4, the measured bridge responses include girder vertical displacement, longitudinal strain at the girder bottom and girder vertical acceleration.

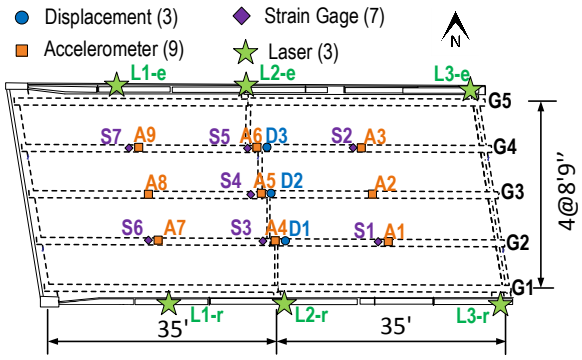

(a) Sensor instrumentation

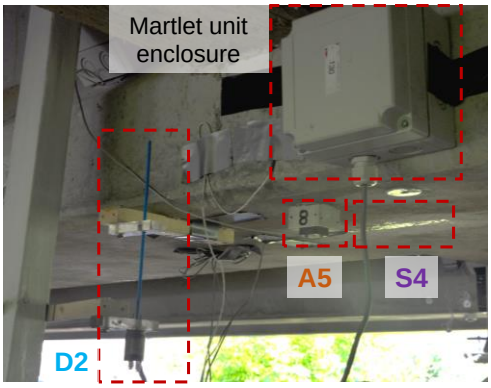

(b) Sensors at mid-length of girder G3

Figure 5-21 Instrumentation plan of *Martlet* wireless sensing system

In order to obtain vehicle speed required by the moving load estimators, 3 pairs of laser sensors are used to estimate the speed of passing vehicles. Specifically, each pair of laser sensors includes a laser emitter (Figure 5-22(a) and denoted as L#-e in Figure 5-21(a)) and a laser receiver (Figure 5-22(b) and denoted as L#-r in Figure 5-21(a)). The laser emitter is used to generate laser beam, and the laser receiver has three photodiodes used to sense the laser beam. The laser sensors were installed at the top of the two bridge barriers on each side, as shown in Figure 5-22(c).

Before testing, each pair of laser emitter and receiver was properly aligned such that the laser beam from the emitter aims at the photodiodes of the receiver. As a result, the voltage output from the photodiodes stays relatively constant. When a vehicle passes through the bridge and blocks the laser beam, the voltage output from the photodiodes drops significantly, thus indicating the presence of a vehicle. The voltage output from the photodiodes is sampled by the *Martlet* wireless sensing system and automatically synchronized with all other sensing channels.

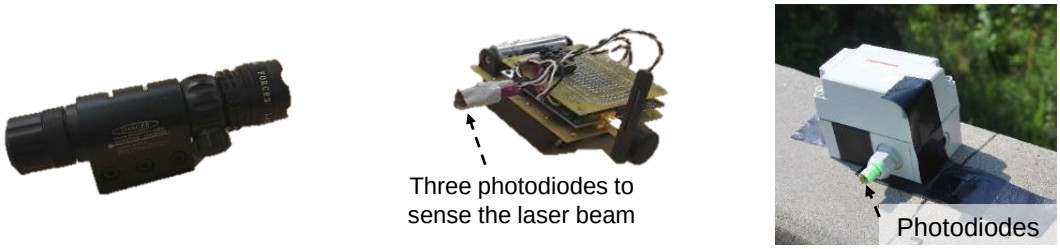

(a) Laser emitter (b) Laser receiver (c) Laser receiver on barrier

Figure 5-22 Laser sensors for detecting vehicle speed

Figure 5-23 shows the relative voltage changes from three laser receivers when truck A and B drove through the bridge, respectively. Recall that for each laser receiver, three photodiodes are combined to achieve reliable measurements (Figure 5-22(b)). Therefore, each laser receiver provides three voltage signals. For all three laser receivers, significant voltage drop can be observed when a truck blocks the laser beam. The time lag between voltage drops at different laser receivers can be obtained. Dividing the distance between each laser receiver by the time lag, the speed of the moving vehicle can be calculated.

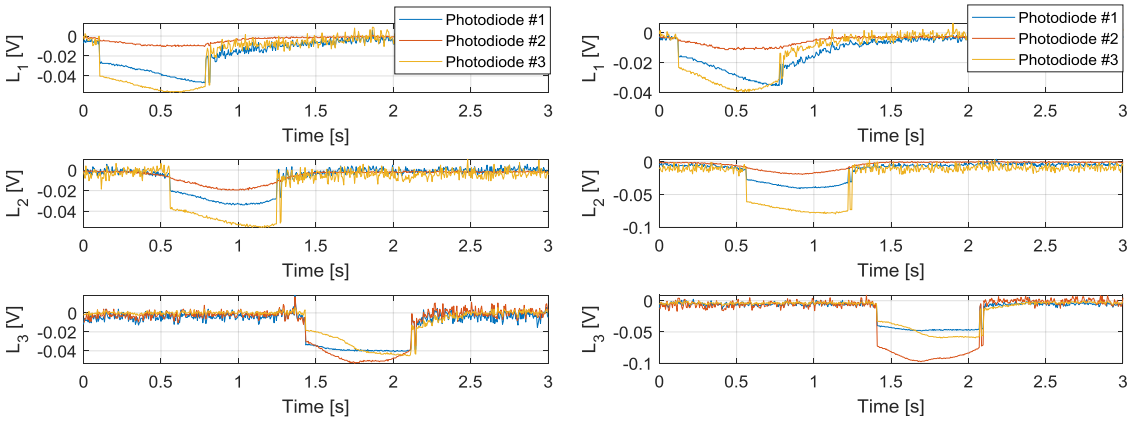

(a) Laser voltage change: truck A (b) Laser voltage change: truck B

Figure 5-23 Relative votlage change from laser sensors as a truck drives through

Finally, the average speed among all laser measurements is taken as the vehicle passing speed. Based on the laser measurements, the average speed of truck A is 460 inch/s (26 mph) and the average speed of truck B is 477 inch/s (27 mph). These speed values are then provided to the moving load estimators for truck weight estimation.

5.3.5.3 Vehicle Weight Estimation

Based on the simulation results in Section 5.3.4, all three types of measurements are used to estimate the moving loads. For comparison, the experimental measurements are up-sampled from 200 Hz to 1000 Hz and synchronized with the simulated bridge response. Using the speed value, the time of each vehicle axle enters and passes through the bridge span are summarized in Table 5-3.

Table 5-3 Timing of truck axles on the bridge span

Truck	Case	1st axle (front)	2nd axle (rear)	3rd axle (rear)
A	Enter	0.05 s	0.45 s	0.56 s
	Exit	1.94 s	2.34 s	2.46 s
B	Enter	0.05 s	0.43 s	0.55 s
	Exit	1.88 s	2.26 s	2.38 s

To determine the vehicle location at each time instant, bridge responses are generated in simulation first based on the available vehicle speed. A total of 70 modes are used to reduce the system order through modal decomposition. The proposed FIC and LFB

estimators are applied. The estimator covariances are kept the same as in Section 5.3.4. Specifically, the process noise covariance is set as $\Sigma_{w,est} = 10^{-12}I$. For measurement noise covariance $\Sigma_{v,est}$, the standard deviations of measurement noise corresponding to each type of sensors are set as $\sigma_{v,sim}^{\text{disp}} = 10^{-4}$ inch, $\sigma_{v,sim}^{\text{strain}} = 0.1$ με and $\sigma_{v,sim}^{\text{acc}} = 0.3$ mg. For state initialization, μ_{x_0} is set as zero and covariance is set as $\Sigma_{x_0} = 10^{-10}I$. The FIC estimator uses an input covariance $\Sigma_{u,est}$ of $10^8 I$ lbs^2 for both trucks. The LFB estimator uses a low-pass 4$^{\text{th}}$ order Chebyshev filter as the input model. The filter has a cutoff frequency of 5 Hz and a peak-to-peak passband ripple of 0.1 dB. The noise covariance $\Sigma_{\xi,est}$ of the LFB estimator is set as $10^8 I$ lbs^2, same as $\Sigma_{u,est}$ of the FIC estimator.

The estimation results from both FIC and LFB estimators are shown in Figure 5-24, including the estimation of front axle load u_1, combined rear axle loads $u_{2,3} = u_2 + u_3$ and the total load u_t. The estimated total load u_t is obtained as the sum of all estimated axle loads at each time step. The measured static axle weights and GVW are indicated as the dashed red lines with the corresponding $\pm 5\%$ and $\pm 10\%$ error intervals in each plot. In general, the FIC and LFB estimators have similar performance with almost coinciding estimates. For each axle, larger estimation error occurs when the axles are close to the beginning or end of the span. For GVW estimation, larger estimation error is observed when the rear axles enter the bridge span (shortly before 0.5s) and when the first axle is close to the end of the span.

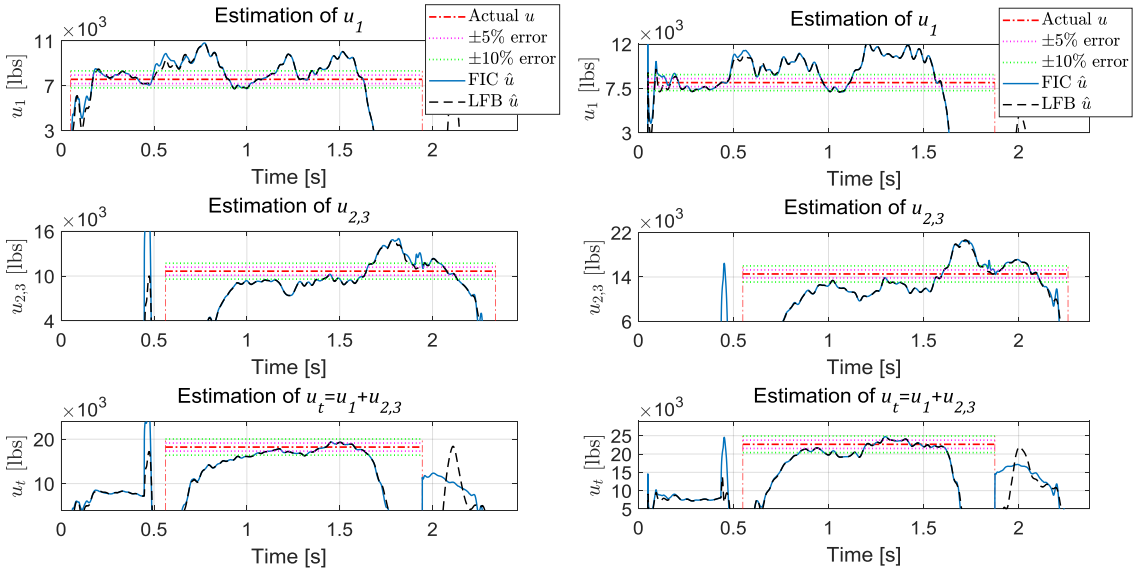

(a) Estimated loads of truck A

(b) Estimated loads of truck B

Figure 5-24 Estimated moving loads of truck A and B

To find the axle weights and GVW of both trucks from the moving load estimates, mean value of the estimated loads are calculated. For front axle weight estimation, mean value of front load $\hat{u}_1$ is calculated using 80% of the time duration after the front axle enters and before third axle enters the bridge span. For combined rear axle weight estimation, mean value of $\hat{u}_{2,3}$ is calculated using 55% of the time duration when both rear axles are on the bridge span. For GVW estimation, mean value of total load $\hat{u}_t$ is calculated using 40% of the time duration when all three axles are on the bridge span. The estimated weights of both trucks and the corresponding computation time from both estimators are summarized in the Table 5-4. For both trucks, the GVW are within 3% error, and the estimates of axle weights are within 4% error compared to the actual truck weight. The computation time of both estimators are similar, with the LFB estimator performing slightly faster.

Table 5-4 Comparison of truck weight estimation among different estimators

Truck	Estimator	Front axle e_{u_1} (%)	Rear axles $e_{u_{2,3}}$ (%)	GVW e_{u_t} (%)	Computation time (unit: second)
A	FIC	-1.79	-0.24	-2.82	3.32
	LFB	-3.57	-1.43	-2.88	4.54
B	FIC	-0.98	-3.39	-2.27	3.22
	LFB	-3.49	-4.07	-2.33	4.36

5.4 Summary

This chapter generalizes the previously proposed input-state estimators for moving input estimation, especially for application in bridge weigh-in-motion (B-WIM). Heterogeneous sensor measurements, including displacement, acceleration and strain, are fused together to estimate the moving inputs/loads. To validate the proposed estimators, a simply supported girder and a full-scale pre-stressed concrete highway bridge are used. Modal decomposition is applied to reduce the system order and improve estimator performance. For the simply supported girder, simulated displacement and acceleration measurements are used to estimate the moving load(s). Good estimates of vehicle axle weights can be obtained from the estimated moving loads with an error of less than 1%, using both the FIC and LFB estimators.

For the highway bridge, simulated sensor measurements are first used to estimate axle weights and gross vehicle weight (GVW) of a three-axle truck. The noise

contaminated measurements include displacement, strain and acceleration responses of the bridge span. Three different sensor instrumentation scenarios are discussed here. When a larger number of modes are used in model reduction, the estimated weights are closer to the actual weights. When acceleration measurements are available, the estimated GVW is within 3% error and the estimated axle weights are within 9% error. When only displacement and strain measurements are available, the FIC estimator is not able to estimate the moving loads, but the delayed FIC-10 estimator can provide good estimate. In addition, the LFB estimator is not only able to perform similarly well as the FIC estimator when acceleration measurements are available, but also performs well with only displacement and strain measurements.

Finally, experimental measurements from a B-WIM field test are used to estimate axle weights and GVW of two different three-axle trucks. A wireless sensing system named *Martlet* is instrumented on the bridge span. To find the passing vehicle speed, laser sensors are instrumented on the bridge. Using the displacement, strain and acceleration measurements from the field test, the estimated truck weights are compared with the static weight measured by portable scales. The results demonstrate that both the FIC and LFB estimators can provide relatively good estimates of axle weights and GVW with an overall error of less than 4%. In addition, the computation time is less than 6s for each vehicle.

CHAPTER 6. SUMMARY AND FUTURE WORK

To simultaneously estimate unknown input and state of a dynamical system, this research proposes and validates several input-state estimators for systems with and without direct feedthrough of the input based on a unifying minimum mean square error (MMSE) framework. In addition, the location of the unknown input can be both time-invariant and time varying depending on different applications. Two field tests are used to validate the proposed estimators, including a full-scale concrete frame and an in-service highway bridge. This chapter first summarizes the main conclusions of the dissertation and then discusses potential topics for future research.

6.1 Summary and Conclusions

The main conclusions of this research can be summarized as follows:

1. For simultaneous estimation of unknown input and state of a dynamical system, an estimator that adopts a white Gaussian input model with an explicit estimate of the unknown input is proposed in Chapter 2 for systems with and without direct feedthrough of the input. The estimator, short-named as the FIC (finite input covariance) estimator, can utilize prior statistical knowledge of the unknown input to achieve better estimation results. Compared with two other well-known estimators, e.g. an augmented Kalman filter (AKF) and a weighted least-squares (WLS) estimator, the FIC estimator can eliminate potential drift error in the estimated input along with a tighter estimation confidence interval. Furthermore, proof of equivalence between the WLS estimator and the FIC estimator with

infinite input covariance is derived based on a unifying MMSE framework. To generalize the FIC estimator for systems with rank deficient feedthrough matrix, an estimator with multi-step delayed measurements is also derived, short-named as the FIC-d estimator. Numerically simulated responses of a 4-story shear structure are used to validate the proposed FIC and FIC-d estimators in different input and output scenarios. For both systems with and without feedthrough, the FIC estimator can provide good estimation of the unknown input and state with a tight estimation confidence interval. In addition, the FIC-d estimator is shown to perform well even when the feedthrough matrix does not have full column rank.

2. Different state space models can be used to describe the dynamics of unknown input, and prior knowledge of such input models can be incorporated into the estimators to further improve estimation results. Based on the same MMSE framework, two estimators are proposed by assuming a general form of an exogenous input model for both systems with and without direct feedthrough. With the exogenous input model, not only a theoretical unification of the AKF and FIC estimators can be obtained, but also prior knowledge of the frequency bandwidth of the unknown input can be utilized by the proposed estimator. Specifically, a state space realization of a digital bandpass filter can be used as the exogenous input model, short named as the LFB (limited frequency bandwidth) estimator. The same 4-story shear structure is used to validate and compare the proposed LFB and FIC estimators with a larger measurement noise level. The LFB estimator is shown to perform better in both scenarios when input and measurement are collocated and non-collocated, respectively.

3. Experimental acceleration measurements from a full-scale concrete frame are used to validate the proposed FIC, FIC-d and LFB estimators in comparison to the conventional WLS estimator combined with an online drift filter (WLSF estimator). Based on the experimental measurements, the estimated force input generated by a shaker located on the roof of the frame is compared with the actual measured shaker force. Because of the large dimension of the original state space model, modal decomposition is used to reduce system order. After system order reduction, effect of sensor instrumentation on input estimation is investigated by examining the magnitude of the feedthrough matrix. A finite element (FE) model of the frame is first calibrated through non-convex optimization by minimizing modal property differences between the nominal model and the experimentally identified results. Next, two instrumentation scenarios are used to compare estimator performance: (i) measurements including the shaker location, and (ii) measurements far away from the shaker location. In both scenarios, except the WLSF estimator, all other estimators perform consistently well in estimating the shaker input. Although the online drift filter of the WLSF estimator can reduce drift error when only acceleration measurements are available, the estimation error covariance cannot be reduced and the WLSF estimator cannot converge to steady state. In contrast, the shaker force estimated by the FIC, FIC-d and LFB estimators are in good agreement with the actual measured shaker input, and all three estimators converge to steady state after a few seconds.

4. When input location is time varying, all the proposed estimators can be modified for applications in bridge weigh-in-motion to estimate moving vehicle weight based on the vibration responses of a bridge. To account for the moving input/load, the input location

matrix in the state space model is used to map the input to specific DOFs of an FE model as a function of time. Numerical studies of a simply supported girder is performed first to validate the proposed FIC and LFB estimators for estimating a single pair of moving loads and two pairs of moving loads, respectively. Using noise contaminated displacement and acceleration measurements, good estimates of axle weights can be obtained by the FIC and LFB estimators with an error of less than 1%. Furthermore, an in-service highway bridge is used as the test structure to validate and compare estimator performance. Both simulated and experimental heterogeneous measurements are used for estimation of moving vehicle weights. Different sensor instrumentation scenarios are discussed in simulation first. When acceleration measurements are available, the estimated gross vehicle weight (GVW) is within 3% error and the estimated axle weights are within 9% error for both FIC and LFB estimators (Table 5-1). When only displacement and strain measurements are available, the FIC estimator is not able to estimate the moving loads, but the delayed FIC-d and the LFB estimator can provide good estimates. Experimental heterogeneous measurements obtained from the *Martlet* wireless sensing system are then used to validate the proposed estimators. In addition, laser sensors are interfaced with the *Martlet* sensing system and used to estimate the vehicle speed. Two different trucks were arranged to drive through the bridge, respectively. The corresponding displacement, strain and acceleration responses of the bridge are used by the FIC and LFB estimators to estimate the moving truck weights in comparison to the static weights measured by portable wheel scales. The results demonstrate that both the FIC and LFB estimators can provide relatively good estimates of axle weights and GVW with an overall error of less than 4% and a fast computation time

of less than 6s per vehicle (Table 5-4). In addition, the *Martlet* wireless sensing system shows reliable performance during the field test and the potential to be used toward a B-WIM system.

6.2 Future Work

Based on current results, following are some recommendations for future research:

1. The input covariance of the FIC estimator and the noise covariance of the input model in the LFB estimator are important estimator parameters, which need to be properly tuned using prior statistical knowledge of the unknown input. Sensitivity analysis of the effect of covariance values on estimation accuracy can be performed based on the estimation error covariance. Furthermore, because the input covariance of the FIC estimators may be different from the actual statistical property of the input, an update of the input covariance can be combined if a better estimate of the unknown input covariance is desired. For the delayed FIC-d estimator, stability condition of the estimator needs to be further studied, and computational efficiency can be improved. In addition, when experimental acceleration measurements are used, the effect of accelerometer frequency bandwidth on input-state estimation should be considered.

2. In this research, the system model needed by the proposed input-state estimators is obtained from a frequency domain FE model updating approach. As recent studies have shown promising results using time domain based approach to estimate both system parameters and unknown input [83, 84], input estimation combined with system parameter identification as well as identifiability condition can be further investigated. Moreover, the

damping model used in this research is the Rayleigh damping model, which may not be the best model to describe the actual structure. Therefore, further studies on damping modeling are recommended.

3. In the numerical study of moving load estimation, the contact between vehicle and bridge is modeled using the wheel-rail contact algorithm provided by LS-DYNA [80]. This contact algorithm uses a predefined simple penalty function to ensure the vehicle nodes follow the straight track. To obtain more accurate modeling of the vehicle-bridge contact, other contact algorithms from LS-DYNA can be further studied. In addition, the effect of FE model mesh size and bridge barrier modeling on input estimation accuracy can be further investigated.

4. This research demonstrates that the proposed moving load estimator can estimate moving vehicle loads with reasonable accuracy, but prior knowledge about vehicle location and vehicle axle distance is assumed to be available. To obtain such prior knowledge, camera-based machine learning techniques can be adopted. For example, Ojio, *et al.* [85] proposed a contactless B-WIM system using cameras to detect vehicle axles and to obtain bridge deflection under vehicle loads. Hou, *et al.* [86] used computer vision and convolutional neural network to extract truck features and re-identify the same truck as it passed through different weigh-in-motion stations. These novel techniques can be further investigated and may significantly improve the performance of B-WIM systems. Other important factors to consider may include road roughness, multiple vehicles passing at the same time, vehicle velocity effect [87, 88] on estimation accuracy.

REFERENCES

[1] J. Chen and R. J. Patton, "Optimal filtering and robust fault diagnosis of stochastic systems with unknown disturbances," *IEEE Proceedings-Control Theory and Applications,* vol. 143, pp. 31-36, 1996.

[2] J. Chen, R. J. Patton, and H.-Y. Zhang, "Design of unknown input observers and robust fault detection filters," *International Journal of control,* vol. 63, pp. 85-105, 1996.

[3] P. K. Kitanidis, "Unbiased minimum-variance linear state estimation," *Automatica,* vol. 23, pp. 775-778, 1987.

[4] Y. Bar-Shalom, X. R. Li, and T. Kirubarajan, *Estimation with applications to tracking and navigation: theory algorithms and software*: John Wiley & Sons, 2004.

[5] W.-H. Chen, J. Yang, L. Guo, and S. Li, "Disturbance-observer-based control and related methods—An overview," *IEEE Transactions on Industrial Electronics,* vol. 63, pp. 1083-1095, 2015.

[6] B. Jacob and V. Feypell-de La Beaumelle, "Improving truck safety: Potential of weigh-in-motion technology," *IATSS research,* vol. 34, pp. 9-15, 2010.

[7] B. Friedland, "Treatment of bias in recursive filtering," *IEEE Transactions on Automatic Control,* vol. 14, pp. 359-367, 1969.

[8] E. I. Verriest, "Optimal filtering for crypto-deterministic systems with application to delay systems with unknown initial data," in *Proceedings of the 47th IEEE Conference on Decision and Control*, 2008, pp. 49-54.

[9] M. Darouach and M. Zasadzinski, "Unbiased minimum variance estimation for systems with unknown exogenous inputs," *Automatica,* vol. 33, pp. 717-719, 1997.

[10] M. Darouach, M. Zasadzinski, and M. Boutayeb, "Extension of minimum variance estimation for systems with unknown inputs," *Automatica,* vol. 39, pp. 867-876, 2003.

[11] C.-S. Hsieh, "Robust two-stage Kalman filters for systems with unknown inputs," *IEEE Transactions on Automatic Control,* vol. 45, pp. 2374-2378, 2000.

[12] S. Gillijns and B. De Moor, "Unbiased minimum-variance input and state estimation for linear discrete-time systems," *Automatica,* vol. 43, pp. 111-116, 2007.

[13] S. Gillijns and B. De Moor, "Unbiased minimum-variance input and state estimation for linear discrete-time systems with direct feedthrough," *Automatica,* vol. 43, pp. 934-937, 2007.

[14] K. Maes, A. Smyth, G. De Roeck, and G. Lombaert, "Joint input-state estimation in structural dynamics," *Mechanical Systems and Signal Processing,* vol. 70, pp. 445-466, 2016.

[15] E. Lourens, C. Papadimitriou, S. Gillijns, E. Reynders, G. De Roeck, and G. Lombaert, "Joint input-response estimation for structural systems based on reduced-order models and vibration data from a limited number of sensors," *Mechanical Systems and Signal Processing,* vol. 29, pp. 310-327, 2012.

[16] K. Maes, K. V. Nimmen, E. Lourens, A. Rezayat, P. Guillaume, G. D. Roeck, and G. Lombaert, "Verification of joint input-state estimation for force identification by means of in situ measurements on a footbridge," *Mechanical Systems and Signal Processing,* vol. 75, pp. 245-260, 2016.

[17] E. Lourens, E. Reynders, G. De Roeck, G. Degrande, and G. Lombaert, "An augmented Kalman filter for force identification in structural dynamics," *Mechanical Systems and Signal Processing,* vol. 27, pp. 446-460, 2012.

[18] P. C. Hansen, "Analysis of discrete ill-posed problems by means of the L-curve," *SIAM review,* vol. 34, pp. 561-580, 1992.

[19] K. Maes, E. Lourens, K. Van Nimmen, E. Reynders, G. De Roeck, and G. Lombaert, "Design of sensor networks for instantaneous inversion of modally

reduced order models in structural dynamics," *Mechanical Systems and Signal Processing,* vol. 52, pp. 628-644, 2015.

[20] S. E. Azam, E. Chatzi, and C. Papadimitriou, "A dual Kalman filter approach for state estimation via output-only acceleration measurements," *Mechanical Systems and Signal Processing,* vol. 60, pp. 866-886, 2015.

[21] S. E. Azam, E. Chatzi, C. Papadimitriou, and A. Smyth, "Experimental validation of the Kalman-type filters for online and real-time state and input estimation," *Journal of vibration and control,* vol. 23, pp. 2494-2519, 2017.

[22] F. Naets, J. Cuadrado, and W. Desmet, "Stable force identification in structural dynamics using Kalman filtering and dummy-measurements," *Mechanical Systems and Signal Processing,* vol. 50, pp. 235-248, 2015.

[23] X. Liu and Y. Wang, "Input estimation of a full-scale concrete frame structure with experimental measurements," in *Proceedings of the 37th International Modal Analysis Conference (IMAC XXXVII),* Orlando, FL, USA, 2019.

[24] S. Z. Yong, M. Zhu, and E. Frazzoli, "A unified filter for simultaneous input and state estimation of linear discrete-time stochastic systems," *Automatica,* vol. 63, pp. 321-329, 2016.

[25] S. Z. Yong, M. Zhu, and E. Frazzoli, "Simultaneous input and state estimation with a delay," in *2015 54th IEEE Conference on Decision and Control (CDC)*, 2015, pp. 468-475.

[26] J. L. Massey and M. K. Sain, "Inverses of linear sequential circuits," *IEEE Transactions on Computers,* vol. 100, pp. 330-337, 1968.

[27] J. Jin and M.-J. Tahk, "Time-delayed state estimator for linear systems with unknown inputs," *International Journal of Control, Automation, and Systems,* vol. 3, pp. 117-121, 2005.

[28] S. Sundaram and C. N. Hadjicostis, "Comments on “Time-delayed state estimator for linear systems with unknown inputs”," *International Journal of Control, Automation, and Systems,* vol. 3, pp. 646-647, 2005.

[29] S. Sundaram and C. N. Hadjicostis, "Optimal state estimators for linear systems with unknown inputs," in *Decision and Control, 2006 45th IEEE Conference on*, 2006, pp. 4763-4768.

[30] K. Maes, S. Gillijns, and G. Lombaert, "A smoothing algorithm for joint input-state estimation in structural dynamics," *Mechanical Systems and Signal Processing*, vol. 98, pp. 292-309, 2018.

[31] C. Johnson, "Further study of the linear regulator with disturbances--The case of vector disturbances satisfying a linear differential equation," *IEEE Transactions on Automatic Control*, vol. 15, pp. 222-228, 1970.

[32] W.-H. Chen, "Disturbance observer based control for nonlinear systems," *IEEE/ASME transactions on mechatronics*, vol. 9, pp. 706-710, 2004.

[33] L. Guo and W. H. Chen, "Disturbance attenuation and rejection for systems with nonlinearity via DOBC approach," *International Journal of Robust and Nonlinear Control: IFAC‐Affiliated Journal*, vol. 15, pp. 109-125, 2005.

[34] F. Moses, "Weigh-in-motion system using instrumented bridges," *Journal of Transportation Engineering*, vol. 105, 1979.

[35] C. Rowley, A. Gonzalez, E. O'Brien, and A. Znidaric, "Comparison of conventional and regularized bridge weigh-in-motion algorithms," in *Proceedings of the international conference on heavy vehicles*, 2008, pp. 19-22.

[36] E. J. O'Brien, C. Rowley, and A. González, "A regularised solution to the bridge weigh in motion equations," *International Journal of Heavy Vehicle Systems*, vol. 16, pp. 310-327, 2009.

[37] A. N. Tikhonov and V. I. Arsenin, *Solutions of ill-posed problems* vol. 14: Wiley, New York, 1977.

[38] E. J. O'Brien, M. Quilligan, and R. Karoumi, "Calculating an influence line from direct measurements," *Bridge Engineering, Proceedings of the Institution of Civil Engineers*, vol. 159, pp. 31-34, 2006.

[39] E. J. OBrien, L. Zhang, H. Zhao, and D. Hajializadeh, "Probabilistic bridge weigh-in-motion," *Canadian Journal of Civil Engineering*, vol. 45, pp. 667-675, 2018.

[40] R. Peters, "AXWAY-a system to obtain vehicle axle weights," in *Proceedings of 12th Australian Road Research Board (ARRB) Conference*, Hobart, Austrialia, 1984.

[41] R. Peters, "CULWAY, an unmanned and undetectable highway speed vehicle weighing system," in *Proceedings of 13th Australian Road Research Board (ARRB) Conference*, Adelaide, Australia, 1986, pp. 70-83.

[42] A. Žnidarič, J. Kalin, and M. Kreslin, "Improved accuracy and robustness of bridge weigh-in-motion systems," *Structure and Infrastructure Engineering*, vol. 14, pp. 412-424, 2018.

[43] R. E. Snyder, F. Moses, B. E. Burke, and D. A. Kennedy, "Bridge weigh-in-motion system," ed: Google Patents, 1992.

[44] A. Dempsey, E. O'Brien, and J. O'Connor, "A bridge weigh-in-motion system for the determination of gross vehicle weights," in *European Conference on Weigh-in-Motion of Road Vehicles, 1st, 1995, Zurich, Switzerland*, 1995.

[45] A. Žnidaric, J. Žnidaric, and S. Tercelj, "Determination of the True Traffic Load in the Process of Safety Assessment of Existing Bridges," in *Proceedings of the 12th Congress of Structural Engineers in Slovenia*, 1991, pp. 241-246.

[46] B. Jacob and E. J. O'Brien, "WAVE-A European research project on weigh-in-motion," in *National Traffic Data Acquisition Conference (NATDAQ'96)*, Albuquerque, New Mexico, 1996, pp. 659-668.

[47] A. Znidaric, I. Lavric, and J. Kalin, "The next generation of bridge weigh-in-motion systems," in *Third International Conference on Weigh-in-Motion (ICWIM3) Iowa State University, Ames*, 2002.

[48] E. OBrien, A. Znidaric, and T. Ojio, "Bridge weigh-in-motion—Latest developments and applications world wide," in *Proceedings of the International Conference on Heavy Vehicles*, 2008, pp. 19-22.

[49] B. Jacob, E. J. O'Brien, and S. Jehaes, "European specification on weigh-in-motion of road vehicles," ed. Paris: COST 323, 1999, p. 66.

[50] SiWIM. *Accuracy of the measurement*. Available: https://www.cestel.eu/113/more-about-siwim-system

[51] H. Sekiya, "Field verification over one year of a portable bridge weigh-in-motion system for steel bridges," *Journal of Bridge Engineering,* vol. 24, p. 04019063, 2019.

[52] C. O'Connor and T. H. T. Chan, "Dynamic wheel loads from bridge strains," *Journal of Structural Engineering,* vol. 114, pp. 1703-1723, 1988.

[53] T. H. Chan, S. Law, T. Yung, and X. Yuan, "An interpretive method for moving force identification," *Journal of sound and vibration,* vol. 219, pp. 503-524, 1999.

[54] S. Law, T. H. Chan, and Q. Zeng, "Moving force identification: a time domain method," *Journal of Sound and vibration,* vol. 201, pp. 1-22, 1997.

[55] S. Law, T. H. Chan, and Q. Zeng, "Moving force identification—a frequency and time domains analysis," *Journal of dynamic systems, measurement, and control,* vol. 121, pp. 394-401, 1999.

[56] S. Law and Y. Fang, "Moving force identification: optimal state estimation approach," *Journal of Sound and Vibration,* vol. 239, pp. 233-254, 2001.

[57] T.-C. Chen and M.-H. Lee, "Research on moving force estimation of the bridge structure using the adaptive input estimation method," *Journal of Structural Engineering,* vol. 8, pp. 20-208, 2008.

[58] A. González, C. Rowley, and E. J. OBrien, "A general solution to the identification of moving vehicle forces on a bridge," *International journal for numerical methods in engineering,* vol. 75, pp. 335-354, 2008.

[59] S. Law, J. Bu, X. Zhu, and S. Chan, "Vehicle axle loads identification using finite element method," *Engineering Structures,* vol. 26, pp. 1143-1153, 2004.

[60] S. Law, T. H. Chan, Q. Zhu, and Q. Zeng, "Regularization in moving force identification," *Journal of engineering mechanics,* vol. 127, pp. 136-148, 2001.

[61] X. Zhu and S. Law, "Moving loads identification through regularization," *Journal of engineering mechanics,* vol. 128, pp. 989-1000, 2002.

[62] X. Zhu and S.-S. Law, "Recent developments in inverse problems of vehicle–bridge interaction dynamics," *Journal of Civil Structural Health Monitoring,* vol. 6, pp. 107-128, 2016.

[63] D. Feng, H. Sun, and M. Q. Feng, "Simultaneous identification of bridge structural parameters and vehicle loads," *Computers & Structures,* vol. 157, pp. 76-88, 2015.

[64] Y. Yu, C. Cai, and L. Deng, "State-of-the-art review on bridge weigh-in-motion technology," *Advances in Structural Engineering,* vol. 19, pp. 1514-1530, 2016.

[65] X. Q. Zhu and S. S. Law, "Identification of vehicle axle loads from bridge dynamic responses," *Journal of sound and vibration,* vol. 236, pp. 705-724, 2000.

[66] L. Yu and T. H. Chan, "Moving force identification based on the frequency–time domain method," *Journal of Sound and Vibration,* vol. 261, pp. 329-349, 2003.

[67] L. Deng and C. Cai, "Identification of parameters of vehicles moving on bridges," *Engineering Structures,* vol. 31, pp. 2474-2485, 2009.

[68] J. Kim and J. P. Lynch, "Experimental analysis of vehicle–bridge interaction using a wireless monitoring system and a two-stage system identification technique," *Mechanical Systems and Signal Processing,* vol. 28, pp. 3-19, 2012.

[69] T. R. Wright, "Full-scale Seismic Testing of a Reinforced Concrete Moment Frame Using Mobile Shakers," Ph.D., Civil and Environmental Engineering, Georgia Institute of Technology, Atlanta, GA, USA, 2015.

[70] E. Yu, D. H. Whang, J. P. Conte, J. P. Stewart, and J. W. Wallace, "Forced vibration testing of buildings using the linear shaker seismic simulation (LSSS) testing method," *Earthquake engineering & structural dynamics,* vol. 34, pp. 737-761, 2005.

[71] X. Dong, X. Liu, T. Wright, Y. Wang, and R. DesRoches, "Validation of wireless sensing technology densely instrumented on a full-scale concrete frame structure," *Proceedings of International Conference on Smart Infrastructure and Construction (ICSIC)*, Cambridge, U.K., 2016.

[72] Y. Wang, N. Uddin, L. J. Jacobs, and J.-Y. Kim, "Field validation of a drive-by bridge inspection system with wireless BWIM+ NDE devices," School of Civil and Environmental Engineering, Georgia Institute of Technology2016.

[73] M. Kane, D. Zhu, M. Hirose, X. Dong, B. Winter, M. Häckell, J. P. Lynch, Y. Wang, and A. Swartz, "Development of an extensible dual-core wireless sensing node for cyber-physical systems," *Proceedings of SPIE, Nondestructive Characterization for Composite Materials, Aerospace Engineering, Civil Infrastructure, and Homeland Security*, San Diego, California, USA, 2014.

[74] X. Liu, X. Dong, and Y. Wang, "Field testing of Martlet wireless sensing system on an in-service pre-stressed concrete highway bridge," *Proceedings of SPIE 2016, Health Monitoring of Structural and Biological Systems*, Las Vegas, NV, USA, 2016.

[75] D. Simon, *Optimal state estimation: Kalman, H infinity, and nonlinear approaches*: John Wiley & Sons, 2006.

[76] P. Horowitz and W. Hill, *The Art of Electronics*, 2nd ed. Cambridge, England: Cambridge University Press, 1989.

[77] P. Van Overschee and B. De Moor, "N4SID: Subspace algorithms for the identification of combined deterministic-stochastic systems," *Automatica*, vol. 30, pp. 75-93, 1994.

[78] R. S. Pappa, K. B. Elliott, and A. Schenk, "Consistent-mode indicator for the eigensystem realization algorithm," *Journal of Guidance, Control, and Dynamics*, vol. 16, pp. 852-858, 1993.

[79] Y. Wang, X. Dong, D. Li, and Y. Otsuki. (2019). *SMU: MATLAB Package for Structural Model Updating*. Available: https://github.com/ywang-structures/Structural-Model-Updating

[80] L. S. T. Corporation, *LS-DYNA Keyword User's Manual Version R8.0* vol. I, 2015.

[81] L. S. T. Corporation, *LS-DYNA Theory Manual*. CA, USA, 2006.

[82] X. Dong, D. Zhu, Y. Wang, J. P. Lynch, and R. A. Swartz, "Design and validation of acceleration measurement using the Martlet wireless sensing system," *Proceedings of the ASME 2014 Smart Materials, Adaptive Structures and Intelligent Systems (SMASIS)*, Newport, RI, 2014.

[83] R. Astroza, H. Ebrahimian, Y. Li, and J. P. Conte, "Bayesian nonlinear structural FE model and seismic input identification for damage assessment of civil structures," *Mechanical Systems and Signal Processing*, vol. 93, pp. 661-687, 2017.

[84] H. Ebrahimian, R. Astroza, J. P. Conte, and C. Papadimitriou, "Bayesian optimal estimation for output‐only nonlinear system and damage identification of civil structures," *Structural Control and Health Monitoring*, vol. 25, p. e2128, 2018.

[85] T. Ojio, C. Carey, E. J. OBrien, C. Doherty, and S. E. Taylor, "Contactless bridge weigh-in-motion," *Journal of Bridge Engineering*, vol. 21, p. 04016032, 2016.

[86] R. Hou, S. Jeong, K. H. Law, and J. P. Lynch, "Reidentification of trucks in highway corridors using convolutional neural networks to link truck weights to bridge responses," in *Sensors and Smart Structures Technologies for Civil, Mechanical, and Aerospace Systems 2019*, 2019, p. 109700P.

[87] X. Zhu and S. Law, "Identification of moving interaction forces with incomplete velocity information," *Mechanical systems and signal processing*, vol. 17, pp. 1349-1366, 2003.

[88] S. P. Brady, E. J. O'Brien, and A. Žnidarič, "Effect of vehicle velocity on the dynamic amplification of a vehicle crossing a simply supported bridge," *Journal of Bridge Engineering*, vol. 11, pp. 241-249, 2006.